

DEVELOPMENT OF CARBON BASED MATERIALS WITH SiC COATING FOR HIGH TEMPERATURE NUCLEAR APPLICATIONS

By

RAMANI VENUGOPALAN

BHABHA ATOMIC RESEARCH CENTRE

*A thesis submitted to the
Board of Studies in Chemical Sciences Discipline*

In partial fulfillment of requirements

For the Degree of

DOCTOR OF PHILOSOPHY

of

HOMI BHABHA NATIONAL INSTITUTE



June, 2011

Homi Bhabha National Institute

Recommendation of the Viva Voce Board

As members of the Viva Voce Board, we certify that we have read the dissertation prepared by **Smt Ramani Venugopalan** entitled “**Development of carbon based materials with SiC coating for high temperature nuclear applications**” and recommended that it may be accepted as fulfilling the dissertation requirement for the Degree of Doctor of Philosophy,

_____ **Date:02/11/2011**

Chairman- Dr.(Smt.) Shyamala Bhardwaj

_____ **Date: 02/11/2011**

Guide-Dr. A. K. Tyagi

_____ **Date: 02/11/2011**

Member-1- Prof. Maheswar Sharon

_____ **Date: 02/11/2011**

Member-2: Dr. Dr. D. Sathiyamoorthy

_____ **Date: 02/11/2011**

Member-3: Dr. V. K. Jain

_____ **Date: 02/11/2011**

Member-4: Dr. R. K. Vatsa

Final approval and acceptance of this dissertation is contingent up on the candidates submission of the final copies of the dissertation to HBNI.

I hereby certify that I have read this dissertation prepared under my direction and recommend that it may be accepted as fulfilling the dissertation requirement.

Date: 02/11/2011

Place: BARC, Mumbai

STATEMENT BY AUTHOR

This dissertation has been submitted in partial fulfillment of requirements for an advanced degree at Homi Bhabha National Institute (HBNI) and is deposited in the library to be made available to borrowers under rules of the HBNI.

Brief quotations from this dissertation are allowable without special permission, provided that accurate acknowledgement of source is made. Requests for permission for extended quotation from or reproduction of this manuscript in whole or in part may be granted by the Competent Authority of HBNI when in his or her judgment the proposed use of the material is in the interests of scholarship. In all other instances, however, permission must be obtained from the author.

(Ramani Venugopalan)

DECLARATION

I, hereby declare that the investigations presented in the thesis have been carried out by me. The work is original and has not been submitted earlier as a whole or in part for a degree / diploma at this or any other Institution / University.

(Ramani Venugopalan)

Dedicated to my dear parents

ACKNOWLEDGEMENTS

It is a great pleasure in presenting my thesis on completion of my project and in expressing my deepest regards and deep sense of gratitude and sincere thanks to my research guide Dr. A. K. Tyagi,, Head, Solid State Chemistry Section, Chemistry Division, for his valuable guidance in hours of need, constant encouragement, keen interest, good wishes and valuable suggestions throughout my entire research tenure. I am also grateful to him for critically reviewing this thesis.

It gives me immense pleasure to acknowledge Dr. D. Sathiyamoorthy, Head, Powder Metallurgy Division (PMD), for his constant support and for critically evaluating my research activities from time to time and also for providing the facilities and valuable suggestions for completion of this work.

It is also my great pleasure to thank Dr. A. K. Suri, Director, Materials Group for his support in carrying out the research work.

I also wish to extend my heart filled thanks to my colleagues Jyoti Prakash, P. T. Rao, Dr. Selvakumar, Kinshuk Dasgupta and other colleagues from Process Engineering Section, PMD for helping me in my experimental work and providing constructive suggestions throughout the work. I would also like to acknowledge the magnanimous cooperation extended to me by the colleagues from other Divisions in my research activities.

I wish to express my sincere gratitude and indebtedness to my parents, late parents-in-laws for their blessings, for their love and support to me. I am extremely thankful to my husband and my son for their patience and understanding.

Last but not the least, I also wish to thank all my friends for their constant unconditional support.

CONTENTS

	Page Number
SYNOPSIS	xiv-xxv
LIST OF FIGURES	xxvi-xxxii
LIST OF TABLES	xxxiii
CHAPTER 1	1-36
INTRODUCTION AND LITERATURE SURVEY	
1.Introduction	2
1.1 Carbon-carbon composites	7
1.1.1 Carbon Fibers	8
1.1.2 Matrix	11
1.2 Conventional processing of carbon/carbon composites	11
1.3 Liquid impregnation Route	14
1.4 Gas Impregnation Route	17
1.4.1 Isothermal Chemical Vapour Infiltration (ICVI)	17
1.4.2 Thermal gradient Chemical Vapour Infiltration Process	20

1.4.3 Differential pressure process	21
1.4.4 Forced flow-thermal gradient CVI (FCVI)	21
1.4.5 Film boiling CVI (Kalamazoo)	22
1.5 Mechanical properties	24
1.6 Oxidation behavior and protection	30
1.7 Applications	35
1.8 Plan of the present work	36

CHAPTER 2 **37-59**

**CHARACTERISATION TECHNIQUES AND METHODS FOR
PROPERTY EVALUATION OF CARBON/CARBON COMPOSITE
MATERIALS**

2. Introduction	38
2.1 Preparation of carbon/carbon composite samples	39
2.2 Densification of the samples	40
2.3. Characterization of the samples	40
2.3.1 Characterization techniques	41
2.3.1.1 Chemical analysis	41

2.3.1.2 Density of the composites	41
2.3.1.3 Powder X-ray diffraction:	42
2.3.1.4 X-ray Tomography	43
2.3.1.5 Scanning electron microscopy (SEM)	46
2.3.1.6 Thermomechanical Analyser (TMA)	48
2.3.1.7. Differential Scanning Calorimetry (DSC)	49
2.4. Spectroscopic Techniques	50
2.4.1. Raman Spectroscopy	50
2.4.2. Small angle scattering studies	53
2.4.3 X-ray Photon Spectroscopy	56

CHAPTER 3 **60-86**

**PREPARATION, EVALUATION OF STRUCTURAL AND THERMOPHYSICAL
PROPERTIES OF CARBON COMPOSITES**

3. Introduction	61
3.1. Experimental	62
3.1.1 Petroleum coke based samples	62
3.1.2 Carbon black based samples	62

3.1.3.1 Chopped carbon fiber based samples	64
3.1.3.2 Matted carbon fiber based samples	65
3.2 Chemical analysis	67
3.3 Density of the composites	67
3.4 Characterization	73
3.4.1 XRD characterization studies	73
3.4.2. Optical microscopy and Scanning electron microsc	77
3.4.3. Tomography studies	83
3.5 Conclusion	85
CHAPTER 4	87-120
SPECTROSCOPIC STUDIES ON CARBON COMPOSITES	
4. Introduction	88
4.1 Experimental	90
4.1.1 Preparation of Carbon/Carbon composite Samples	90
4.2 Thermophysical property measurement	90
4.2.1 CTE and Cp measurements	90
4.2.2. Compressive strength measurement	96

4.3.Raman Spectroscopy studies	97
4.3 X-ray Photoelectron Spectroscopy (XPS) Studies	108
4.4 Small angle scattering studies	113
4.5 Conclusion	119
CHAPTER 5	121-146
RADIATION STABILITY OF CARBON COMPOSITES	
5. Introduction	122
5.1 Radiation effects in solids	123
5.2 Experimental	129
5.2.1 Preparation of carbon/carbon composite samples	129
5. 2.2 Irradiation of the samples	131
5. 2.3 Characterization of the irradiated sample	131
5. 3 Results and discussion	132
5. 3.1 Raman spectroscopy studies	132
5. 3. 2 XRD studies	138
5. 3. 3 DSC studies	141
5. 4 Conclusions	145

DEVELOPMENT OF SiC COATINGS ON CARBON COMPOSITES AND ITS CHARACTERIZATION

6 Introduction	148
6. 1. 1 Carbothermal Reduction Process	149
6. 1. 2 Physical Vapour Transport	149
6. 1. 3 Sublimation Growth	150
6. 1. 4 Two Step Sol-gel Process	150
6.1.5 Laser Pyrolysis of Polycarbosilane	151
6.1.6 Using Supersonic beam of C ₆₀	152
6.1.7 Chemical vapour deposition growth	152
6. 2. Experimental procedure	157
6. 3 Results and discussion	160
6. 3.1. Effect of MTS feed rate	165
6. 3. 2 Effect of hydrogen gas flow rate on deposition rate	167
6. 3. 3 Effect of inert gas flow rate on coating rate	171
6. 4 Conclusions	175

CHAPTER7	176-184
SUMMARY AND FUTURE SCOPE OF THE WORK	
Summary and future scope of the work	177
An extension of the present work not included in thesis	181
REFERENCES	185-195
LIST OF PUBLICATIONS	196-197
PUBLISHED PAPERS	

**SYNOPSIS OF THE THESIS TO BE SUBMITTED TO THE HOMI BHABHA
NATIONAL INSTITUTE FOR THE DEGREE OF DOCTOR OF PHILOSOPHY IN
CHEMICAL SCIENCE**



Name of the Candidate : **RAMANI VENUGOPALAN**

Name of the Guide : **Prof. A. K. TYAGI**
**Chemical Science, Homi Bhabha National
Institute, Mumbai - 400094, INDIA**

Registration Number : **CHEM01200604027**

Date of Registration : **22-02-2007**

Title of the Thesis : **DEVELOPMENT OF CARBON BASED
MATERIALS WITH SiC COATING FOR
HIGH TEMPERATURE NUCLEAR
APPLICATIONS**

Place of Research Work : **Powder Metallurgy Division
Bhabha Atomic Research Centre
Mumbai - 400 085, INDIA**

Signature of the Candidate :

Signature of the Guide :

SYNOPSIS

Title: DEVELOPMENT OF CARBON BASED MATERIALS WITH SiC COATING FOR HIGH TEMPERATURE NUCLEAR APPLICATIONS

Carbon is a wonderful material having a wide range of structures and possess several properties such as capability to withstand high temperature (in protective environment), acceptable strength up to 2500⁰C, chemical inertness, low coefficient of thermal expansion, low friction, good thermal and electrical conductivities, low density and excellent thermal shock resistance. Carbon and carbon-based materials are used in nuclear reactors. In the recent past there has been a growing interest to develop graphite and carbon-based materials for high temperature thermal nuclear and fusion reactors. Efforts are underway to develop carbon materials with high density as well as amorphous isotropic carbon for use in thermal reactors. For some of these applications amorphous structure is required so as to avoid accumulation of Wigner energy [1-6], which is the stored energy in graphite lattice due to dislocation of atoms induced by irradiation. Graphitic carbon, due to its excellent neutron scattering properties, continues to be the unanimous choice for the moderator material in high-temperature nuclear reactors [7-9] where the aforesaid drawbacks are essentially overcome due to high-temperature annealing. This amorphous carbon should be isotropic and dense in order to achieve dimensional stability under irradiation.

Carbon is used as moderator and reflector due to its heat transfer properties, corrosion resistance, stability under irradiation, mechanical strength, low atomic weight with high neutron scattering cross section, low neutron capture cross section. In addition to, these properties, the lower cost and its easy availability are other attractive features with carbon. Since graphite as a moderator as well as structural material in high temperature reactors is the most favored choice, there is a need to develop high density isotropic graphite with suitable coatings for safe application of carbon based materials even in oxidizing or water vapor environment. Carbon-carbon (C/C) composite materials as against conventional graphite materials are now being contemplated as the promising materials for the fusion reactor due to their high thermal conductivity and high thermal resistance. The present study encompasses with the preparation and application of carbon materials for various nuclear reactors related issues and addresses the

current need for focused research on novel carbon materials for future new generation nuclear reactors.

C/C composites also possess a number of properties such as low atomic number, high thermal shock resistance, high sublimation temperature and high thermal conductivity, which makes them a good choice for the fusion reactors. C/C component materials may be the choice for the next generation Tokamak fusion reactors such as International Thermonuclear Experimental Reactor (ITER) which must endure severe environment including high-heat fluxes, high armor, surface temperature and eddy-current induced stresses during plasma disruption. The plasma-facing carbon-carbon composite materials are likely to suffer structure and property degradation as a result of carbon atom displacements and crystal lattice damage, caused by impinging high-energy fusion neutrons. As C/C composites are infinitely variable family of materials, the processing and design variables such as; (1) architectures viz. 1D, 2D, 3D or random fiber distribution; (2) fiber precursor, i.e., pitch, polyacrylonitrile (PAN) or vapor grown; (3) matrix, i.e., liquid impregnation (pitch or resin) or chemical vapour infiltration (CVI), and (4) final graphitization temperature will influence the properties and behavior of C/C composites. Burchell et al. [10-15] subjected 1D, 2D, and 3D C/C composites to irradiation at 600°C and to damage doses up to 1.5dpa, which revealed that 3D C/C composites have more isotropic dimensional changes than that of 1D or 2D composites. Pitch fiber composites were shown to be dimensionally more stable than PAN fiber composites and high graphitization temperatures were found to be beneficial.

Graphite and carbon fibre reinforced carbon composites are the candidate materials for high temperature applications due to their superior properties [16-22]. However, they are prone to oxidation at high temperatures as normal carbon materials when exposed to oxidizing atmospheres. In order to exploit the advantage of these properties from an environment ranging from of vacuum or inert gases to an oxidizing atmosphere, these materials should be protected by an oxidation resistant material, by giving a protective coating.

SiC is a material with high temperature oxidation resistance along with good thermal shock properties and stability against hot corrosion. These properties make it an oxidation resistant material. SiC coating has the combination of unique physicochemical and mechanical properties such as high strength, extreme hardness as well as excellent resistance to wear oxidation and

corrosion. SiC coating can be obtained by several methods [23-29] such as cementation packing chemical vapor deposition CVD, Laser Induced Chemical Decomposition (LICD) etc. Among the different techniques to grow SiC on various substrates, the CVD is the most frequently used technique. CVD can be used to deposit materials with near theoretical density with good adherence to the substrate.

Objective of the present study

The present studies were aimed to develop carbon-carbon (C/C) composite using non-graphitizing precursors such as polyacrylonitrile (PAN) fiber and phenolic resin matrix. The main focus was to arrive at a final composite material which is non-graphitic in nature and is stable under irradiation. These C/C composites are typically having 40 vol% of PAN fibre which was found to be amorphous. In the present studies C/C composites have been prepared using 2D matted PAN carbon fibers. The composites were densified using resin impregnation technique under pressure followed by curing and then carbonization. The effect of pressure and time duration on the density was studied by varying the pressure and time duration of impregnation. The materials were characterized by X-ray Diffraction (XRD), Small Angle X-ray Scattering (SAXS), Small Angle Neutron Scattering (SANS), X-ray tomography and Raman Spectroscopy. These composites have been irradiated by neutrons and were characterized before and after irradiation. Although these materials possess excellent properties, they are prone to oxidation at high temperatures as normal carbon materials when exposed to oxidizing atmospheres. Therefore, these composites were given protective coating. Hence studies on coating with SiC by chemical vapor deposition technique using a hot wall reactor with methyl trichlorosilane as precursor for SiC was carried out.

The thesis will be divided into several chapters, briefly described as follows:

Chapter 1: Introduction

The chapter describes general introduction of carbon/carbon composites. These are a generic class of synthetic, pure carbon materials consisting of carbon fibers reinforced in a carbon matrix. Their characteristic properties for example light weight, high thermal shock resistance, low co-efficient of thermal expansion, strength retention at high temperatures, high impact

resistance, high stiffness etc. catapulted them initially as a preferred material for various high technology applications. The quest for high temperature structural material for selected critical components of advanced air force exit and re-entry systems provided the impetus for research. They included improvements in properties of the constituent materials, viz., carbon fibers and carbon matrix precursors and design allowables. These properties were attained by an intelligent combination of two different constituents. The reinforcement is used in the form of fibers which possess a very high modulus. The matrix serves to protect the fibers from damage due to the environment and also it plays a very important role of stress transfer, which helps in attaining excellent properties.

In this chapter, an explicit description of the various aspects of carbon-carbon composites development is given. It commences from the description of their manufacturing techniques and proceeds to explain the effect of various parameters on final properties exhibited. Fabrication method of C/C composites involves fabrication of 1D (one directional reinforced), 2D (two directional reinforced), 3D (three directionally reinforced) or MD (multi directional reinforcement) of porous carbon fiber preforms having the desired shape or a porous carbon-carbon skeleton (UD, 2D, 3D or MD). Carbon-carbon composites are manufactured by using different techniques such as all solid pyrolysis using thermosetting resins, or pitch route using liquid infiltration carbonization route or CVD route.

Chapter 2: Instrumentation

Carbon/ carbon composite was prepared by making a 2-D preform using PAN based fibers and phenolic resin. These preforms were first carbonized. These preform samples have density of 1100 kg/m^3 . These samples were densified using phenolic resin at varying pressures such as 30, 50 and 70 bar at varying time period 10, 15, 20 and 25hrs. Two cycles of impregnation were performed for each sample. Impregnation was followed by curing and carbonization of the samples. The effect of pressure and time duration of impregnation on the density and microstructural parameters has been studied. The densities of the samples were determined by Archimedes principle. XRD technique was employed to characterize the degree of graphitization of carbon-carbon composites with low crystallinity. Raman Spectroscopy was

also used to characterize the composites. The coefficient of thermal expansion (CTE) and the specific heat of the sample have been measured using thermomechanical analyzer (TMA) and differential scanning calorimetry (DSC), respectively. X-ray tomography studies of these samples were carried out on the composites to determine the homogeneity and cracks/pores in the sample. SAXS and SANS studies were carried out on the C/C composite prepared from carbonized PAN fiber and phenol formaldehyde resin to evaluate the porosity in the composite materials. XPS studies were carried out to determine the ratio of sp^2 and sp^3 hybridised carbon atoms in these composites.

Chapter 3: Preparation, structural and thermophysical properties of carbon composites

The fabrication of a suitable preform is the first step for manufacturing the carbon-carbon composite. This may also be referred to as fiber architecture. It not only imparts rigidity to the composite, but also in conjunction with fiber properties it determines the properties of the composite. In the present study, preform has been made using PAN carbon fibers. These fibers have been matted and stacked to a 2-D preform using phenol formaldehyde resin. Green preform in the shape of rectangular blocks have been fabricated. This preform was cut into 250mm X 250mm X 60mm size and carbonized at a slow heating rate. The carbonized preforms were then used for further studies. The carbonized sample is highly porous and needs to be densified for further any application. The samples have been densified by impregnation technique up to two cycles. The liquid phenol formaldehyde resin was impregnated under a varying pressure of 30, 50 and 70 bar and with varying time duration of 10, 15, 20 and 25 h. The impregnated sample was then carbonized at 1000°C under inert atmosphere with a heating rate of 6°C/h. The samples were then subjected to a second cycle of impregnation at the same pressure and varying time duration as carried out during the first cycle. These samples were then cured and carbonized as done in the first cycle. Two cycles of impregnation and carbonization were carried out. The density of the samples were measured after two cycles by Archimedes principle. Few samples were subsequently heat-treated at 1800°C to study the effect of high-temperature processing on the micro-structural modification of the materials. X-ray diffraction studies were also performed. X-ray tomography studies have been carried out on composites subjected to different pressures for densification. The dimension of the carbon

composite was 11mm x 12mm x 6.4mm. 400 radiographs, each of 15 second exposure, were taken at 60kV and 400 to 450 micro-amp (keeping the power constant for constant flux during operation) setting of the microfocus source. The reconstruction grid dimension is 787x787x256 pixels.

Chapter 4: Spectroscopic and Small Angle Scattering characterization of carbon composites

Raman spectroscopy investigations have been used extensively on different carbon materials to determine the degree of crystallinity ranging from poorly ordered carbon to graphite and diamond. Raman spectroscopy is based on Raman effect, which originates from the scattering of electromagnetic radiation by the electron sheaths of the investigated molecules. Raman spectroscopy was used for the structural analysis and to find if graphitization was occurring during the processing of the samples. Usually Raman spectra of most of the carbon- graphite materials contain two bands at $\sim 1580\text{ cm}^{-1}$ and at $\sim 1360\text{ cm}^{-1}$ except for natural graphite, which has a single sharp Raman band at 1580 cm^{-1} [15]. The ratio of the integrated intensities of the two peaks, I_D/I_G has been considered to be a crucial parameter to estimate the degree of graphitization. The higher the ratio of I_D/I_G , lower is the degree of graphitization of the carbon materials.

XPS is a quantitative spectroscopic technique which measures the chemical state and electronic state of elements and the elemental composition that exist in the material. C1s XPS spectra were recorded in slow scan mode. The spectra is deconvoluted using Gaussian function into the distinct features at $\sim 283.4\text{ eV}$ and 285 eV . The feature at $\sim 285\text{ eV}$ corresponds to sp^3 hybridised carbon atoms while $\sim 283.4\text{ eV}$ corresponds to sp^2 hybridised carbon atoms. The intensity ratio of these peaks gives an estimate of the sp^2/sp^3 carbon fraction.

Small-angle neutron scattering (SANS), unlike mercury intrusion porosimetry (MIP), is a non-destructive and non-intrusive technique used for pore size measurement in porous solids. Furthermore, SANS can probe open, closed and ink-bottle pores. Hence, SANS was used to investigate the effect of impregnation parameters (pressure and time) on the pore morphology of C/C composites. SAXS experiments were carried out using SAXS set-up based on line-slit

geometry to examine the pore structure of neutron irradiated PAN carbon fiber-carbon composites.

Chapter 5: Radiation stability of some representative carbon composites

The main focus of this chapter is on the particle irradiation which might lead to the formation of crystalline phase in the amorphous carbon leading to storage of Wigner energy. There is a possibility of self-organization phenomenon under irradiation leading to localized ordered arrangement in disordered structure of atoms in amorphous samples leading to crystallinity. In the present work, neutron irradiation on the carbon- carbon composites was carried out. These samples were characterized for various structural parameters like extent of local ordering along c axis, the average spacing of the $d_{(002)}$ i.e. the (002) crystallographic planes using X-ray diffraction (XRD) technique. The salient observations were further validated using Raman spectroscopy. The carbon-carbon (C/C) composite samples have been irradiated with thermal neutrons at APSARA Reactor, Bhabha Atomic Research Center, Trombay. Two samples (denoted as sample-1 and sample-2) with density of 1314 kg/m^3 and 1310 kg/m^3 , respectively, were used for these studies. Sample-1 was prepared by impregnation of the resin at 30 bars for 10h while sample-2 was prepared by impregnation at 30 bars for 20h. The irradiation flux was $1 \times 10^{12} \text{ n/cm}^2/\text{s}$ for seven, fourteen and twenty hours for both sample-1 and sample- 2. The respective fluence was $2.52 \times 10^{16} \text{ n/cm}^2$, $5.04 \times 10^{16} \text{ n/cm}^2$ and $7.2 \times 10^{16} \text{ n/cm}^2$ at temperature of 313 K during the irradiation. The stored energy in the composite due to irradiation was measured using DSC and the changes in the structure were observed by X-ray diffraction and Raman spectroscopy. These results will be discussed in this chapter.

Chapter 6: Development of SiC coatings on carbon composites and their characterization

Graphite and carbon fibre reinforced carbon composites are candidate materials for high temperature applications due to their superior properties such as high sublimation temperature combined with high resistance against cyclic thermal stress, superior specific tensile strength up to 2273 K. In order to harness the advantage of these properties even if environment changes from vacuum or inert gases to an oxidizing atmosphere, these materials should be protected by a

oxidation resistant material. SiC is a material with high temperature oxidation resistance along with good thermal shock properties and stability against hot corrosion. This makes it an ideal oxidation resistant material. SiC coating has the combination of unique physicochemical and mechanical properties such as high strength, extreme hardness as well as excellent resistance to wear oxidation and corrosion. Among the different techniques to grow SiC on different substrates, the CVD is the most frequently used technique. CVD can be used to deposit materials at near theoretical density with good adherence to the substrate. The deposition rate by CVD process is higher than most other coating techniques except plasma spraying method. As the CVD technique does not require line of sight with the vapor source, the coatings can be uniformly deposited over complex shapes and internal surfaces. Even materials having high melting point can be deposited at low temperatures by using suitable CVD reaction precursor. SiC coating can be formed by using various Si and C compounds. The present study has been carried out with methyl trichlorosilane (MTS) as the SiC precursor. These experiments were carried out with varying feed flow rates of MTS at 1673K along with hydrogen and argon as the carrier gas using a high temperature vertical graphite reactor. Various parameters such as hydrogen flow rate and feed rate of MTS were optimized to get the best coatings. The SiC coatings have been characterized by X-Ray Diffraction (XRD) and Raman spectroscopy for phase identification. Scanning electron microscopy (SEM) analysis with EDS was also carried out for microstructure and elemental analysis. A detailed study on the effect of operating parameters is presented in this chapter. The present objective of this work was to coat graphite or carbon composites with SiC using CVD technique in order to obtain a dense isotropic β -SiC phase and to study the effect of the operating parameters such as MTS, hydrogen flow rate and feed rate of MTS. The experiments were carried out at 1673K.

Chapter 7: Conclusion and future scope

Carbon-carbon composites with density of 1470 kg/m^3 have been prepared with two cycles of impregnation. From the XRD and Raman analysis, it was found that though there was small ordering taking place due to the effect of pressure and time duration on impregnation of samples but the material is still predominantly amorphous in nature. The X-ray tomography studies showed that the sample with density of 1470 kg/m^3 showed uniform structure with absence of

large pores. Neutron irradiation studies showed the tendency to get ordered crystalline structure which is observed from both XRD and Raman spectroscopy. However the stored energy is very less compared to that of graphite. The simple defects are created at lower fluence which are annealed at around 100°C while at higher fluence levels complex defects are formed and annealed at higher temperatures. Even after irradiation, the samples are still amorphous in nature though there is a tendency to get ordered structure at fluence of 10^{16} n/cm². SiC coating on C/C composites was achieved using CVD technique.

Future work includes development of composites with higher density by choosing proper variation in process parameters. The present irradiation studies were carried out at available lower fluences, irradiation studies at higher fluencies of 10^{21} n/cm² will be carried out. The irradiation studies of SiC coated sample are also underway.

References

- [1] Graphite Moderator Lifecycle Behavior
IAEA – Tecdoc., 32 (1998) 32.
- [2] G. B. Engle and Eatherly, W. P.
High Temp.–High Press., 119 (1972) 4.
- [3] B. T. Kelly, editor.
Physics of Graphite., London: Applied Science Publishers (1981).
- [4] B. T. Kelly and T. D Burchell
Carbon, 499 (1994) 32.
- [5] R. E. Nightingale
Nuclear Graphite (Academic Press, New York, London) (1962).
- [6] B. T. Kelly
Prog. Nucl. Energ., 21(1978) 2.
- [7] T. D. Burchell
Phys. Scripta T., 17(1996) 64.
- [8] T. Iwata
J. Nucl. Mater., 361(1985) 134.
- [9] K. Dasgupta, M. Roy, A. K. Tyagi, S. K. Kulshreshtha, Ramani Venugopaln
and D. Sathiyamoorthy
Compos. Sci. Technol., 1794-1801 (2007) 67.
- [10] T. D. Burchell, Carbon Materials for Energy production and Storage, In Design and
Control of structure of Advanced Carbon materials for Enhanced Performance. B. Rand et
al, editor. Kluwer Academic Publishers., 277-294(2001).
- [11] F. Banhart
Rep. Prog. Phys., 1181(1999) 62.
- [12] A. Seeger
Rad. Eff. Defects Solids., 111-112(1989) 355.
- [13] A. Seeger and W. Frank
Solid State Phenomena., 3-4(1988) 125.
- [14] K. Dasgupta, P. Barat, A. Sarkar, P. Mukherjee, D. Sathiyamoorthy
Applied Physics A- Materials Science and Processing., 721-726 (2007) 87.
- [15] S. D. Preston, G. T. Melvin, Results from the 1997/98 Stored energy Survey of Windscale
Pile I, IAEA Technology plc Report AEAT-3400 WPTC., 73 (1998).
- [16] J. D. Buckley
Ceram Bull., 67, (1988) 364.
- [17] J. E. Sheehan
Ann Rev Mater Sci., 24 (1994)19.
- [18] M. E. Westwood, J. D. Webster, R. J. Day, F.H. Hayes and R. Taylor
J Mater Sci., 31 (1996) 1389.
- [19] H. Fritze, J. Jojie, T. Witke, C. Ruscher, S. Weber, S. Scherrer
J Eur Ceram Soc., 18-23 (1988) 51.
- [20] F. Smeacetto and M. Ferraris
Carbon, 40 (2002) 583.
- [21] L. F. Cheng, Y.D. Xu and L.T. Zhang
Carbon, 38 (2000) 1493
- [22] S. Lloyd , N. Avery and M. Pal

- Carbon.,39 (2001) 991.
- [23] A. Ordine, C.A. Achete, O.R. Mattosa, I.C.P. Margaret, S.S. Camargo Jr and T.Hirsch
Surf Coat. Technol., 133-134 (2000) 583
- [24] S. K. Gong, H.B. Xu, Q.H. Yu, C.G. Zhou
Surf. Coat. Technol. 130 (2000) 128.
- [25] K. L. Choy
Prog. Mater. Sci., 48 (2) (2003) 57.
- [26] W. G. Zhang and K. J. Huttinger
Chem. Vap. Deposition., 13(7) (2001) 167.
- [27] Y. J. Lee, D. J. Choi, S.S. Kim, H. L. Lee, H.D. Kim
Surf. Coat. Technol., 177-178 (2004) 415.
- [28] A. K. Costa, S.S. Camargo Jr., C.A. Achete and R.Carius
Thin Solid Films., 243. (2000) 377.
- [29] T. M. Bessman, B. W. Sheldon, T. S. Moss III and M. D. Kaster
J. Am. Ceram Soc., 75 (1992) 2899.

LIST OF FIGURES

1.	Fig. 1.1: Techniques for producing anisotropic carbon fibers	9
2.	Fig. 1.2: Classification of carbon architecture [6]	11
3.	Fig. 1.3: Processing of carbon/carbon composites by RSM and RTM method [6]	15
4.	Fig. 1.4: Processing of carbon/carbon composites [1]	16
5.	Fig. 1.5: Sketch of basic infiltration techniques [12, 13]	18
6.	Fig. 1.6: Description of the densification effect using the coating thickness and amount of porosity [13]	19
7.	Fig. 1.7: Schematic representation of thermal gradient CVD technique [7, 14]	20
8.	Fig. 1.8: Schematic of the FCVI process [7]	21
9.	Fig. 1.9: Schematic comparison of isothermal and thermal gradient CVI [16]	23
10.	Fig. 1.10: Summary of the parameters and responses in CVI processes [12, 17]	24
11.	Fig. 1.11: Anisotropy of the chemical bonds in the graphite lattice causes anisotropic mechanical and physical properties [18].	25
12.	Fig. 1.12: Possible orientations of the matrix structure [18]	27
13.	Fig. 1.13 (a): Plot of weight loss vs. oxidation temperature [21]	31
14.	Fig. 1.13(b): Plot of weight loss rate vs. oxidation time duration [26]	31
15.	Fig. 1.14: Oxidation Arrhenius curve for C/C composites [26]	32
16.	Fig. 2.1: Schematic diagram of the principle of X-ray attenuation tomography	45
17.	Fig. 2.2: Schematic diagram of the various interaction of electron beam with specimen	46

18.	Fig. 2.3: Schematic diagram of a Scanning Electron Microscope.	47
19.	Fig. 2.4: Schematic diagram of a Raman spectrometer.	53
20.	Fig. 2.5: Schematic of SANS instrument at GT-Lab of Dhruva Reactor	55
21.	Fig. 2.6: Schematic for the XPS instrument	58
22.	Fig. 3.1: Flow sheet for the preparation of amorphous carbon/carbon composite starting from carbon black and phenolic resin	63
23.	Fig. 3.2: Indigenously fabricated Impregnator Unit	66
24.	Fig. 3.3: Flowsheet for the preparation of C/C Composite	66
25.	Fig. 3.4: Variation of density in both PAN based carbon fiber and Carbon black samples as a function of their constituents.	69
26.	Fig. 3.5: Open porosity for Carbon Black based samples as a function of their constituents.	69
27.	Fig.3.6: Effect of carbon black and binder amount on the density of the composite	70
28.	Fig. 3.7(a): Effect of impregnation pressure on density	72
29.	Fig. 3.7(b): Effect of time of impregnation on density	72
30.	Fig. 3.8: Degree of graphitization of petroleum coke based samples with heat treatment temperature	75
31.	Fig. 3.9 Effect of time duration and pressure of impregnation on the d_{002} peak	76

32.	Fig. 3.10(a): Optical micrograph of petroleum coke sample treated at 800°C showing micro crystallinity	78
33.	Fig. 3.10(b): Optical micrograph of petroleum coke sample treated at 1500°C showing development of larger crystals	78
34.	Fig. 3.11: Polarized optical micrographs of carbon composites made from (a)20% PAN based carbon fiber, (b) 50% PAN based carbon fiber heat-treated at 1000°C and (c)20% PAN fiber heat-treated at 1500°C.	80
35.	Fig. 3.12 (a): Optical image of the carbon black- resin carbon composite treated at 1000 ⁰ C showing isotropy.	81
36.	Fig. 3.12(b) Optical image of the carbon black- resin carbon composite treated at 1900 ⁰ C showing no development of anisotropy.	81
37.	Fig. 3.13: SEM micrographs of C/C composites prepared using matted PAN fibers	82
38.	Fig. 3.14(a): Reconstructed 3D image of Sample(a)	84
39.	Fig. 3.14 (b): Contrast stretched 3-D image showing individual fibers	84
40.	Fig. 3.15: Crack propagation in the X direction at different Y planes (specified in each image), due to application of pressure (encircled portion)	84
41.	Fig.3.16: Reconstructed 3D image of sample (b)	85
42.	Fig. 3.17: The three images of XY slices at different Z points shows that the sample(b) has much more uniform bonding throughout as compared to sample(a).	85

43.	Fig. 4.1: Variation of coefficient of thermal expansion along (a) parallel and (b) perpendicular directions in PAN based carbon fiber and Carbon Black based samples as a function of their constituents	95
44.	Fig. 4.2: Variation of specific heat in the temperature range of 50 -500°C for both PAN carbon fiber and carbon black based samples as a function of their constituents	96
45.	Fig.4.3: Variation of compressive strength in both PAN carbon fiber and carbon black based samples as function of their constituents	97
46.	Fig. 4.4: Raman spectra of carbon composites made with 0, 5 and 15wt.% of carbon black (CB) along with graphite sample	99
47.	Fig. 4.5: Raman spectra of 15wt.% CB composites before and after impregnation cycles. Inset: corresponding polarized optical micrographs	100
48.	Fig. 4.6(a) and (b): Change in intensity vs. wave number for impregnation carried out at 30 bar pressure and 50 bar pressure respectively	102
49.	Fig. 4.6(c): Change in intensity vs. wave number for impregnation carried out at 70 bar pressure	103
50.	Fig. 4.7: Raman spectra for few representative samples impregnated at 30 bar and 70 bar pressure for varying time duration	104
51.	Fig. 4.8: Variation of D/G ratio with time of impregnation for two sets of representative samples showing greater extent of graphitization at higher pressure.	105
52.	Fig. 4.9: Effect of pressure on structure of the C/C composite	107
53.	Fig. 4.10(a): XPS spectra of sample impregnated at 30bar for 15 h $sp^2/sp^3 = 0.6$	109

54.	Fig. 4.10(b): XPS spectra of sample impregnated at 30bar for 20 h $sp^2/sp^3 = 1.3$	110
55.	Fig. 4.10(c): XPS spectra of sample impregnated at 30bar for 25 h $sp^2/sp^3 = 1.1$	110
55.	Fig. 4.10(d): XPS spectra of sample impregnated at 50bar for 10 h $sp^2/sp^3 = 1$	111
56.	Fig. 4.10(e): XPS spectra of sample impregnated at 50bar for 20 h $sp^2/sp^3 = 1.5$	111
57.	Fig. 4.10(f): XPS spectra of sample impregnated at 70bar for 10 h $sp^2/sp^3 = 1.4$	112
58.	Fig. 4.10(g): XPS spectra of sample impregnated 70bar for 15 h $sp^2/sp^3 = 1.2$	112
59.	Fig. 4.11: Variation of sp^2-C/sp^3-C ratio indicating different extent of graphitization at two different impregnation pressures.	113
60.	Fig. 4.12: Scattering profiles of 1.0cm and 0.5 cm samples.	114
61.	Fig. 4.13: SANS profiles with fit. Inset shows pore size distribution in two samples.	115
62.	Fig. 4.14: SSPs of S2 and S3 with fit. Insets show comparison of their large and small pores size distributions.	117
63.	Fig. 4.15: SAXS profiles of neutron irradiated carbon-carbon composites	119
64.	Fig. 5.1: Crystal lattice defects introduced by fast neutron irradiation [80]	126
65.	Fig. 5.2: Radiation damage in graphite showing the induced crystal dimensional change along a and c direction	127
66.	Fig. 5.3: Stored energy release curves for graphite irradiated at 30°C in Hanford K reactor cooled test channel [74].	128
67.	Fig. 5.4: Photograph of the carbon/carbon composite sample	130

68.	Fig. 5.5 (a) and (b): Change in I_G/I_D for unirradiated and irradiated carbon/carbon composites sample-1 at different fluence levels	134
69.	Fig. 5.5 (c) and(d): Change in I_G/I_D for unirradiated and irradiated carbon/carbon composites sample-1 at different fluence levels	135
70.	Fig. 5.6 (a) and (b): Change in I_G/I_D for unirradiated and irradiated carbon/carbon composites sample-2 at different fluence levels	136
71.	Fig. 5.6 (c) and (d): Change in I_G/I_D for unirradiated and irradiated carbon/carbon composites sample-2 at different fluence levels	137
72.	Fig. 5.7: Crystal structure of graphite	138
73.	Fig. 5.8 (a) and (b): XRD patterns of irradiated carbon/carbon composite sample-1 and sample-2 at different fluences.	139
74.	Fig. 5.9(a) and (b): Stored energy release spectra of carbon/carbon composite sample-1 and sample-2 at different fluence levels.	143
75.	Fig. 6.1: Schematic of the experimental setup for coating using CVD technique	158
76.	Fig. 6.2: XRD pattern of the coatings obtained for various operating conditions as per Table 6.2	161
77.	Fig. 6.3 (a-i): SEM micrographs of the coatings obtained with various processing parameters (a) deposition at $H_2/MTS= 4.66$ (b) deposition at $H_2/MTS=2.33$ (c) deposition at $H_2/MTS=1.16$ (d) deposition at $H_2/MTS= 9.3$ (e) deposition at $H_2/MTS= 4.65$ (f) deposition at $H_2/MTS=2.32$ (g) deposition at $H_2/MTS=14. 0$ (h) deposition at	163

	H ₂ /MTS=7.0 (i) deposition at H ₂ /MTS=3.5	
78.	Fig. 6.4: EDS spectrum of the coating for conditions of deposition at (a) H ₂ /MTS= 7 and (b) deposition at H ₂ /MTS= 4.66	164
79.	Fig. 6.5(a): Effect of variation of MTS feed rate at different hydrogen concentration on the deposition rate	166
80.	Fig. 6.5(b): Plot of ln (no. of moles of MTS) vs. ln of (deposition rate) at different hydrogen concentration.	166
81.	Fig. 6.6(a): Effect of H ₂ content in the diluent gases on deposition rate	168
82.	Fig. 6.6(b): Plot of ln of (no. of moles of hydrogen) vs. ln of (deposition rate) at different MTS flow rate	168
83.	Fig. 6.6 (c): Effect of H ₂ content in the diluent gases on the microstructure of deposit at MTS=1.0 ml/min for (a)60% hydrogen & (b)20% hydrogen	169
84.	Fig. 6.7: Effect of total gas in the diluent gases on microstructure for (a) Total flow at 2 lpm & (b) 4 lpm	172
85.	Fig. 6.7(a): Effect of argon gas on the deposition rate	173
86.	Fig. 6.7(b): Plot of ln of (no of moles of argon) with ln (deposition rate)	173
87.	Fig. 6.7(c): Effect of argon gas on the microstructure at (a) 0% Ar, (b) 40% Ar, (c) 60% Ar, (d) 100% Ar	174
88.	Fig.7.1: Schematic of TRISO coated fuel particle, compact and single fuel bed	182
89.	Fig. 7.2: SEM images of the TRISO coated zirconia particle	183

LIST OF TABLES

1. Table 1.1: Main parameters controlling the bulk properties of all carbon and graphite materials by three parameters: (1) preferred orientation, (2) volume and character of porosity, (3) Degree and type of crystalline disorder. [18]	26
2. Table 1.2: Methods of protection of C/C composites from oxidation	33
3. Table 3.1: Chemical analysis of different carbon samples	67
4. Table 3.2: Bulk density of the petroleum coke based samples with varying binder composition and heat treatment temperature	68
5. Table 3.3: Effect of time duration and pressure of impregnation on density of the sample	73
6. Table 3.4: Effect of Time duration and pressure of impregnation on the d_{002} values (Å)	75
7. Table 4.1: Thermo-mechanical properties of heat treated petroleum coke based samples	92
8. Table 4.2: Characteristics of fiber based samples	92
9. Table 4.3: Variation of density, open porosity and compressive strength of the composite with carbon black and binder composition	94
10. Table.4.4: Variation of I_G/I_D with Pressure at 10 h and 25 h of impregnation	106
11. Table 5.1: Variation of I_G/I_D with irradiation fluence levels	133
12. Table 5.2: Variation of L_c with irradiation	140
13. Table 5.3: Stored energy at different irradiation fluence levels	142
14. Table 6.1: Comparison of commercial available precursors	156
15. Table 6.2: Experimental details of SiC coating by CVD method with varying parameters	159

CHAPTER 1

CHAPTER 1

INTRODUCTION AND LITERATURE SURVEY

1. Introduction

Carbon is a unique solid that can be manipulated to exhibit a broad variety of structures and properties as is seen from the well known allotropes of carbon such as diamond, graphite, carbynes and fullerenes. Each of these allotropes has significant scientific and technological importance. Some modifications of carbon are extremely strong, hard and stiff while other forms are soft. Many carbon materials are highly porous and exhibit a large surface area while others are impervious to liquids and gases. The most abundant allotrope graphite, can exist in many forms with respect to microstructure ranging from amorphous to highly crystalline structure and exhibit a wide range of densities from highly dense 2200 kg/m^3 to highly porous with density 500 kg/m^3 . These types of graphite are called synthetic carbons and in technical terms, engineered carbons. Solid carbons are preferred for structural applications under extreme environmental conditions of temperature or corrosion (liquid as well as gaseous). This is mainly because theoretically carbon materials which have covalently bonded atoms possess very high specific mechanical strengths ($40\text{--}50\text{GPa}$), which is retained even at elevated temperatures over 1500°C . Carbon fibers are a few microns thick, light in weight, very strong and stiff synthetic fibers with long aromatic molecular chains comprising mainly carbon. Carbon fiber reinforced carbon matrix composites or the so called carbon-carbon (C/C) composites are a generic class of synthetic materials consisting of carbon fibers reinforced in a carbon matrix. They possess densities in the range $1600\text{--}2000 \text{ kg/m}^3$, much lower than those of metals and ceramics. They can be classified according to the type of reinforcement used and also

depending on the type of process used for their manufacturing. Some of the most important and useful properties of C/C composites are light weight, high strength at high temperature (3000°C) in non-oxidizing atmospheres, low coefficient of thermal expansion, high thermal conductivity (higher than that of copper and silver), high thermal shock resistance and low recession in high pressure ablation environments. The mechanical strength of C/C composites increases with temperature, in contrast to the strength of metal and ceramics. The main application areas of these are in military, space and aircraft industries which include brake discs, rocket-nozzles etc. They also possess numerous applications in the field of general mechanical engineering. Some of the emerging applications include their use as critical parts in advanced nuclear reactors.

Carbon and carbon-based materials have been used in nuclear reactors and in the recent past there has been a growing interest to develop graphite and carbon based materials for high temperature nuclear and fusion reactors. Efforts are underway to develop carbon materials with high density as well as amorphous isotropic carbon for use in thermal reactors. An amorphous structure is needed in order to avoid accumulation of Wigner energy [1], which is the stored energy in graphite lattice due to dislocation of atoms induced by irradiation. Graphitic carbon due to its excellent neutron scattering properties, continues to be the unanimous choice for the moderator material in high-temperature nuclear reactors [2-4] where the aforesaid drawbacks are essentially overcome due to high-temperature annealing. This amorphous carbon should be isotropic and dense in order to achieve dimensional stability under irradiation.

Carbon is used as moderator and reflector due to its neutron interaction characteristics, heat transfer properties, corrosion resistance, stability under

irradiation, mechanical strength, and low atomic weight with high neutron scattering probability and low capture probability. In addition to these the lower cost and its availability is other attractive feature with carbon. Since graphite as a moderator and as structural material in high temperature reactors is the most favoured choice, it is now felt to develop high density isotropic graphite with suitable coating for safe application of carbon based materials even in oxidizing or water vapour environment.

Graphite in conjunction with other materials is also used in the nuclear industry other than moderator and reflector. Graphite as a moderator and structural material stands as a material of favorable choice particularly for high temperature nuclear reactor. The structural behavior of graphite is a complex function of the source material, manufacturing process, chemical environment, temperature and irradiation history. Under neutron irradiation, graphite undergoes irradiation-induced changes, which are quite important in reactor design and operation. Such property changes in HTR reactors operating in the temperature range of 400 to 1700°C are greatly reduced but it still continues to be a major factor in reactor technology. The radiation causes the displacement of carbon atoms by high-energy neutrons and recoil carbon atoms. These high-energy particles become lodged between carbon layer planes in the graphite and cause a relatively large increase in interlayer distance due to low binding energy of the layer planes. At low temperatures, the graphite expands and at high temperatures it undergoes radiation-induced contraction which is related to the recrystallization phenomena or radiation induced stress annealing.

Wigner Energy: When neutrons having energy of 30 MeV impinges on carbon, 30,000 carbon atoms are released. Hence when carbon based materials are used in nuclear reactors its properties change due to irradiation damage. Thus it is imperative to study in detail the radiation damage of the carbon materials before its use in nuclear

components and the design as a whole. Graphite in particular tends to accumulate or store energy due to lattice displacement, which results due to knock down of carbon atoms by energetic particles such as neutrons or electrons. The stored energy is known as Wigner energy [1]. It may be noted that the binding energy of carbon atom in the graphite lattice is about 7ev. Actually on an average 30ev is required to displace a carbon atom from its equilibrium position. The energy stored for graphite under irradiation at ambient temperature is 2720 J/g which when released adiabatically would cause its temperature to rise to 1300°C. In order to reduce or limit the stored energy it is essential to anneal the irradiated graphite. However, it is noted that stored energy ceases us to be a problem at temperature of irradiation above 300°C.

To avoid the Wigner energy, graphite has to be annealed frequently to remove the stored energy. If the structure is perfectly graphitic, the initial energy of the system is minimum, so it can have lot of possibility to store energy, whereas if the structure itself is highly energetic in the beginning, the chances of more energy storage are less. This is the main reason for the carbon to be non-graphitic in nature if used in low temperature thermal nuclear reactors. In other words, amorphous carbon in place of graphite is an alternate choice in place of graphite. But the research on the development of such materials and irradiation studies are scant.

The irradiated graphitic require high activation energy to overcome the activation barrier to reach at a lower energy state (stable form) and therefore higher temperature is required. The disordered carbon is already at higher energy level and the activation energy barrier is less, as compared to graphite therefore lesser temperature is sufficient to overcome the activation energy barrier. This study deals with the preparation and application of carbon materials on various nuclear reactors

related issues and addresses the current need for focused research on novel carbon materials for future new generation nuclear reactors.

Carbon-carbon composite materials as against conventional graphite materials are now contemplated as the promising materials for the fusion reactor due their ability to have high thermal conductivity and high thermal resistance. The carbon/carbon composites can be tailor made according to the requirement in terms of its application. C/C composites possess a number of properties such as low atomic number, high thermal shock resistance, high sublimation temperature and high thermal conductivity, which makes it a good choice in the fusion reactors. C/C components materials may be the choice for the next generation Tokamak fusion reactors such as International Thermonuclear Experimental Reactor (ITER) which must endure severe environment including high-heat fluxes, high armor, surface temperature and eddy-current induced stresses during plasma disruption. The plasma-facing carbon-carbon composite materials are likely to suffer structure and property degradation as a result of carbon atom displacements and crystal lattice damage, caused by impinging high-energy fusion neutrons and energetic helium ions for carbon transmutations.

As C/C composites are infinitely variable family of materials, the processing and design variables such as; (a) architecture, i.e., 1D, 2D, 3D or random fiber distribution; (b) fiber precursor, i.e., pitch, polyacrylonitrile (PAN) or vapour grown; (c) matrix, i.e., liquid impregnation (pitch or resin) or CVI and (d) final graphitization temperature will influence the properties and behavior of C-C composites. Burchell et al. [5] irradiated 1D, 2D, and 3D C-C composites at 600°C to damage doses up to 1.5dpa. 3D C/C composites were shown to have more isotropic dimensional changes than that of 1D or 2D composites. Pitch fiber composites were shown to be more

dimensionally stable than PAN fiber composites and high graphitization temperatures were found to be beneficial.

The main objective of this investigation is to fabricate carbon-carbon composites followed by densification impregnation method and to characterize the final microstructure. Thermo-physical properties of the carbon composite like density, co-efficient of thermal expansion have been evaluated. Scanning Electron Microscope imaging (SEM), X-ray Diffraction (XRD), Raman spectroscopy and X-ray tomography studies of the carbon composites have also been carried out as an attempt to study the effect of different processing parameters like impregnation time duration, pressure, number of cycles of impregnation on the final product.

This chapter deals with the various aspects of carbon-carbon composites, the various processing techniques of carbon-carbon composites are reviewed with their characteristics to gain a comprehensive understanding. It starts from the description of their manufacturing techniques and proceeds to explain the effect of various parameters on final properties exhibited. The microstructure and its role in governing the desired properties are discussed to establish a correlation between the two.

1.1. Carbon-carbon composites

These are a generic class of synthetic, pure carbon materials consisting of carbon fibers reinforced in a carbon matrix. Their characteristic properties for example light weight, high thermal shock resistance; low coefficient of thermal expansion, strength retention at higher temperatures, high impact resistance, high stiffness etc. made them initially a preferred material for space shuttle program. The quest for high temperature structural material for selected critical components of advanced air force exit and re-entry systems provided the impetus for research, on

these materials includes improvements in properties of the constituent materials, i.e., carbon fibers and carbon matrix precursors and design allowables. These properties were attained by an intelligent combination of two different constituents. The reinforcement is used in the form of fibers that possess a very high modulus. The matrix serves to protect the fibers from damage due to the environment and also it plays a very important role of stress transfer, which helps in attaining excellent properties finally. Each constituent is described below in the following sections:

1.1.1. Carbon fibers

They are generally classified based on the type of precursor used for their manufacture and also based on the final properties they attain. Among the various precursors only three precursor namely–rayon, polyacrylonitrile(PAN) and pitch are considered for commercial processes. Although rayon was used to produce carbon fiber–reinforced composite, the carbon fibers used for the advanced composites are made using PAN and pitch precursors. The schematic of the three commercial routes for preparing carbon fibers is shown in Fig. 1.1.

a) PAN based fibers

PAN has proven to be the most suitable precursor for developing the carbon structure for high strength fibers. Their synthesis starts with the PAN precursor which is a linear polymer containing 68% carbon. Subsequently a controlled transformation to carbon fiber is affected through a series of heat treatment steps in different environments at progressively increasing temperatures.

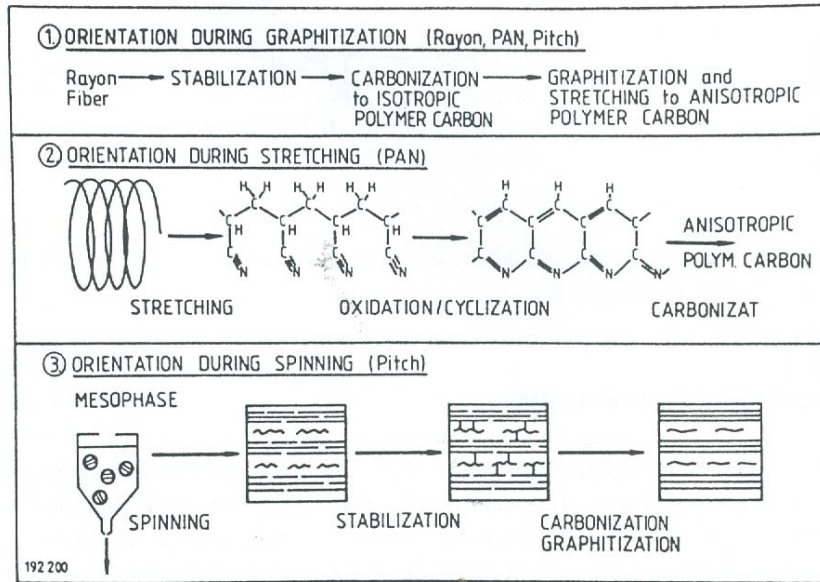


Fig. 1.1: Techniques for producing anisotropic carbon fibers

The basic process involves three steps: preoxidation or stabilization (heating in air at temperature range of 200-230°C), followed by carbonization (heat treatment in an inert atmosphere at temperature of 1000°C to 1500°C), and final high temperature thermal treatment (approximately 2000-3000°C in an inert atmosphere). These steps develop high strengths because of the final morphology of the fiber which is a direct consequence of the various chemical reactions that take place during the fabrication.

b) Pitch based fibers

These are again of two kinds depending on the initial precursor which may be isotropic or anisotropic. While the isotropic carbon fibers have very low strength and moduli, thus are of no value for advanced composites, they can be used in insulation felts and as fillers for concrete. For carbon fiber to develop a high modulus, it is critical that the preferred orientation of the polyaromatic layers is parallel to the fiber

axis. The preferred orientation can be achieved in rayon-based and isotropic pitch based carbon fibers by cumbersome and costly high temperature stretching process.

In PAN based carbon fiber process the preferred molecular orientation parallel to the fiber axis is developed by first stretching the molecules of the polymeric precursor fiber and subsequent heat treatment. This can be developed in carbon fibers during melt spinning after which they are subjected to heat treatments in tandem in varying environments and at different temperatures which are generally meant to retain the developed structure and also to get rid of the hetero-elements present in the initial precursor. Their densities are generally 10-15% higher than that of PAN fibers. In addition, their electrical and thermal conductivities are higher because of a high degree of orientation [6, 7].

Once the type of fibers is selected depending on the end application the next crucial job would be the fabrication of a suitable preform that forms the starting material for manufacturing the composite. This may also be referred as fiber architecture. It not only imparts rigidity to the composite, but also in combination with fiber properties it determines the properties of the composite. All known types of carbon fibers are used in different types of architecture as highlighted in the Fig 1.2.

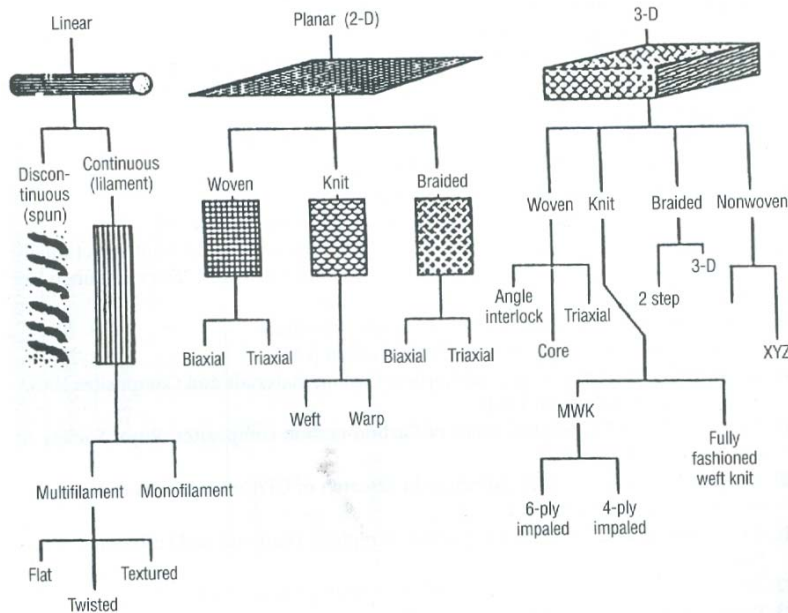


Fig. 1.2: Classification of carbon architecture [6]

1.1.2. Matrix

In carbon/carbon composites, the matrix is also made up of pure carbon. It can be developed from various precursors, which intrinsically possess some specific characteristics that determine the final properties. Hence matrix precursor should also be decided depending on final application. The various sources of matrix precursors are:

- Pure hydrocarbons
- Oxygen containing hydrocarbons
- Nitrogen containing hydrocarbons
- Sulphur- and halogen-containing compounds

1.2. Conventional processing of carbon/carbon composites

From the thermodynamic equilibrium phase diagram of graphite, it is observed that carbon or the equilibrium phase graphite melts only under conditions of high

temperature and pressure. Hence chemical methods of fabrication, such as melting or sintering cannot be applied for the fabrication of carbon products. The fabrication methods employing filler and binder phases used for fabrication of carbon products are similar to the ceramic process. They differ from the ceramic sintering in that the strong covalent bonding between the carbon atoms does not allow the movement of atoms at high temperatures and hence thermal sintering is not achievable in carbon particles. Instead carbon particles are combined with a temporary binder, which then acts as precursor for the secondary carbon formed during the baking (carbonization). This results in all carbon materials with two different phases, the primary carbon as filler carbon and secondary carbon as binder carbon. The principle routes of manufacturing make use of carbonizable compounds initially. Carbon-carbon composites can also be manufactured by using different techniques which are broadly the three methods of manufacturing C/C composites [8, 9], (a) Chemical vapour deposition (CVD), (b) Pyrolysis of thermoset or thermoplastic resins and (c) Pyrolysis of hydrocarbon pitches obtained from petroleum coal tar, synthetic mesophase pitch.

Carbon-carbon composites are generally highly porous after first step of production. They consist of primary carbons only a small part of the binder bridges constituting the secondary carbon. The subsequent process of densification is achieved by impregnation with carbonaceous precursor such as liquid or gases followed by carbonization.

Densification may be achieved by two different impregnation routes, gas phase impregnation or liquid impregnation. The most economical liquid impregnation method has gained importance for carbon/carbon composite. This process involves vacuum or pressure impregnation of porous solid with carbon yielding liquid precursor, thereby the impregnant liquid has access to the inner fine pore. This can be

used to make composites with complex structures. Composites with much higher densities can be prepared by a combination of liquid infiltration and CVI as the small pores resulting from multiple impregnations can be filled. The ultimate properties of the C/C composites are dependent on the structure and properties of the carbon matrix which in turn is controlled by their precursors. Therefore the selection of precursor for matrix is extremely important. It should give high carbon yield i.e. low weight loss during carbonization, the precursor should have low viscosity to enter into the fine pores and control on wetting of fibers should give favorable microstructure on carbonization. The precursors used for impregnation can be classified in two categories, i. e. the thermosetting resin and thermoplastic pitches.

Thermosetting resins

Thermosetting resins commercially have been used for long time as impregnants for wide range of applications due to its availability in liquid state with moderate viscosity at room temperature. They polymerise into highly cross-linked non melting solid at temperature of 200°C. The carbon yield is determined by the carbon content of the precursor and the extent to which the volatile carbon containing species are released during carbonization. Polyfurfuryl alcohol and phenolics have been used as binders and impregnants in the carbon industries for a long time. These resins polymerise at 150-250°C to give highly polymerized cross-linked non melting solids which undergoes solid state pyrolysis and hence well contained in the filler particle. During pyrolysis of the resins, condensation, oxidation, dehydration and decomposition reactions occur simultaneously or sequentially. The weight loss of the polymer is during pyrolysis is accompanied by volume shrinkage. The matrix shrinkage during pyrolysis has a dominating effect on the microstructure and

performance of the carbon-carbon composites. Excessive shrinkage during carbonization generates stresses at the fiber/matrix interface and often results in matrix cracks and fiber damage.

Pitches

They are the essential constituent of 80% of carbon products. They are used both as binder and for impregnation and densification. The attractive characteristics of pitches are its high carbon yield, low cost and graphitizability and its controllable viscosity. Pitches are classified based on their origin such as, coal tar pitch, petroleum pitch and synthetic pitch. The coal tar pitch is obtained from the coal tar by distillation and heat treatment. The petroleum pitches is obtained from the residues at the bottom of catalytic crackers of naphtha, crude oil distillation or refineries. The carbonization of pitches consists of aromatic growth and polymerization to two dimensional order of graphite. Pitch is as matrix precursor for advanced carbon-carbon composite due to its high coke yield. The yield depends on the composition of the precursor and the pyrolysis conditions. Chemically modified pitches mostly lead to isotropic carbons.

1.3. Liquid impregnation route

The two methods of manufacturing C/C composites from thermoset resin are shown in Fig.1.3. The first one is the conventional or solvated resin method whereas the second is the resin transfer molding (RTM) method. In both the process the steps involved are (a) Fabrication of a rigid prepreg/preform (green or as cured), (b) carbonization of the preform and (c) densification. The first two steps are common to both the methods. The resin solution method is used for materials like phenolic resin commonly used in the industries.

RESIN SOLUTION METHOD

RTM METHOD

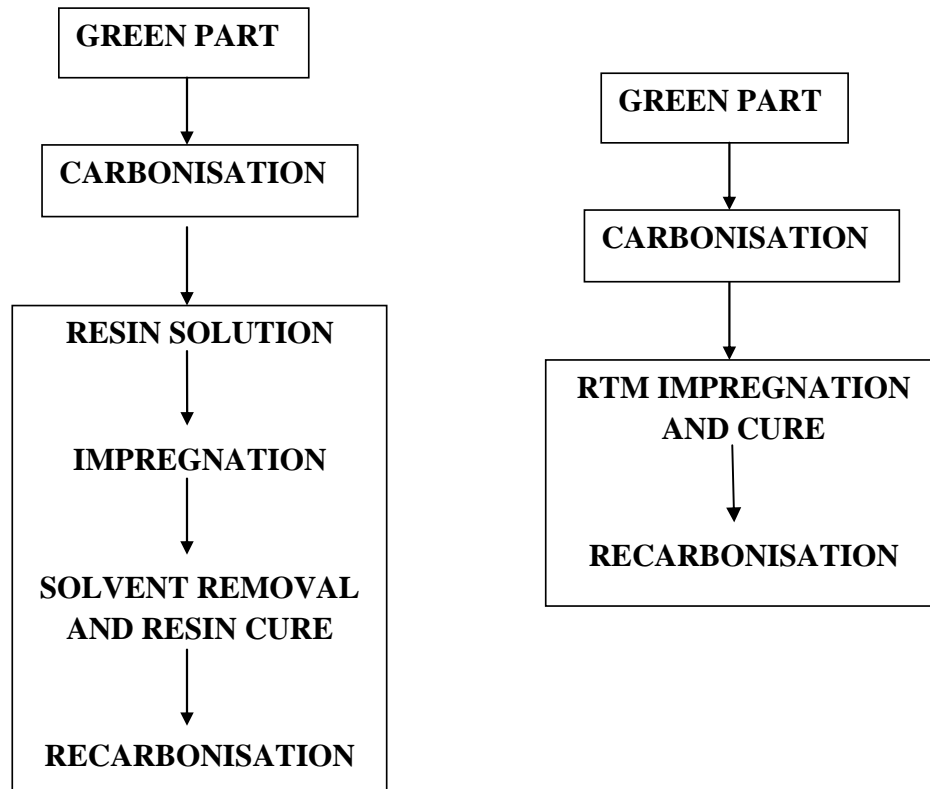


Fig. 1.3: Processing of carbon/carbon composites by RSM and RTM method [6]

The resin transfer molding (RTM) process was developed in the late seventies by French Commission for Atomic Energy [10]. The RTM process consists of immersing the porous substrate to be densified into a liquid hydrocarbon which acts as the matrix precursor. The preform is heated to a temperature higher than the cracking temperature of the hydrocarbon which is in contact with the hot substrate, which is vaporized and cracked to give the carbon deposit. Though the pyrolytic carbon (PyC) is obtained from gaseous phase it cannot be classified as CVD process because of direct contact between substrate and precursor. The process has been classified as liquid–vapour phase densification.

Fabrication method of C/C composites involves fabrication of 3D (three directionally reinforced) or MD porous carbon fiber preforms having the desired shape or a porous carbon-carbon skeleton (UD, 2D or 3D). The schematic in the Fig 1.4 outlines the possible processing routes of carbon/carbon composites. The solid-state pyrolysis involves heat treatments like carbonization to get rid of the hetero-elements and also to improve the carbon yield. After that they are subjected to graphitization to achieve desired properties by organization of the microstructure. The main drawback in the conventional processes is the differential shrinkage of matrix and fiber during carbonization which damages the fibers. Differential shrinkage also leads to the formation of closed porosity which in turn reduces the final density of the composite [11]. In order to avoid this, the impregnation needs to be repeated 5 to 6 times after which the final density reaches a constant value.

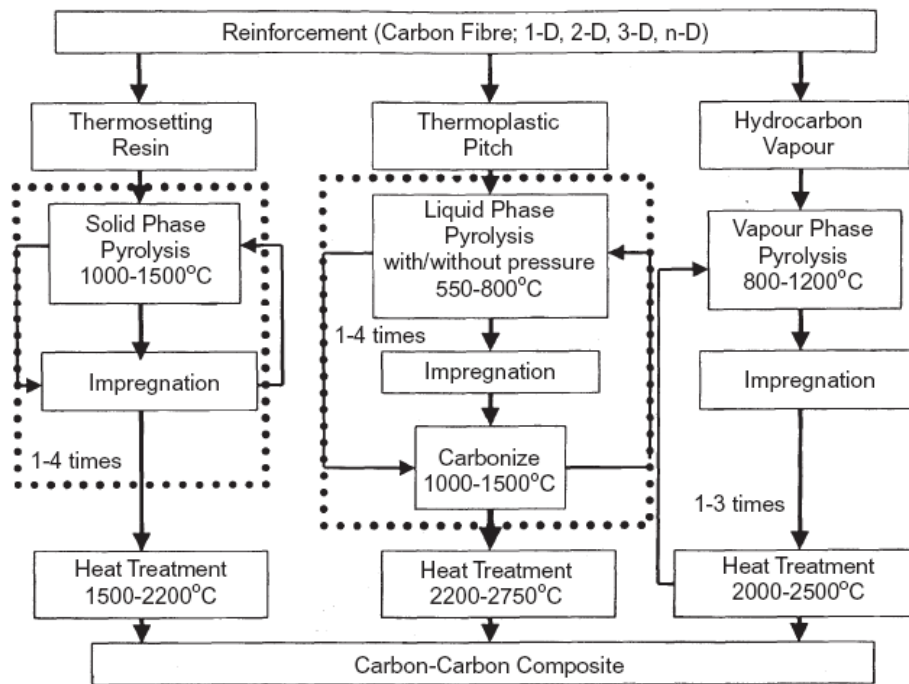


Fig. 1.4: Processing of carbon/carbon composites [1]

In order to avoid the drawbacks of liquid impregnation method a novel method of gas phase impregnation has been developed which will be discussed in great detail in the next section.

1.4. Gas impregnation route

The chemical vapour deposition (CVD) process uses hydrocarbon compounds such as methane, ethane, propane and benzene as precursors for carbon. Thermal degradation is achieved on hot surfaces of the substrate, resulting in a pyrolytic carbon deposit and volatile byproducts, which mainly consists of hydrogen. The process of fabricating carbon/carbon composites through this route is in fact, analogous to the technique applied to densify highly porous skeleton, i.e. so-called CVI. In this case porous skeleton is replaced by carbon fiber woven preform. Therefore this process is used for densification of preforms alone or rigidized carbon structures. In this process, the feed gas undergoes a series of various vapour phase interactions as it diffuses into the preform, forming intermediate species which further react to deposit carbon on all heated surfaces in the vicinity of the gas. From all the experimental studies a general trend has been outlined to provide an overall reaction model which considers two classes of reactions [12].

1.4.1. Isothermal Chemical Vapour Infiltration (ICVI)

In this process, a woven preform called substrate is placed inside the susceptor of an induction furnace and hydrocarbon gases are introduced into the susceptor to allow infiltration into the substrate. The substrate and the gas are maintained at a uniform temperature, which is around 1050-1100°C, and reduced pressures, with the

flow rate of hydrocarbon gas predetermined depending on the substrate surface area [13].

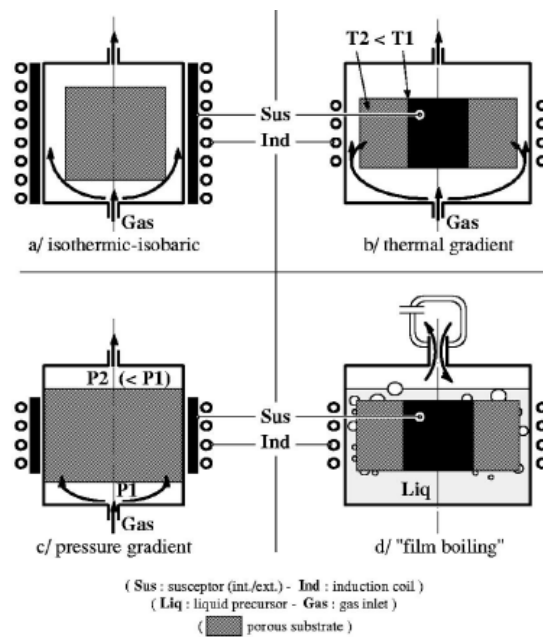


Fig. 1.5: Sketch of basic infiltration techniques [12, 13]

As the cracking gas enters deep into the preform, its concentration becomes less because of deposition at the surface resulting in gradient within, which in turn is the driving force for the hydrocarbon gas to diffuse inside the substrate. As a consequence of this, a density gradient is also established which is a function of the distance from the outer surface, depending on the geometry of the furnace. In the composites fabricated by this method, the density of the composites with varying geometry was different although they are processed under similar conditions. Therefore, in order to achieve higher density the process has to be operated at lower temperatures which consequently increase the processing times. Moreover a crust also forms on the surface that must be machined away in between the infiltration cycles to achieve more infiltration and high ultimate density of the composites. Its main advantage is precise parameter control, in particular for large furnaces where a large

number of specimens can be densified together. The drawbacks include long processing times with very slow rate of carbon deposition associated with very low overall precursor efficiency. Fig. 1.6 shows the change in coating thickness and porosity at different locations along the radial cross-section after infiltration. The uniformity in the densification process can be seen from the slope of the curves in it. Coating on the adjacent fibers overlap and finally pyrolytic carbon becomes the continuous phase. It can be noticed that the deposition at the centre is very small even after very long time during which the outer surface of the preform gets very dense. The effects of the fiber content in the initial preform and dimensionality of the reinforcement on the densification behaviour is discussed in the subsequent sections.

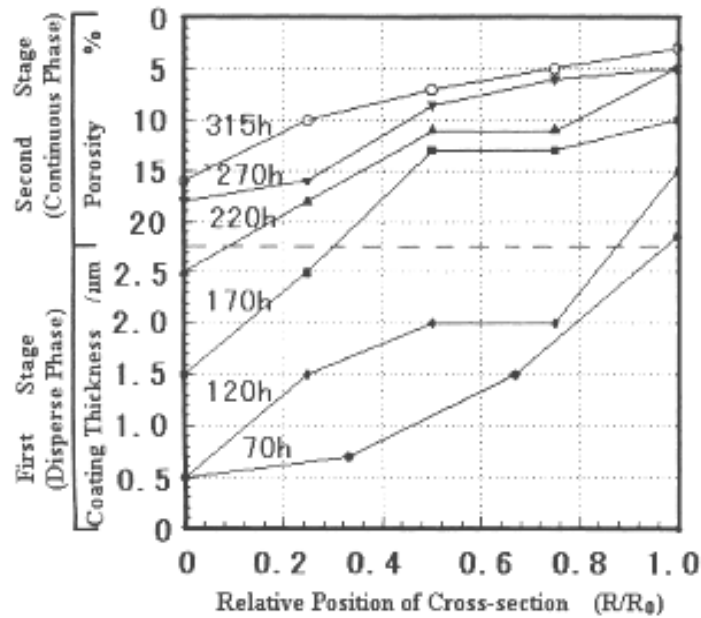


Fig. 1.6: Description of the densification effect using the coating thickness and amount of porosity [13]

1.4.2. Thermal gradient Chemical Vapour Infiltration Process

This method comprises of maintaining a temperature gradient through the substrate thickness. The outer surface of the substrate, i.e., the entry point of the gas is at a lower temperature than the innermost surface. This is achieved by keeping the woven preform over a graphite mandrel which is inductively heated. The mandrel and the induction coil need to be tailored according to the substrate. The surface near the mandrel is at a very high temperature in the order of 1300-1400°C. Therefore the deposition starts at the surface near the mandrel. The densified region exhibits a better thermal conductivity and results in the migration of the hot zone through the thickness. Therefore the densification progresses through the substrate towards the colder surface. The gas velocity is faster compared to the previous process and formation of crust on the outer surface is avoided here. This is useful for relatively thin structures and is limited to a single item per furnace. Large cross sections can cause turbulence and uncertain gas phase pyrolysis. The schematic representation of the process is shown below in Fig 1.7.

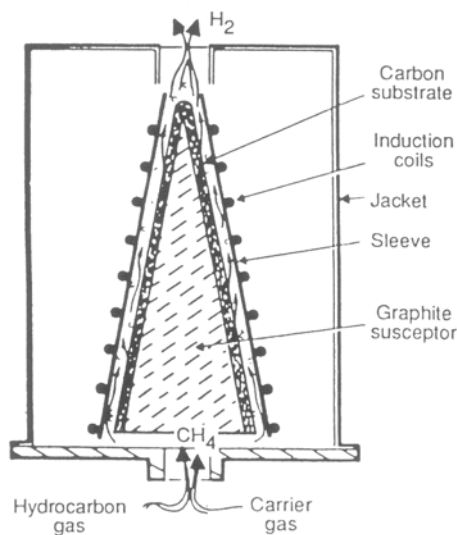


Fig. 1.7: Schematic representation of thermal gradient CVD technique [7, 14]

1.4.3. Differential pressure process

This is a modification of the isothermal technique. In this technique the substrate is heated to a constant temperature while the gas is fed into the middle of the substrate under positive pressure with respect to the furnace chamber. A pressure difference is thus created between the centre and the outer walls of the substrate and gas is forced to flow through the complete substrate. This process has limited applications. Depletion of reagent while flowing through the preform results in non-uniform densification and plugging of the flow path at the surface where the reagent first contacted the preform.

1.4.4. Forced flow-thermal gradient CVI (FCVI)

This method incorporates the advantages of both the forced flow of the reagent and the thermal gradient across the preform. It was found to be very effective in rapid fabricating of SiC/SiC composites [15]. This process was also applied for carbon/carbon composite manufacturing using propylene, propane or methane. Fig 1.8 depicts a schematic of the FCVI process

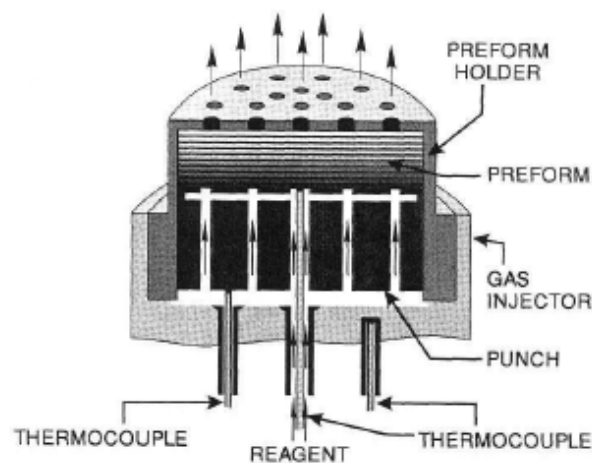


Fig. 1.8: Schematic of the FCVI process [7]

The height of the preform holder affects the temperature and the temperature gradient across the preform. The temperature difference between the hot and the cold side of the preform for the holder will be around 150°C. The temperature gradient is established by keeping the bottom of the preform cool by the water cooled gas injector and the top of the preform heated by the furnace. The pressure gradient forces the gas through the preform. As the infiltration progresses, reduction in porosity will cause an increase in the back-pressure. The runs will be typically terminated once the back-pressure reaches a practical value for a standardized gas flow rate of propane and of hydrogen. The temperatures of the preform top and bottom are monitored using K-type thermocouples during the infiltration. With this method fabrication of the carbon/carbon composites with a matrix of uniformly high thermal conductivity infiltrated onto conventional sized fibers is realized in a few hours under controlled parameters. In the work reported in literature [15], it was inferred that the three variables namely temperature of the bottom of the preform, hydrocarbon concentration and flow rate, affected the infiltration time and the deposition rate. Uniform density was achieved at low concentrations of hydrocarbons.

1.4.5. Film boiling CVI (Kalamazoo)

New routes to develop rapid infiltration techniques have been explored in particular the thermal gradient one, coupled to an in-situ vaporized liquid precursor. This process known as ‘Kalamazoo’ is presently in a pre-industrial state [16]. The Fig. 1.9 shows the schematic comparison of the isothermal and thermal gradient CVI processes. As compared to the isothermal process, a mobile densification front is created by a strong thermal gradient, inside the porous preform. The mass and heat fluxes being opposite inside the sample, the precursor is pyrolysed at the very place

needed. Subsequently, a high rate of mass deposition is observed which is about one or two orders of magnitude larger than in classical isothermal CVI.

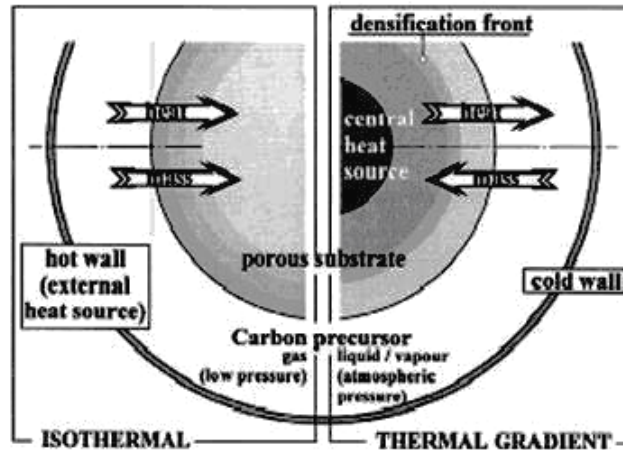
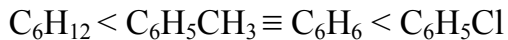


Fig. 1.9: Schematic comparison of isothermal and thermal gradient CVI [16]

The rapid densification process consists of immersing the porous substrate directly into a liquid hydrocarbon. In a pilot reactor the heater is an axial graphite susceptor inductively heated, the preform being wrapped around it. The key parameters are the resistor temperature T which is to be maintained at $1000-1300^{\circ}\text{C}$ and the selected precursor which in this particular reference was cyclohexane. By comparison of the efficiency associated to each precursor the infiltration rates can be classified as:



This confirms the influence of the precursor nature; both aromacity and the presence of halogen increase the efficiency and the yield that is quite high as compared to the isothermal CVI.

The infiltration process is dependent on two kinds of parameters, which are the easiest to handle i.e. the process conditions such as: (a) Temperature of the preform, (b) Total pressure, (c) Precursor concentration and (d) Gas velocity and the microstructural properties of the starting preform such as: preform permeability, preform porosity, average pore size and pore distribution, preform thickness, specific surface area available for deposition. The summary of the parameters and the responses in CVI process is given in the Fig. 1.10.

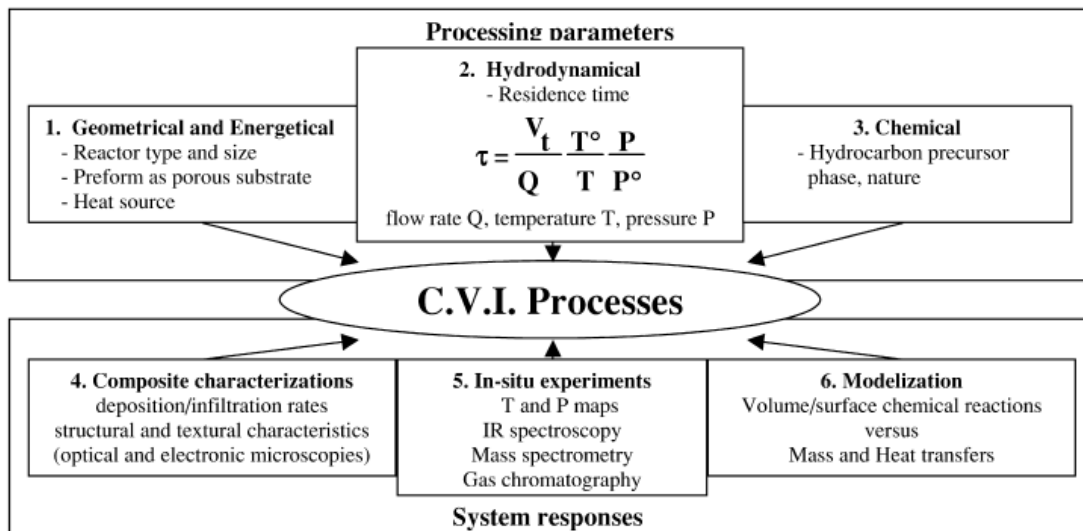


Fig. 1.10: Summary of the parameters and responses in CVI processes [12, 17]

1.5. Mechanical properties

All types of polygranular carbon and graphite materials take advantage of the extremely high strength of σ -bonds in elemental carbon, which also accounts for the low thermal expansion along ‘*a*’ and ‘*b*’ directions in graphite, and a high proportion of the phonon part of the thermal conductivity. This combination of physical properties has made possible the application of carbon and graphite materials at high

temperatures and under severe thermal shock conditions [18]. The availability of graphite fibers has become the key to a nearly quantitative use of the σ -bond strength in bulk carbon and graphite materials. With such fibers, components for load carrying systems are available which promise much better utilization of the chemical bond strength of elemental carbon. The bonding force acting between two neighbouring atoms can be directly demonstrated as a function of interatomic separation.

The same can be done for the potential energy of the atoms. As shown in Fig.1.11 the curves resulting from attraction and repulsion give directly the interatomic distance ' d ' for the ' a ' and ' c ' directions. Since the macroscopic elastic strain results from a change in inter atomic spacing in a given direction, the Young's modulus is proportional to the curvature of the potential curve at d_o .

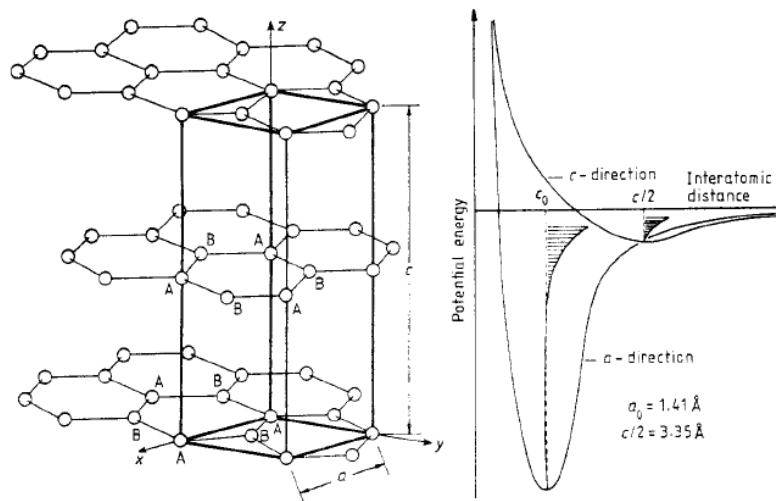


Fig. 1.11: Anisotropy of the chemical bonds in the graphite lattice causes anisotropic mechanical and physical properties [18]

Thermal expansion can be determined directly from this curve by its degree of asymmetry. The differences between both curves are consistent with the known high anisotropy of Young's modulus, strength and thermal properties of carbon in both directions. The Table 1.1 summarizes the three main parameters to control the effect

of the chemical bonds between the carbon atoms on bulk properties namely preferred orientation, volume and character of porosity and amount and type of crystalline order.

Table 1.1: Main parameters controlling the bulk properties of all carbon and graphite materials by three parameters: (1) preferred orientation, (2) volume and character of porosity, (3) Degree and type of crystalline disorder. [18]

	Monolithic carbon			Heterogeneous carbon		
	Glass-like	Pyrolytic	C-fibre	C/C composite	Polygranular carbon	
					Ultra fine grained type	Coarse grained needle type
Preferred orientation	Minimum Not variable	Maximum planar Can be partly modified	Maximum cylindrical Can be partly modified	Variable up to maximum	Minimum Nearly isotropic	Limited preferred orientation by grain structure
Porosity (all types of voids exceeding lattice defects (> 1 nm))	Minimum only micropores				Not avoidable, but variable in volume and pore characteristic	
Crystalline disorder (defect concentration)	Maximum Only 2-dimensional Not variable	Minimum obtainable Variable by deposition parameters and HT	Medium mainly 2-dimensional order Limited variability by HT		Low disorder possible Variable by raw material and HT	

A significant contribution of the matrix to the modulus of the composite can only be expected in the case of a suitable preferred orientation of the matrix C layers as shown below in the Fig.1.12

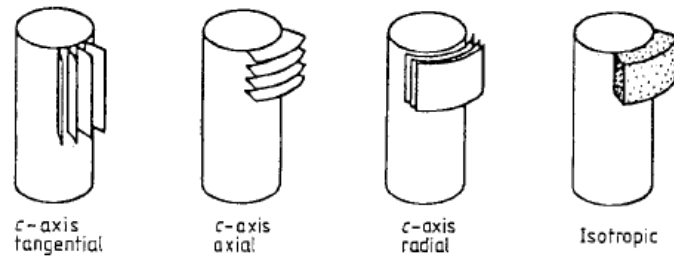


Fig. 1.12: Possible orientations of the matrix structure [18]

The condition of the carbon fiber surface is of great importance in determining the mechanical properties of a carbon/carbon (C/C) composite. The presence of functional groups on the fiber surface and roughness of the surface control to a great extent the tensile strength, fracture toughness and interlaminar shear strength [19]. An optimization has to be made between a weak interfacial bond which improves fracture toughness by the debonding and fiber pull-out mechanism, but results in a low tensile strength and a strong interfacial bonding which leads to a catastrophic failure.

Thus fiber-matrix interactions have to be studied in order to determine the correlation between the conditions of the carbon fiber surface and the mechanical properties of C/C composites. The critical mechanical properties for design are tensile, compression, shear, bearing and transverse tensile strength. The flexural properties of C/C composite are required to determine the deformation of these composites under stress. A good chemical bonding between the fiber and matrix in C/C composite, results in a poor flexural strength. Strong chemical fiber-matrix interactions can cause a large tensile stress to be developed during the cooling process of the fabrication. This may result in the transverse cracks in the matrix, which can propagate through the fiber upon tensile loading and cause the matrix to crack.

In addition, a strong chemical interfacial bonding provides no debonding mechanism which is necessary to increase fracture toughness. On the other hand, a

poor interfacial bonding allows a relatively free thermal deformation to occur in the matrix, so the fiber breakage occurs only when the tensile strength of the fibers is exceeded. The strength of such composites will depend on statistical distribution of fiber breakage. A weak interfacial bond will also lead to a crack deflection at the fiber matrix interface and/or fiber pullout resulting in an increased fracture toughness of C/C composite. If the interfacial bonding is in the right range, crack will deflect at the interface and toughness and strength will be achieved. Future structural applications of C/C composites will require an improvement in the translation of mechanical properties of carbon fibers into C/C composite [19]. This can be only accomplished in three ways

- (a) An optimum bonding between the fibers and the matrix.
- (b) No bonding but a large compressive stress is exerted by the matrix on the fibers. The compressive stress exerted by the matrix on the fibers results in a higher interfacial bonding between the fiber and matrix, resulting in a smaller amount of the fiber pull-out. This improved bonding will result in a better load transfer between the fiber and matrix leading to synergetic mechanism of the matrix and improved tensile, flexure and interlaminar shear strength value.
- (c) A large coefficient of friction between the fiber and the matrix. Since a strong chemical bonding is detrimental to the mechanical properties of C/C composites, weak chemical bonding and/or mechanical bonding should be used.

Failure behavior of C/C composites prepared by the CVD technique is unique among such composites because the pyrolytic carbon matrix is highly anisotropic [20]. In C/C composites, there are not only fiber/matrix (F/M) interfaces but also planes of circumferential microcracks parallel to the fibers in front of the advancing

crack. Therefore, the propagation path of the crack can deviate along the planes of circumferential microcracks as well as at F/M interfaces. These circumferential microcracks, which are likely to behave as “new interfaces,” interrupt the path of the cracks advancing through the matrix, and hence relax the stress concentration within the composites. The number of microcracks is controlled by varying the cooling rate of the composites from the deposition temperature. On rapid cooling, a large number of microcracks may be initiated instantaneously because of the need for rapid accommodation of the residual thermal stresses. The microcracks do not grow to large sizes since almost all the stresses can be removed only by such crack formation. On slow cooling, however, the limited number of microcracks initiated at the beginning of cooling relaxes the stresses by further propagation or by being linked together on continued cooling, resulting in more opening and more extension around the fiber.

The influence of microcracks on C/C composite properties is thought to also depend on the fiber orientation within the substrate. Since the axes of all the fibers and thus the planes of microcracks are oriented perpendicular to the advancing crack plane in composites using a carbon cloth substrate, the microcracks are always expected to increase the composite properties as described previously.

In the case of a carbon felt substrate, however, fibers have a quasi-random array and the microcrack planes that may be formed in a smooth laminar structure meet the advancing crack plane at various angles. Therefore, the microcracks perpendicular to the crack have an advantage of improving the properties whereas those parallel to it serve as a rapid path of crack propagation.

1.6. Oxidation behavior and protection

Graphite and carbon fibre reinforced carbon composites are candidate materials for high temperature applications due to their superior properties [21-25] such as high sublimation temperature combined with high resistance against cyclic thermal stress, superior specific tensile strength up to 2000 °C. In order to make use of the advantage of these properties from an environment ranging from vacuum to inert gases to an oxidizing atmosphere, these materials should be protected by an oxidation resistant material. Although these materials possess excellent properties, they are prone to oxidation at high temperatures as normal carbon materials when exposed to oxidizing atmospheres. Their oxidation behavior also depends on the type of structure developed during the process of fabrication [26].

The accompanying Fig.1.13(a & b) depicts the relationship of weight loss with oxidation temperature and time respectively. From the apparent calculations of the activation energy, an understanding can be obtained on the possible mechanisms of oxidation existing in those particular regimes. One such example is shown in the Fig.1.14. Generally at lower temperatures, the oxidation rates are controlled by the surface reaction of the oxygen with active sites on the surfaces of the specimens, while at higher temperatures they are not only controlled by surface reaction but also by the diffusion of oxygen through the boundary layer on the surface of the composites into the pores. Initially oxidation commences from pores on the surfaces produced during preparation of the specimens. Once oxidation starts, these pores progressively become larger and new pores arise as oxidation proceeds.

Since the microcracks not only exist between carbon fibers and CVI carbon, but also among ring-like CVI carbon, owing to the effect of reactive edge sites present in the carbon fiber and the matrix carbon, both are oxidized simultaneously. In the

process of oxidation, the carbon fibers appear to become thinner, and the CVI carbon becomes more flimsy.

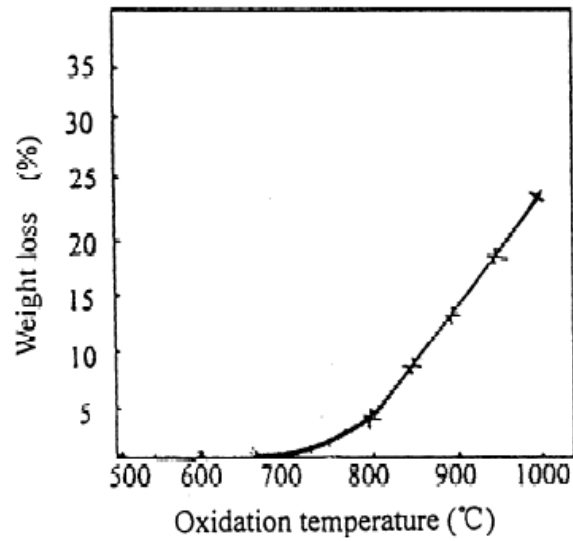


Fig. 1.13(a): Plot of weight loss vs. oxidation temperature [21]

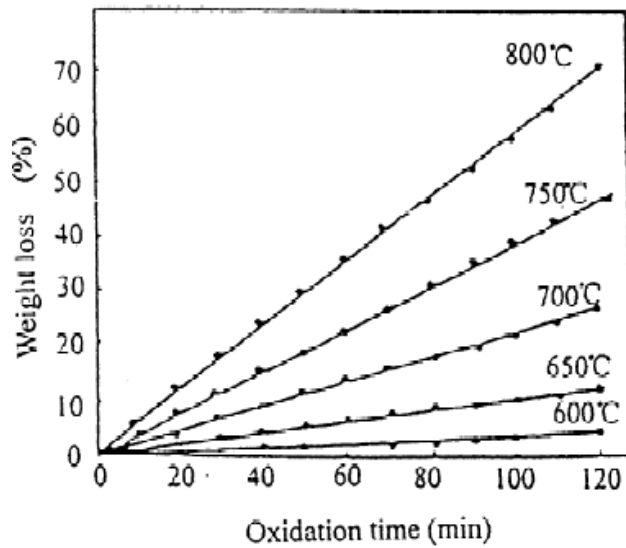


Fig. 1.13(b): Plot of weight loss rate vs. oxidation time duration [26]

Also, at very high burn-off rates, carbon fibers are more prone to oxidation than the matrix carbon, this results from differences between the fibers and the matrix either in microstructural order and preferred orientation or in impurities.

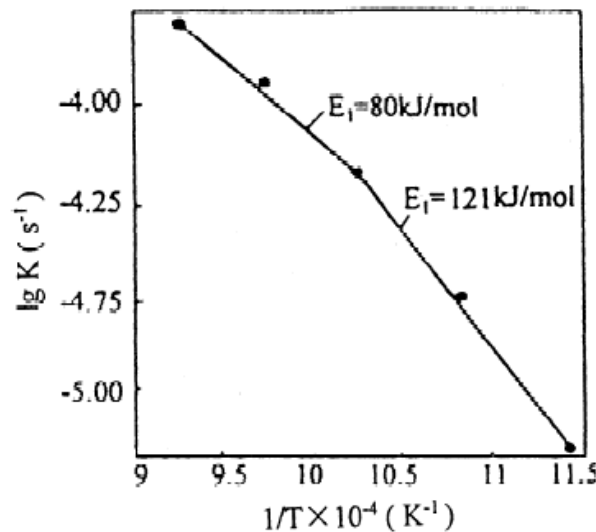


Fig. 1.14 Oxidation Arrhenius curve for C/C composites [26]

Various approaches which have been described in the open literature for protection of carbon/carbon composites are summarized in Table 1.2. These can be grouped into two categories: (a) inhibitors and sealants to block the active sites and slow down the oxidation rate and (b) diffusion barriers consisting of coatings and overcoats to prevent oxygen ingress and carbon egress [27]. Often the protection systems used are complementary and are dictated by the end application of the composite.

These coatings are applied to the substrate by pack cementation, CVD, vapour phase deposition, plasma spray, electro-deposition etc. Most of the works referred in literature are based on pack cementation and the CVD processes since these produce material in the purest form. As is evident from the available thermal expansion data

silicon based ceramics become the unanimous choice for their best thermal compatibility with the C/C composites and exhibit lower oxidation rate among the high temperature ceramics. One of the principal limiting factors for its success is the formation of crack patterns in the SiC coating.

Table 1.2: Methods of protection of C/C composites from oxidation

Inhibitors and sealants	Barrier coatings and overcoats
Halogens	Noble metals
Phosphorus compounds	Borides
Boron compounds	Carbides/nitrides
Polysiloxanes	Silicides
Silicon	Intermetallic compounds
Borate and silicate glasses	Engel/beewer compounds

SiC is a material with high temperature oxidation resistance along with good thermal shock properties and stability against high temperature corrosion [28, 29]. This makes it an oxidation resistant material. SiC coating has the combination of unique physicochemical and mechanical properties such as high strength, extreme hardness as well as excellent resistance to wear oxidation and corrosion [30-32]. This makes it a preferred material for high temperature applications such as in structural material in high temperature reactors.

SiC coating can be obtained by several methods such as cementation packing [33] chemical vapor deposition CVD [34-37] laser induced chemical decomposition (LICD) [38] plasma spray, electro-deposition etc. Most of the works referred in

literature are based on pack cementation and the CVD processes since these produce material in the purest form. As is evident from the available thermal expansion data silicon based ceramics become the unanimous choice for their best thermal compatibility with the C/C composites and exhibit lower oxidation rate among the high temperature ceramics. The principal limiting factors for its success is the formation of crack patterns in the SiC coating. In order to avoid this, two stage pack cementation methods are employed in which the precursors are slightly varied so that during the second stages a glassy SiO₂ forms and seals off the crack. Additionally the free silicon distributing in the SiC coating could relax the mismatch of thermal expansion between the coating and the composite. The SiC coating can effectively protect the composite from oxidation at temperatures above 1600°C.

The key issues to be tackled in order to develop efficient protective systems are: thermal stability of the material, adhesion with the C/C composite, chemically compatible interfaces through out the coating architecture, oxygen ingress and carbon egression, thermal mismatch stresses causing spallation and crack formation, erosion in hot gases.

Among the different techniques to grow SiC on different substrates, CVD is the most frequently used technique. CVD can be used to deposit materials at near theoretical density with good adherence to the substrate. The deposition rate by CVD process is higher than most other coating techniques except plasma spraying method. SiC coating can be formed by various Si and C compounds.

The typical systems used include SiH₄/CH₄ in hydrogen or nitrogen SiCl₄/CH₄ in hydrogen, (CH₃)₂SiCl₂ with hydrogen, CH₃SiCl₃ in hydrogen, SiHCl₃ / C₃H₈ with hydrogen and (CH₃)₄Si in hydrogen. In the CVD process, a precursor is used to deposit SiC and this precursor should have some requisite properties such as stability

at room temperature, low vaporization temperature and high saturation of vapor pressure, should undergo decomposition at a temperature far below the melting point of the substrates. In the present studies SiC coating has been developed using CVD method at atmospheric pressure using MTS precursor along with hydrogen and argon as carrier gas.

1.7. Applications

The main applications of C/C composites today are mainly in defense, space and aircraft industry while those in the field of mechanical engineering are picking up steadily. There is great potential for the wider applications of these materials. Due their excellent friction and wear characteristics these were the obvious choice as brake discs for aircraft braking systems. In aerospace industry they are used for thermal protection system of space shuttles, rocket nozzles, exit cones, nose tips of re-entry vehicles. Their use in jet engine was as rotors and stators, which are operating at temperatures 500-600°C higher than those used in conventional engines with high temperature alloys. These can be used as refractory materials in non-oxidizing environments and also as hot press dies in hot forging processes. They find application in high temperature corrosion resistant fasteners. The most advanced applications include Radio Frequency (RF) antennae, cladding elements for the nuclear fusion reactor, plasma-facing surfaces and reflectors for satellite communications.

1.8. Plan of the present work

Having considered the details of the processing of carbon-carbon composites by liquid impregnation method the plan of work for the project was as follows

- 1) Fabrication of green preforms to make carbon-carbon composites. Carbonization of the preforms. Its operation will be optimized with respect to the required microstructure.
- 2) To achieve the aforementioned, samples from experiments conducted with varying process controls would be characterized after suitable heat treatments.
- 3) Optical microscopy with polarized light, electron microscope, XRD analysis, X-ray Tomography and Micro laser Raman spectroscopy will be used to characterize the microstructure and get a clear understanding of the micro- and nano-structural details and to estimate the degree of graphitization that is achieved finally.
- 4) Density, CTE, and compressive strength measurements will be performed to characterize the physical, thermal and mechanical properties of the composite.
- 5) As the main aim of this is to develop a composite for advanced reactor applications; hence, due concern would be given to the radiation damage studies of these materials by conducting relevant irradiation experiments.
- 6) Finally a correlation shall be obtained between synthesis, microstructure and the properties attained.

CHAPTER 2

CHAPTER 2

CHARACTERISATION TECHNIQUES AND METHODS FOR PROPERTY EVALUATION OF CARBON/CARBON COMPOSITE MATERIALS

2. Introduction

Carbon-carbon (C/C) composite consists of carbon fibers embedded in a carbon matrix. The carbon fibre reinforced C/C composites are promising materials for varied applications [24,25,39-41] due to their excellent properties such as high specific strength and stiffness, high specific modulus, high thermal conductivity, low coefficient of thermal expansion (CTE) and excellent creep resistance. Apart from these advantages they are chemically resistant and can be used at elevated temperature [42-44], bio-compatible and possessing pseudo-plastic fracture behaviour. Carbon in various forms has been used in nuclear reactors and there has been growing interest to develop graphite and carbon based materials for upcoming high temperature nuclear and fusion nuclear reactors. C/C composite materials compared to conventional graphite materials are now considered as the promising materials for the fusion reactor due their excellent properties of high thermal conductivity and high thermal resistance.

There are three known conventional methods of preparing C/C composites [45]. They are chemical vapour deposition (CVD), pyrolysis of thermoset and thermoplastic resin and pyrolysis of hydrocarbon pitches derived from coal tar, synthetic mesophase and petroleum products. Most of the C/C composite work on thermoset resin has been carried out using phenolic resin because of its excellent char

yield (about 65%). The amount of the matrix depends on the char yield. In the present work, C/C composites have been prepared using 2D matted polyacrylonitrile (PAN) carbon fibers and phenolic resin. This preform was carbonized to remove the volatile material.

2.1. Preparation of carbon/carbon composite samples

The different carbon/carbon composites were prepared for these studies they are petroleum coke based, carbon black and phenolic resin carbon based, chopped carbon fiber reinforced and 2-D matted carbon fiber based composites. The petroleum coke and carbon black composites were prepared by mixing them with phenolic resin. Chopped carbon fibers were dispersed in phenol formaldehyde resin matrix and cast followed by heat-treatment. The 2-D preform of carbon composite was prepared by stacking the matted PAN fiber using phenol formaldehyde resin. The carbonized sample is highly porous and it needs to be densified for any further application.

In the present studies the conventional or solvated resin solution method is used for development of the C/C composite made from carbon fiber. This involves the following steps (a) fabrication of preform (green or as cured part), (b) carbonization of the preform and (c) densification. The densification includes resin impregnation, drying to remove the solvents and curing. This is followed by carbonization to decompose the polymeric matrix into carbon and to remove the volatile molecules by pyrolysing the matrix in an inert atmosphere. The phenolic resin gives a char yield of 65% along with the removal of other volatiles which causes some porosity during the evacuation of the gases. These pores are to be filled by impregnating with resin followed by curing and carbonization till a maximum achievable density is obtained.

These fibers have been matted and stacked to a 2-D preform using phenol formaldehyde resin. Green preform in the shape of rectangular blocks has been fabricated. This preform was cut into 2.5 X 2.5 X 0.6 cm size and carbonized at a slow heating rate. The carbonized preforms were then used for the studies. The carbonized sample is highly porous and hence needs to be densified for any application.

2.2. Densification of the samples

The samples have been densified by impregnation technique over two cycles for 2D matted carbon fiber preform while the chopped carbon fiber composites were densified for four cycles of impregnation. The impregnated samples were then carbonized at 1000°C under inert atmosphere with a heating rate of 0.1°C/min. The samples were then subjected to a second cycle of impregnation at the same pressure and varying time duration as carried out during the first cycle. These samples were then cured and carbonized as done in the first cycle. The samples were subsequently heat-treated at 1800°C to study the effect of high-temperature processing on the micro-structural modification of the materials.

2.3. Characterization of the samples

The densities of the samples were determined by Archimedes principle. The pellets were characterized by X-ray diffraction and Raman spectroscopy to verify the amorphous nature. The coefficient of thermal expansion (CTE) and the specific heat of the sample have been measured using thermo mechanical analyzer (TMA) and Differential Scanning Calorimetry (DSC), respectively.

2.3.1. Characterization techniques

The various characterization techniques employed in the present investigation to characterize the C/C composites are given in this section. The basic principles methodology and the objective of using these techniques are described briefly as follows.

2.3.1.1. Chemical analysis

Chemical analysis of the samples was done by Atomic Emission Spectroscopy (AES). Nuclear grade (N-grade) material was obtained by both the proposed synthetic routes and also from N-grade petroleum coke. Chemical analysis of the composite showed that the boron content was less than 1 ppm whereas cadmium and cobalt were not detected. This was due to the purity of the precursor matrix and the carbon black. Elemental analysis of the samples (Table 2.1) shows impurities like boron, cadmium and cobalt, with very high neutron cross-section below ppm level. Other impurities also comply with nuclear standards. These metallic impurities especially iron are believed to have been incorporated during milling of the samples

2.3.1.2. Density of the composites

The density of the samples was measured using water displacement method. It was found that density of the petroleum coke-based samples at a given temperature increased initially and then decreased steadily with weight fraction of the binder. Density of carbon fiber based samples increases monotonically with fiber content i.e., with decreasing matrix element. Carbon-black (CB) based samples have higher density than carbon fiber based. In the case of matted PAN fiber composite it is observed that maximum sample density of 1470 kg/m^3 was achieved after the two

cycles of impregnation was obtained at 50 bar with 10 h impregnation. While at 30 bar and 70 bar the density first increased with time duration of impregnation and then decreased after 20 h. The density increases after extending the impregnation duration to 25 h.

2.3.1.3. Powder X-ray diffraction:

Basic principle: The X-ray diffraction (XRD) analysis for crystallographic structure determination in principle is based on the Bragg's law of diffraction [46, 47]

$$n \lambda = 2d \sin \theta \quad (2.1)$$

Eq. (2.1) relates to the 'd' spacing (Å) between the (hkl) planes of the lattice and the glancing angle 'θ' of the monochromatic beam of X-ray of wavelength (λ). The positions (2θ) of the diffraction peaks depend on the dimensions and geometry of the unit cell, while the relative intensities (I/I₀) depend on the way specific atoms are arranged at the lattice sites. The detection limit (for a phase) is normally 2-5 wt. %

Methodology: XRD measurements in the present investigation were carried out using Philips model PW-3710 X-ray diffractometer employing Cu-K_α radiation. The intensity component due to the Cu-K_β radiation was suppressed by using a graphite monochromator with the instrument. Standard silicon sample, supplied by the manufacturer was employed as a standard for calibration. The precision of angular reproducibility using the above diffractometer was ±0.001°. The sample was placed in a collimated monochromatic X-ray beam (Cu-K_α radiation) and the intensity of the diffracted beam was measured as a function of diffraction angle (2θ). Using Bragg's

relation, the ' d ' values were obtained for each peak (2θ values) and the corresponding (hkl) values were assigned by indexing. Depending up on the requirement two types of scan speeds were used for recording the XRD pattern. Namely the normal scan and the slow scan were used for recording the XRD pattern.

Objective: The normal scan consisting of a scanning speed of $2^\circ/\text{min}$ was employed for the phase identification whereas slow scan consisting of a scanning speed $1^\circ/\text{min}$ was used for estimating the peak broadening to calculate the crystallite size and to resolve the closely spaced peaks. The crystallites size were calculated using the standard Scherrer's formula given in eq. (2. 2)

$$D = 0.9\lambda / \beta \text{ Cos } \theta \quad (2.2)$$

Where D is the crystallite size in nm, λ is the radiation wavelength (0.154 nm) θ is the diffraction peak angle and β is the line width at half peak intensity. β can be calculated using the Warne's formula as given below in eq. (2.3)

$$\beta^2 = \beta_m^2 - \beta_s^2 \quad (2.3)$$

Where β_m is the measured full width at half maximum (FWHM) and β_s is FWHM of standard silicon sample.

2.3.1.4. X-ray Tomography

Basic principle: An X-ray beam is sent on a sample mounted on a rotator; a series of N number of radiographs corresponding to N angular positions of the sample in the beam is recorded on a detector which is generally a CCD in modern tomography setup. A reconstruction software is used to obtain the three dimensional distribution of

the X-ray attenuation coefficient μ within the sample. The distribution forms a 3D image whose elementary unit is called a voxel which can be viewed using appropriate imaging softwares. The schematic diagram of the principle of X-ray tomography is shown in Fig. 2.1.

For the reconstruction step two mathematical methods i.e. algebraic and analytical methods can be used. The algebraic methods consist of solving a linear system of equations whereas the analytical method principle is to back project the intensities of the radiographs via Fourier transform approach the algorithm for the filtered back projection method depends on the type of source used. The analytical filtered back projection method is used to reconstruct a slice of the sample perpendicular to the rotation axis. The 3D volume is obtained by stacking the reconstructed slices.

Micro-computed tomography (μ CT) has become commercially available with instruments having micron range resolution that is used for non- destructively examine the samples in three dimensions (3D). μ CT has been used [48-51] for carbon based materials for various applications such as graphite oxidation, relationship between density and mechanical properties of C/C composites and the porosity effect on mechanical properties of graphite.

The porosity in carbon materials is very important in its numerous diverse applications as it may be beneficial or detrimental depending upon the application. Therefore a number of techniques are utilized to characterize porosity which has their merits and demerits as no single method can characterize the entire range of pore size distribution.

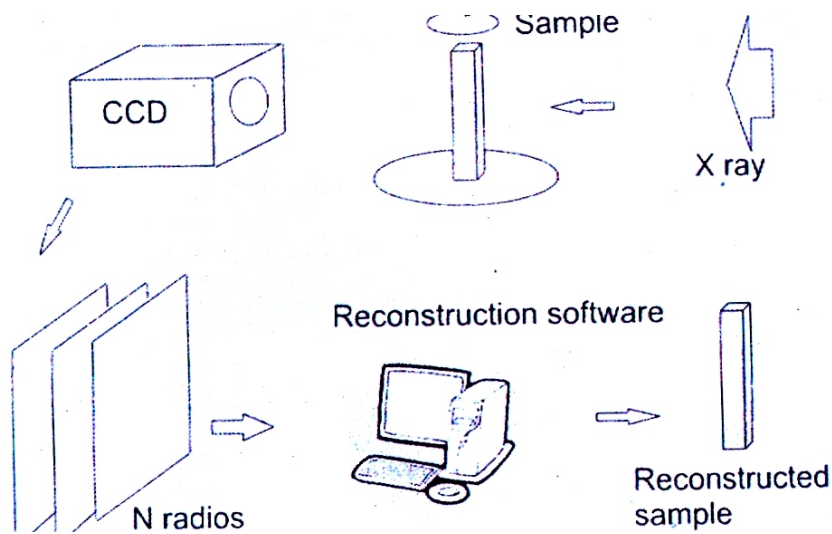


Fig. 2.1: Schematic diagram of the principle of X-ray attenuation tomography

Methodology: Carbon composites made up of carbon fibers and impregnated with phenolic resins to fill the pores present in the fibers with carbons were characterized by tomography. These have been subjected to different pressures for densification. Sample (a) is prepared at a lower pressure of 30 bar and sample (b) at a much higher pressure of 50 bar. The dimension of the carbon composite was 1.1 x 1.2 x 0.64 cm. 400 radiographs, each of 15 second exposure, were taken at 60 kV and 400 to 450 micro-ampere (keeping the wattage constant for constant flux during operation) setting of the microfocus source. The reconstruction grid dimension is 787x787x256 pixels.

Objective: This technique has been used to determine the homogeneity of the sample. The bonding of the fiber and matrix can be determined. The porosity and the cracks developed in the matrix as result of pressure can be determined.

2.3.1.5. Scanning Electron Microscopy (SEM)

Basic principles: When a finely focused electron beam interacts with the matter mainly three phenomenons occur by emission of secondary electrons, back scattering of electrons transmission of electron, emission of characteristic X-rays, cathode luminescence and absorption of electrons also occur during the interaction of primary electrons with the matter. The various interaction of electron beam with the specimen is shown in Fig. 2.2 depending on which the various techniques like SEM. AES, EPMA, EELS, and TEM etc are based on.

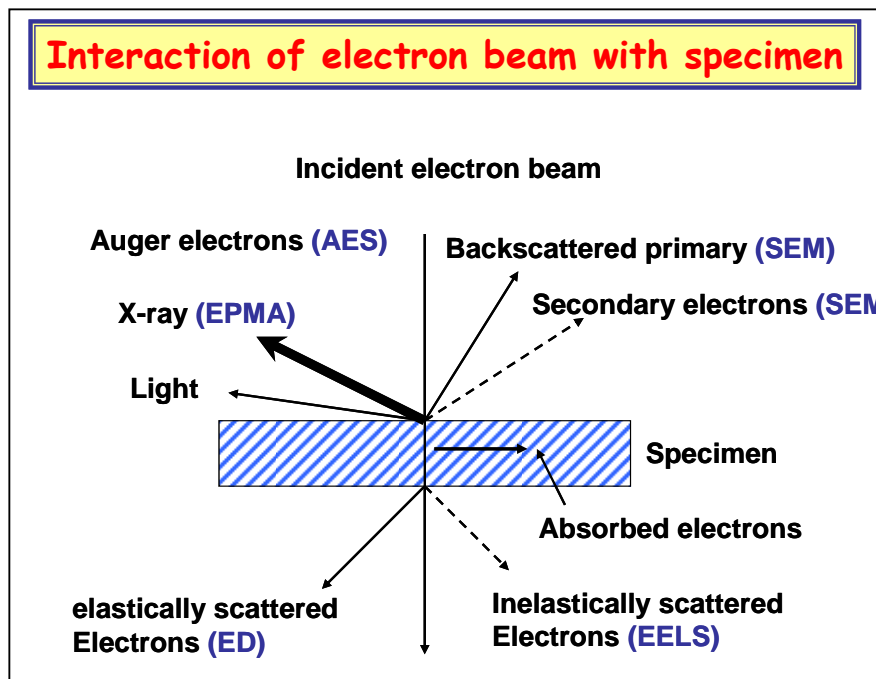


Fig. 2.2: Schematic diagram of the various interaction of electron beam with specimen

In Scanning Electron Microscopy (SEM) the signals generated from the surface by secondary and back scattered electrons are detected and are fed to a synchronously

scanned cathode Ray Tube. (CRT) as an intensity modulating signal which displays a specimen image on the CRT screen. The CRT raster divided by the electron probe scanning width determine the image magnification. Scanning electron microscope is composed of electron optical system specimen stage display and recording system vacuum system. Morphological features of the samples were examined by scanning electron microscopy (SEM). The samples were then examined employing SEM at different magnifications.

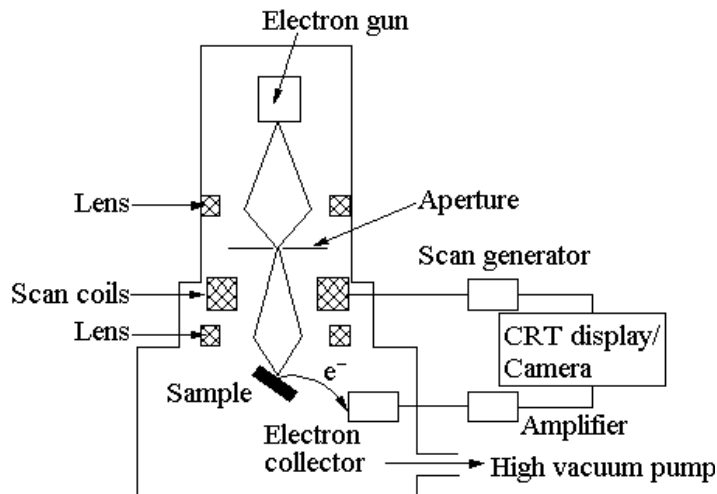


Fig. 2.3: Schematic diagram of a Scanning Electron Microscope.

Methodology: SEM (SERON Inc, Korea, Model: AIS2100) was used to examine the morphology of the porous samples at different magnifications. The microstructure was revealed in the samples. For chemical composition determination the EDX (Oxford Instruments, UK Model No: INCA E350) was used in the present studies. As the carbon samples are conducting there was no specific requirement of giving any

conductive coating to the samples. The schematic of scanning electron microscope is given in Fig. 2.3.

Objective: The technique was used to study the porosity, uniformity and homogeneity of the samples with varying impregnation parameters. The C/C composites were coated with SiC using chemical vapour deposition technique. The effect of processing parameters during deposition of SiC on the microstructure has been studied using SEM analysis

2.3.1.6. Thermo mechanical Analyzer (TMA)

Basic principle: In this technique the change in the length of the sample with temperature is detected by the movement of the push rod and measured by means of a dial gauge of a transducer device Linear Variable differential transformer (LVDT) attached to the top of the push rod [60, 61].

Methodology: The measurements were carried out from ambient temperatures to 1123 K in air at a heating rate of 5K using a fused quartz push rod dilatometer (TMA813). The sample in the form of rectangular block was kept between small quartz dice which was placed inside the quartz tube. The entire assembly along with the quartz push rod and thermocouple was inserted in the furnace; a calibrated chromel alumel thermocouple was placed near the sample and was used for temperature measurement. The dilation of the sample was read on a calibrated Mitutoyo Dial gauge with an accuracy of $\pm (0.0005\text{mm})$

Objective: The technique was used for comparative study of the bulk thermal expansion behavior of C/C composite with varying densities after two cycles of impregnation at varying time and pressure.

2.3.1.7. Differential Scanning Calorimetry (DSC)

Basic principle: It is a technique where the difference in energy inputs into a reference and sample material is measured as a function of temperature while the reference and sample material are subjected to controlled temperature programme. There are two modes in which DSC is performed i.e. power compensation DSC and heat flux DSC.

In the power compensation DSC both the reference and sample materials are connected to the heaters to maintain same temperature for reference as well as sample material. This method yields direct calorimetric measure of energy transition. In the heat flux method both the reference and the sample material holders are surrounded by thermopile. The heat flux (the differential heat flow) is measured using a thermopile.

Methodology: The DSC experiments were performed using a SETARAM simultaneous TG/DTA instrument on a part of the dried gel precursors in the flowing air atmosphere with a heating rate of 10°C/min. The precursor sample and the reference material were placed in two identical platinum crucibles. The weight loss of sample a function of temperature was monitored with the help of a thermo-balance. The temperature difference between sample and reference material as well as sample temperature was monitored using two thermocouples simultaneously.

Objective: In the present investigations the DSC technique was used to determine the specific heat of the sample and also determine the stored energy in the irradiated samples.

2.4. Spectroscopic Techniques

2.4.1. Raman Spectroscopy

Basic principle: Raman spectroscopy is a useful technique for the identification of a wide range of substances in different states viz. solids, liquids, and gases. It is a straightforward, non-destructive technique requiring no sample preparation. Raman spectroscopy involves illuminating a sample with monochromatic light and using a spectrometer to examine light scattered by the sample. At the molecular level photons can interact with matter by absorption or scattering processes. Scattering may occur either elastically, or inelastically. The elastic process is termed Rayleigh scattering, while the inelastic process is termed Raman scattering.

The electric field component of the scattering photon perturbs the electron cloud of the molecule and this process may be regarded as exciting the system to a 'virtual' state. Raman scattering occurs when the system exchanges energy with the photon and the system subsequently decays to vibrational energy levels above or below that of the initial state. The frequency shift corresponding to the energy difference between the incident and scattered photon is termed the Raman shift. Depending on whether the system has lost or gained vibrational energy, the Raman shift occurs either as an up or downshift of the scattered photon frequency relative to that of the incident photon. The down-shifted and up-shifted components are called the Stokes and anti-Stokes lines respectively. A plot of detected number of photons versus Raman shift from the incident laser energy gives a Raman spectrum. Different materials have different vibrational modes, and therefore characteristic Raman spectra. This makes Raman spectroscopy a useful technique for material identification. There is one important distinction to make between the Raman spectra of gases and liquids, and those taken from solids-in particular, crystals. For gases and

liquids it is meaningful to speak of the vibrational energy levels of the individual molecules which make up the material. Crystals do not behave as if composed of molecules with specific vibrational energy levels; instead the crystal lattice undergoes vibration. These macroscopic vibrational modes are called phonons.

Carbon has several allotropes and can exist in a wide range of disordered forms. Raman spectroscopy was found to be quite sensitive to these structures and to changes that perturb the translational symmetry of the analyzed sample, such as those that take place in small-dimensional crystals or small grain size (polycrystalline). It is thus a powerful method for characterizing carbons [52-55]. Since the Raman signal is sensitive to short range disorder, it can also reveal different forms of amorphous carbons.

Natural diamond exhibits one main Raman active vibration which manifests itself as a sharp first order peak in the Raman spectrum at $\sim 1332 \text{ cm}^{-1}$ and a weak second order feature at $\sim 2750 \text{ cm}^{-1}$. In diamond films grown by CVD, carbon is also incorporated into the film in non-diamond forms. These non diamond carbons may be graphitic or amorphous carbon regions in the film. The Raman spectrum of an infinite crystal of pure graphite (or a large single crystal sample, in practice) would show one sharp peak at 1580 cm^{-1} . For small crystallite sizes, the selection rules concerning the Raman inactivity of certain phonons in infinite graphite crystals are relaxed as the crystal can no longer be regarded as infinite. The sharp graphite peak becomes a broad band (the G-band) and a 'disordered' (or D-band) peak [56-59] appears in the spectrum at $\sim 1350 \text{ cm}^{-1}$. Amorphous carbon produces a broad asymmetric hump in the region $1000\text{-}1600 \text{ cm}^{-1}$. Both graphite and amorphous carbon have Raman scattering efficiencies greater than that of diamond. This means that for identical numbers of sampled atoms in the three carbon forms-diamond, graphite, and

amorphous carbon, the graphite and amorphous carbon samples would give a much larger Raman signal than the diamond sample. These scattering efficiency ratios, relative to diamond have been reported to be ~50 times for graphite, and ~233 times for amorphous carbon, both measured using 514.5 nm laser radiations.

Raman spectra of most of the carbon-graphite materials contain two peaks at around 1580 and 1360 cm^{-1} , except for natural graphite, which has a single sharp Raman band at 1580 cm^{-1} . The 1580 cm^{-1} peak is known to correspond to the graphite structure and the 1360 cm^{-1} peak is correlated with graphitized carbon structure and the ratio of the integrated intensities of the two peaks, I_{1360}/I_{1580} , can be considered to be a good parameter to estimate the degree of graphitization. The higher this ratio the lower is the degree of graphitization. The 1580 cm^{-1} peak mainly comes from the flex vibration of chemical bonds in atomic hexagonal net plane, however, the 1360 cm^{-1} band of the spectra is closely associated with one kind of local asymmetrical structure, which exists in graphitized carbon or non-integrity graphite crystals containing defects introduced by grinding process, it can be inferred that this kind of local structure is obtained by loss of symmetry or conversion from a hexagonal symmetry to a much lower symmetry.

Methodology: In modern Raman spectrometers (Fig. 2.4), lasers are used as a photon source due to their highly monochromatic nature and high beam fluxes. This is necessary as the Raman Effect is weak, typically the Stokes lines are ~105 times weaker than the Rayleigh scattered component. In the visible spectral range, Raman spectrometers use notch filters to cut out the signal from a very narrow range centered on the frequency corresponding to the laser radiation. Most Raman spectrometers for material characterisation use a microscope to focus the laser beam to a small spot (<1-100 μm diameter).

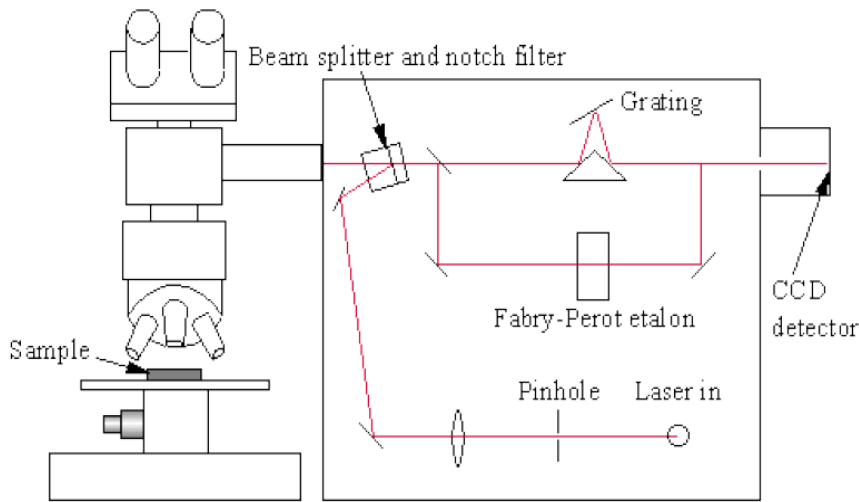


Fig. 2.4: Schematic diagram of a Raman spectrometer

Light from the sample passes back through the microscope optics into the spectrometer. Raman shifted radiation is detected with a charge-coupled device detector (CCD) and a computer is used for data acquisition and curve fitting. These factors have helped Raman spectroscopy to become a very sensitive and accurate technique.

Objective: The degree of graphitization of the composite is considerably dependent on that of the fiber and the pyrolytic carbon, of which the composite is composed, the difference on the degree of graphitization between the fiber and the matrix carbon will still be kept in the composite leading to its heterogeneity, which can be characterized by Raman spectroscopy.

2.4.2. Small angle scattering studies

Basic principle: Small-angle scattering refers to the scattering at small wave-vector transfer and is caused by the variation of scattering length density over a distance

exceeding the normal inter-atomic distances in condensed systems. It is distinct from Bragg or diffuse scattering in the sense that it refers to scattering at that region of wave-vector transfer whose magnitude is small compared to that of the smallest reciprocal lattice vectors in crystalline substances. Generally X-rays or neutrons are used as probing radiation for small angle scattering SAS investigations and the techniques are termed as Small-angle X-ray scattering (SAXS) or Small-angle neutron scattering (SANS) respectively. Small-angle X-ray scattering (SAXS) as X-rays get scattered by electrons, probes in homogeneities in electron density in contrast to the small-angle neutron scattering (SANS) that probes in homogeneities in nuclear scattering length density. SAXS and SANS are complementary in nature. However, for specific cases, one technique is more suitable than the other. In the scattering process, the electrons in case of SAXS and the nuclei in case of SANS, emit coherent secondary waves by passing of X-rays or neutrons respectively, which interfere with each other. The strength of the scattering interaction is determined by "scattering length". For an incident plane wave $\exp(i\mathbf{k}_0 \cdot \mathbf{r})$ interacting with a fixed scatterer at origin $\mathbf{r} = 0$, the scattered wave is represented as $-\frac{b(\theta)}{r} \exp(i\mathbf{k} \cdot \mathbf{r})$, where \mathbf{k}_0 and \mathbf{k} are incident and scattered wave-vector respectively. For elastic scattering $k = |\mathbf{k}_0| = |\mathbf{k}|$ and the wave-vector transferred in the scattering $\mathbf{q} = \mathbf{k} - \mathbf{k}_0$, $q = |\mathbf{q}| = |\mathbf{k} - \mathbf{k}_0| = (4\pi \sin\theta)/\lambda$, where λ is the wavelength of the probing radiation and 2θ is the scattering angle. The quantity $b(\theta)$ has the dimension of length and is called the "scattering length". In the case of X-ray scattering, scattering length is proportional to atomic number of an element and hence heavier the element the more it scatters. In addition, X-ray scattering length is always positive and for small angle scattering region it is almost independent of θ .

Methodology: A double crystal (Si (111)) based diffractometer (DCD) at Guide Tube Lab. of Dhruva reactor was used for SANS experiments as shown in Fig. 2.4. SANS data were recorded over the accessible scattering wave vector ' q ' ($q = 4\pi\sin\theta/\lambda$) range of $0.003 - 0.17 \text{ nm}^{-1}$ of the diffractometer. The schematic diagram of the instruments is installed at Guide Tube Laboratory of Dhruva reactor at Trombay, India [62-66] is shown in Fig. 2.5.

The DCD consists of a non-dispersive (1, -1) setting of 111 reflections from a pair of perfect silicon crystals. The scattered intensities of each specimen at several values of scattering vector q [$= 4\pi\sin(\theta)/\lambda$, where 2θ is the scattering angle and the incident neutron wavelength λ is 0.312 nm] was recorded by automated rotation of analyzer crystal with fine step size of 0.0012° . The pinhole instrument uses a BeO filter. The mean wavelength of incident neutron beam is 0.52 nm with a wavelength spread of approximately 15%. The scattered neutrons are detected in an angular range of $1-15^\circ$ using a linear He-3 filled position sensitive detector.

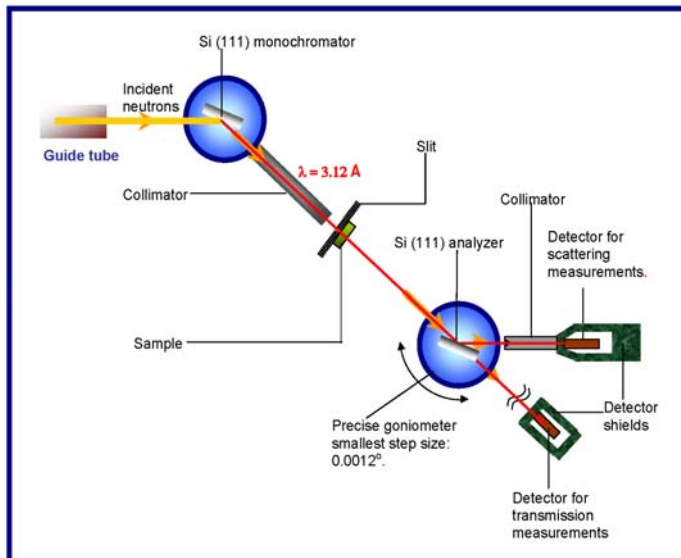


Fig. 2.5: Schematic of SANS instrument at GT-Lab of Dhruva Reactor

Objective: Small-angle scattering (SAS) is a powerful technique to investigate structural features of the inhomogeneities (particles) or the density fluctuations in condensed matter, on a length scale ranging from one nanometer up to one micron. “Structural features” include size or size distribution, shape, dimensionality, inter-particle spatial correlation etc. The consideration of scattering at low wave-vector transfer makes the SAS technique suitable to study gross-scale structural properties of a medium overlooking the specific details over inter-atomic distances.

Small-angle neutron scattering (SANS), unlike mercury intrusion porosimetry (MIP), is a non-destructive and non-intrusive technique used for pore size measurement in porous solids. Furthermore, SANS can probe open, closed and ink-bottle pores [66]. Hence, SANS was used to find the effect of impregnation parameters (pressure and time) on the pore morphology of C/C composites.

2.4.3. X-ray Photoelectron Spectroscopy (XPS)

Basic principle: XPS is a quantitative spectroscopic technique that measures the chemical state, electronic state and elemental composition, empirical formula, of the elements that exist within a material. XPS spectra are obtained by irradiating a material with a beam of aluminium or magnesium X-rays while simultaneously measuring the kinetic energy (KE) and number of electrons that escape from the top 1 to 10 nm of the material being analyzed. XPS requires ultra-high vacuum (UHV) conditions. The detection limits for most of the elements are in the range of parts per thousand. The detection limits of parts per million (ppm) are possible, but require special conditions: concentration at top surface or very long collection time (overnight).

XPS is a surface chemical analysis technique that can be used to analyze the surface chemistry of a material in its "as received" state, or after some treatment such as: fracturing, cutting or scraping in air or UHV to expose the bulk chemistry, ion beam etching to clean off some of the surface contamination, exposure to heat to study the changes due to heating, exposure to reactive gases or solutions, exposure to ion beam implant, exposure to ultraviolet light, for example. XPS can be performed using either a commercially built XPS system, an indigenously built XPS system or a Synchrotron-based light source combined with a custom designed electron analyzer.

Methodology: The present commercial XPS instruments use either a highly focused 20 to 200 μm beam of monochromatic aluminium K_{α} X-rays or a broad 10-30 mm beam of non-monochromatic (polychromatic) magnesium X-rays. A few, special design XPS instruments can analyze volatile liquids or gases, materials at non ambient temperatures or materials at about 1 torr vacuum. However there are relatively few of these types of XPS systems. The schematic diagram of the XPS instrument is shown in Fig. 2. 6.

The energy of a particular X-ray wavelength equals a known quantity; it is possible to determine the electron binding energy (BE) of the emitted electrons by using an equation that is based on the work of Ernest Rutherford

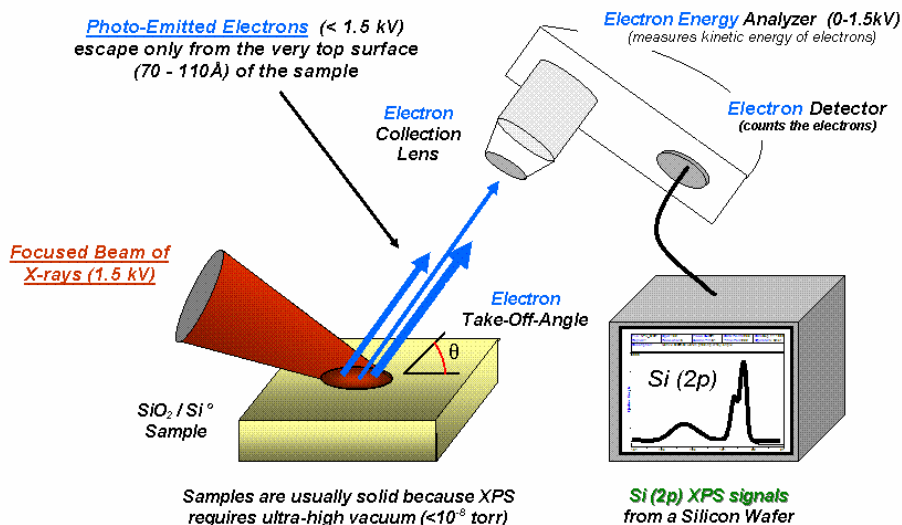


Fig. 2.6: Schematic for the XPS instrument

$$E_{binding} = E_{photon} - E_{kinetic} - \Phi$$

Where, $E_{binding}$ is the energy of the electrons emitted from one electron configuration within the atom, E_{photon} is the energy of the X-ray photons being used, $E_{kinetic}$ is the kinetic energy of the emitted electrons as measured by the instrument and Φ is the work function of the spectrometer (not the material).

A typical XPS spectrum is a plot of the number of electrons detected (Y-axis, ordinate) versus the binding energy of the electrons detected (X-axis, abscissa). Each element produces a characteristic set of XPS peaks with characteristic binding energy values which directly identify each element that exist in or on the surface of the material being analyzed. These characteristic peaks correspond to the electron configuration of the electrons within the atoms, e.g. 1s, 2s, 2p, 3s, etc. The number of detected electrons in each of the characteristic peaks is directly related to the amount

of element within the area (volume) irradiated.

To generate atomic percentage values, each raw XPS signal must be corrected by dividing its signal intensity (number of electrons detected) by a "relative sensitivity factor" (RSF) and normalized over all of the elements detected. To count the number of electrons at each KE value, with the minimum of error, XPS must be performed under ultra-high vacuum (UHV) conditions because electron counting detectors in XPS instruments are typically one meter away from the material irradiated with X-rays.

It is important to note that XPS detects only those electrons that have actually escaped into the vacuum of the instrument. The photo-emitted electrons that have escaped into the vacuum of the instrument are typically those which originate from within the top 10 to 12 nm of the material. All of the deeper photo-emitted electrons, which were generated as the X-rays penetrated 1–5 micrometers of the material, are either recaptured or trapped in various excited states within the material. For most applications, it is, in effect, a non-destructive technique which reveals the surface chemistry of any material.

Objective: In the present investigations the 1s XPS spectra of carbon based samples is recorded in slow scan mode. The spectra is deconvoluted using Gaussian into the distinct features at ~283.4 eV and 285 eV. The feature at ~285 eV corresponds to sp^3 hybridised carbon atoms while ~283.4 eV corresponds to sp^2 hybridised carbon atoms. The intensity ratio of these peaks gives an estimate of the sp^2/sp^3 carbon fraction.

CHAPTER 3

CHAPTER 3

PREPARATION AND STRUCTURAL EVALUATION OF CARBON/CARBON COMPOSITES

3. Introduction

Carbon based materials due to their wide range of structures and several desirable properties are used in nuclear reactors. In the recent past there has been a growing interest to develop speciality carbon material for high temperature nuclear reactors. Research on carbon materials with high density and amorphous isotropic carbon for their use in thermal reactors to avoid accumulation of Wigner energy is also being carried out. Due to its excellent neutron scattering properties, graphite continues to be the unanimous choice for the moderator material in high-temperature nuclear reactors where the aforesaid drawbacks are essentially overcome due to high-temperature annealing. Graphite and carbon fibre reinforced carbon composites are the candidate materials for high temperature applications due to their superior mechanical properties.

This chapter describes the synthesis routes for fabrication of novel carbon composites that not only retain isotropicity over a wide range of stock composition but also remain amorphous when heat-treated at high temperatures. An exhaustive study has been carried out on different thermo-mechanical and other material properties of the samples using a wide range of characterization techniques. In this chapter the results of the investigation on carbon composites made from carbonized polyacrylonitrile (PAN) fiber (i.e. carbon fibers both chopped and matted) and carbon composites using carbon

black in comparison with a standard carbon composite sample made from petroleum coke are reported.

3.1. Experimental

3.1.1. Petroleum coke based samples

Samples were prepared using nuclear grade petroleum coke mixed with phenol formaldehyde as the binder. The binder amount was varied between 15-40 wt.%. The samples were then heat treated at different temperatures (viz. 800, 1000, 1200 and 1500 °C) in argon atmosphere. In order to get a reference, a sample was prepared from nuclear grade petroleum coke mixed with 25% phenol formaldehyde binder following standard recipe available in the literature. Pellets (10 mm diameter and 10 mm height) were made using a uniaxial press under a pressure of 350 MPa. They were then heat-treated at 1000 °C in an inert atmosphere to get the desired product.

3.1.2. Carbon black based samples

Phenol formaldehyde resin (liquid Resole type) was cured at 200 °C and crushed into small pieces. They were subsequently carbonized at a temperature of 1000 °C in an inert atmosphere. The heating rate was maintained at 1.66 °C/min in the temperature range of 200–750 °C. The carbonized product was milled and sieved into different size fractions. The powder was leached with hydrochloric acid to remove metallic impurities like iron which get incorporated during the milling. Powder having size below 75 µm was used in the present study. This carbon powder was mixed with 0–15 wt% of carbon black (N330 grade, surface area 83 m²/g) and phenol formaldehyde binder varying from 10 to 20% by weight. Pellets (10 mm diameter and 10 mm height) were made using a uniaxial press

under a pressure of 350 MPa. The green pellets were heat treated up to 1000°C at a heating rate of 0.83°C/min in inert atmosphere to remove volatile organic impurities from the binder. Fig.3.1 gives the flow sheet adopted for the preparation of the carbon black based samples.

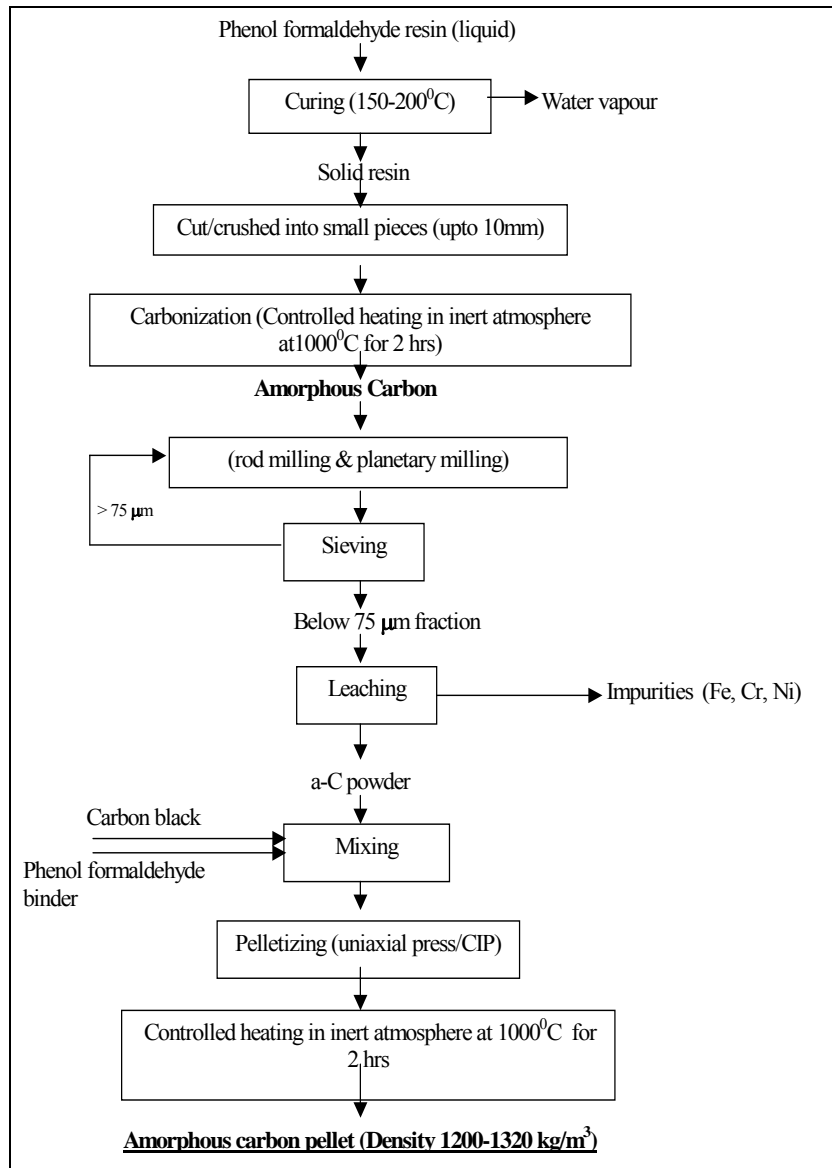


Fig.3.1: Flow sheet for the preparation of amorphous carbon/ carbon composite starting from carbon black and phenolic resin

Densification of carbon samples was carried out by resin impregnation technique. The residual open pores in the samples were impregnated with liquid phenol formaldehyde resin under pressure of 24 bar and then it was cured and carbonized at 1000°C under an inert atmosphere. Heating rate was maintained at 1.66°C/min. Impregnation for different span of time and subsequent carbonization was carried out in cycles until there was no appreciable change in the density of the samples. All the samples were subsequently heat-treated at 1500°C to investigate the effect of high-temperature processing on the micro-structural modification of the materials. The pellets were also characterized by polarized light optical microscopy to study the isotropic nature. The phenolic resin carbon and carbon black powder were characterized by X-ray and Raman spectroscopy.

3.1.3.1. Chopped carbon fiber based samples

Carbonized PAN (polyacrylonitrile) carbon fibers were chopped into pieces typically 2 mm in length and dispersed in phenol formaldehyde resin matrix in different weight fractions. The resin along with the fiber was then cast in a dye having 10 mm diameter and 10 mm height and was heat-treated to 1000°C in argon atmosphere at the rate of 0.83°C/min to obtain the desired product. Carbon composites were made with 10, 20, 30 and 50 wt% of carbon fibers.

They were heat treated up to 1000°C with a heating rate of 0.1°C/min in inert (argon/nitrogen) atmosphere. The samples were subjected to four cycles of impregnation with phenolic resin and carbonization. They were characterized in terms of bulk density and structure using polarized light optical microscopy and X-ray diffraction.

3.1.3.2. Matted carbon fiber based samples

In the present studies, carbon-carbon (C/C) composite samples have been prepared using non-graphitizing matted PAN fibers in phenolic resin matrix. A typical sample of C/C composite at 40 vol% of PAN fibre was found to be amorphous. These fibers have been used to make a 2-D preform and phenol formaldehyde resin was impregnated as the matrix. The impregnation was followed by carbonization at 1000°C under inert atmosphere. All these samples have been characterized for their density, micro structure. The preform has been made using carbonized PAN carbon fibers (PANEX-35). These fibers have been matted and stacked to a 2-D preform using phenol formaldehyde resin. Green preforms in the shape of rectangular blocks have been fabricated. This preform was cut into 2.5 X 2.5 X 0.6 cm size and carbonized at a slow heating rate of 0.1°C/min. The carbonized preforms were then used for the subsequent studies. The carbonized sample is highly porous and hence needs to be densified for any application. The impregnation was carried out using indigenously designed and fabricated impregnator shown in Fig. 3.2.

The samples have been densified by impregnation technique up to two cycles. The liquid phenol formaldehyde resin was used for impregnation under varying pressure of 30, 50 and 70 bar and for varying time duration of 10, 15, 20 and 25 h. The impregnated sample were then cured and subsequently carbonized at 1000°C under inert atmosphere with a heating rate of 0.1°C/min. The second cycle of impregnation was followed by curing and carbonization as carried out as in the first cycle. The flow sheet developed for the preparation of the carbon/carbon composite is shown in Fig. 3.3. After two cycles the densities of the samples were measured. Few samples were subsequently

heat-treated at 1800°C to study the effect of high-temperature processing on the micro-structural modification of the materials.



Fig.3.2: Indigenously fabricated Impregnator Unit

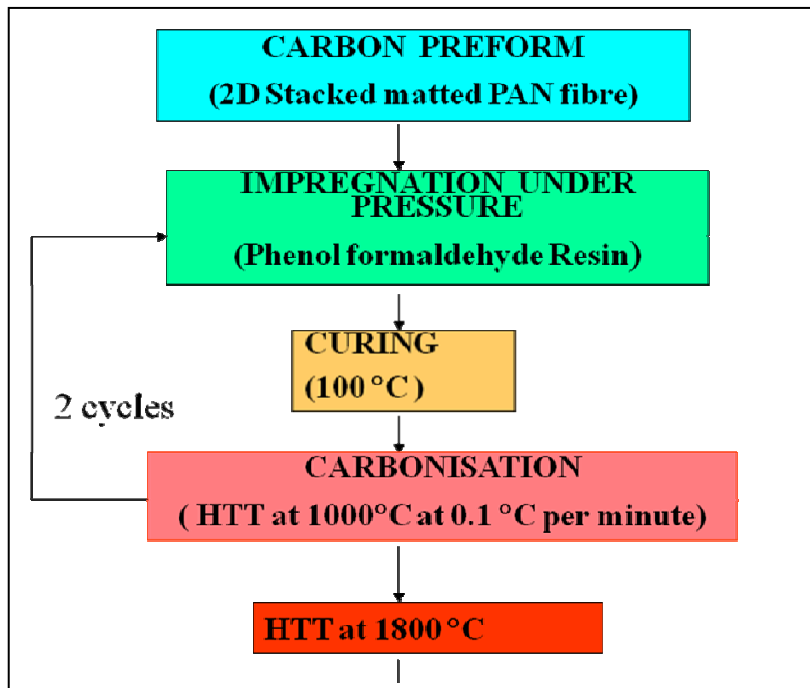


Fig.3.3: Flowsheet for the preparation of C/C Composite

3.2. Chemical analysis

Chemical analysis of the samples was performed by Atomic Emission Spectroscopy (AES). Chemical analysis of these composites showed that the boron content was less than 1 ppm whereas cadmium and cobalt were below the detection limit. This was due to the purity of the precursor matrix and the carbon black.

Table 3.1: Chemical analysis of different carbon samples

Sample	Boron (ppm)	Cadmium (ppm)	Cobalt (ppm)	Iron (ppm)
Nuclear grade petroleum coke	<1	0.5	0.3	380
PAN based sample	<1	0.7	0.6	400
Carbon black-phenolic resin composite	<1	ND	ND	620

ND: Not Detectable

3.3. Density of the composites

Bulk density of the samples was measured by conventional Archimedes principle using distilled water. It was found that density of the petroleum coke-based samples at a given temperature increased initially and then decreased steadily with weight fraction of the binder. Initially the binder bridges the inter-particulate gap thus increasing the sample density, while excess of it contributes to porosity in the sample as it volatilizes during carbonization. Maximum density (1710 kg/m^3 at 1000°C) was obtained with 25 wt.% of

binder composition as seen in Table 3.2. A standard carbon sample synthesized by cracking this stock composition i.e. 75% petroleum coke and 25% binder at 1000°C has been used during the present study as a reference material for comparing its thermo-mechanical and other material properties with those obtained from carbon fiber and carbon black.

Table 3.2: Bulk density of the petroleum coke based samples with varying binder compositions and heat treatment temperature

Heat treatment temperature (°C)	Binder Composition(wt.)					
	15%	20%	25%	30%	35%	40%
	Density in kg/m ³					
800	1510	1620	1680	1650	1640	1610
1000			1710			
1200			1720			
1500			1720			

The variation in density of the two sets of samples as a function of their constituents is shown in Fig. 3.4. The dotted line represents the standard sample made from petroleum coke. Density of carbon fiber based samples increases monotonically with fiber content i.e., with decreasing matrix element. Incomplete binding of the matrix resin with fiber leads to open porosity and hence decrease in the sample density with decreasing percentage of fiber.

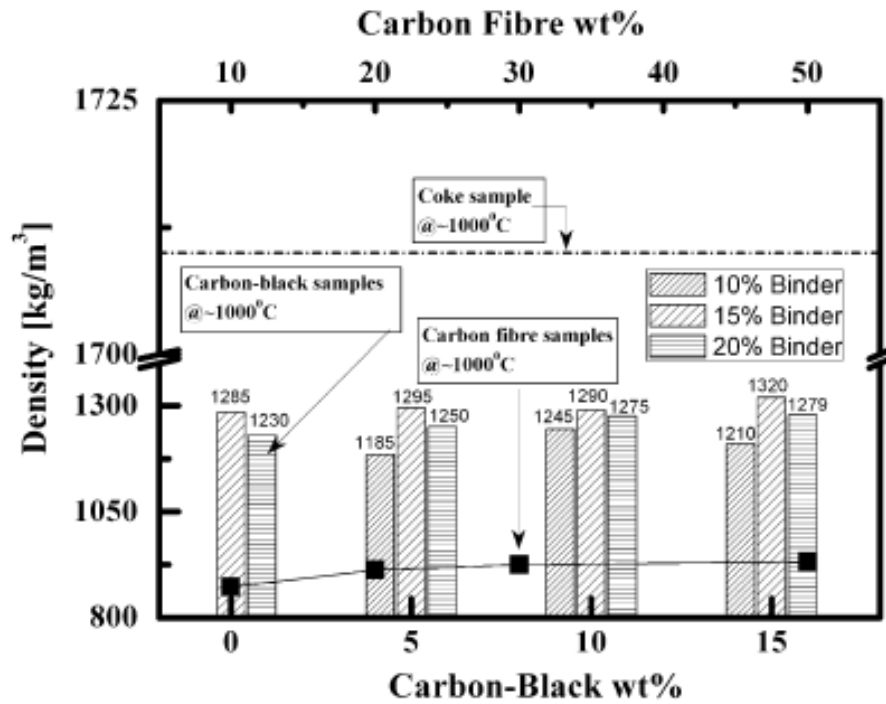


Fig. 3. 4: Variation of density in both PAN based carbon fiber and Carbon Black samples as a function of their constituents

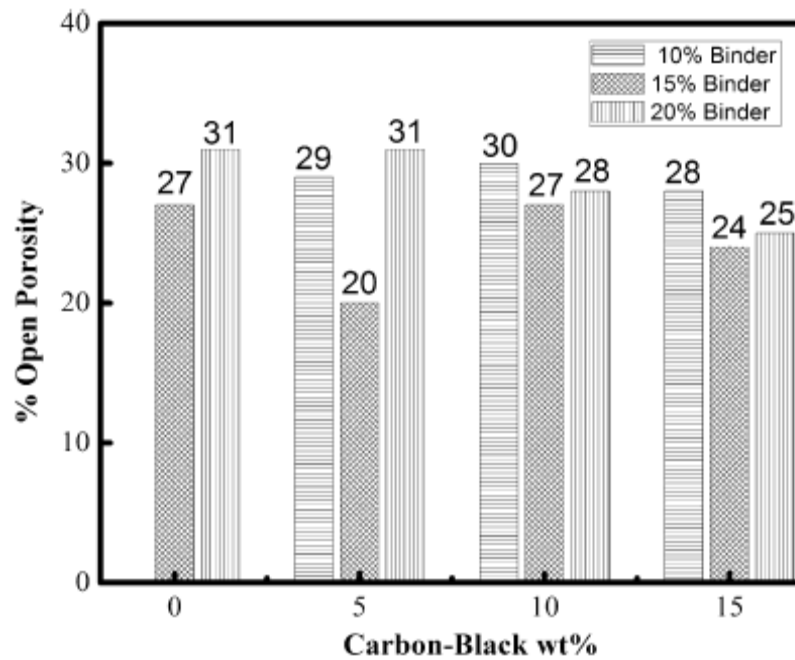


Fig. 3.5: Open porosity for Carbon Black based samples as a function of their constituents

Carbon-black (CB) based samples have higher density than carbon fiber based samples because of lower percentage porosity but no systematic variation of the sample density as a function of wt% of carbon-black is observed for these samples. For a given wt.% of CB, highest sample density attained was with 15 wt.% binder which falls off on both sides of it due to the binder-effect as has already been explained in the case of petroleum coke based samples. This can be observed from the open pore analysis of CB samples (Fig. 3.5) that shows samples made with 15 wt.% binder having lowest percentage of open porosity for a given wt% of CB. The density of the standard coke sample was however considerably much higher as compared to both carbon fiber and CB based samples.

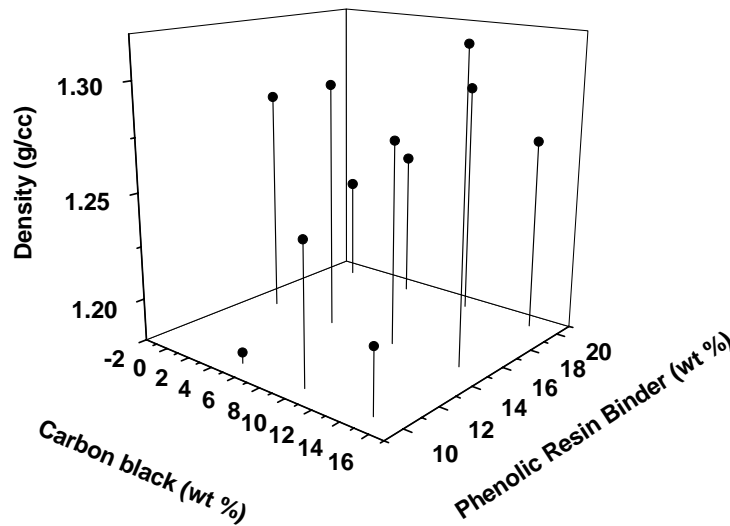


Fig.3.6: Effect of carbon black and binder amount on the density of the composite

It is also clear that the effect of binder amount is more pronounced than that of the carbon black amount. Fig.3.6 shows the 3D plot of the effect of carbon black and binder on

density. In order to further increase their density, the samples were subjected to impregnation and subsequent carbonization as described in detail in the experimental part. After several cycles of impregnation it was found that density increased only by 15% (density 1512 kg/m³) in case of 15 wt% CB sample while it increased by more than 40% (density 1510 kg/m³) in case of 20 wt% PAN based carbon fiber sample, indicating greater percentage of open pores in as-grown carbon fiber samples. However, one major disadvantage of this impregnation technique is that during high-temperature processing, stress is developed in the samples due to unequal expansion of the matrix and core material, often resulting in the formation of cracks in them.

The variation of density with varying pressures for a particular time period of impregnation for C/C composites prepared using 2D matted PAN carbon fibers is given in Table 3.3. The effect of pressure on impregnation (of liquid phenol formaldehyde resin followed by its carbonization) is shown in Fig. 3.7(a) shows. The graphical representation of the effect of time on density of the composite is shown in Fig. 3.7(b). The density of the impregnated samples was measured using water displacement method. The density increased with increase in pressure of impregnation initially and then decreased. It was observed that maximum sample density of 1470 kg/m³ was achieved after the two cycles of impregnation was obtained at 50 bar with 10h impregnation. While at 30 bar and 70 bar the density first increased with time duration of impregnation and then decreased after 20h. The density further increased after 25h.

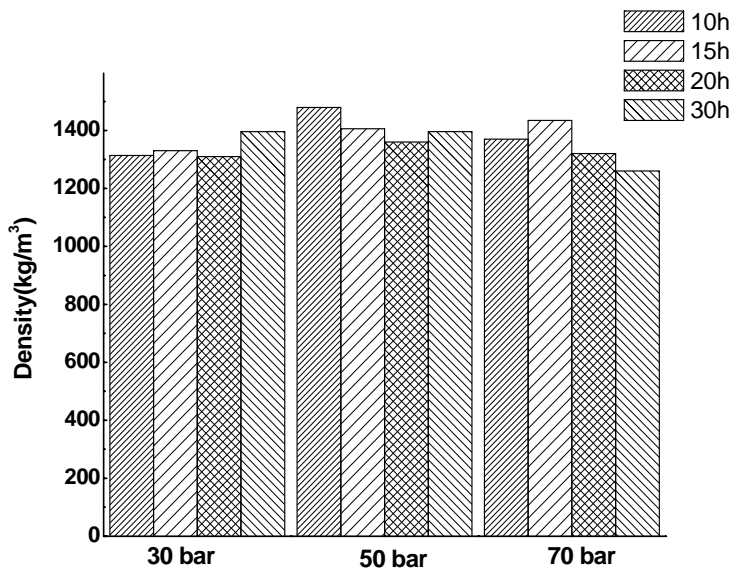


Fig. 3.7(a): Effect of impregnation pressure on density

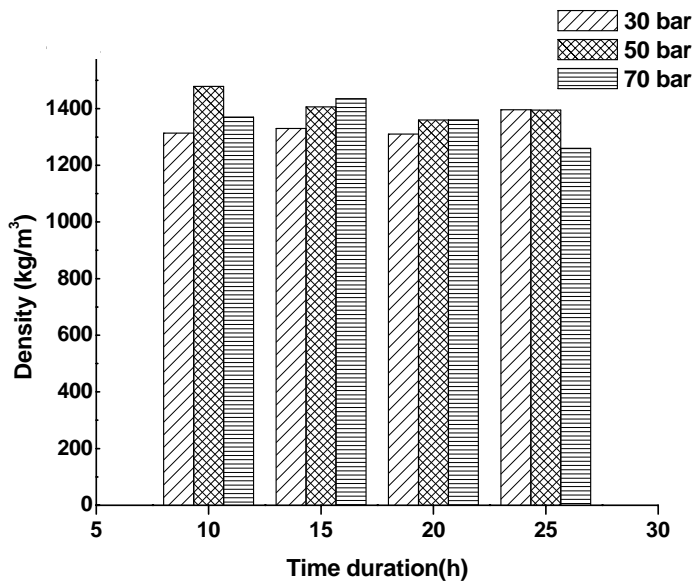


Fig. 3.7(b): Effect of impregnation time on density

Table 3.3: Effect of time duration and pressure of impregnation on density of the sample

S. No.	Pressure of Impregnation (bar)	Impregnation time (h)			
		10	15	20	25
		Density (kg/m ³)			
1	30	1314	1330	1310	1396
2	50	1470	1406	1360	1395
3	70	1370	1435	1320	1260

3.4. Characterization

3.4.1. XRD characterization studies

X-ray diffraction technique was employed to characterize the degree of graphitization of carbon-carbon composites with low crystallinity. The interlayer spacing d_{002} (Å) can be obtained from XRD and on the basis of the model given by Maire and Maring, the degree of graphitization can be calculated from the equation given below.

$$g (\%) = (3.440 - d_{002} / 3.440 - 3.354) \times 100 \quad (1)$$

where g is the degree of graphitization, 3.440 Å is the interlayer spacing of fully non graphitized carbon, 3.354 Å is the interlayer spacing of the ideal graphite crystallite and the d_{002} is interlayer spacing obtained from XRD. The 3.440 Å represents a specific

structure proposed by Franklin, who considered it as interlayer spacing of non graphitic carbon, i.e. the turbostratic structure put forward by Warren and co-workers. The variation of degree of graphitization with heat treatment temperature for the sample having maximum density with 25% binder is shown in Fig.3.8. It is clear that the sample is amorphous at 800 °C but it graphitizes up to 70% at 1500 °C.

The XRD patterns of 10%, 20% and 30% samples are diffused in nature but that of the 50% sample is sharp. It is seen that the degree of graphitization in the case of 50 vol% sample is 73%. This finding is quite interesting, even though both PAN fiber and phenolic resin are non-graphitizing in nature.

XRD patterns for the carbon-carbon composites as prepared by impregnation of resin at varying time durations for pressures of 30 and 50 are shown in Fig.3.9. The d_{002} values were calculated using Bragg's law. It is seen from Table 3.4 that the d_{002} value decreased with increasing time duration of impregnation indicating some sort of small range crystallinity being formed. However it was seen from these values that there was no graphitization occurring which was also corroborated from the Raman spectroscopy which is discussed in detail in Chapter 4.

Table 3.4: Effect of Time duration and pressure of impregnation on the d_{002} values

S.No.	Time duration of impregnation (h)	Pressure (bar)		
		30	50	70
		$d_{002}(\text{Å})$		
1	10	3.71	3.61	3.59
2	15	3.62	3.60	3.64
3	20	3.64	3.61	3.61
4	25	3.59	3.59	3.62

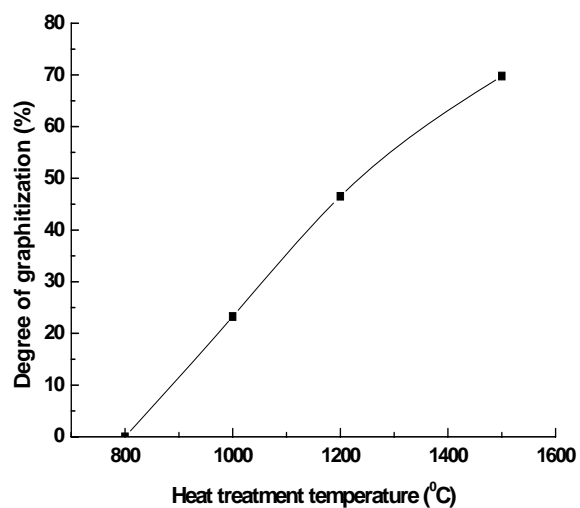


Fig. 3.8: Degree of graphitization of petroleum coke based samples with heat treatment temperature

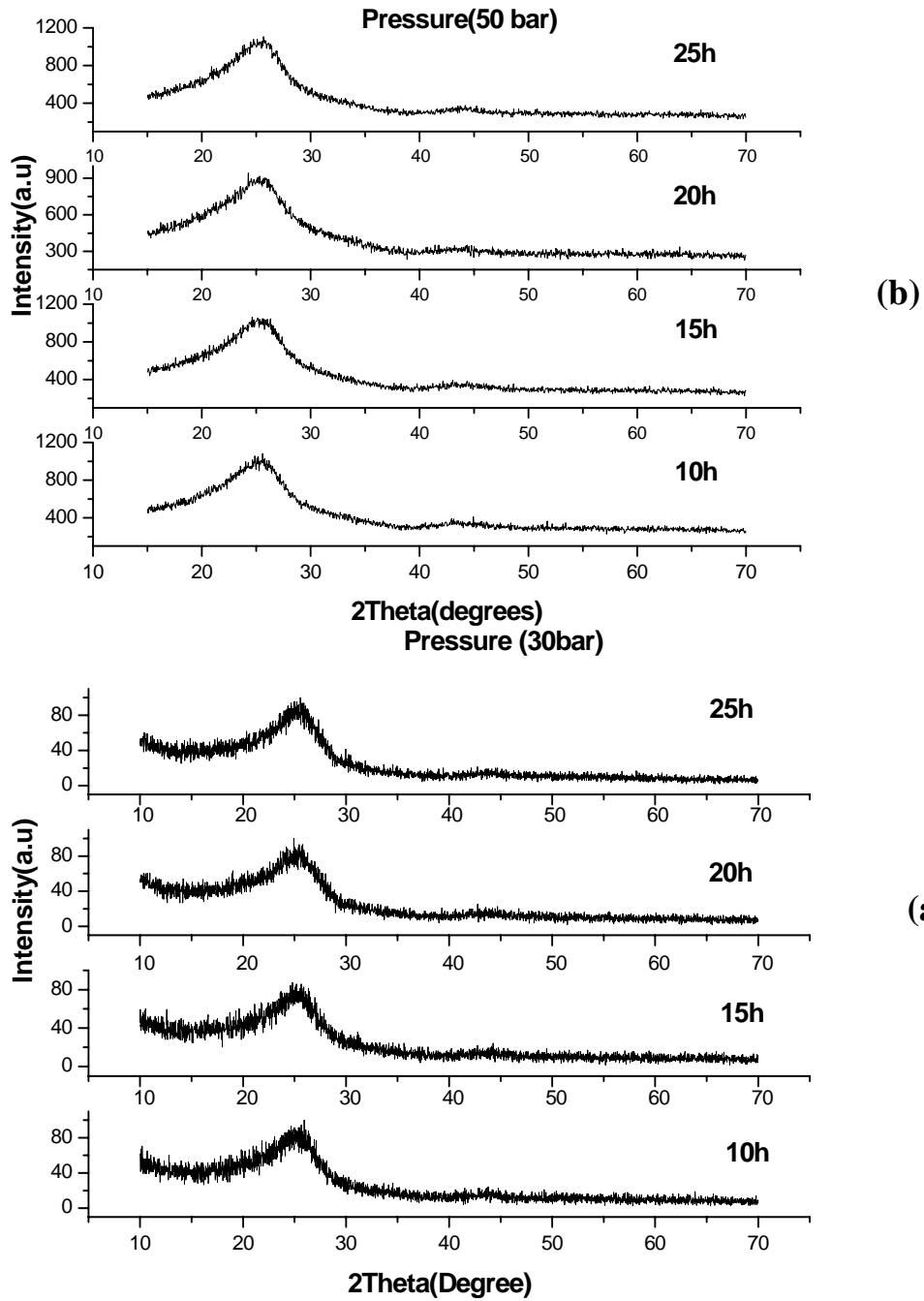


Fig. 3.9: Effect of time duration and pressure of impregnation on the d_{002} peak (a)at 30 bar and (b)50bar

3.4.2. Optical and Scanning Electron Microscopy

The extent of anisotropy in amorphous carbon sample due to formation of graphitic phase can be qualitatively studied using an optical polarized microscope equipped with a set of cross-polarizer and a retarder plate (λ -plate). According to Newton's chart for evaluation of the phase shifts, a λ -plate that introduces a phase shift of 551 nm would show up an isotropic phase as blurred magenta colored background [black in gray scale], while the anisotropic graphite crystals would appear either as greenish blue or deep yellow (bright patches with contrast in gray scale) depending on whether its aromatic plane is perpendicular or parallel to the λ -plate. Development of such coloration (greenish/yellowish) due to anisotropic graphite phase is referred to as optical activity. Fig. 3.10(a) shows the micrograph of the standard coke sample that clearly shows development of optical activity due to the formation of graphite micro-crystallites. The micrograph of the same sample heat treated at 1500°C is shown in Fig. 3.10(b). It is evident from the figure that the graphite micro-crystallites have grown larger upon heat treatment resulting in enhanced optical activity of the sample. It was seen that the sample treated at 800°C consists of microcrystallites and they grow in size at 1500°C. This observation was in full conformity with the degree of graphitization calculated from the X-ray diffraction data.

Cracks were present in the 10 vol % sample, attributed to the shrinkage of the matrix during carbonization. 10 vol % of fiber was too less to arrest the cracks. Otherwise the sample is isotropic and amorphous in nature as indicated by the magenta colour in the micrograph. The composites with 20 and 30 vol % samples also showed very little optical activity. The composites with 50 vol % fibre showed high optical activities. The green

and the yellow colour indicate the development of the graphitic structure mostly in the fiber/matrix interface. This may be due to the stress-induced graphitization. The fiber ends are acting as the stress raisers.

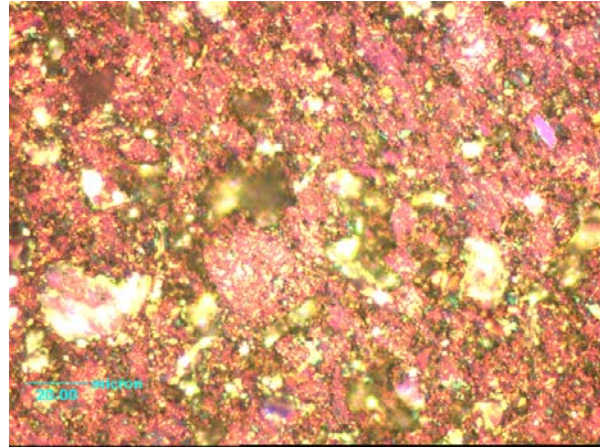


Fig. 3.10(a): Optical micrograph of petroleum coke sample treated at 800°C showing micro crystallinity

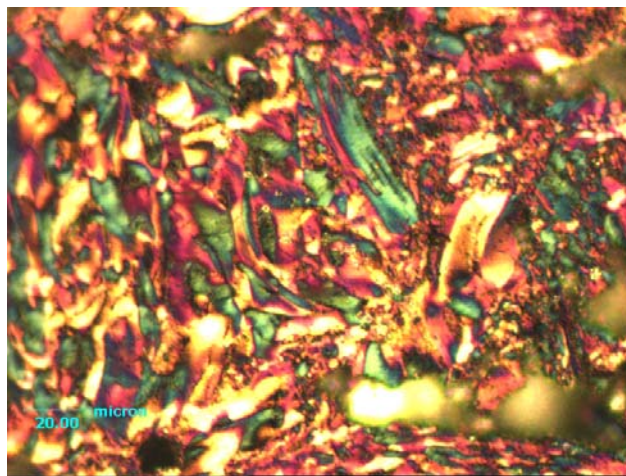


Fig. 3.10(b): Optical micrograph of petroleum coke sample treated at 1500°C showing development of larger crystals

The micrographs of two typical samples grown with 20% and 50% carbon fiber are shown in Fig. 3.11(a,b). The optical activity of the 50% fiber sample is quite high as seen in Fig. 3.11(b), whereas the 20% fiber sample barely shows any activity as seen from Fig. 3.11(c). This has been explained on the basis of graphitization due to stress induced by the fiber ends. The stress distribution along the fiber length due to fiber matrix interaction during heat treatment of composite is uneven. The stress is maximum at the fiber end and minimum at the fiber centre. The greater is the fiber content the more is the stress generated at the fiber matrix interface, which lead to anisotropy by means of graphitization.

However, even after heating to 1500°C, no optical activity is developed in the 20% fiber sample as observed in Fig. 3.11(c). The carbon-black samples on the contrary do not show up any activity for the entire range of composition discussed earlier. The micrograph of a typical CB sample with 15% CB and 15% binder composition is shown in Fig. 3.12(a). Extensive magenta background (black in gray scale) confirms the isotropic nature of the composite. The sample remains isotropic and amorphous even when heated to 1900°C as seen in Fig. 3.12(b) implying that no stress is developed at the interface of as-grown CB samples.

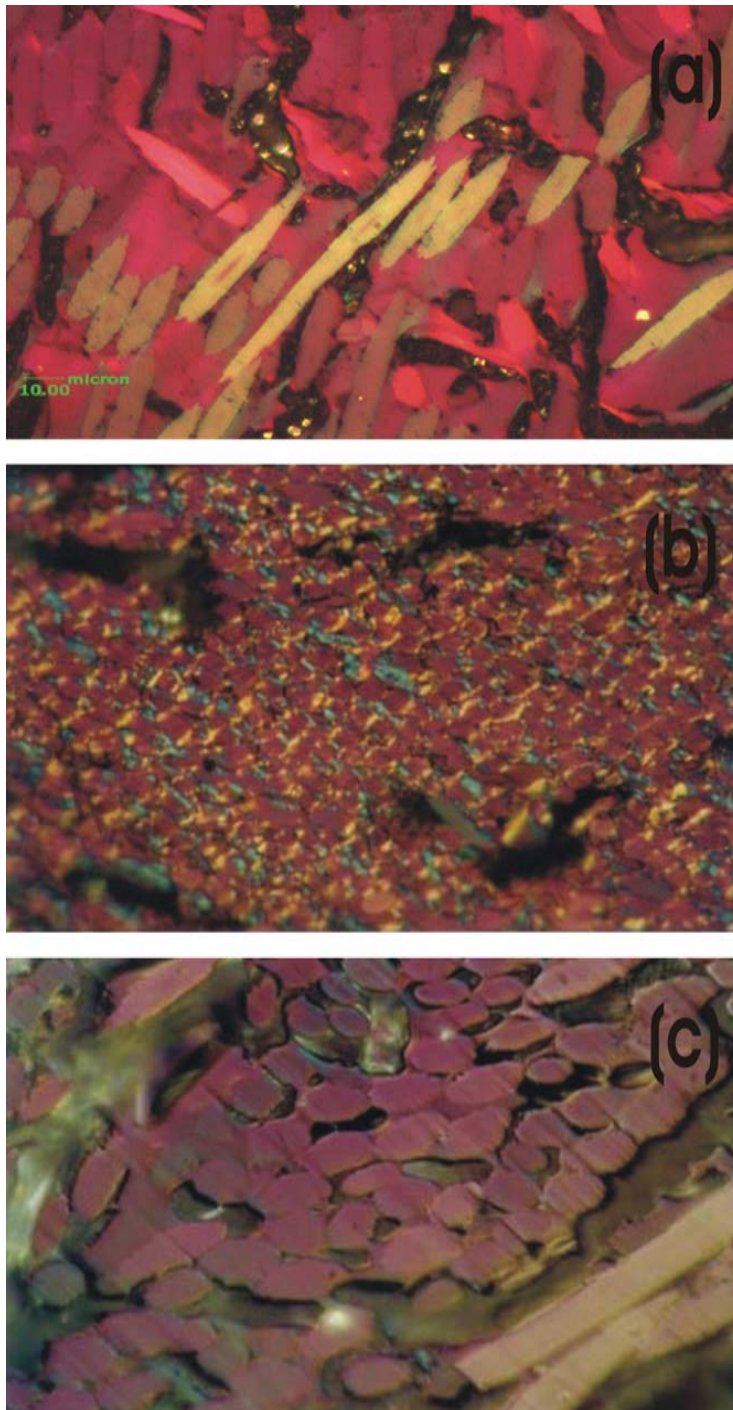


Fig. 3.11: Polarized optical micrographs of carbon composites made from (a) 20% PAN based carbon fiber, (b) 50% PAN based carbon fiber heat-treated at 1000°C and (c) 20% PAN fiber heat-treated at 1500°C

Here, the CB particles because of their near spherical geometry actually act as stress reliever as against the pointed fiber ends in carbon fiber based samples

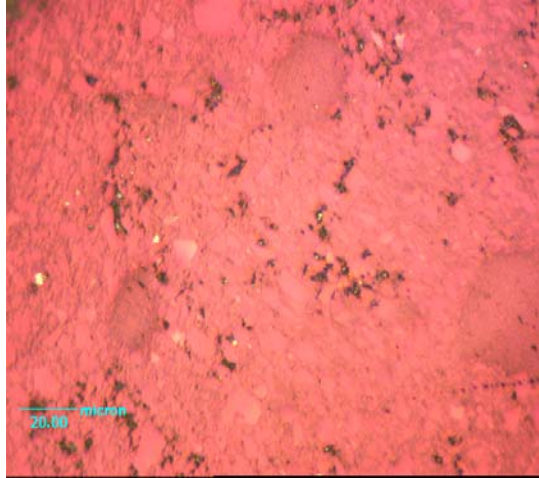


Fig. 3.12 (a): Optical image of the carbon black- resin carbon composite treated at 1000°C showing isotropy

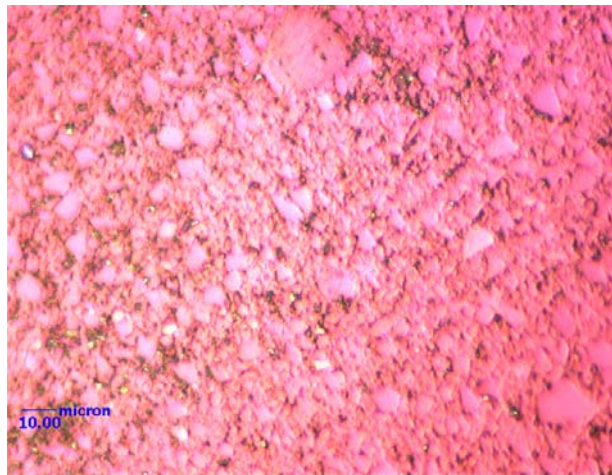


Fig. 3.12 (b): Optical image of the carbon black- resin carbon composite treated at 1900°C showing no development of anisotropy

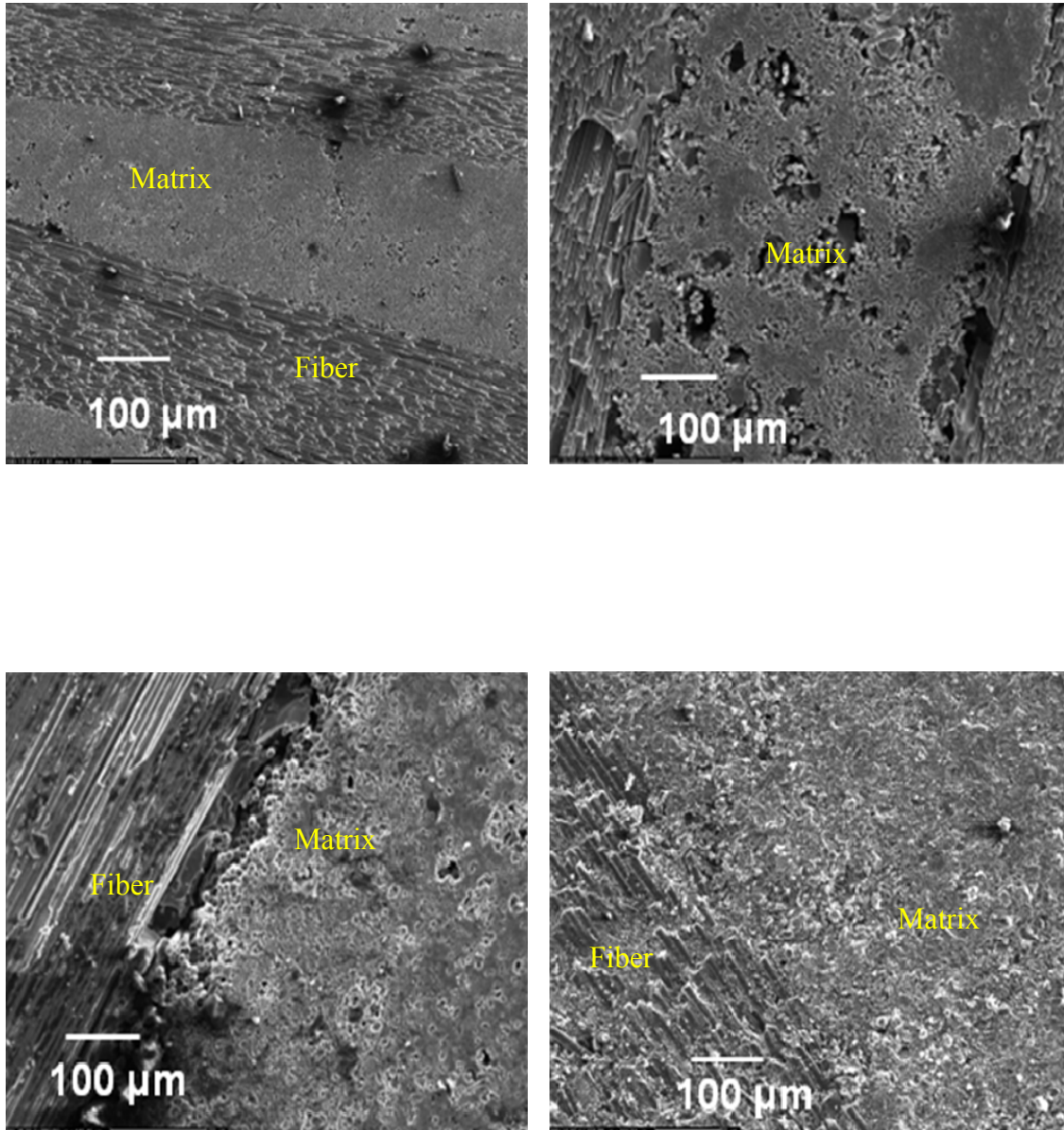


Fig. 3.13: SEM micrograph of C/C composites prepared using matted PAN fibers

The SEM images of C/C composites prepared using matted carbon PAN fibres densified by impregnation at varying pressure and time duration is shown in Fig. 3.13. The SEM micrographs of carbon/carbon composite as seen in Fig. 3.13 made by multiple impregnation, exhibits the various interfaces. The interfaces depend on the type of fibers,

matrix and the processing conditions. The interfaces of carbon/carbon composites are complex due to the presence of primary and secondary carbons derived from different precursors.

3.4.3. Tomography studies

Two types of carbon composites made up of carbon fibers and impregnated with phenolic resins to fill the pores present in the fibers with carbons have been taken for the tomography studies. These have been subjected to different pressures for densification. Sample (a) is prepared at a lower pressure (30bar) impregnation and sample (b) at a much higher pressure (50 bar) of impregnation. The dimension of the carbon composite was 11mm x 12mm x 6.4mm. 400 radiographs, each of 15 second exposure, were taken at 60kV and 400 to 450 μ A (keeping the wattage constant for constant flux during operation) setting of the micro focus source. The reconstruction grid dimension is 787x787x256 pixels. 3D Tomography studies on these C/C composites are shown in Figs. 3.14(a & b). The Fig.3.15 shows crack propagation in the X direction at different Y planes (specified in each image), due to application of pressure (encircled portion) and that it has pores of different distribution and gaps are present in between individual fibre layers.

When the individual carbon fibre layers are bonded with phenolic resins and densification done using external pressure, development of some crack or fissures might take place. It can be seen from the figures that the densification has take place for sample (a) density of 1310kg/m³, to sample (b) density 1470kg/m³. The sample (b) has lot more uniform structure throughout as seen in Figs. 3.16 and 3.17. Absence of large sized pores has also been visualized from this tomographs.



Fig. 3.14 (a): Reconstructed 3D image of sample (a)



Fig. 3.14(b): Contrast stretched 3D image showing individual fibres

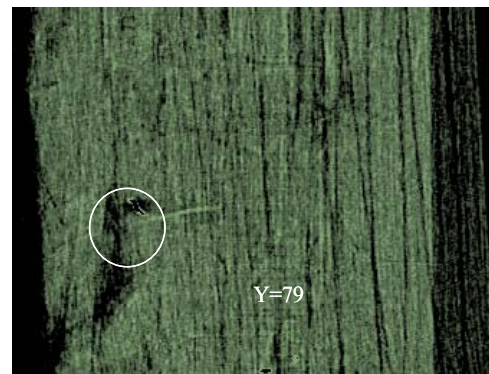
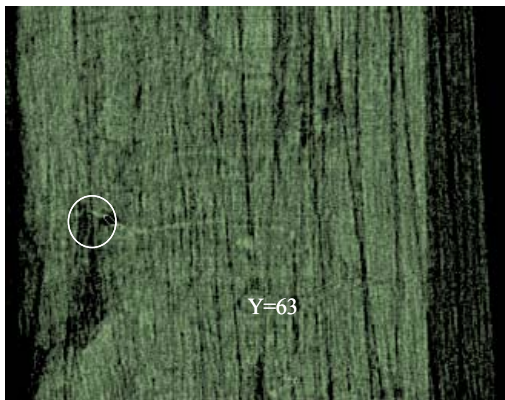


Fig. 3.15: Crack propagation in the X direction at different Y planes (specified in each image), due to application of pressure (encircled portion)

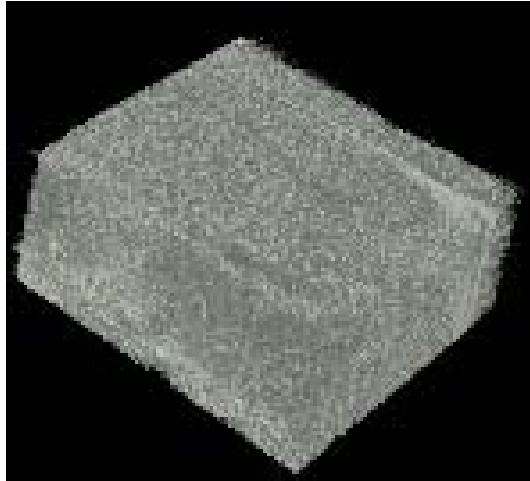


Fig.3.16: Reconstructed 3D image of sample (b)

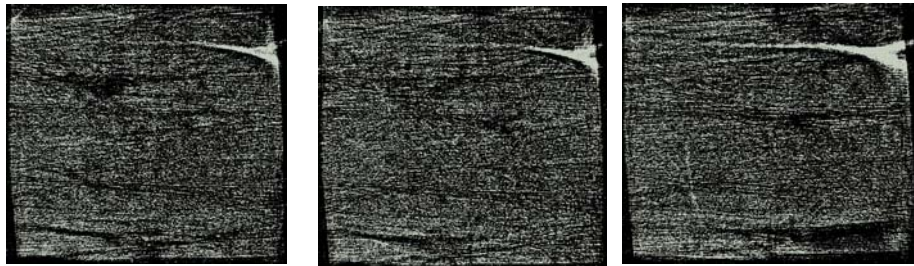


Fig. 3.17: The three images of XY slices at different Z points shows that the sample (b) has much more uniform bonding throughout as compared to sample (a).

3.5 Conclusions

Petroleum coke based samples were found to be amorphous at lower temperatures (below 800°C), but they tend to graphitize at higher temperatures. They also show the accumulation of Wigner energy, which prevents their use as neutron scatterer in Advanced Heavy Water reactor (AHWR). As these samples were found to be graphitizable in nature, next set of samples was made from chopped PAN fiber and phenol formaldehyde resin, which are nongraphitizable in nature. The composite with 20

vol% fiber was heat treated at 1000°C which showed desired properties in terms of amorphousness and isotropicity. Samples with 10 vol% fiber show development of crack during processing. Increase in the percentage of fiber volume enhances stress-graphitization as seen in the case of 50 vol% fiber based sample. The samples with 20 vol% fiber tended to develop anisotropy when heated to 2000°C.

Basically the shape of the fibers causes the development of stress at fiber matrix interface. This limitation was eliminated by choosing the spherical shape of the second phase (carbon black). Carbon black-phenolic resin composites have been prepared through a novel technique. The carbonization of the phenolic resin pieces prior to composite preparation helps in many ways. The shrinkage of the product was found to be less and lesser volatile matter was evolved during carbonization. Therefore the possibility of crack formation also reduces.

Hence higher rate of heating could be employed there by helping in the decrease in production cost. Composite with a density up to 1320 kg/m³ was obtained without any impregnation by this method as compared to 1270 kg/m³ with the PAN fiber based sample after four cycles of impregnation. Structural characterization suggests that the carbon black-phenolic resin carbon composite fulfills the criterion of the scattering material. This material has to be densified to give irradiation stability. C/C composites with density of 1470 kg/m³ were developed with two cycles of impregnation and carbonization. These composites are amorphous in nature revealed by from the XRD even on heat treatment at 1800°C. Further work on irradiation stability was carried out to see the stability of the material under irradiation which is discussed in detail in the fifth Chapter.

CHAPTER 4

CHAPTER 4

THERMOPHYSICAL PROPERTIES AND SPECTROSCOPIC STUDIES ON CARBON/CARBON COMPOSITES

4. Introduction

The carbon fibre reinforced C/C composites are widely used materials for varied applications [3, 42-44] due to their excellent properties. They are chemically resistant and can be used at elevated temperature, bio-compatible and possessing pseudo-plastic fracture behaviour. Due to its excellent neutron scattering properties, graphite continues to be the unanimous choice for the moderator material in high-temperature nuclear reactors [6, 9] where the aforesaid drawbacks are essentially overcome due to high-temperature annealing. Carbon is used as moderator and reflector due to its neutron interaction characteristics, heat transfer properties, corrosion resistance, stability under irradiation, mechanical strength, low atomic weight with high neutron scattering probability, low capture probability combined with its lower cost and easy availability makes carbon an attractive choice. Carbon in various forms has been used in nuclear reactors and there has been a growing interest to develop graphite and carbon based materials for upcoming high temperature nuclear and fusion reactors. C/C composite materials compared to conventional graphite materials are now considered as the promising materials for the fusion reactor due to their excellent properties of high thermal conductivity and high thermal resistance.

Research on carbon materials with high density and amorphous isotropic carbon for its use in thermal reactors to avoid accumulation of Wigner energy [3] is also being carried out. Samples have been prepared with matted PAN fibers in phenolic resin

matrix. All these samples have been characterized for their density, microstructural and thermophysical properties.

There are three known conventional methods of manufacturing C/C composites. They are chemical vapour deposition (CVD), pyrolysis of thermoset and thermoplastic resin and pyrolysis of hydrocarbon pitches derived from coal tar, synthetic mesophase products and petroleum. Most of the C/C composite work on thermoset resin has been carried out using phenolic resin because of its excellent char yield (about 65%) The amount of the matrix depends on the char yield. In the present studies C/C composites have been prepared using 2D matted PAN carbon fibers. The carbon preform was made using the matted carbon fibers and phenolic resin. This preform was carbonized to remove the volatile materials. During carbonization the resin releases moisture as the condensation by product during curing and pyrolysis hence controlled heating rate and evacuation of gases are required to avoid damaging the sample. Porosity is developed during carbonization which may be open or closed type.

The structural imperfections within the composite adversely affect the composite properties. The carbonized perform contains a lot of porosity and hence it needs to be densified using resin impregnation technique. This process aims at filling the open pores /void accessible to the impregnant and must be repeated several times to achieve the desired density. This consists of resin impregnation under pressure followed by curing and then carbonization. This process is repeated to improve the density. This chapter deals with the Raman spectroscopic analysis, SAXS and SANS studies and XPS studies of the C/C composite prepared from carbonized PAN fiber and phenol formaldehyde resin to evaluate the microstructural details and porosity in the composite materials.

4.1. Experimental

4.1.1. Preparation of Carbon/Carbon composite Samples

Four different types of composites were prepared for these studies i.e. petroleum coke based, carbon black/phenolic resin carbon black based, chopped carbon fiber reinforced and 2-D matted carbon fiber based composites. The petroleum coke and carbon black composites were prepared by mixing them with phenolic resin. Pellets were made using a uniaxial press under pressure. Chopped carbon fibers were dispersed in phenol formaldehyde resin matrix in different weight fractions (10-50%) and cast in a dye having 10 mm diameter and 10 mm height which was heat-treated. The 2-D preform of carbon composite was prepared by stacking the matted PAN fiber using phenol formaldehyde resin. The carbonized performs were then used for the studies. The carbonized sample is highly porous and it needs to be densified for any further application.

4.2. Thermophysical property measurement

4.2.1 CTE and Cp measurements

The results on the coefficient of thermal expansion (CTE) in the temperature range 100–550°C for the petroleum coke based samples heat treated at 800 and 1500°C are given in Table 4.1 along the two orthogonal directions. The values ($5.4 \times 10^{-6} \text{ K}^{-1}$ and $6.8 \times 10^{-6} \text{ K}^{-1}$) are not varying much for the sample treated at 800°C; but they vary ($3.8 \times 10^{-6} \text{ K}^{-1}$ and $6.8 \times 10^{-6} \text{ K}^{-1}$) for the 1500°C treated sample. This result indicates the development of anisotropy with heat treatment at higher temperature for the samples.

The values of the specific heat C_p in the temperature range of 50-500°C for the samples heat treated at different temperatures are also given in Table 4.1 which reveals that the C_p decreases with heat treatment temperatures as the sample tends to graphitize. The compressive strength of the samples with 25% binder is also given in Table 4.1 at different heat treatment temperatures. The higher the density the greater is the compressive strength.

Coefficient of thermal expansion (CTE) along two mutually perpendicular directions has been recorded for the carbon fiber based samples and is presented along with that of the standard coke sample in Fig. 4.1(a & b). It is observed that CTE^{\parallel} increases while CTE^{\perp} first increases and then steadily decreases with wt% of fiber in carbon fiber samples. In case of CB samples, CTE^{\parallel} varies rather irregularly while CTE^{\perp} exhibits an increasing trend with wt% CB for a given percentage of binder. However, it may be noted that for the entire range of composition studied CTE values for both carbon fiber and CB samples are very considerably lower than the standard coke sample as required for the proposed application. Moreover, CTE^{\parallel} and CTE^{\perp} values differ significantly in the standard coke sample implying development of anisotropic graphite phase in it, whereas there is not much of difference in the values for the CB and carbon fiber samples except for the 50% fiber composition. The mean values of coefficient of thermal expansion for the fiber based samples in two orthogonal directions in the temperature range of 100-550°C are given in Table 4.2. It is clear from the table that the 50 vol% fiber based sample is more anisotropic in nature than the other samples. It is observed from Table 4.2 that the samples are having higher specific heat than the

graphite structure (around 0.8 J/g/K). The specific heat is the lowest for the 50 vol% sample among these fiber based samples.

Table 4.1: Thermo-mechanical properties of heat treated petroleum coke based samples

Parameters	Heat treatment temperature (°C)			
	800	1000	1200	1500
Specific Heat $\text{Jkg}^{-1}\text{K}^{-1}$ (50-500 °C)	0.9-2.0	0.8-1.7	0.8-1.8	0.8-1.7
CTE ($10^6/\text{K}$) and \perp directions	5.4 & 6.8	Not measured	Not measured	3.8 & 6.8
Compressive strength (MPa)	36	41	42	41

Table 4.2: Characteristics of fiber based samples

Parameters	Fiber volume percentage			
	10	20	30	50
Specific Heat $\text{Jkg}^{-1}\text{K}^{-1}$ (50-500°C)	1.71	1.12	0.97	0.84
CTE ($10^6/\text{K}$) and \perp directions	1.6 & 2.1	2.5 & 3.1	1.9 & 2.4	1.1 & 5.2
Compressive strength (MPa)	11	32	30	42
d_{002} (Å)	3.50	3.49	3.48	3.377
Degree of graphitization	0	0	0	73

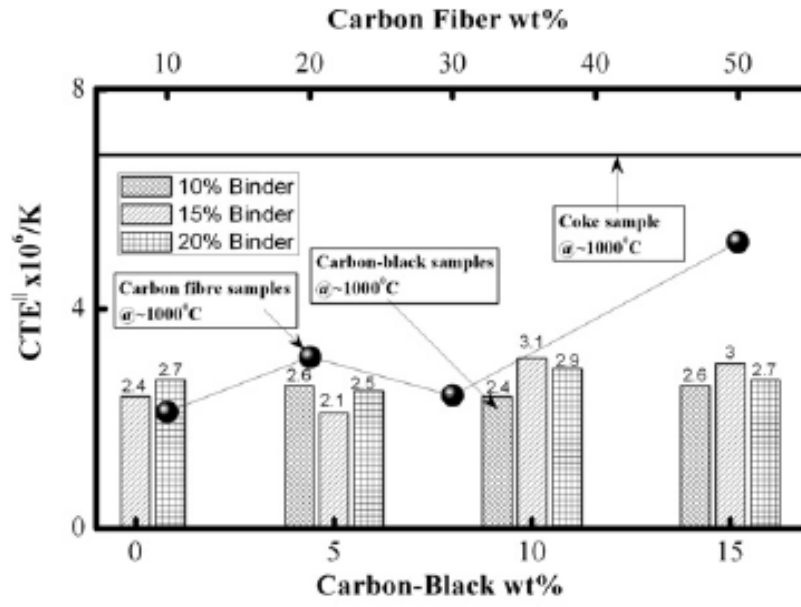
The specific heat of the CB samples was measured in the temperature range of 50-550°C. Sample S1 is without carbon black and it has the lowest specific heat among the various samples. This indicates that the presence of carbon black increases the specific heat values. The variation in density, open porosity and the compressive strength of different samples is given in Table 4.3. It was found that the sample with 15% carbon black and 15% binder has the maximum compressive strength of 65 MPa.

Specific heat (C_p) data were obtained using a differential scanning calorimeter (DSC). The mean specific heat values of the carbon fiber samples and CB samples with 15% binder composition over the temperature range of 50–550°C are shown in Fig.4.2. Samples with 15% binder have been typically chosen as they exhibit higher specific heat and excellent material properties over other binder compositions. Mean specific heat decreases drastically from 1710 to 1120 $\text{Jkg}^{-1}\text{K}^{-1}$ as fiber increases from 10 to 20% and then tends to saturate at higher wt% of fiber. In contrast, specific heat first increases significantly from 1210 to 1700 $\text{Jkg}^{-1}\text{K}^{-1}$ upon addition of 10% carbon black and then decreases at higher wt.% of CB. It is well known that higher specific heat minimizes the risk of suddenly releasing Wigner energy. The arrows in the graph describe the mean (1250 $\text{Jkg}^{-1}\text{K}^{-1}$), upper (1700 $\text{Jkg}^{-1}\text{K}^{-1}$) and lower (800 $\text{Jkg}^{-1}\text{K}^{-1}$) limiting values of specific heat for the standard coke sample in the specified range. Although the mean values are slightly lower for carbon fiber samples, they are very much on the higher side for CB samples as compared to the standard. In addition all the data points for both the samples measured in the specified temperature range lie within the limiting band for the standard sample.

Table 4.3: Variation of density, open porosity and compressive strength of the composites with carbon black and binder composition

Sample	Carbon black (%)	Binder (%)	Density (g/cc)	Open porosity%	Compressive strength (MPa)
S1	0	15	1.285	27	35.2
S2	0	20	1.230	31	18.4
S3	5	10	1.185	29	11.5
S4	5	15	1.295	20	54.7
S5	5	20	1.250	31	27.3
S6	10	10	1.245	30	24.5
S7	10	15	1.275	28	30.2
S8	10	20	1.290	28	55.5
S9	15	10	1.210	28	20.5
S10	15	15	1.320	24	65.0
S11	15	20	1.270	25	43.7

a



b

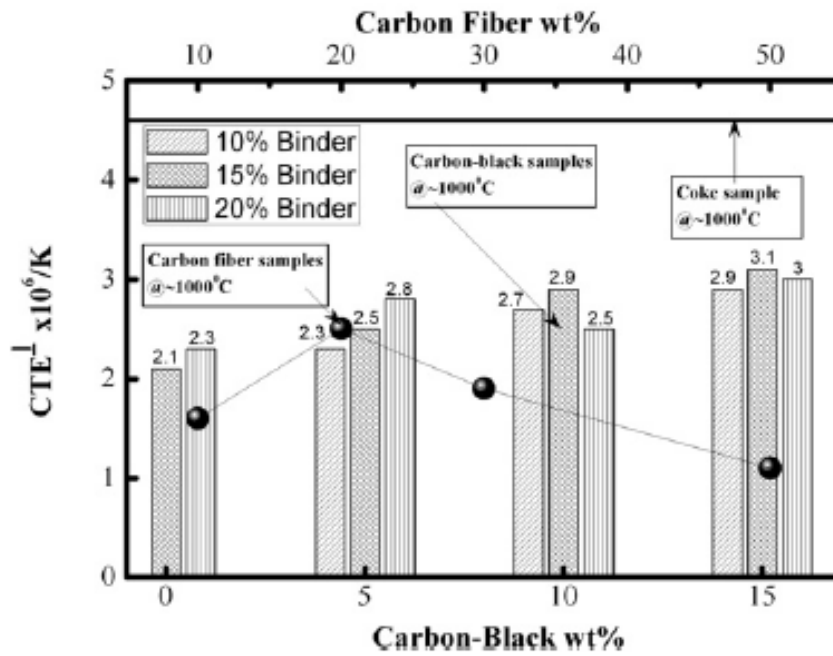


Fig. 4.1: Variation of coefficient of thermal expansion along (a) parallel and (b) perpendicular directions in PAN based carbon fiber and carbon black based samples as a function of their constituents

In the case of carbon composites prepared from matted PAN carbon fibers the coefficient of thermal expansion for the samples impregnated at 30 bar were measured using thermo-mechanical analyzer, which revealed that the values ranged from $0.6 \times 10^{-6}/^{\circ}\text{C}$ to $4.58 \times 10^{-6}/^{\circ}\text{C}$.

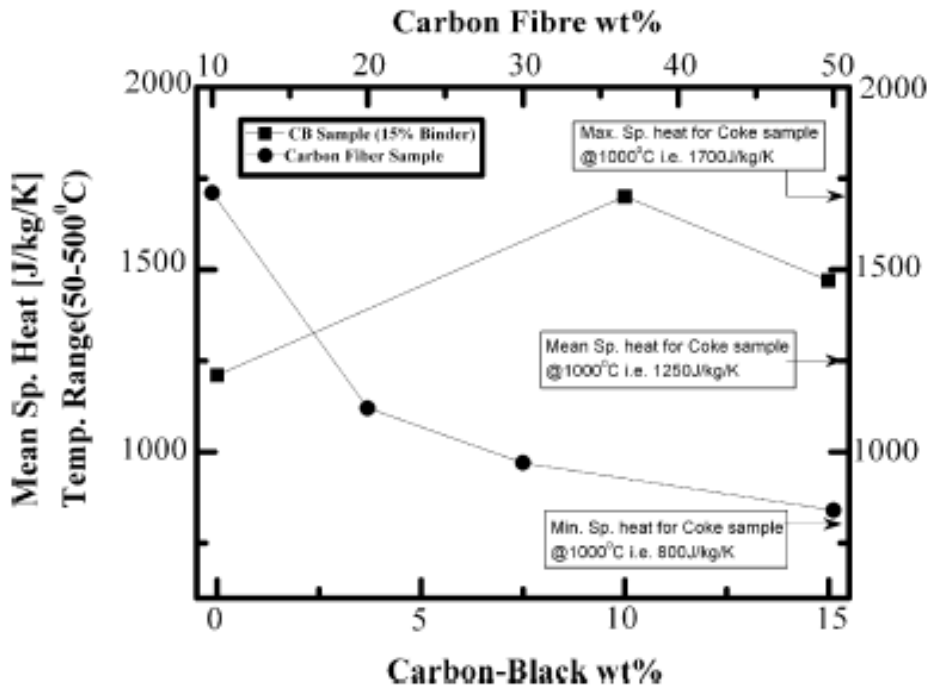


Fig. 4.2: Variation of specific heat in the temperature range of 50 -500°C for both PAN carbon fiber and carbon black based samples as a function of their constituents

4.2.2. Compressive strength measurement

Compressive strength measurements were carried out using a dilatometer and a universal testing machine. The variation in compressive strength of the same set of samples as a function of their constituents is shown in Fig. 4.3. The dotted line as in the previous graph represents the standard coke sample. It was found that the trend is the

same as that was observed in the case of density. In case of CB samples, 15% binder yields the highest compressive strength irrespective of wt% of CB, while it was highest for 50% in the case of carbon fiber sample. The most significant observation was that compressive strength of the 50% PAN based carbon fiber sample and a few other CB samples far exceeded that of the standard coke sample.

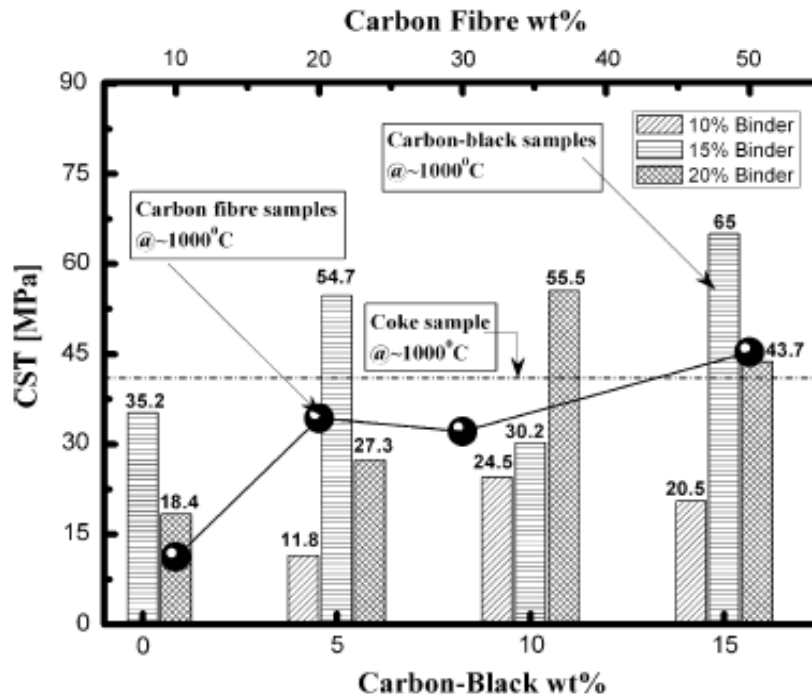


Fig.4.3: Variation of compressive strength in both PAN carbon fiber and Carbon Black based samples as function of their constituents

4.3. Raman Spectroscopy studies

μ -Raman spectroscopy and X-ray photoelectron spectroscopy were used to find out whether there is a change in the sp^2/sp^3 hybridised carbon ratio in the composites prepared from PAN fibers after different cycles of impregnation. This was done to find out if graphitization has occurred during the densification process.

Raman spectroscopy was used for the structural analysis to find if graphitization was occurring during the processing of the samples. Raman spectra of standard graphitic sample show a strong and sharp peak at $\sim 1580\text{ cm}^{-1}$ corresponding to zone center vibrational mode of E_{2g} symmetry labeled 'G' peak and a hump at $\sim 1355\text{ cm}^{-1}$ called 'D' peak, assigned to have originated due to the disorder, induced in the Lorentzian shape used to determine the peak position, FWHM and G/D ratio from the fitted parameters.

Raman spectra of most of the carbon-graphite materials contain two peaks at around 1580 and 1360 cm^{-1} , except for natural graphite, which has a single sharp Raman band at 1580 cm^{-1} . The 1580 cm^{-1} peak is known to correspond to the graphite structure and the 1360 cm^{-1} peak is correlated with graphitized carbon structure and the ratio of the integrated intensities of the two peaks, I_{1360}/I_{1580} , can be considered to be a good parameter to estimate the degree of graphitization. The higher this ratio, the lower is the degree of graphitization.

Fig. 4.4 shows the micro Raman spectra of the samples made using varying percentage of carbon black with 15% binder. From the Lorentzian fitting the exact peak position from the FWHM and the D/G ratio was also obtained. It may be seen from the graph that both the 'D' and 'G' bands get broadened and D/G ratio increases in case of samples made from 0% and 5% of CB as compared to that of graphite, implying significant disorder in the samples.

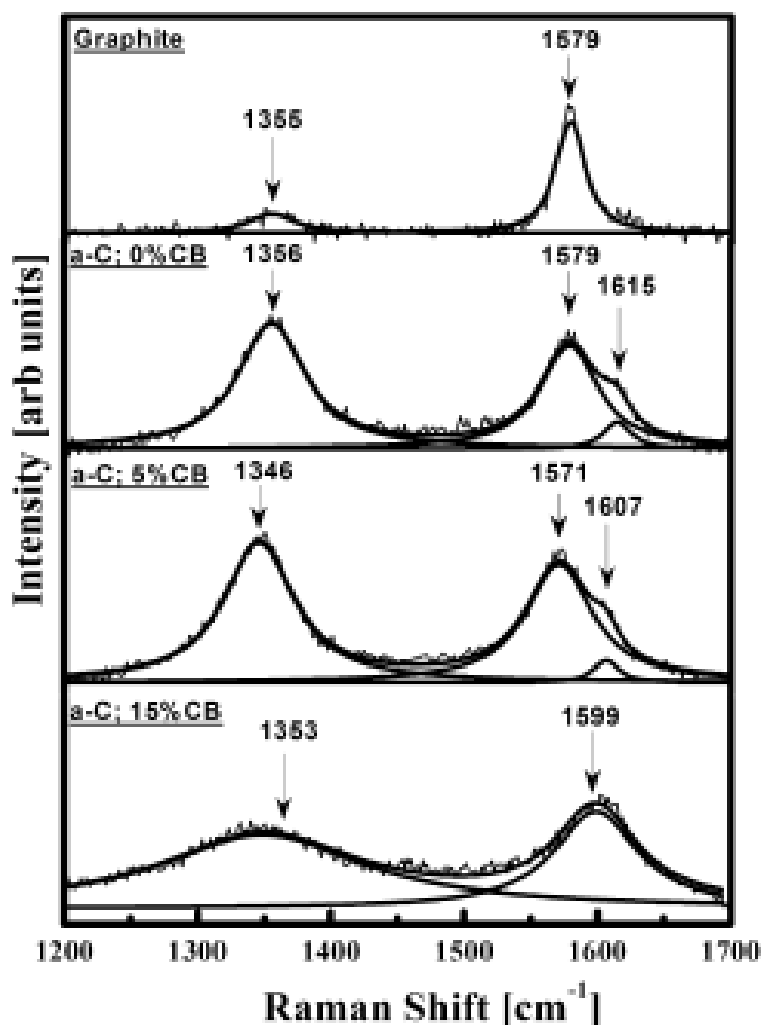


Fig. 4.4: Raman spectra of carbon composites made with 0, 5 and 15 wt.% of carbon black (CB) along with graphite sample

Apart from the 'D' and 'G' bands, another band at 1610 cm⁻¹ that corresponds to the first order zone boundary phonon mode also appears in these samples. The bands are further broadened in case of samples made from 15% CB indicating an increase in their amorphous nature with increasing weight percentage of CB. Fig. 4.5 shows the Raman spectra of 15% CB sample before and after impregnation cycle. No appreciable change in the Raman profile could be observed following impregnation of the samples.

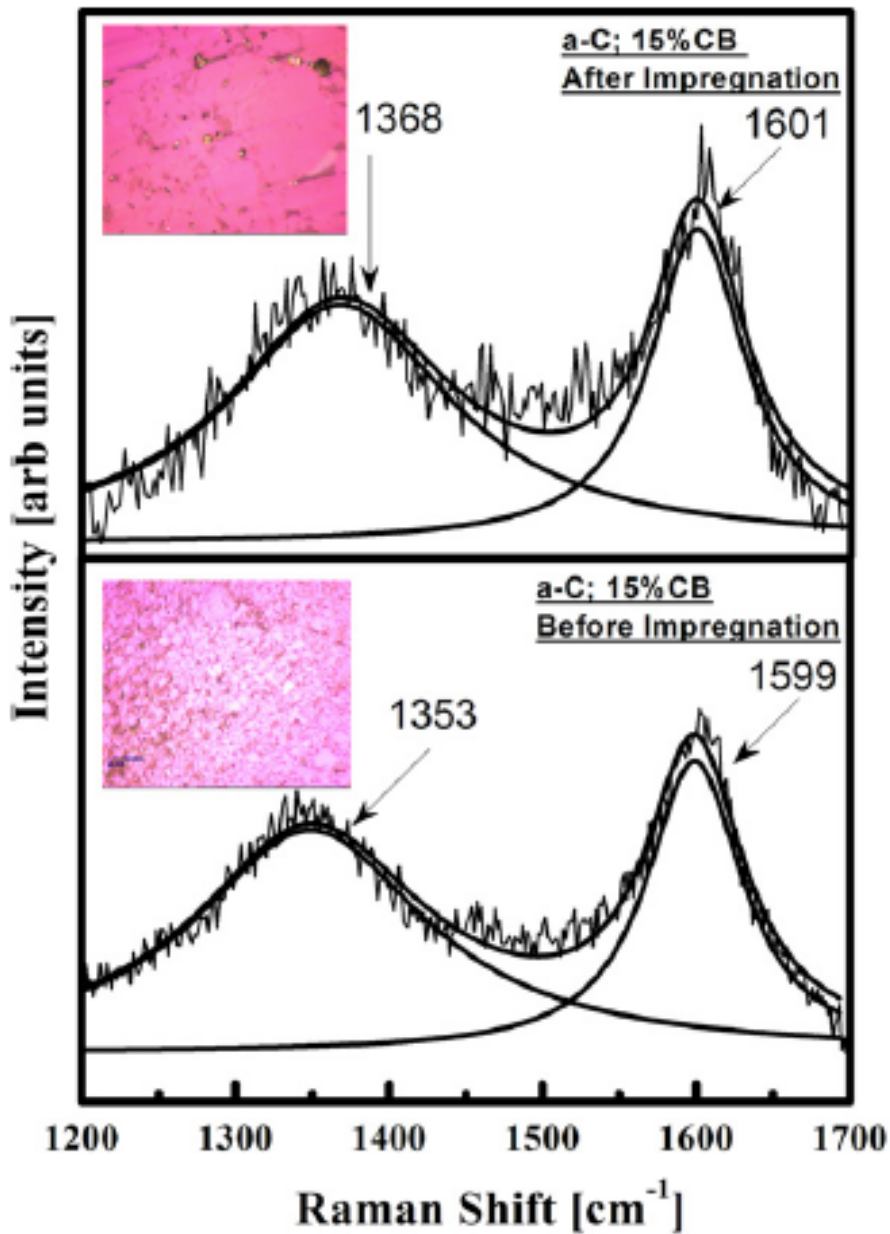
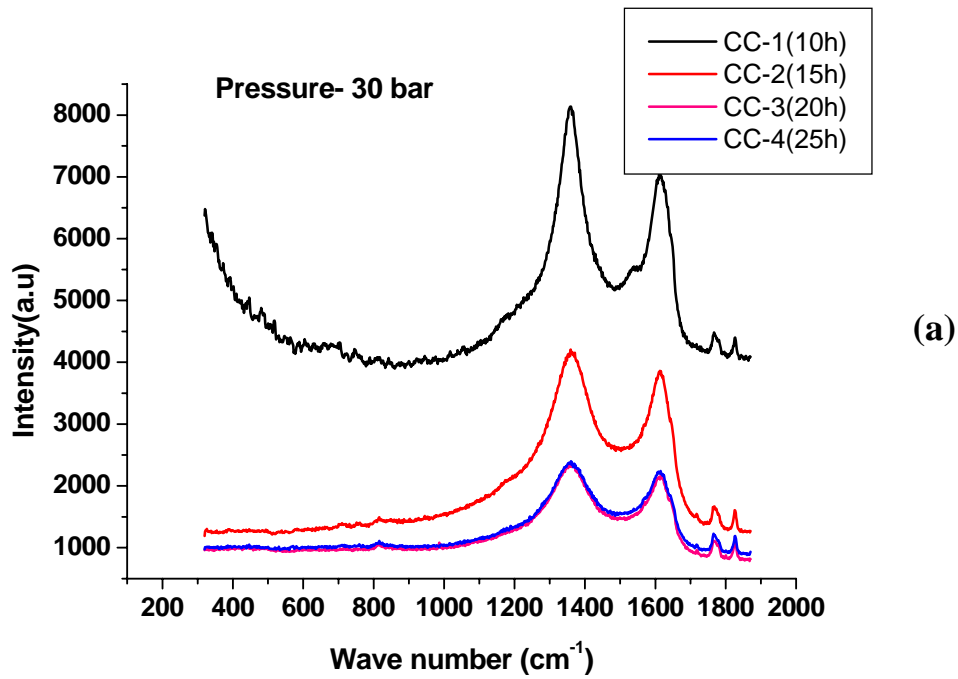


Fig. 4.5: Raman spectra of 15wt% CB composites before and after impregnation cycles. Inset: corresponding polarized optical micrographs

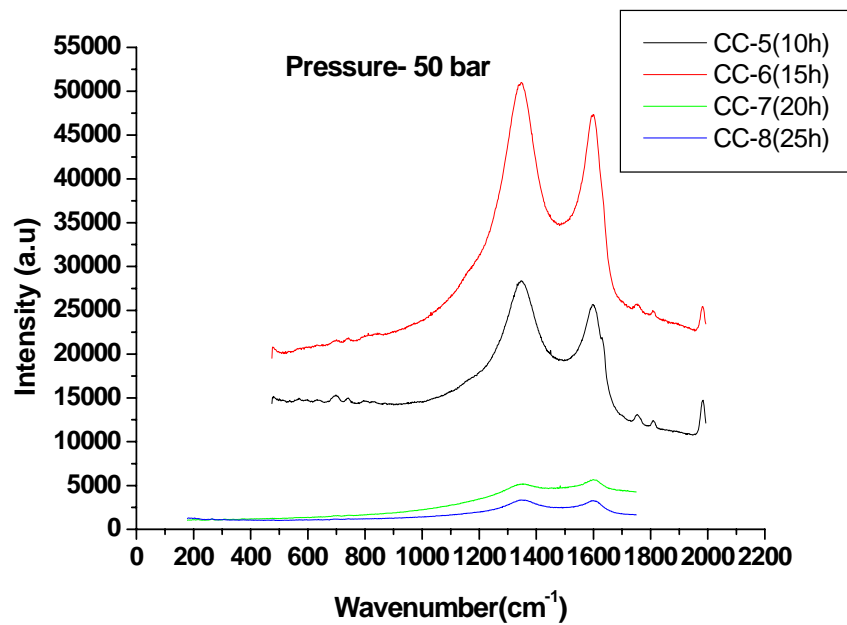
Fig.4.6 (a, b &c) shows the Raman spectra of a few representative samples of carbon composites prepared using the matted PAN matted fiber composites obtained after

impregnation at different pressures and for different impregnation period. They exhibit an intense peak at $\sim 1580 \text{ cm}^{-1}$ (G-peak) assigned to the zone centre E_{2g} mode of graphite. The peak arises due to the in-plane C-C vibration of the six-member aromatic rings present in the short range order of the carbon composites. They also exhibit a relatively broader peak at $\sim 1355 \text{ cm}^{-1}$ (D-peak). The D-peak is observed in defective graphite sample and is believed to have originated from disorder induced in the samples along its graphitic planes [67].

It is known from the literature that with decreasing long-range order in graphitic materials (i.e. with amorphization), D-peak intensity relative to that of G-peak (i.e., D/G ratio) increases, often exceeding that of the latter. The G-peak is associated with the relative motion of sp^2 -C pairs irrespective of their configuration (cluster or open chain) and is not significantly affected by the introduction of defects. However, the intensity of the D-peak relative to that of the G-peak i.e. D/G increases as the D-peak strength changes with the introduction of defects. Hence, in a completely disordered amorphous structure, if local ordering of sp^2 -C takes place (e.g. due to graphitization), D/G ratio should go down. Similar observation was reported previously for carbon black samples [68].

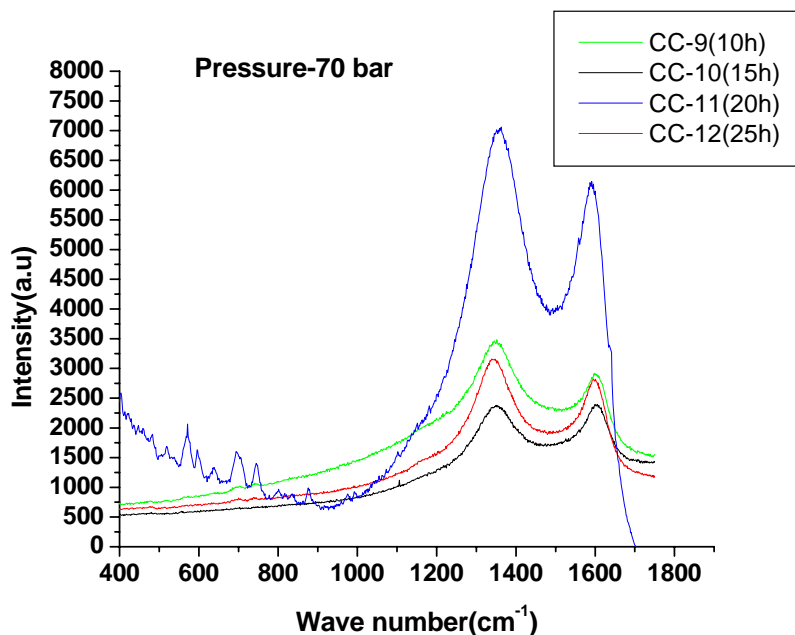


(a)



(b)

Fig. 4.6(a) and (b): Change in intensity vs wave number for impregnation carried out at (a)30 bar pressure and (b)50 bar pressure



(c)

Fig. 4.6(c): Change in intensity vs. wave number for impregnation carried out at 70 bar pressure

In order to extract quantitative information regarding peak position, FWHM and D/G ratio, the Raman spectra of the samples were fitted with multi-Lorentzian line shape after correcting the background. It may be noted that two Lorentzian peaks centered at D-band and G-band did not produce a good fit to the raw data. Hence, two more Lorentzian peaks centered at $\sim 1180\text{cm}^{-1}$ and 1540cm^{-1} were added to take care of the residual contributions from different types of carbon structures present in the composite samples. The peak at $\sim 1180\text{cm}^{-1}$ arises because of the possible presence of sp^3 -carbon rich nano-crystalline and/hexagonal diamond phase while that at $\sim 1540\text{cm}^{-1}$ is due to the semicircular stretching of the aromatic rings. During fitting, either position or width of the broad peak at $\sim 1180\text{cm}^{-1}$ was kept constrained at a time, while the rest of the parameters were allowed to vary freely.

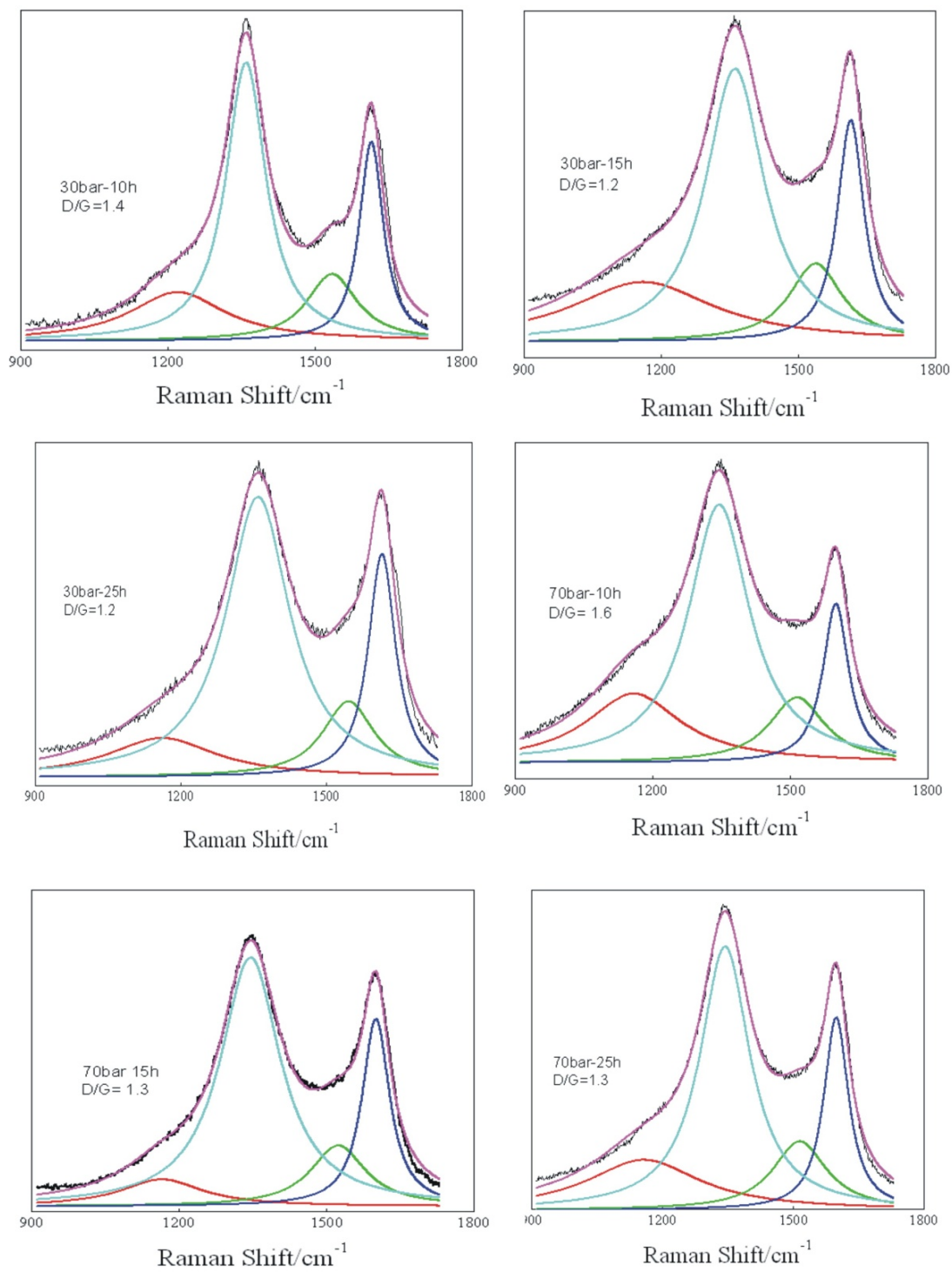


Fig. 4.7: Raman spectra for few representative samples impregnated at 30 bar and 70 bar pressure for varying time duration

For calculating D/G ratio, we have taken ratio of the height of the D and G peaks instead of their area. Fig. 4.7 shows the variation of D/G ratio with time of impregnation for the two extreme pressures used. For better comparison of data from two sets of samples, D/G ratio was normalized to their respective values after 10h of impregnation. The value decreases, more sharply at higher pressure, and then becomes steady after 15h of impregnation. It indicates that during the high-pressure densification process graphitization has taken place due to stress generated at open pores and the extent of graphitization is higher for higher impregnation pressure. However, it may be noted that μ -Raman provides only local information around the spot of shining of the laser and may not reflect the bulk properties of the samples.

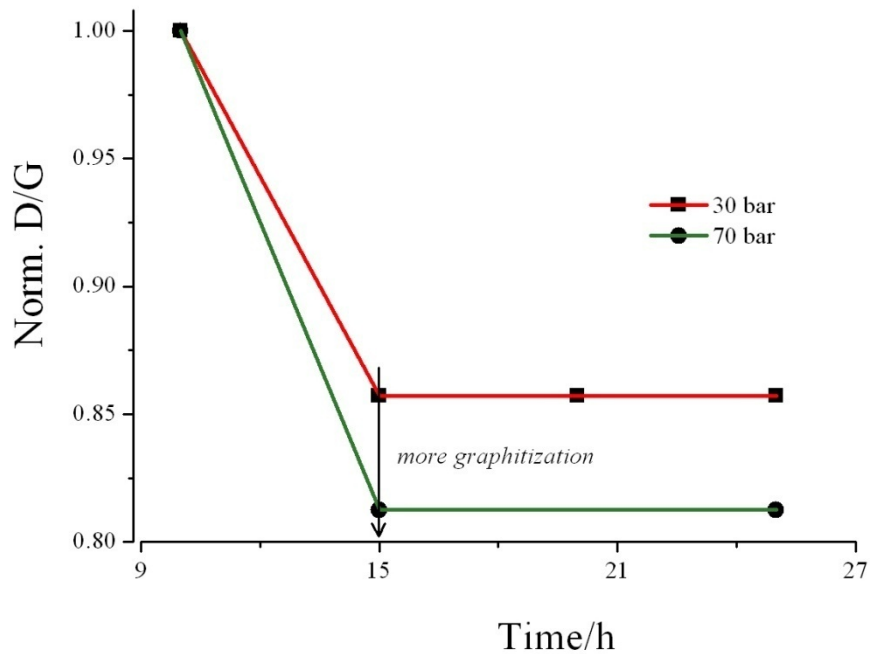


Fig. 4.8: Variation of D/G ratio with time of impregnation for two sets of representative samples showing greater extent of graphitization at higher pressure.

The variation in D/G ratio with impregnation for two sets of samples is shown in Fig. 4.8. It is observed that with increase in pressure of impregnation the graphitization also increases.

From Fig.4.6 and 4.9 it is seen that I_G/I_D ratio initially increases when pressure of impregnation is increased from 30 bars to 50 bars after which it decreases on further increasing the pressure to 70 bars in both cases i.e. for impregnation carried for 10h and 25 h respectively. The I_G/I_D ratio is higher in the impregnation carried out for 25h at 50bar indicating tendency to graphitize as compared to the impregnation carried out for 10h as shown in Table.4 4.

Table.4.4: Variation of I_G/I_D with Pressure at 10 h and 25 h of impregnation

S.No	Pressure(bar)	I_G/I_D	I_G/I_D
		10 h duration of impregnation	25 h duration of impregnation
1	30	0.76	0.63
2	50	0.78	0.88
3	70	0.65	0.63

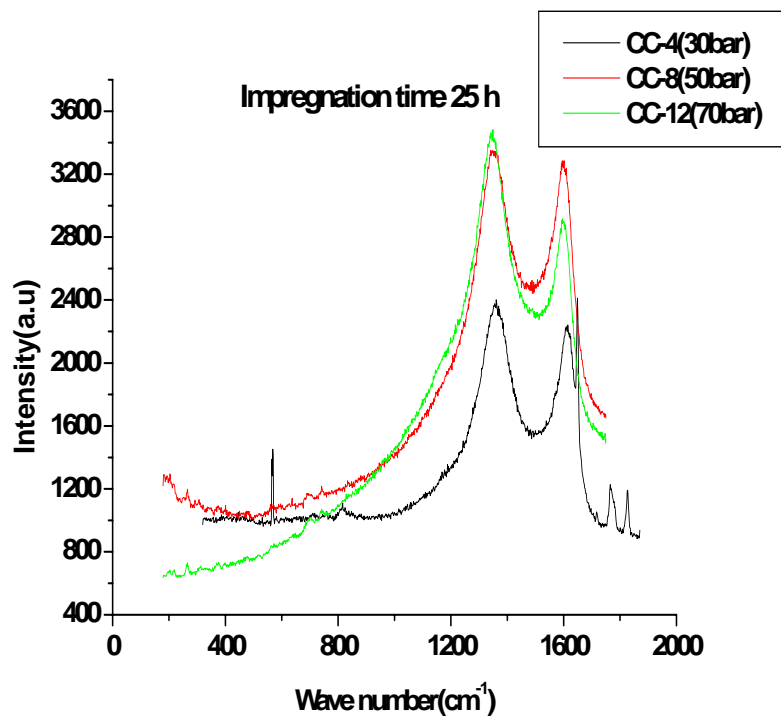
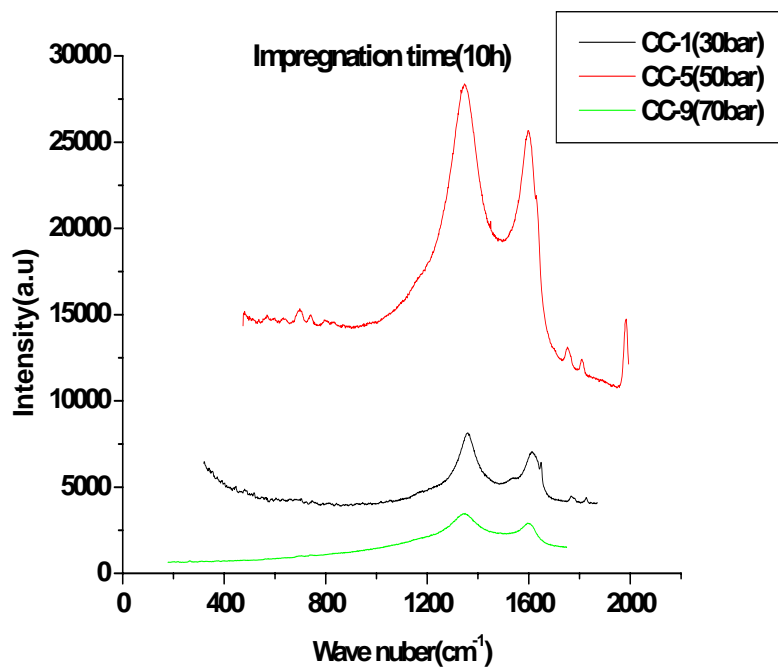


Fig. 4.9: Effect of pressure on structure of the C/C composite

4.4. X-ray Photoelectron Spectroscopy (XPS) Studies

It is a quantitative spectroscopic technique that measures the elemental composition, empirical formula, chemical state and electronic state of elements which exist in the material. The material is irradiated with X-rays while simultaneously measuring the K.E and number of electrons that escape from the top 1- 10 nm of material. Each element produces characteristic set of XPS peaks at characteristic binding energy values that directly identify the element present in the sample.

Another way to look at the problem is to monitor sp^2 -C/ sp^3 -C ratio using X-ray photoelectron spectroscopy. Fig. 4.10(a-g) shows the set of main core level C1s XPS spectra of two representative samples along with their deconvoluted features obtained by fitting the spectrum with line shapes having different Gaussian: Lorentzian ratios, after approximating the background contribution with a Tougaard-type baseline. All the parameters viz. peak position, FWHM and the area under the curves were taken for optimization as fixing any one of them would have made the quality of the fit worse. Small χ^2 values denote that the deconvoluted features nicely represent the raw data. Fitting was carried out with “XPS peak 4.1” software freely available in the web and the optimized values of the fitted parameters are tagged as insert on the respective curves in the figure. The C1s spectrum upon deconvolution exhibits four peaks at ~ 284.3 eV, 285eV, 288eV and 290eV. The peaks at ~ 283.4 and 285 eV are respectively attributed to sp^2 and sp^3 bonded carbon atoms. The other two peaks are due to carbon atoms associated with the ester or carboxylic groups formed upon oxidation of surface species. The ratio of the peak areas under the first two component curves provides a direct estimate of the sp^2 -

C/sp³-C carbon fraction in the composite. Fig. 4.11 shows Variation of sp²-C/sp³-C ratio indicating the extent of graphitization at two different impregnation pressures.

The ratio of sp²-C/sp³-C is higher for sample impregnated at higher pressure indicating greater extent of graphitization in it. Nevertheless XPS provides information only about the surface layers (depth resolution is only 3 nm) and does not reflect the bulk property of the composite.

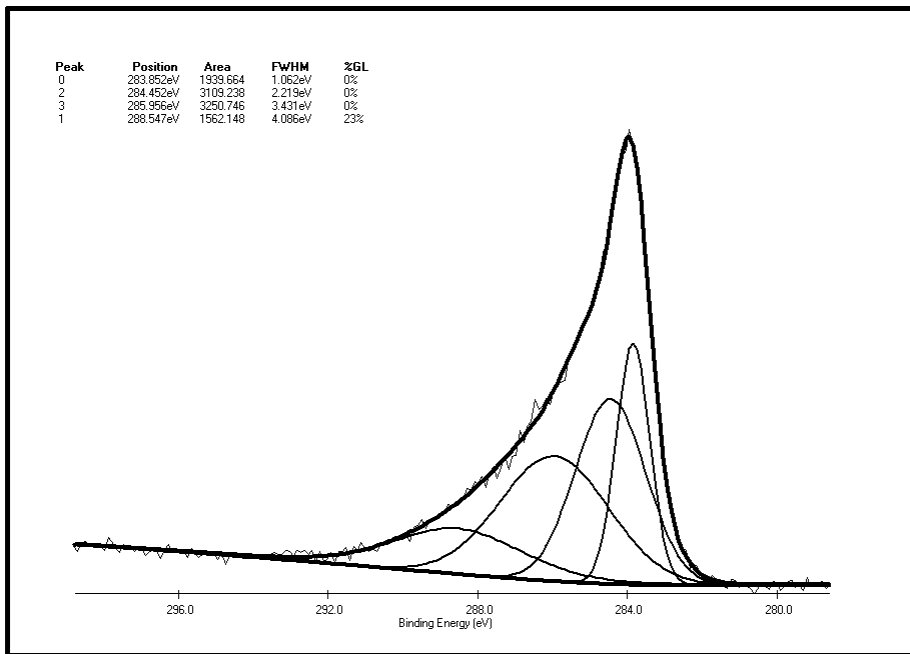


Fig. 4.10(a): XPS spectra of sample impregnated at 30 bar for 15 h $sp^2/sp^3 = 0.6$

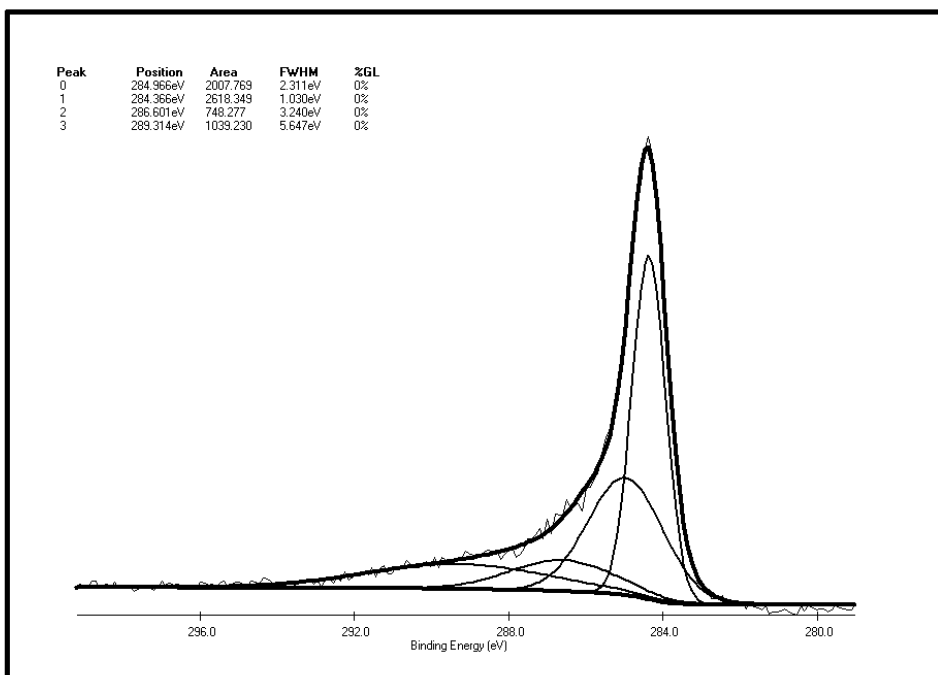


Fig. 4.10(b): XPS spectra of sample impregnated at 30 bar for 20 h $sp^2/sp^3 = 1.3$

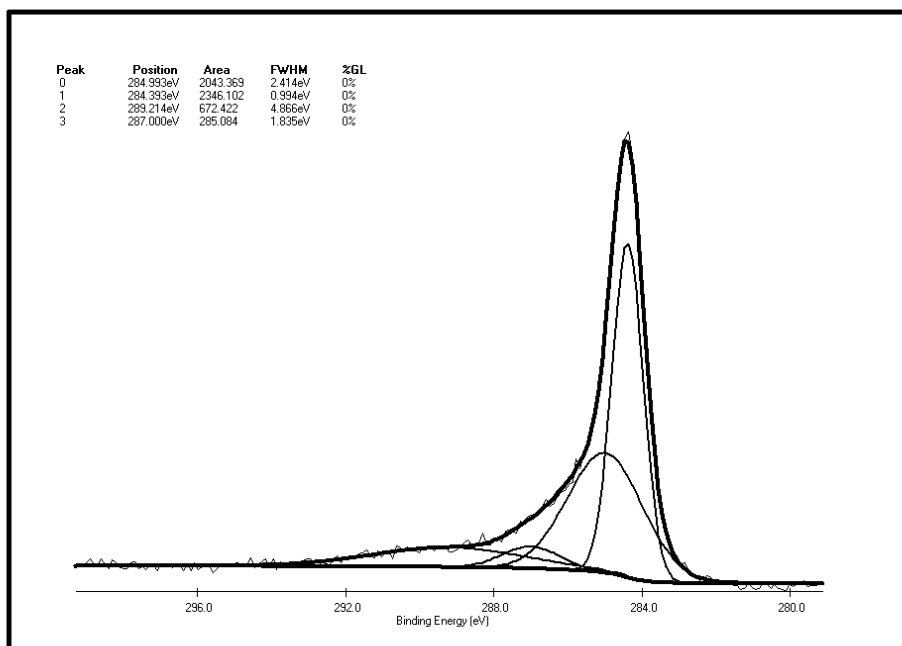


Fig. 4.10(c): XPS spectra of sample impregnated at 30 bar for 25 h $sp^2/sp^3 = 1.1$

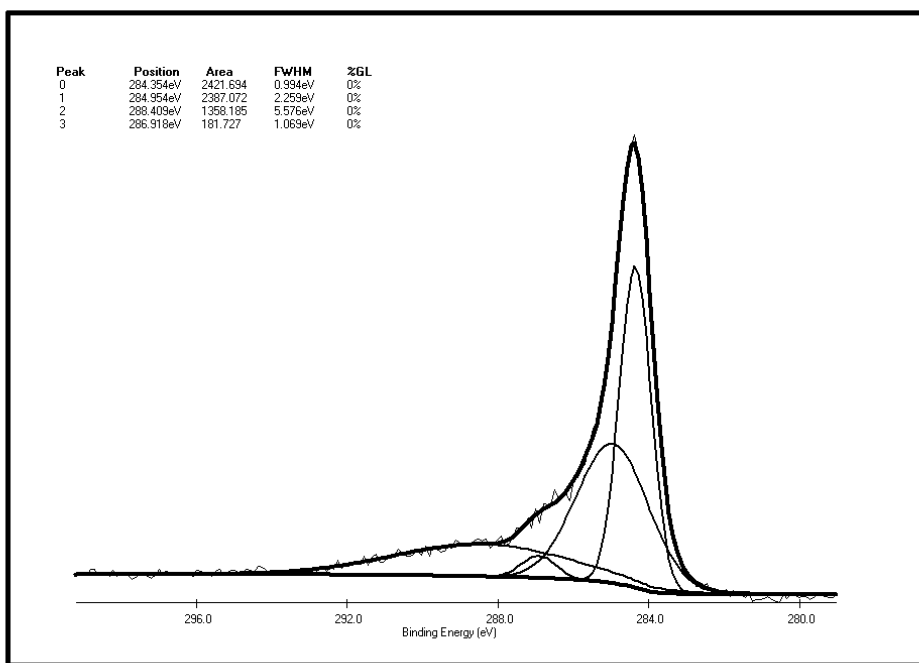


Fig. 4.10(d): XPS spectra of sample impregnated at 50 bar for 10 h $sp^2/sp^3 = 1$

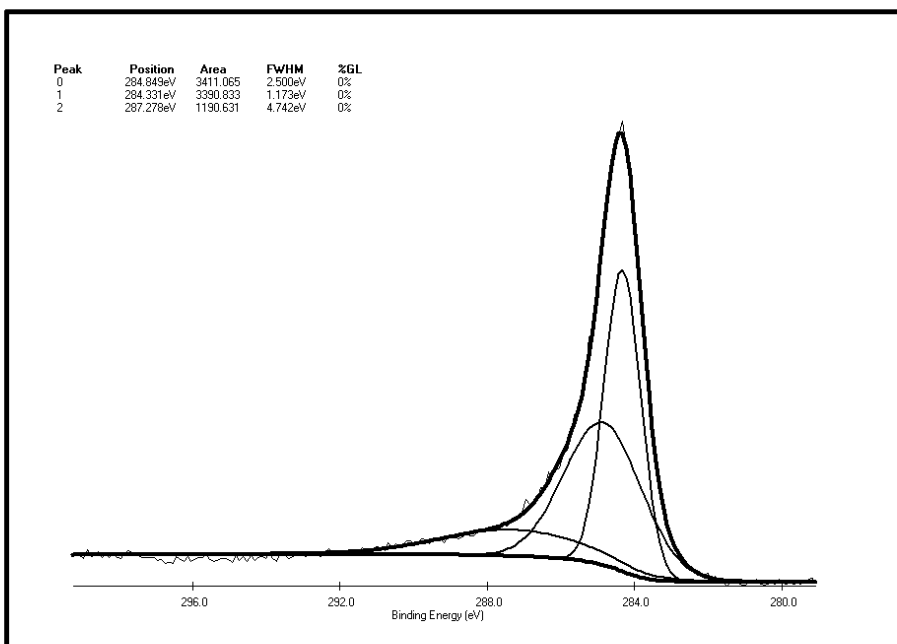


Fig. 4.10(e): XPS spectra of sample impregnated at 50 bar for 20 h $sp^2/sp^3 = 1.5$

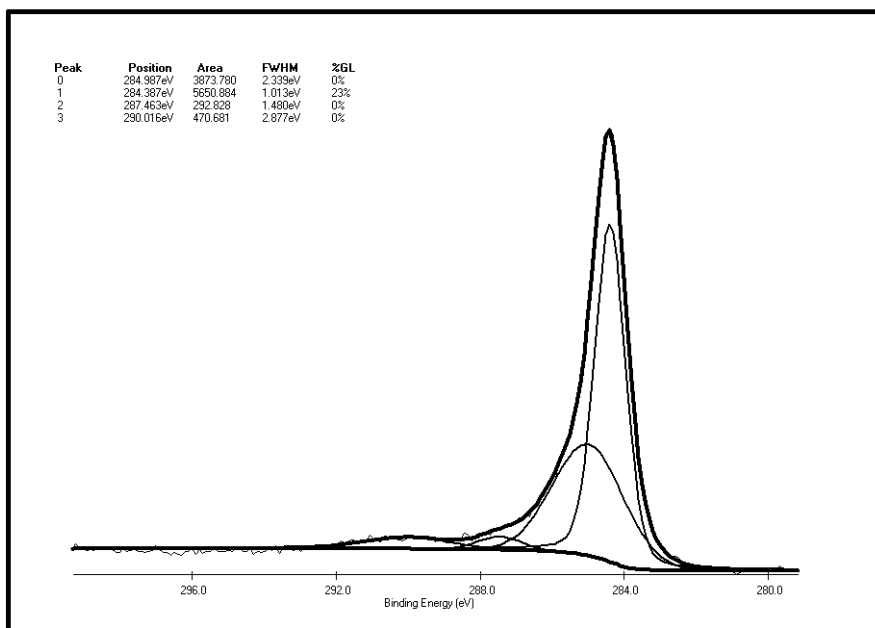


Fig. 4.10(f): XPS spectra of sample impregnated at 70 bar for 10 h $sp^2/sp^3 = 1.4$

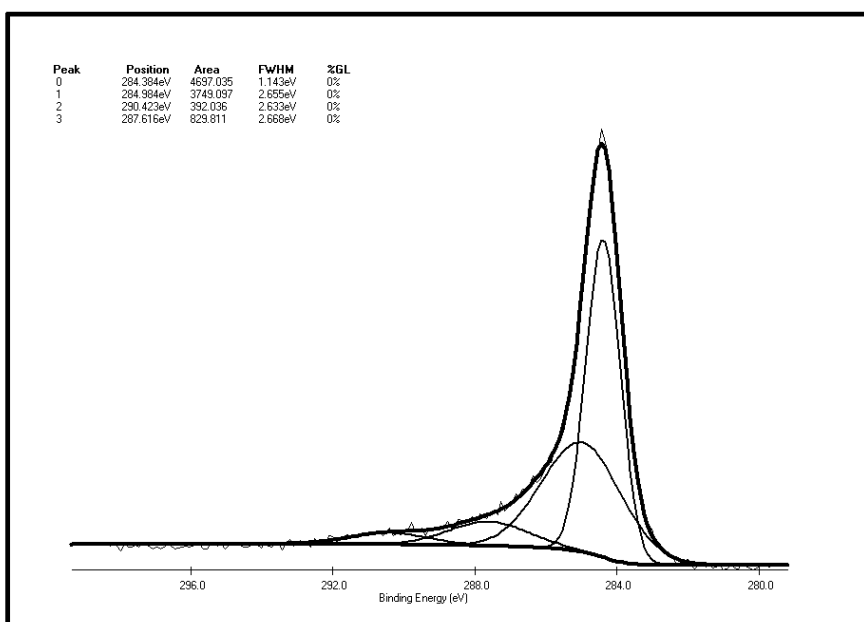


Fig. 4.10(g): XPS spectra of sample impregnated at 70 bar for 15 h $sp^2/sp^3 = 1.2$

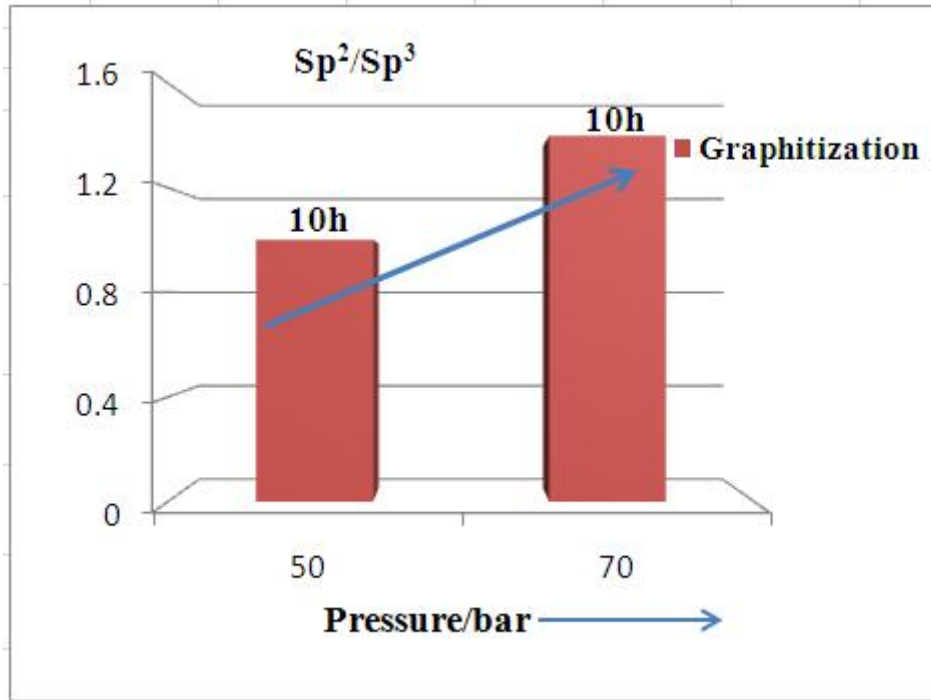


Fig. 4.11: Variation of sp²-C/sp³-C ratio indicating different extent of graphitization at two different impregnation pressures.

4.5. Small Angle Scattering Studies

Small Angle Neutron Scattering (SANS), unlike mercury intrusion porosimetry (MIP), is a non-destructive and non-intrusive technique used for pore size measurement in porous solids. Furthermore, SANS can probe open, closed and ink-bottle pores [66, 69]. Hence, SANS was used to find the effect of impregnation parameters (pressure and time) on the pore morphology of C/C composites. C/C composite specimens of 1.0cm x 1.0cm cross-section and 1.0cm and 0.5cm thicknesses cut from larger blocks were used for SANS experiments. A double crystal (Si (111)) based diffractometer (DCD) at Guide Tube Lab. of Dhruva reactor was used for SANS experiments [63]. SANS data were recorded over the accessible scattering wave vector 'q' ($q = 4\pi\sin\theta/\lambda$) range of 0.003nm^{-1} – 0.17nm^{-1} of the diffractometer.

It is clearly seen from Fig. 4.12 that the scattering profiles of 1.0 cm and 0.5 cm thick specimens of sample S1 are functionally different particularly, at low 'q' regime. The thickness dependence feature of profiles of S1 suggests that the scattering data contain a component of neutrons that have been scattered more than once [70, 71].

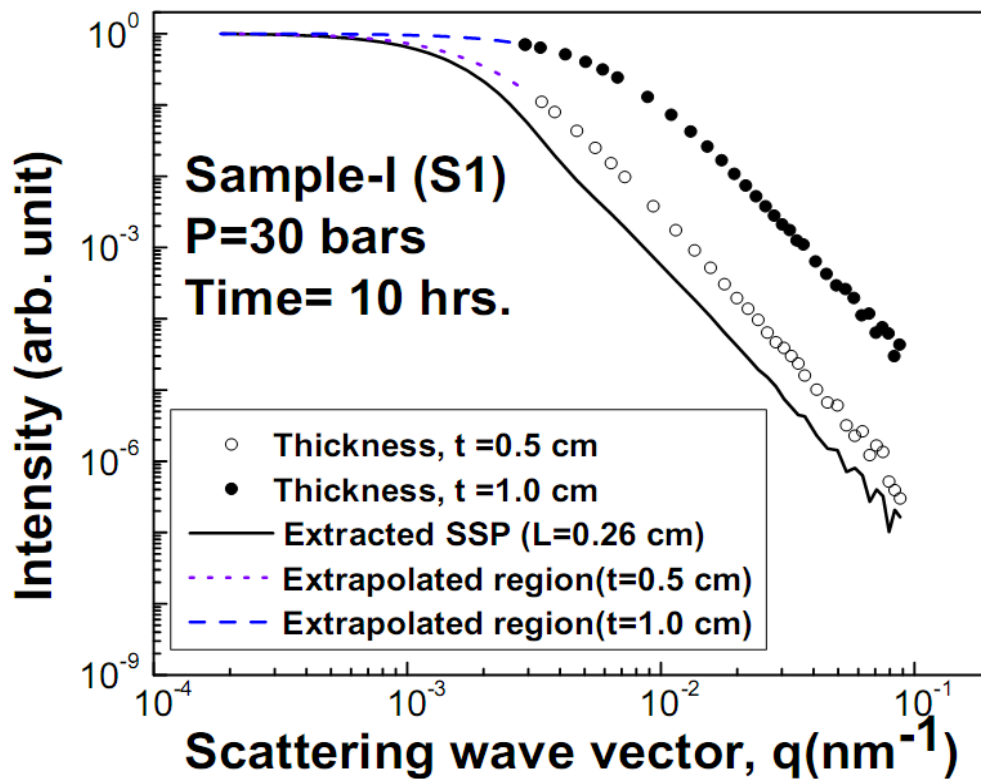


Fig. 4.12: Scattering profiles of 1.0cm and 0.5 cm samples.

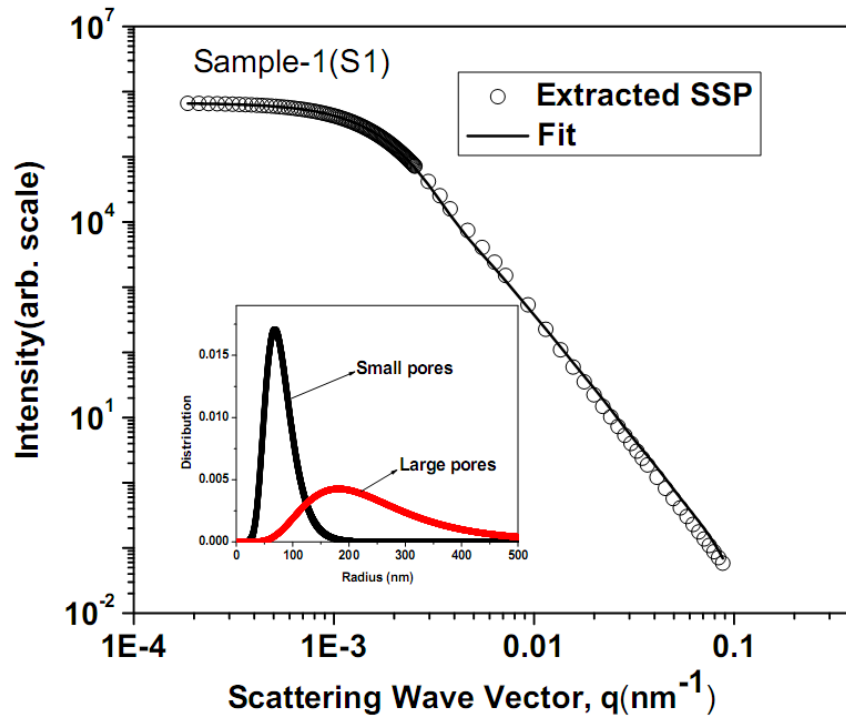


Fig. 4.13: SANS profiles with fit. Inset shows pore size distribution in two samples.

Due to such multiple scattering effects, profile of thicker (1.0cm) specimen has become broader than that of thinner (0.5cm) sample. In order to obtain correct real space information about pore morphology, the single scattering profile (SSP) as shown in Fig. 4.13 has been extracted by making use of the profiles of two different thicknesses [70, 71]. The same procedure has been adopted for samples 2 and 3 also. In Fig.4.14 only SSPs of samples 2 and 3 are shown.

After obtaining SSP for all the samples, SANS data have been modeled by assuming polydisperse ensemble of spherical pores following bimodal size distribution. The model profile, $I(q)$ in such a situation is expressed by

$$\begin{aligned}
I(q) = & c_1 \int_{R_{a \min}}^{R_{a \max}} P(q, R) D_1(R) (V(R))^2 dR \\
& + c_2 \int_{R_{b \min}}^{R_{b \max}} P(q, R) D_2(R) (V(R))^2 dR
\end{aligned} \tag{4.1}$$

Where, the first and the second terms of eq. (4.1) represent scattering contributions from large and small pores, respectively. Higher ‘q’ regime of all the profiles could only be fitted by taking contributions of small pores. P (q, R) and V(R) denote square of the form factor [62] and volume of the sphere of radius R, respectively. C₁ and C₂ are two scaling parameters associated with population of large and small pores, respectively. D₁(R) and D₂(R) denote size distributions for large and small pores respectively. Standard log normal function has been used for D₁(R) and D₂(R). D₁(R) and D₂(R) of different samples are shown in the insets of Figs 4.13 and 4.14

It could be noticed from Fig.4.14 that for S2 and S3 increase in impregnation time does not show any change in small pores size distribution D₂(R). SANS investigations reveal that there is reduction of pore size in the C/C composites with increase in both impregnation pressure and time.

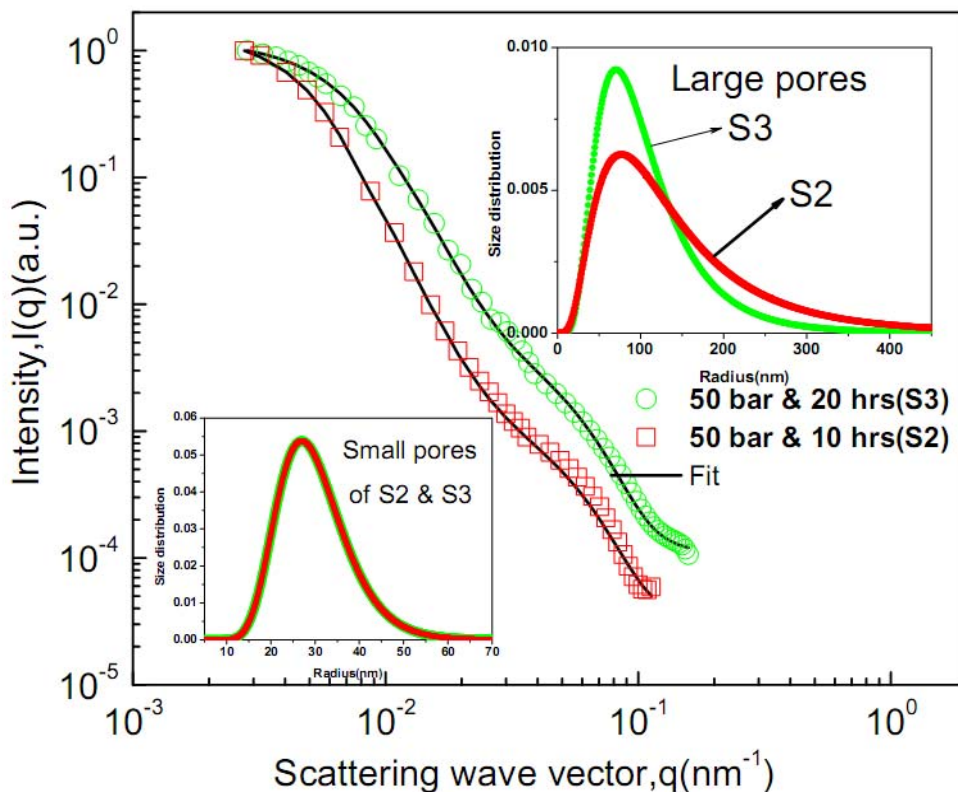


Fig. 4.14: SSPs of S2 and S3 with fit. Insets show comparison of their large and small pores size distributions.

Carbon based materials are useful in aerospace applications, for high-temperature nuclear and fusion reactors due to mechanical strength and thermal resistance. However, their durability gets affected due to pores created during constant exposure to radiations. Recently, high-dense fiber based carbon-carbon based composites are being developed for better properties and performance for these applications. In this work, we have examined the pore structure of neutron irradiated PAN carbon fiber-carbon composites using small angle x-ray scattering (SAXS) technique. Previous studies indicated increase in pore size in the carbon matrix with treatment at high-temperatures [72] and the irradiation makes the amorphous structure more ordered. The present samples were prepared using PANEX 35 carbon fibers

which were stacked in to 2-D using phenol formaldehyde resin (PFR) and carbonized at a heating rate of 0.1°C/min in inert atmosphere.

Samples were irradiated with thermal neutrons at APSARA reactor, BARC with a neutron flux of 10^{12} n/cm²/sec for 7h, 14h and 20 h [74]. SAXS experiments were carried out using SAXS set-up based on line-slit geometry, 12 KW Rigaku rotating anode x-ray source with CuK α radiation. The intensities $I(Q)$ (where Q is the scattering vector $4\pi\sin\theta/\lambda$) were corrected for absorption and slit-smearing effects. The SAXS profiles as displayed on log-log scale indicating linear profiles with two distinct slopes as seen in Fig.4.15. Thus, the intensity $I(Q)$ varies as a power-law $Q^{-\beta}$ with the value of β different at low- Q (larger pores) and high- Q (smaller pores) regions. For larger pores (of minimum size 40 nm), β changes gradually from about 3.8 to 4.05 with increase in irradiation time, suggesting an initial rough surface tends to smoothen with the irradiation.

On the other hand, the smaller pores show mass (pore) fractal nature with an average fractal dimension about 2.4. The lowering of intensity at low- Q with different irradiation timings indicates a relatively reduction in specific surface area of the pores due to increase in the average pore radius. These observations are expected to have considerable impact on the mechanical properties of the composites.

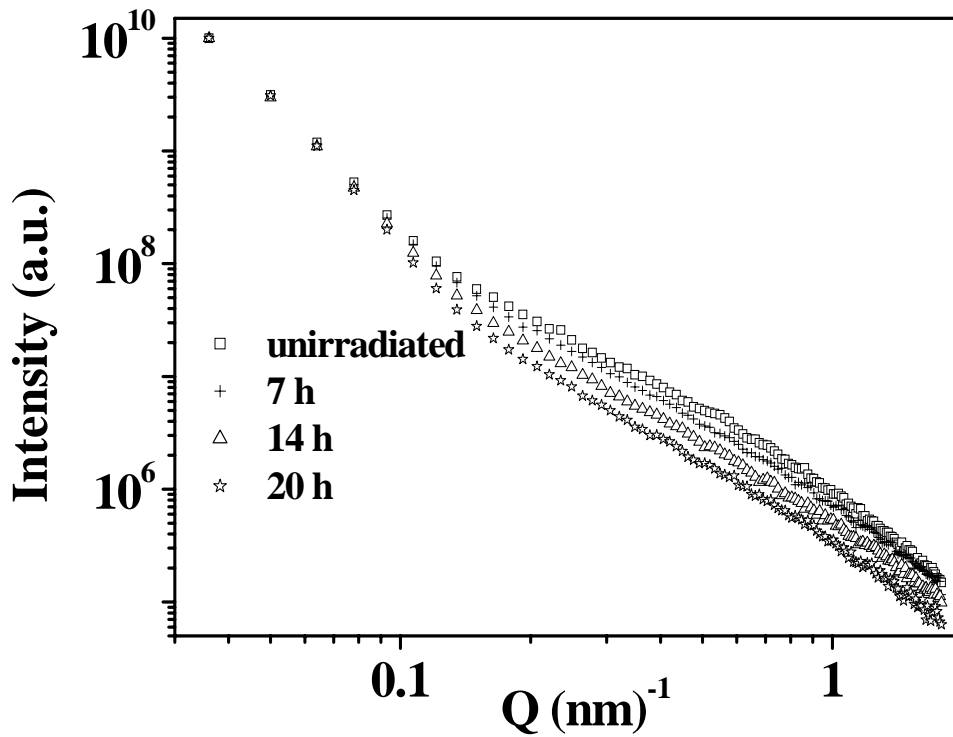


Fig. 4.15: SAXS profiles of neutron irradiated carbon-carbon composites

4.6 Conclusions

From the thermophysical property measurements it was found that the C_p value of the composites is more than that of the graphite, which suggests a reduced probability of release of Wigner energy. In addition, these materials offer excellent thermo-mechanical properties such as low coefficient of thermal expansion, high specific heat and high compressive strength. The Raman analysis of the composites made from carbon black showed that both the 'D' and 'G' bands get broadened and D/G ratio increases in case of samples made from 0% and 5% of CB as compared to that of graphite, implying significant disorder in the samples. The increase in broadness in case of samples made from 15% CB indicates an increase in their amorphous nature with increasing weight percentage of CB. No appreciable change in the Raman profile could be observed

following impregnation of the samples. While in the case of carbon composites made from matted PAN fibers showed that the D/G ratio value decreases, more sharply at higher pressure, and then becomes steady after 15h of impregnation. This indicates that during the high-pressure densification process graphitization has taken place due to stress generated at open pores and the extent of graphitization is higher for higher impregnation pressure. It is observed that with increase in pressure of impregnation the graphitization also increases. From the XPS studies it was observed that the ratio of sp^2 -C/ sp^3 -C is higher for sample impregnated at higher pressure indicating greater extent of graphitization in these samples. It was inferred from the SANS investigations that there is reduction of pore size in the C/C composites with increase in both impregnation pressure and time. It was observed that increase in impregnation time does not show any change in small pores size distribution. From the SAXS studies, it was found that for larger pores (of minimum size 40 nm), β changes gradually from about 3.8 to 4.05 with increase in irradiation time, suggesting an initial rough surface tends to smoothen with the irradiation while on the other hand, the smaller pores show mass (pore) fractal nature with average fractal dimension about 2.4. The lowering of intensity at low-Q with different irradiation timings indicates a relatively reduction in specific surface area of the pores due to increase in the average pore radius.

CHAPTER 5

CHAPTER 5

RADIATION STABILITY OF CARBON COMPOSITES

5. Introduction

Carbon and carbon-based materials have been extensively used in nuclear reactors and in the recent past there has been growing interest to develop graphite and carbon-based materials for high temperature nuclear and fusion reactors. The associated problems of using graphite in low temperature reactor is the Wigner energy storage. Hence an amorphous structure is needed in order to avoid accumulation of Wigner energy [1], which is the stored energy in carbon lattice due to dislocation of atoms induced by irradiation. This amorphous carbon should be isotropic and dense in order to achieve dimensional stability under irradiation.

Graphitic carbon due to its excellent neutron scattering properties, continues to be the unanimous choice for the moderator material in high-temperature nuclear reactors [2-4] where the aforesaid drawbacks are essentially overcome due to high-temperature annealing. The effect of particle irradiation on graphite has gained lot of importance due to its use as nuclear material. Some literature on irradiation behavior of graphite [75-77] and stored energy in graphite [78, 79] is available. However, the studies on radiation damage in the disordered forms of carbon are scant. Few investigations on heavy ion irradiation of disordered carbon in carbon /carbon composite made of particulates and chopped carbon fibers have been reported, but there is not much literature on architecture carbon/carbon composites. Burchell et al. [5] irradiated 1D, 2D, and 3D C-C composites

at 600°C up to damage doses 1.5 dpa. 3D C-C composites were shown to have more isotropic dimensional changes than that of 1D or 2D composites.

The effects of particle irradiation in solids have been a field of intense research since the 1950's. The early studies focused on radiation damage in metals, semiconductors and insulators in view of their radiation resistance in nuclear technology. The modifications of carbon have been the subject of many early irradiation studies; in particular graphite has attracted much attention as a reactor material. The early studies of radiation damage in graphite are still of considerable advantage, since from the renewed interest in radiation phenomena in graphitic structures a need for data about the behavior of graphite under particle irradiation has arisen. Radiation defects in graphite have, in fact, been characterized with many techniques, including electron microscopy. However, the resolving power of electron microscopes at that time was insufficient for lattice imaging; therefore the nature of defect agglomerates remained unknown. Nowadays, modern high-resolution electron microscopes permit detailed insight into the structure of lattice defects on an atomic scale and lead to a new understanding of radiation defects in graphite and eventually in graphitic nanostructures. Meanwhile, it has turned out that many early results are out-dated and that the subject needs to be thoroughly revisited.

5. 1. Radiation effects in solids

When a highly energetic particle such as an electron, neutron or ion strikes the atoms of a target, different mechanisms of energy or momentum transfer take place. The most important primary radiation effects are (a) electronic excitation or ionization of individual atoms, (b) collective electronic excitations, e.g. plasmons, (c) breakage of

bonds or cross-linking, (d) generation of phonons, leading to heating of the target, (e) displacement of atoms in the bulk of the target and (f) sputtering of atoms from the surface. Secondary effects are (a) emission of photons, e.g. X-rays or visible light and (b) emission of secondary or Auger electrons, leading to a charging of the target. The importance of these different contributions is reflected by the cross sections for the respective interaction. The energy of the projectile is of particular importance as the different phenomena show different energy dependences.

Atom displacements occur by knock-on collisions of highly energetic electrons or ions with the nuclei of the atoms in the specimen. Graphite is a semi-metal and behaves like metals under irradiation where ionization is a negligible factor and knock-on atom displacements are the main source of radiation damage. The knock-on displacement event occurs within a very short time. The time scales during the production of atomic defects are

- 10⁻²¹ s: energy transfer from the particle to the nucleus (primary knock-on)
- 10⁻¹³ s: interatomic collisions (cascade)
- 10⁻¹¹ s: dissipation of epithermal energy (stable defects and clusters)
- >10⁻¹¹ s: thermal migration of point defects.

When radiation effects in carbon are considered, it is useful to divide these contributions into those that lead to a displacement of atoms (knock-on effects) and those that do not (excitations). The interaction which is of primary interest from materials point of view is the elastic collisions. If the ion or neutron imparts sufficient energy and momentum to overcome an atom's binding energy (E_d carbon is 20-30 eV), the carbon atom is displaced from its original lattice position. If this primary knock on carbon atoms

(PKAs) from the primary displacement has received enough transferred energy which is sufficient to displace further atoms, a series of displacement events or a cascade occurs. The Kinchin–Pease model as shown in Fig. 5.1 is used to calculate the total number of atoms displaced.

The secondary knock-on atoms (SKAs) tend to cluster in small groups of 5-10 atoms. The total number of displaced atoms depends on the energy of the PKA, which in turn is function of the neutron energy spectrum and the neutron flux. The carbon atoms once displaced recoils within the graphite lattice displacing other carbon atoms and creating vacant lattice sites. The displaced carbon atoms diffuse between graphite layer planes and high proportion of them will recombine with lattice vacancies. Some will coalesce to form C₂, C₃, C₄ linear molecules. These in turn acts as nucleus of dislocation loop-a new graphite plane. The interstitial clusters may on further irradiation be destroyed by a fast neutron or by a carbon knock on atom (irradiation annealing). The adjacent lattice vacancies in the same graphitic plane may collapse to the layers thereby forming sinks for other vacancies which are highly mobile at temperatures of 600°C. The interaction of high energy neutrons is similar to that of ions except for the amount of energy transferred in a single collision and the distance over which the collision takes place. An ion which has a larger radius interact coulombically and loses its energy over a shorter distance i.e. few microns while the mean free path for neutrons is ~10 cm in case of a 14.1 MeV fusion neutron.

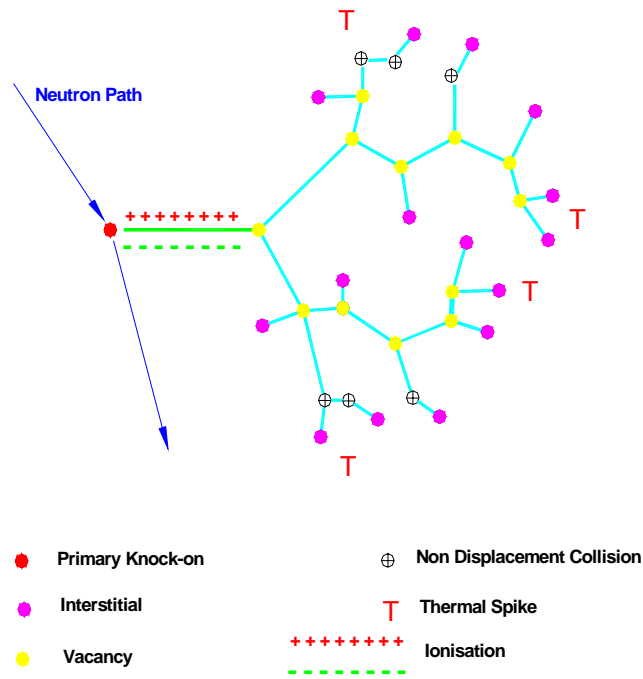


Fig. 5.1: Crystal lattice defects introduced by fast neutron irradiation [80]

The principal result of carbon atom displacements is the crystallite dimensional change. The interstitial defects will cause crystallite growth perpendicular to the layer plane i.e. the c-axis direction while the coalescence of the vacancies will cause shrinkage parallel to the layer plane i.e. a-axis direction. The damage mechanism and associated dimensional changes are illustrated in Fig. 5.2. It is reported in literature that the a-axis shrinkage increased linearly with dose but the magnitude of shrinkage at any dose decreased with increasing graphitization temperature. Similar trends were observed for c-axis expansion. Higher graphitization temperatures reduce the initial number of defect sites which are available to trap the irradiation induced vacancies, and thereby reduce the rate of damage accumulation.

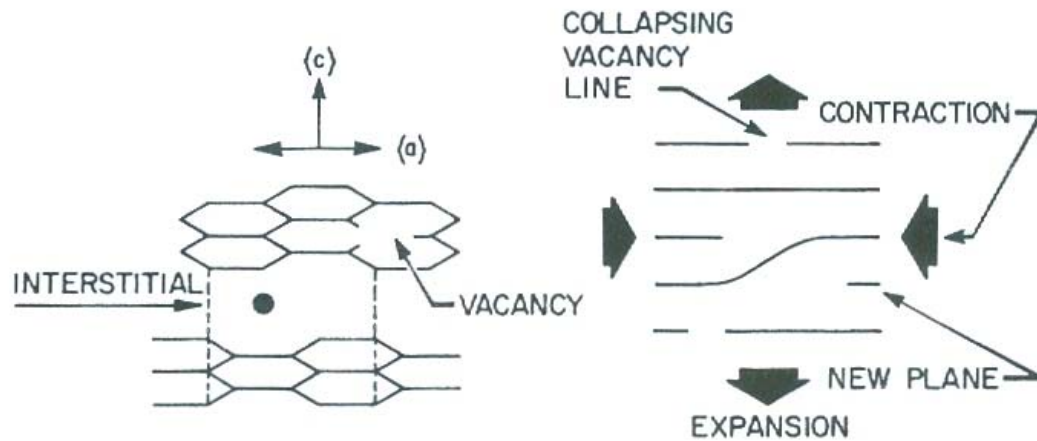


Fig. 5.2: Radiation damage in graphite showing the induced crystal dimensional change along a and c directions

The irradiation induced displacement processes causes an excess energy which is associated with the vacancy/ interstitial pairs in the graphite crystallites. The release of stored energy or Wigner energy, named after the Physicist who first postulated its existence, is the radiation damage in graphite. When the interstitial carbon atom and lattice vacancy recombine, their excess energy is given up. If sufficient damage has been accumulated in the graphite, the release of this stored energy can result in increase in temperature. This poses problems in graphite moderated reactors operating at low temperatures. The rate of release of stored energy with temperature for samples irradiated at 30°C at three different doses (0.01, 0.1 and 0.6 dpa) is shown in Fig. 5.3.

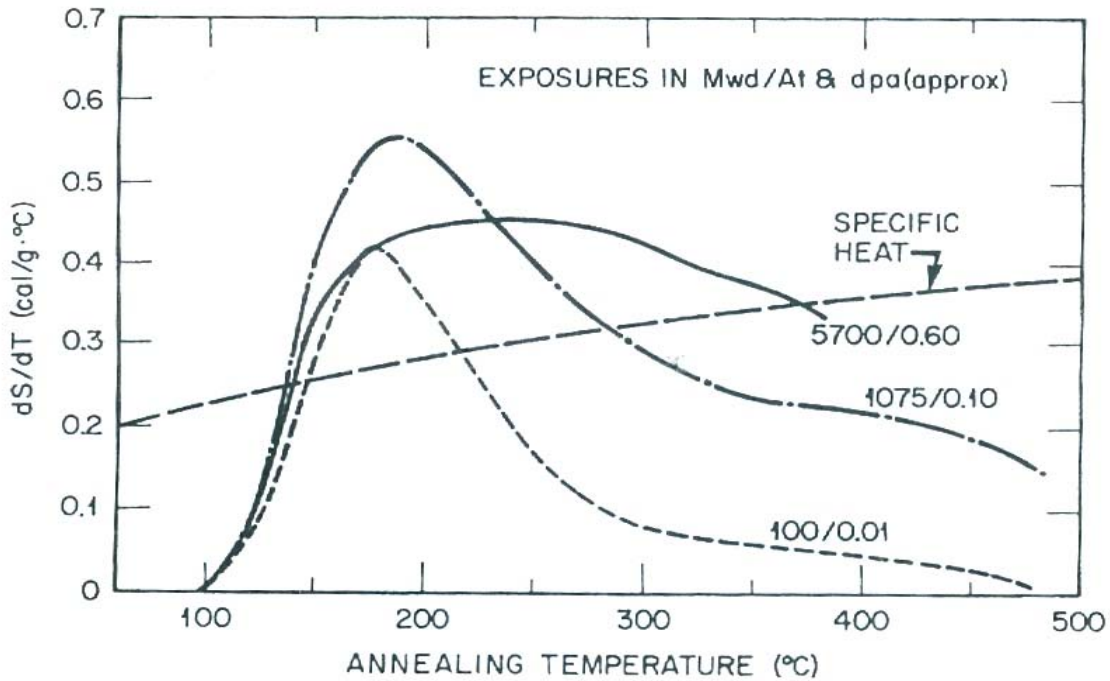


Fig. 5.3: Stored energy release curves for graphite irradiated at 30°C in Hanford K Reactor cooled test channel [74]

The release curves are characterized by a peak occurring at 200°C which is associated with the recombination of single interstitials and vacancies. This peak becomes broader with increasing neutron dose and the maximum release rate is reduced. If the release rate exceeds the specific heat under adiabatic conditions the graphite temperature would rise sharply. In order to limit the total amount of stored energy it is necessary to periodically anneal the graphite.

The present study aims at determining if the particle irradiation causes formation of crystalline phase in the amorphous carbon leading to any storage of Wigner energy. There is a possibility of self-organization phenomena under irradiation leading to localized ordered arrangement in disordered structure of atoms in amorphous samples

leading to crystallinity [80-82]. In the present work, neutron irradiation on the carbon-carbon composites were studied out. The structural parameters like extent of local ordering along c axis, the average d spacing of the d_{002} i.e. the (002) crystallographic planes were characterized using X-ray diffraction (XRD) technique. This is further validated using Raman spectroscopy.

5.2. Experimental

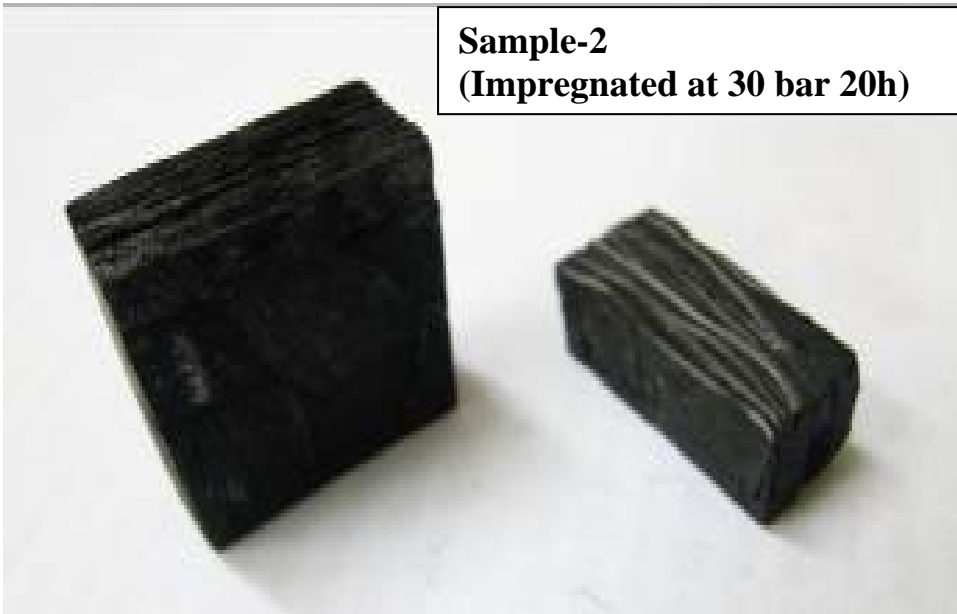
5.2.1. Preparation of carbon/carbon composite samples

The fabrication of a suitable preform is the first step for manufacturing the carbon-carbon composite. This may also be referred to as fiber architecture. It not only imparts rigidity to the composite, but also in combination with fiber properties it determines the properties of the composite. In the present studies the preform has been made using PAN carbon fibers. PANEX 35 carbon fiber of yield 48K has been used. The carbon fiber diameter was 7.2 μm . In the present work green preform in the shape of rectangular blocks have been fabricated using 2D matted PAN carbon fiber have been stacked to a 2-D preform using phenol formaldehyde resin. This preform was cut into 2.5 X 2.5 X 0.6 cm size and carbonized at a slow heating rate of 0.1°C/min in inert atmosphere. This carbonized samples had density of 1100 kg/m³. The carbonized sample is highly porous and has to be densified for any further application. Hence these samples were densified by resin impregnation technique up to two cycles. The liquid phenol formaldehyde resin was impregnated under a pressure of 30 bar and with varying time duration of 10 and 20 hours. The impregnated samples were cured and then carbonized at 1000°C under inert atmosphere with a heating rate of 0.1°C/min. The samples were then

further subjected to a second cycle of impregnation at the same pressure and varying time duration as carried out during the first cycle. These samples were subsequently cured and carbonized as done in the first cycle. Two cycles of impregnation and carbonization were carried out and these samples as shown in Fig. 5. 4 were used for irradiation studies.



Sample-1
(Impregnated at 30 bar 10h)



Sample-2
(Impregnated at 30 bar 20h)

Fig. 5.4: Photograph of the carbon/carbon composite samples

5.2.2. Irradiation of the samples

The carbon-carbon (C/C) composite samples have been irradiated with thermal neutrons at APSARA reactor in Bhabha Atomic Research Center, Trombay. The energy spectrum for irradiation was 98% thermal neutron component for which neutron energy was up to 0.55 eV and 2% is epithermal component (above 0.55 eV).

Two samples, sample-1 and sample-2 having density of 1314 kg/m³ and 1310 kg/m³ respectively were selected for these studies. Sample-1 was prepared by impregnation of resin at 30 bars for 10h while the sample-2 was prepared by impregnation at 30 bars for 20h. The irradiation was carried out at a flux of 1×10^{12} n/cm²/s for seven hours, fourteen hours and twenty hours for both these samples. The desired respective fluence was 2.52×10^{16} n/cm², 5.04×10^{16} n/cm² and 7.2×10^{16} n/cm² at temperature of 40°C during irradiation. After the irradiation the samples are removed from the reactor and kept for cooling (i.e. for the decay of the radioactivity of the radionuclides formed due to irradiation of the impurities if present till it can be handled). The stored energy in the composite due to irradiation was measured using Differential Scanning Calorimetry (DSC) and the changes in the structure were observed by X-ray diffraction and Raman spectroscopy.

5. 2.3. Characterization of the irradiated sample

XRD technique is employed to characterize the degree of graphitization of carbon-carbon composites with low crystallinity. Micro Raman measurements were done using a LABRAM-I spectrometer (ISA) made in a back scattering geometry. The stored

energy release spectra were measured by a DSC at a constant heating rate in argon atmosphere. Both the samples were heated at the rate of $5^{\circ}\text{C}/\text{min}$ from RT to 1000°C .

5. 3. Results and discussion

5. 3.1. Raman spectroscopy studies

Raman spectroscopy was used for the structural analysis and to find if graphitization was occurring during the processing of the samples. Usually Raman spectra of most of the carbon- graphite materials contain two peaks at $\sim 1580\text{ cm}^{-1}$ and at $\sim 1360\text{ cm}^{-1}$ for natural graphite [83]. The 1580 cm^{-1} peak i.e. ‘G’ band is known to correspond to graphite structure and the 1360 cm^{-1} peak is correlated to graphitized carbon structure called ‘D’ peak, assigned to have originated due to the disorder. The ratio of the integrated intensities of the two peaks, $I_{\text{D}}/I_{\text{G}}$ has been considered to be a good parameter to estimate the degree of graphitization. Higher the ratio of $I_{\text{D}}/I_{\text{G}}$, lower is the degree of graphitization of the carbon materials. The 1580 cm^{-1} peak comes from the flex vibration of chemical bonds in atomic hexagonal net plane while the 1360 cm^{-1} peak is associated with local unsymmetrical structure, which exists, in graphitized carbon or non-integrity graphite crystals containing defects.

The change in structural parameters due to displacement of atoms from lattice position during irradiation has been studied using Raman Spectroscopy. The Figs. 5.5 (a-d) shows the variation of $I_{\text{G}}/I_{\text{D}}$ ratio of irradiated Sample-1. The $I_{\text{G}}/I_{\text{D}}$ ratio increased from 0.73 to 0.87 with increase in fluence and then further decreased with further increase in fluence. The variation of $I_{\text{G}}/I_{\text{D}}$ ratio of irradiated sample-2 is shown in Figs.5.6 (a-d). While in sample-2 there was an increase in the ratio of $I_{\text{G}}/I_{\text{D}}$ with increase in fluence from

0.82 to 0.93 and remains almost same on further increase in fluence. Study was carried out to see if the different processing parameters caused marked change in the I_G/I_D ratio of irradiated sample-1 and sample-2. There was no appreciable change observed which may be due to the fact that both had nearly the same density. It can be inferred that density governs the irradiation defects rather than the processing parameter.

Table 5.1: Variation of I_G/I_D with irradiation fluence levels

S.No	Sample code	I_G/I_D			
		Unirradiated	2.52×10^{16} n/cm ²	5.04×10^{16} n/cm ²	7.2×10^{16} n/cm ²
1	Sample-1	0.73	0.87	0.85	0.80
2	Sample-2	0.82	0.92	0.93	0.91

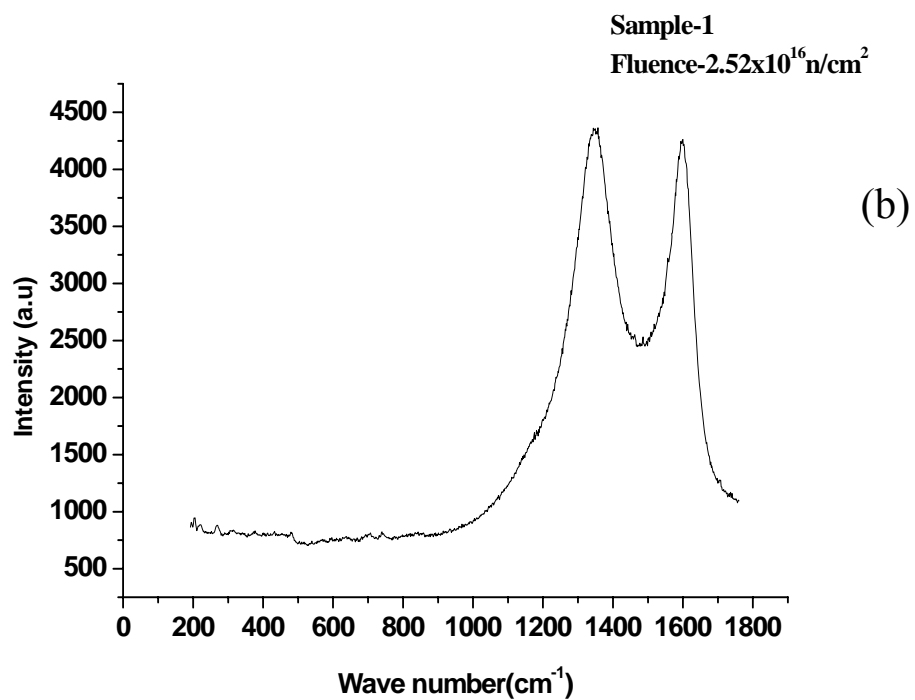
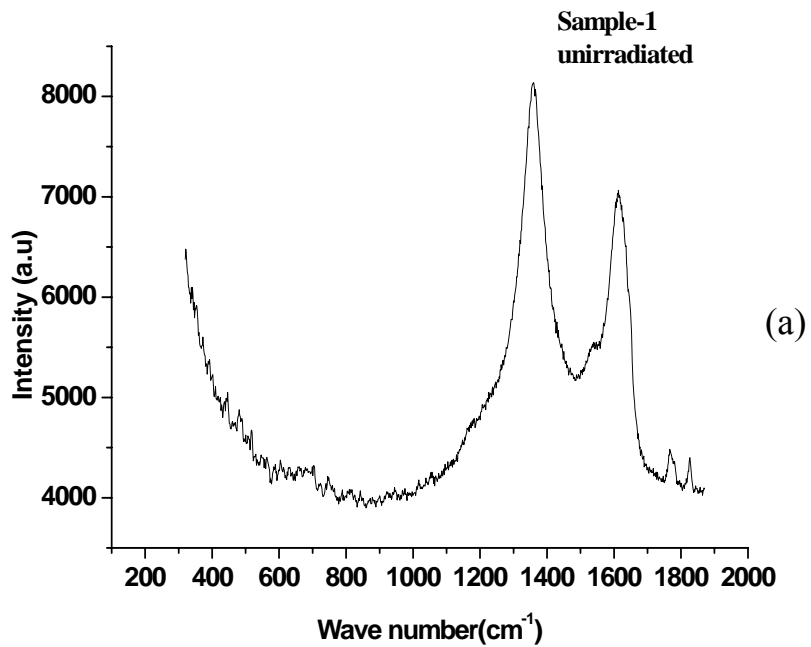


Fig. 5.5 (a) and (b): Change in I_G/I_D for unirradiated and irradiated carbon/carbon composites Sample-1 at different fluence levels

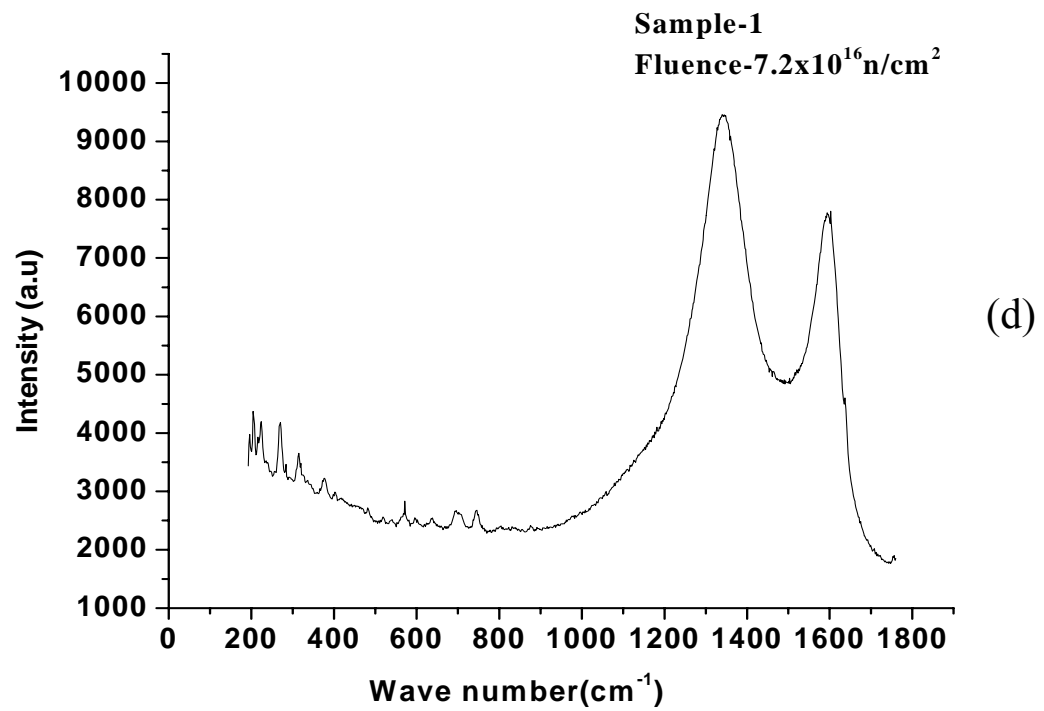
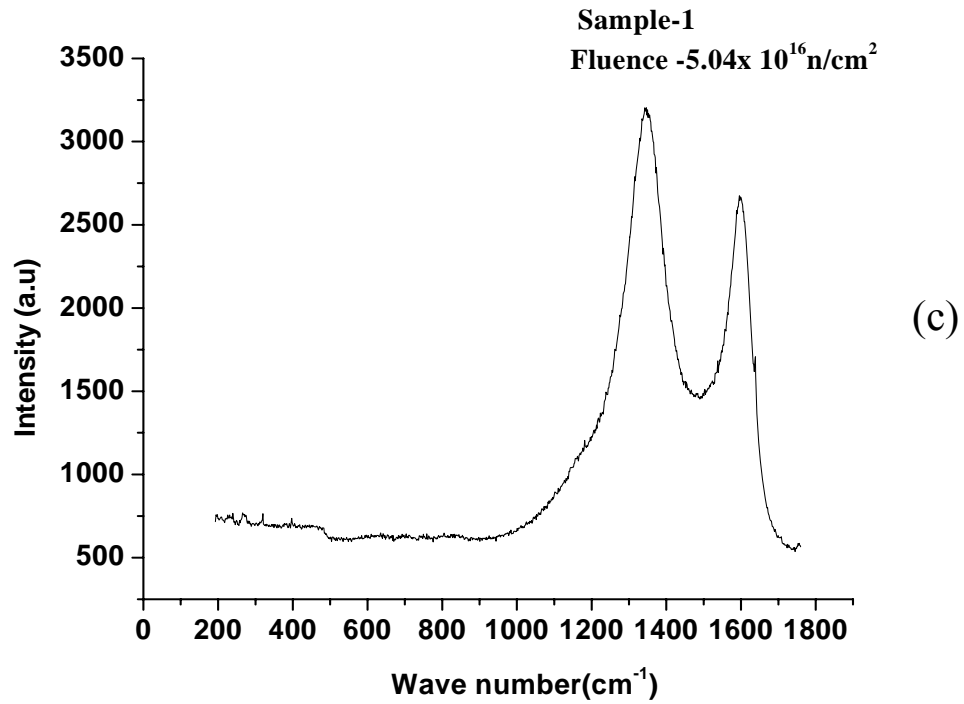


Fig. 5 5 (c) and (d): Change in I_G/I_D for unirradiated and irradiated carbon/carbon composites sample-1 at different fluence levels

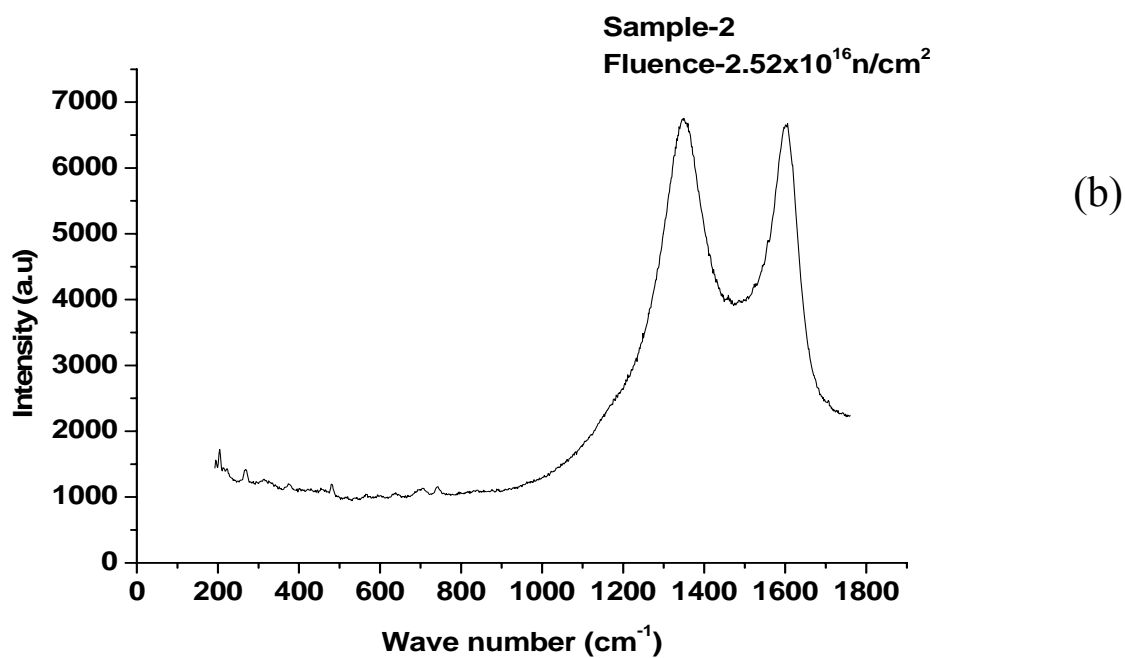
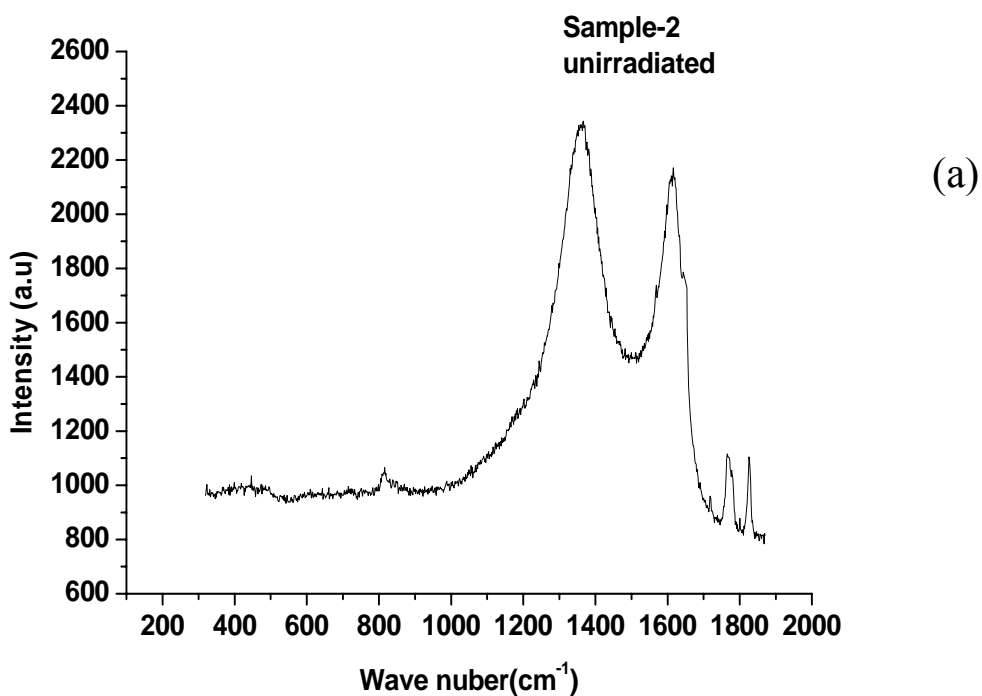


Fig. 5.6 (a) and (b): Change in I_G/I_D for unirradiated and irradiated carbon/carbon composites sample-2 at different fluence levels

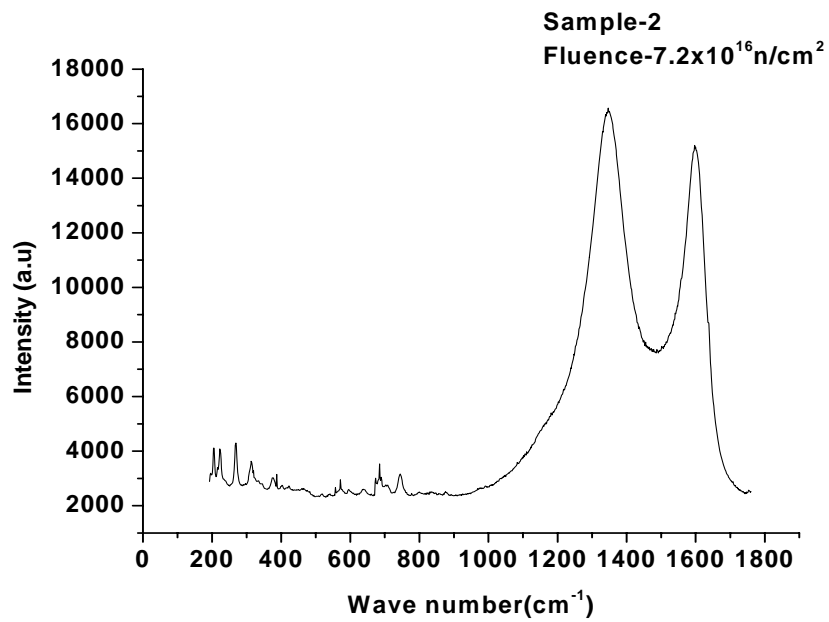
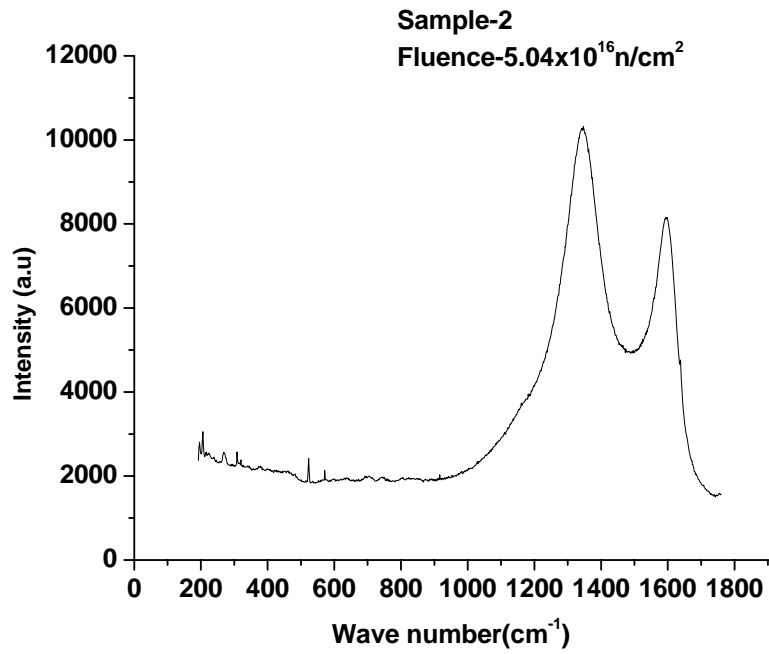


Fig. 5.6 (c) and (d): Change in I_G/I_D for unirradiated and irradiated carbon/carbon composites sample-2 at different fluence levels

5. 3. 2. XRD studies

The degree of graphitization in carbon-carbon composites is inhomogeneous and this is the reason why the material is difficult to graphitize. According to Bragg equation, the interlayer spacing d_{002} can be obtained and on the basis of the model given by Maire and Maring [84], the degree of graphitization can be calculated from the equation given below.

$$g (\%) = (0.3440 - d_{(002)} / 0.3440 - 0.3354) \times 100 \quad (1)$$

where, g is the degree of graphitization, 0.3440 is the interlayer spacing of fully non graphitized carbon (in nm), 0.3354 is the interlayer spacing of the ideal graphite crystallite (Fig. 5.7) and the d_{002} is interlayer spacing obtained from XRD. The inter planar spacing of 0.3440 nm represents a specific structure proposed by Franklin [85] who considered it as interlayer spacing of non graphitic carbon, i.e. the turbostratic structure put forward by Warren and co-workers [86, 87]. Sometimes the apparent

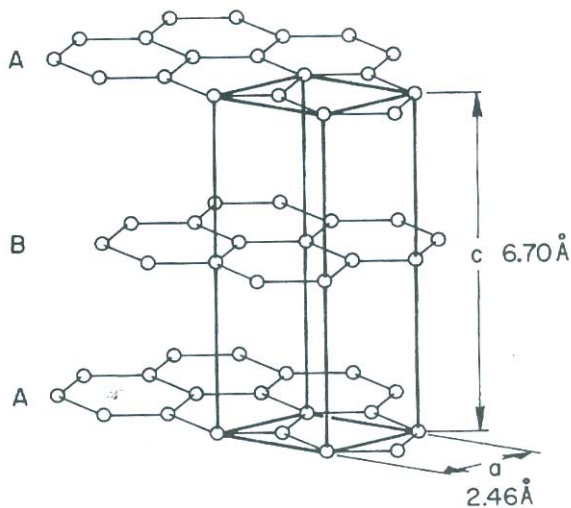


Fig. 5.7: Crystal structure of graphite

interlayer spacing of turbostratic structure is greater than 0.344nm, as $d_{002} > 0.3440\text{nm}$, $g < 0$ in equation (1) represents a structure which is far from ideal graphite structure.

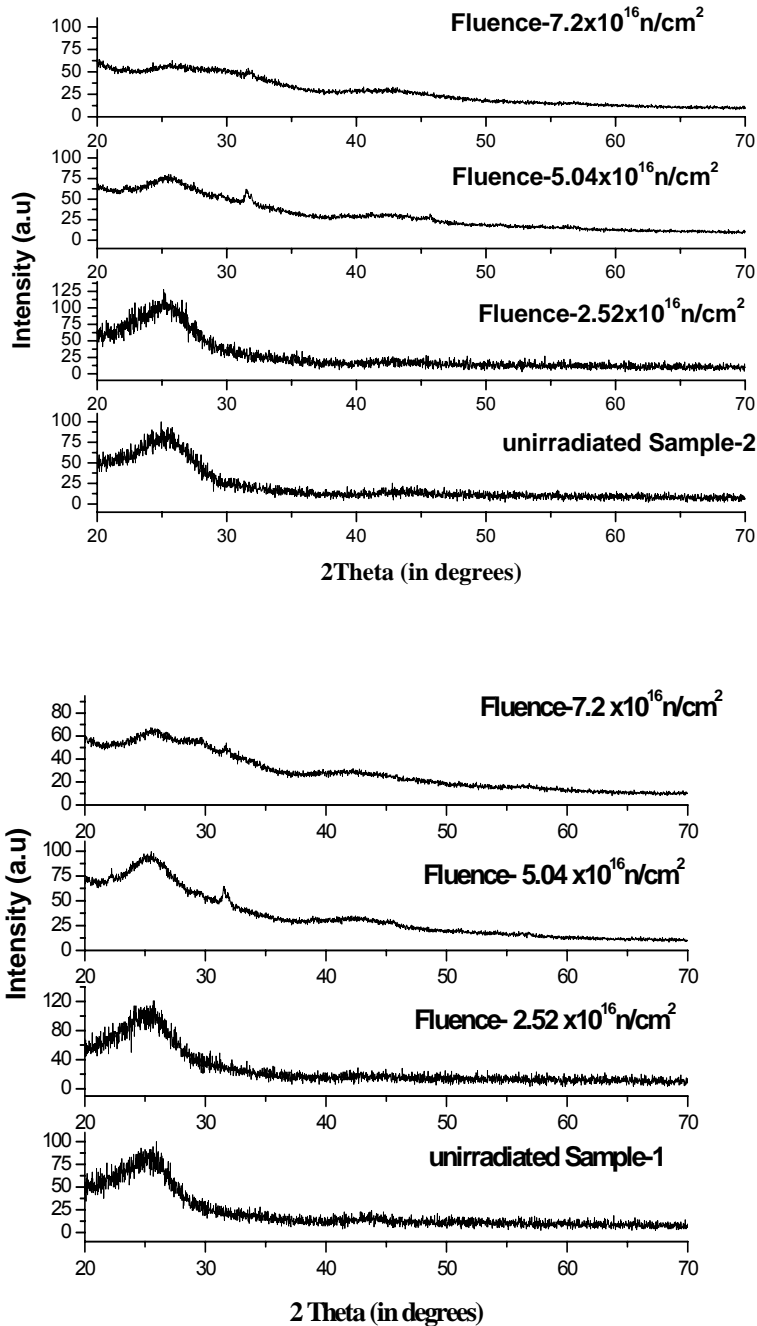


Fig. 5.8 (a) and (b): XRD patterns of irradiated carbon/carbon composite sample-1 and sample-2 at different fluences

From the XRD patterns as seen in Figs. 5.8(a & b) of the irradiated and unirradiated samples it is found that the d_{002} peaks for the irradiated samples are becoming broader and appearance of a new peak indicating the tendency to get ordered structure. The change in d_{002} values of unirradiated and irradiated sample-1 & 2 are shown in Table 5.2.

Table 5.2: Variation of d_{002} with irradiation

Dose(Neutron)(n/cm ²)	Sample -1	Sample -2
	d_{002}	d_{002}
Unirradiated	3.66 Å	3.71 Å
2.52×10^{16}	3.60 Å	3.64 Å
5.04×10^{16}	3.51 Å	3.49 Å
7.2×10^{16}	3.49 Å	3.50 Å

XRD is the most common analytical tool for determining structure of the ordered and disordered carbons [88-91]. In graphite the carbon layers have the ABAB-stacking along the c-axis. In disordered carbon the turbostratic layers are built up of graphite layers, arranged almost parallel to one another, but with random orientation about normal to the layers. Except for (001) reflection, the random orientations prevent the appearance of general (hkl) reflections. The individual layers diffract independently and the two dimensional (hk) reflections are obtained. The interplanar spacing becomes more than

0.344 nm. The correlation lengths of the ordering are given by L_c (stacking along c direction) and L_a (along a direction). The disorder can occur due to random shifts between the adjacent layers, unorganized carbon which are not part of the layer, presence of local 3R stacking and strain in the layers. These defects affect the extent of local ordering L_c along c -axis designated as crystalline height. L_c can be calculated from the (002) peak using the Scherrer [92] equation.

5. 3. 3. DSC studies

Carbon-carbon composite when irradiated with neutrons, they transfer their kinetic energy by knock on of atoms from the lattice. These in turn cause displacement cascades by successive collisions. Stored energy arises due to the fact that after irradiation by neutrons the crystal lattice of graphite possesses increased potential energy due to the presence of defects stable under the conditions at which the irradiation was carried out. The defects are of two general types, vacancy and interstitial, with varying complexity depending on the irradiation conditions.

Defects may be annealed to more stable configuration by increasing the vibrational energy of the lattice by heating. Most of the energy release may be caused by the annihilation of interstitials and vacancies. The stored energy was measured by release of the energy at constant rate.

Table 5.3: Stored energy at different irradiation fluence levels

Dose (n/cm ²)	Sample-1	Sample-2
	Stored energy (J/g) (RT-1000 °C)	Stored Energy (J/g) (RT-1000 °C)
2.52 x 10 ¹⁶	82.2	100.0
5.04 x 10 ¹⁶	119	66
7.2 x 10 ¹⁶	185	51.6

The DSC scans, of the energy release rate with respect to temperature for the irradiated samples are shown in Fig. 5.9(a) & (b). The samples were heated at constant heating rate of 5 °C/min in the range from RT to 1000 °C. The stored energy is obtained from the area under the curve. The stored energy release data for Sample-1 and Sample-2 at varying fluence levels is given in Table 5.3.

The stored energy is found to increase with increasing fluence in sample-1. At lower fluence the defects are simple and are getting annealed at around 100 °C. While at higher fluence levels complex defects are formed which are getting annealed by heating at higher temperatures.

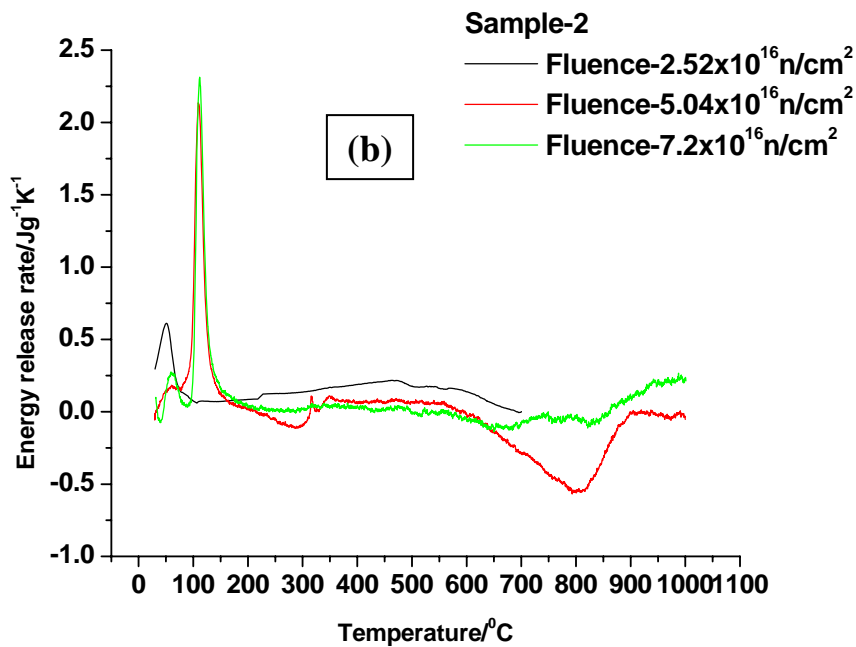
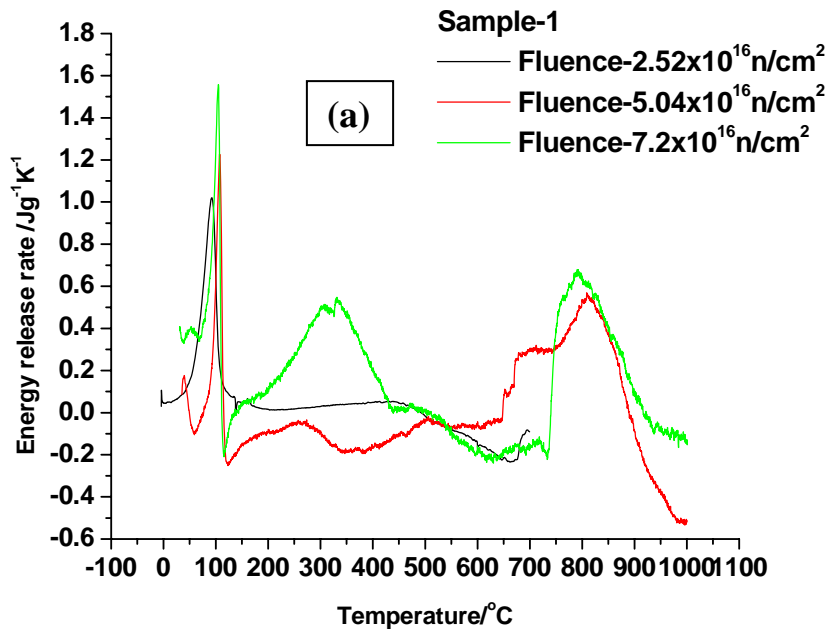


Fig. 5.9(a) and (b): Stored energy release spectra of carbon/carbon composite sample-1 and sample-2 at different fluence levels

In sample-2 the stored energy was found to decrease with increasing fluence indicating that the defects created are less and simple in nature and is getting annealed at lower temperatures. It has been earlier reported in literature [93] that the stored energy decreases with increase in fluence level for ion irradiation of both carbon black based composite and PAN based composite. Irradiation at high doses causes formation of complex defects and the stored energy may be released at higher temperatures. The samples in our experiments are carbon/carbon composites made of reinforced PAN fiber and matrix of carbon char obtained from phenol formaldehyde resin. Both the carbons present in the samples are in disordered form. The amount of energy stored in graphite varies with the crystallite size, more energy being stored in the more crystalline material [94].

In case of irradiated graphitic samples they require high activation energy to overcome the activation barrier to reach at a lower energy state (stable form) and therefore higher temperature is required. Hence the energy release peak is seen around 150-200°C for graphite samples irradiated at 30°C associated with the recombination of single interstitials and vacancies. This peak becomes broader with increasing neutron dose and the maximum release rate is reduced. The disordered carbon is already at higher energy level and the activation energy barrier is less, as compared to graphite therefore lesser temperature is sufficient to overcome the activation energy barrier. The accumulation of stored energy in graphite is both dose and irradiation temperature dependent. With increasing irradiation temperature the total amount of stored energy and its peak rate of release diminish and above temperature of ~300°C stored energy ceases to be a problem. The amount of stored energy in graphite irradiated at ambient temperature

is very large i.e. 2700 J/g, which can be stored as lattice defects. This heat, when released under adiabatic conditions would cause an increase in temperature of $\sim 1300^{\circ}\text{C}$. Annealing is required as observed in highly irradiated graphite [95-98] where the sample has to be heated to 2000°C to release all the stored energy.

5. 4. Conclusions

The neutron irradiated carbon composite samples have been characterized by XRD and Raman spectroscopy before and after neutron irradiation. DSC studies have also been carried out to investigate the stored energy release behavior due to irradiation. From the XRD analysis of the irradiated and unirradiated samples, it is found that the value of d_{002} peak for the unirradiated samples is higher than that of the irradiated samples indicating the tendency to get ordered structure. This is also inferred from the Raman spectroscopy. The I_G/I_D ratio of irradiated samples was found increase with increasing fluence when compared to unirradiated samples initially but decreased further with increasing fluence in sample-1. In sample-2 the ratio of I_G/I_D increases with increase in fluence initially but remains same on further increase in fluence. The stored energy with respect to the fluence level was obtained from the DSC. These results indicate that simple defects created due to low fluence of irradiation are annealed by heating accompanied by release of the stored energy at lower temperature on the other hand the complex defects are formed require high temperatures are required for annealing these defects. The flux/fluence used is lower than the actual scenario in the upcoming compact high temperature reactor; however the present study could definitely be an initial step in the direction of investigation of damage caused by neutrons on carbon/carbon composite

materials for its use in the upcoming reactor. Currently the available flux was low in the range of 10^{12} n/cm²/s. However these samples have to be evaluated by irradiating at a higher dose for potential nuclear application. There were severe limitations of not being able to use the fluence of 10^{20} n/cm². However an extension of work on carbon/carbon (C/C) composites irradiation with higher flux in some international neutron irradiation facility would be taken up in near future. Currently some irradiation studies with high energy neutrons are being carried out. However these investigations are out of scope of the present work and hence will be taken up in future.

CHAPTER 6

CHAPTER 6

DEVELOPMENT OF SiC COATINGS ON CARBON COMPOSITES AND ITS CHARACTERIZATION

6. Introduction

Graphite and carbon fibre reinforced carbon composites are candidate materials for high temperature applications due to their superior properties [21, 24, 25, 41, 93] as discussed earlier. In order to exploit of the advantage of these properties from an environment consisting of vacuum or inert gases or an oxidizing atmosphere these materials should be protected by an oxidation resistant material. The physico-chemical properties of carbon-carbon composites generally meet the desired requirements such as toughness, low density, thermal stability or thermal shock resistance associated with low thermal expansion behavior. A notable drawback consists in the limited resistance to oxidation of carbonaceous materials which react with oxygen to form volatile compounds at temperatures as low as 500°C. SiC is a material with high temperature oxidation resistance along with good thermal shock properties and stability against high temperature corrosion [29, 99]. This makes it an excellent oxidation resistant material. SiC coating has the combination of unique physicochemical and mechanical properties such as high strength, extreme hardness as well as excellent resistance to wear due to oxidation and corrosion [30-32]. SiC can be grown on varying surfaces using different techniques. The nature of the grown SiC depends on many parameters such as crystal structure of surface on which it has to grow, other chemical and physical parameters during growth on surface. The different techniques for the growth of SiC are as follows:

6.1.1. Carbothermal reduction process

It involves inexpensive silicon dioxide and carbon (or carbon precursors) as the starting materials. These materials react to form β -SiC at temperature about 1200°C and the yield of β -SiC increases with increasing reaction temperature [100-102]. In the carbothermal reduction of SiO_2 the commonly accepted mechanism of SiC formation is the gas–solid reaction between $\text{SiO}_{(g)}$ and $\text{C}_{(s)}$ [103, 104]. Carbon is shown to substantially influence the rate of reaction, the morphology and size of the synthesized SiC. However whether the starting SiO_2 does play any role is not clearly demonstrated.

6.1.2. Physical vapour transport

The most common bulk growth technique is based on Physical Vapour Transport (PVT). The technique is also called the modified Lely method or seeded sublimation growth and was invented in 1978 by Tairov et al. In this method, a SiC source (in the form of SiC powder) is sublimed at $\sim 2300\text{-}2500^{\circ}\text{C}$ in a closed crucible and re-crystallized on a seed crystal maintained at a lower temperature. Although the sublimation technique is relatively easy to implement, but the drawbacks are the requirement of high growth temperature and the process is difficult to control, particularly over large substrate areas. The High Temperature Chemical Vapour Deposition, (HTCVD) is an alternate growth technique where transport of the growth species to the seed crystal is directly provided by high purity gas precursors containing Si and C species growth.

6.1.3. Sublimation growth

Sublimation is used for the growth of SiC bulk crystal and it is a complex process in which a number of parameters have to be controlled. The vapour is produced via decomposition of SiC source material with the highest partial pressure which is that of Si. The crystal growth is driven by the shift along a temperature gradient of the equilibrium between the solid SiC and its vapour. Single crystal SiC is formed from deposition of the supersaturated vapour species on a SiC seed crystal. Source materials may be composed of SiC seed crystal, SiC powder or polycrystalline SiC. The vapour transport is performed either in a vacuum or at ambient. Typical temperature and pressure ranges for SiC sublimation growth are 1750 to 2500°C and 10^{-6} to 50 mbar. Usually, the lower temperatures are employed for sublimation epitaxy of SiC, while bulk growth is performed at higher temperatures.

6.1.4. Two step sol-gel process

Sol-gel process has been developed to synthesize the SiC precursors and then convert it to SiC. To obtain high-performance SiC ceramics, fine powders with a narrow particles-size distribution are required which can be obtained by sol-gel process. The main advantage of sol-gel process is homogeneous mixing condition that leads to accelerate reaction rate and to lower the reaction temperature. Tanaka et al. [105] developed a sol-gel processing to mix the reactants in liquid phase, with ethylsilicate liquid and liquid phenolic resin as the sources of SiO₂ and carbon respectively and toluene sulfonic acid as the catalyst. The powders obtained after carbothermal reduction of the gel were sinterable cubic SiC (β -phase), containing no residual SiO₂ and carbon at a proper initial resin content. Similar sol-gel route has also been used to fabricate β -SiC fibers using hydrochloric acid as the catalyst [106].

6.1.5. Laser pyrolysis of polycarbosilane

Solid free-form fabrication (SFF) is a relatively recent manufacturing concept in which shapes are constructed by additive process rather than traditional removal processes like machining. One of the SFF techniques of continuing interest is termed selective laser sintering (SLS) in which a laser scans the surface of a powder bed and then fusing the powder particles together [107-111]. By controlling the pattern scanned by the laser, a two-dimensional layer of fused particles is formed. Thickness is build up by spreading a fresh layer of powder on top of the previously fused layer and repeating the scanning. By changing the scan pattern from layer to layer, a part can be changed to any shape from layer. Laser pyrolysis of polycarbosilanes (PCS) produces controlled β -SiC shapes with nanometer grain size although properties are currently limited by high porosity. The laser pyrolysis process differs significantly from conventional pyrolysis since it is a single step process. PCS is directly pyrolysed by scanning laser in flowing argon to produce a ceramic shape. Avoiding oxygen presence is beneficial because oxygen reduces the high-temperature strength of the product silicon carbide. The processing parameters of concern in laser pyrolysis process are the laser power, scan speed, and scan line spacing which control the pyrolysis time and temperature.

6.1.6. Using supersonic beam of C₆₀

A novel approach has been developed to synthesise SiC on clean Si substrates in ultra high vacuum (UHV), taking advantage of the features offered by a supersonic beam of C₆₀. β -SiC can be grown directly on Si since it is formed at low temperature. The large lattice mismatch (20%) and thermal expansion (8%) coefficients mismatch, combined to the high

carbide temperatures ($>1000^{\circ}\text{C}$) for standard chemical vapour deposition leads to high density of defects in the heteroepitaxial growth [112-114].

The presence of triangular or square shape voids for such films has been widely reported for Si (111) and Si (100) substrates. They are related to diffusion mechanism of Si from the substrate to the SiC surface. Hence, a way to improve the crystallinity of the carbide films and the quality of the SiC/Si interface would be to reduce the synthesis temperature. Aversa et al. [115, 116] have developed a different approach based on investigating the activation of the reaction by the kinetic energy of the precursors. In order to do that they have developed a hyper thermal supersonic beam (HSB) of fullerenes seeded in He. The C_{60} is known to be a good precursor for carbidizing Si [117] and can be accelerated in a supersonic free jet up to 60 eV, which is well above the thermal energy of the standard growth technique (about 0.05eV). They [118] have shown that this makes possible the SiC bond formation by kinetic activation, even at substrate well below 1000°C . Other features of the HSB technique [119] that could be precious in controlling thin film growth are: very low angular divergence and high directionality, the possibility to control, the kinetic energy, velocity spread and flux density by means of different seeding pressures and/or gases, as well as the aggregation state of the beam particles. At temperature below 800°C (below the threshold for thermal bond formation) Si diffusion process becomes less efficient. Under these conditions, SiC hetero epitaxial growth could give films with controlled crystallinity and fewer defects.

6.1.7. Chemical vapour deposition growth

Of late Chemical Vapour deposition, (CVD) technology has found increasing importance in the fields of aerospace, military, science and engineering. The conventional

CVD method, so called thermal activated CVD (TACVD), uses thermal energy to activate the chemical reactions. However, the CVD reactions can also be initiated using different energy sources. This has given rise to other variants of CVD methods such as plasma enhanced CVD (PECVD) [120-123] and photo-assisted CVD (PACVD) [124-128] which use plasma and light, respectively, to activate the chemical reactions. Atomic Layer Epitaxy (ALE) [129-135] is a special mode of CVD where a 'monatomic layer' can be grown in sequence by sequential saturating surface reactions. Such CVD variants are useful for the controlled growth of epitaxial films, and the fabrication of tailored molecular structures. Other variants of CVD include metallo-organic CVD (MOCVD) [136-143] which uses metallo-organic as the precursor rather than the inorganic precursor used in the conventional CVD method. Other CVD variants such as pulsed injection MOCVD [144-149] and aerosol assisted CVD [150-154] use special precursor generation and delivery systems unlike conventional CVD. Flame assisted vapour deposition (FAVD) [155, 156] uses a flame source to initiate the chemical reaction and/or heating the substrate. Electrochemical vapour deposition (EVD) [157-162] is another variant of CVD that is tailored for the deposition of dense films on porous substrates. Chemical vapour infiltration (CVI) [33, 163-167] is a form a CVD that has been adapted for the deposition of a dense ceramic matrix during the fabrication of ceramic fibre reinforced ceramic matrix composites.

SiC coating can be obtained by several methods such as cementation packing [34]. Pack cementation has been used because it can provide for graded distribution of the elements at the interface between SiC coating and C/C composites. Due to mismatch of thermal expansion between SiC coating and C/C composites, cracks are inevitable,

which offer channels for oxygen and results in failure of coating, hence the two step pack cementation is used to fill these cracks. The free Si in this SiC coating can relax the stress at the end of the cracks.

Among the different techniques to grow SiC on different substrates, the Chemical Vapour Deposition (CVD) is the most frequently used technique. In CVD process, a precursor is used to deposit SiC and this precursor should have some requisite properties such as stability at room temperature, low vaporization temperature and high saturation of vapour pressure, it should undergo decomposition at a temperature far below the melting point of the substrates. It should be harmless, non-explosive and non-flammable for safe handling. Methyltrichlorosilane (MTS) is the commercially used precursor which has inherent drawbacks like pyrophoric, corrosive in nature and needs high temperature to deposit SiC.

CVD can be used to deposit materials at near theoretical density with good adherence to the substrate. The deposition rate by CVD process is higher than most other coating techniques except plasma spraying method. As the CVD technique does not require line of sight with the vapor source, coatings can be uniformly deposited over complex shapes and internal surfaces. SiC coating can be formed by various Si and C compounds. The typical systems used include SiH_4/CH_4 in hydrogen or nitrogen $\text{SiCl}_4/\text{CH}_4$ in hydrogen, $(\text{CH}_3)_2\text{SiCl}_2$ with hydrogen, CH_3SiCl_3 in hydrogen, $\text{SiHCl}_3/\text{C}_3\text{H}_8$ with hydrogen and $(\text{CH}_3)_4\text{Si}$ in hydrogen.

In the CVD process, a precursor is used to deposit SiC and this precursor should have some requisite properties for coating applications such as the following:

(a) It should be stable at room temperature.

- (b) It should have low vaporisation temperature and high saturation of vapour pressure.
- (c) It should be vaporized and vapour should be stable at low temperature (i.e. before decomposing or reacting at a higher temperature).
- (d) It should have suitable deposition rate. Low deposition rates for thin film applications (e.g. semiconductor industry) and high deposition rates for thick coating applications.
- (e) It should undergo decomposition/chemical reaction at a temperature below the melting temperature and phase transformation of the substrate depending on the engineering applications.
- (f) It should have low toxicity, explosivity and inflammable for safety of handling chemicals and disposing of the unreacted precursor. This is especially desirable for large scale industrial applications. Example; metallo-organic precursors are generally less toxic, pyrophoric and dangerous than hydrides and are gaining increasing usage in the semiconducting industry for the deposition of III–V and II–VI films.
- (g) It should be cost-effective for thin film or coating deposition.
- (h) It should be readily available with high purity (electronic grade).

The comparison of commercially available precursors for SiC coating is given in Table 6.1. The most widely and commercially used precursor is methyl trichlorosilane (MTS).

Table 6.1: Comparison of commercial available precursors

Precursors	CVD 2000	CVD 4000	MTS plus H ₂ (in exact ratios)	Silane Plus Methane (CH ₄)
Precursors Hazards	Flammable (FP=51°C)	Flammable FP=9°C). Air, moisture reactive at 140°C	Corrosive, toxic, flammable (FP=3°C). Moist air and water reactive at 20°C	Pyrophoric
% SiC in precursor	63% SiC (25% C, 12%H)	91% SiC (9%H)	27% SiC (71%Cl, 2%H)	Silane- 87% SiC (13%H), Silane+ Methane - 83% SiC (17% H ₂)
By Products of the CVD process	H ₂ and Methane (CH ₄)	H ₂	HCl (highly corrosive, must be neutralized) as well as H ₂ and silanes	H ₂
Coating Composition Si:C	Varies with substrate temp., 1:1+5-15% carbon	1:1± 0.5%	1:1±1.2% plus Cl and trace metals	1:01
Deposition temperature	800-900°C	600-900°C	1000-1400°C	200-500°C

In the present studies, SiC coating has been developed using CVD method at atmospheric pressure using MTS precursor along with hydrogen and argon as carrier gas. MTS was the most convenient compound used commercially for obtaining polycrystalline SiC because it has 1:1 molar ratio of silicon and carbon which would result in deposition of stoichiometric SiC deposits. Unlike other systems there is no need to control the Si/C ratio in the gas phase. Though there are many literature reports on CVD of SiC using MTS with hydrogen or argon, the CVD with gas mixtures of hydrogen, argon and MTS is scantily reported especially in the higher temperature i.e.

above 1200°C. The present objective of our work was to coat the entire surface of carbon composites with SiC using CVD technique in order to obtain a dense isotropic β -SiC phase and to study the effect of the operating parameters such as MTS, hydrogen flow rate and feed rate of MTS on the microstructure of the deposits.

6.2. Experimental procedure

The SiC coating was developed on 2D C/C composites (3.5cm×3.5cm×0.5cm) using chemical vapor deposition technique. A high temperature vertical graphite reactor of dimension 40cm length and diameter of 6cm was used for the coating studies. Schematic figure of the coating system is shown in Fig. 6.1. Silicon carbide (SiC) coating has been carried out using methyl trichlorosilane as source for silicon carbide; hydrogen-argon mixture was used as the carrier gas. The furnace was operated at 1400°C during growth under normal atmospheric pressure.

The deposition rate of SiC and nature of SiC deposition has been studied by varying the time duration of deposition, argon flow rate, hydrogen flow rate and MTS flow rate for a particular position of substrate in the vertical furnace having fixed geometry. A controlled MTS flow rate was achieved using a peristaltic pump. MTS was pumped with particular rate to the feed line connected to the vertical furnace which was preheated to temperature of 200°C.

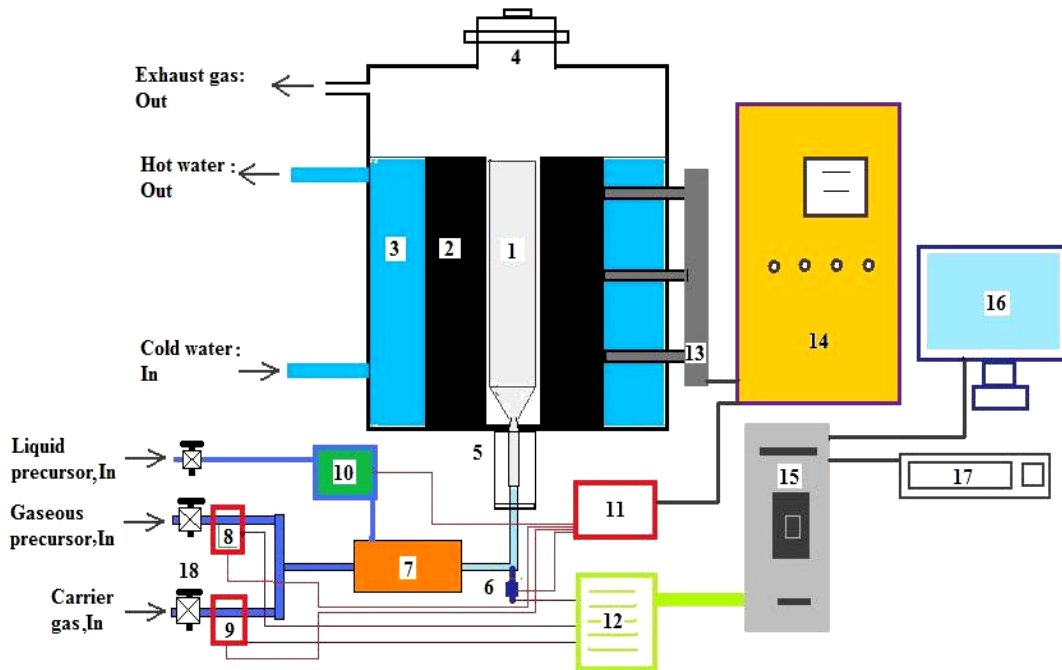


Fig. 6.1: Schematic of the experimental setup for coating using CVD technique

(1)Core graphite reactor, (2) Heating chamber, (3) Water cooling jacket, (4) Reactor opening, (5) gas inlet nozzle (graphite), (6) Pressure sensor, (7) Pre-heater, (8) & (9) MFC gas flow controller, (10) Liquid precursor pump, (11) AC/DC supply, (12) DAQ board, (13) Thermo-coil heating coil (inserted), (14) Reactor temperature control panel, (15) Computer CPU, (16) Computer monitor, (17) Computer key board, (18) Valve

As per literature on this topic and based on our prior experiments the following parameters have been chosen. Hydrogen along with argon was used as carrier gas to sweep the MTS vapors into the reactor. The flow rate of total gas mixture was varied from 2 - 6 lpm (litre per minute) keeping argon/hydrogen flow ratio constant, argon, hydrogen and MTS flow rate were varied from 0.8-4.8 lpm, 0.4-2.0 lpm and 0.5-2.0 ml/min, respectively.

Table 6.2: Experimental details of SiC coating by CVD method with varying parameters

<i>Exp. No.</i>	<i>Total gas flow rate of mixture (lpm)</i>	<i>Ar Flow rate (lpm)</i>	<i>H₂ Flow rate (lpm)</i>	<i>MTS Flow rate (ml/min)</i>	<i>Time duration (min)</i>	<i>H₂/MTS ratio</i>	<i>Deposition Rate (g/min)</i>	<i>Deposition Efficiency (%)</i>
1	2	1.6	0.4	0.5	60	4.66	0.0075	4.37
2	2	1.6	0.4	1.0	30	2.33	0.0195	5.66
3	2	1.6	0.4	2.0	15	1.16	0.0223	3.24
4	2	1.2	0.8	0.5	60	9.3	0.00679	3.95
5	2	1.2	0.8	1.0	30	4.65	0.013	3.62
6	2	1.2	0.8	2.0	15	2.32	0.0229	3.34
7	2	0.8	1.2	0.5	60	14.0	0.00644	3.75
8	2	0.8	1.2	1.0	30	7	0.012	3.11
9	2	0.8	1.2	2.0	15	3.5	0.025	3.59
10	4	3.2	0.8	0.5	60	9.31	0.0062	3.6
11	6	4.8	1.2	0.5	60	14.0	0.0045	2.61
12	2	2.0	0	0.5	60	0	0.0089	5.23
13	2	0	2.0	0.5	60	23.28	0.016	9.35

The total amount of MTS used for all experiment was kept constant (i.e. 30ml) to compare the deposition in all cases. The detail about design of experiment for coating the C/C composites by SiC are given in Table 6. 2. The as grown coatings were characterized by XRD for phase identification. SEM analysis was carried out for the microstructural and morphology details. EDS studies have been performed to get the compositional detail of coating.

6.3. Results and discussion

XRD has been used for the phase identification of the deposits. From the XRD pattern it could be inferred that the coating corresponds to the β -SiC phase in all the experiments as tabulated in the Table 6.2. The XRD pattern (Fig. 6.2) showed the reflections from (111), (220) and (200) corresponding to β -SiC phase. SEM analysis with EDS has been carried out for evaluating the microstructure and its chemical composition. SEM photographs (Fig. 6.3(a-i)) shows varying morphology depending on the deposition conditions.

As deposited SiC films can grow preferentially either along the (111) or (220) plane, depending on the processing conditions. Lee [168] proposed that lower deposition rates and lower temperature for fcc crystals result in development of lowest surface energy plane i.e. (111) plane while higher temperature and higher deposition rates causes development of higher surface energy, i.e. the (110) plane. At higher temperatures and lower deposition rate the preferred orientation occurs in the most densely populated atom planes or the lowest surface energy crystal facets (i.e. (111) plane in SiC crystal).

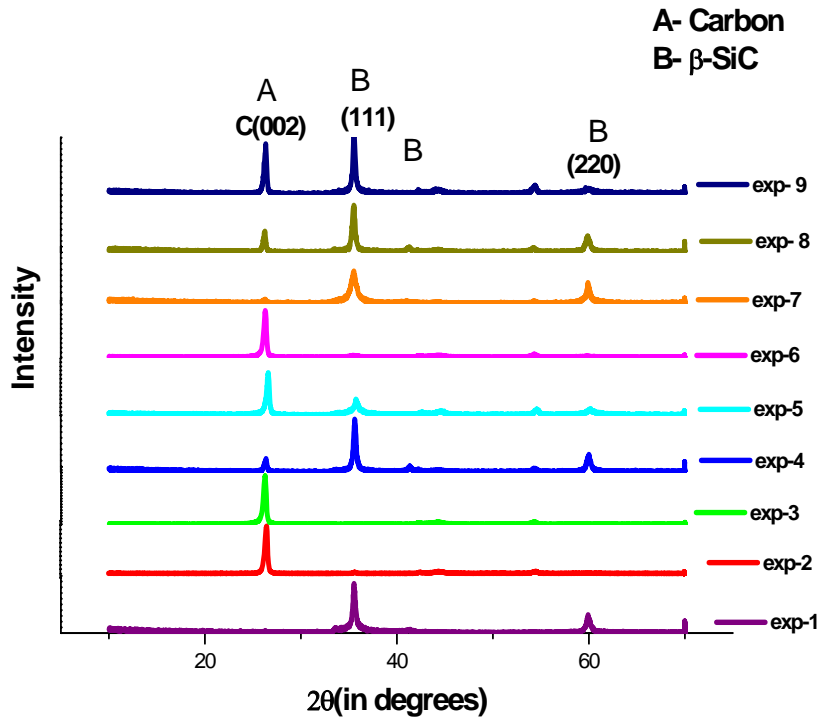


Fig. 6.2: XRD pattern of the coatings obtained for various operating conditions as per Table 6.2

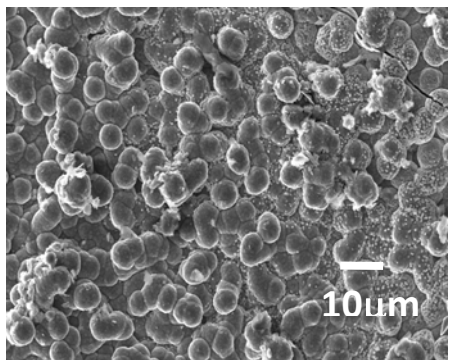
At higher temperatures and high deposition rates the molecules attached to the substrate have the texture that places the less densely populated atomic plane or higher surface energy lattice plane (i.e. $\{110\}$ plane in SiC crystal) parallel to the substrate. The surface morphology of the SiC deposited films largely depend on the preferred orientation. It can be seen from Fig. 6.2 that the deposits are showing preferential orientation of (111) plane and there is some growth in the (220) plane also with varying process conditions.

The deposition temperature, the H_2 / MTS ratio and the total gas flow rate play an important role in determining the microstructure and the properties of the deposit. The morphologies of as deposited SiC crystals are affected primarily by the supersaturating

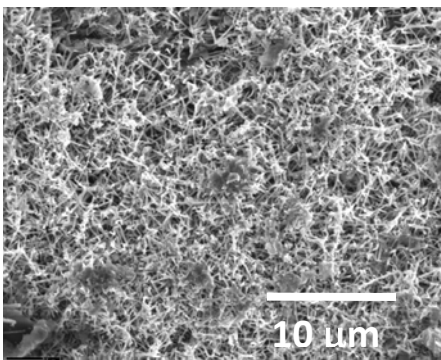
degree of the gaseous reactants which are dependent on the deposition temperature and the concentration of MTS in the reactor. According to stagnant gas layer model [36], growth rates are limited by surface reaction at lower temperature and by mass transfer of vapor at higher temperature. An increase in both temperature and MTS concentration can enhance the supersaturating degree of the gaseous reactants and the driving force of chemical reaction. The reaction temperature and the supersaturating degree of gaseous reactants are the macro scales of reflecting the energy value which affect the morphology.

The high reaction energy can promote SiC crystals to grow along several directions which results in the formation of grains. The present coating experiments were carried out at higher temperature (1400°C), therefore the morphology of SiC deposit was governed by mass transfer mechanism. The EDS spectra's at two different operating conditions, which revealed the presence of Si (60 weight %) and carbon (35 weight %) and some traces of oxygen (5 weight %) are shown in Fig. 6.4.

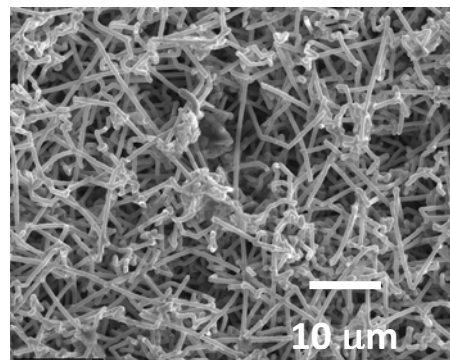
The presence of oxygen may be due to the adsorbed oxygen on the surface or due to the fact that these depositions are carried out under normal atmospheric pressure, not in vacuum. In the next section, the effect of MTS, hydrogen and argon flow rate on the mass transfer of MTS intermediates and on the morphology of SiC deposit has been discussed.



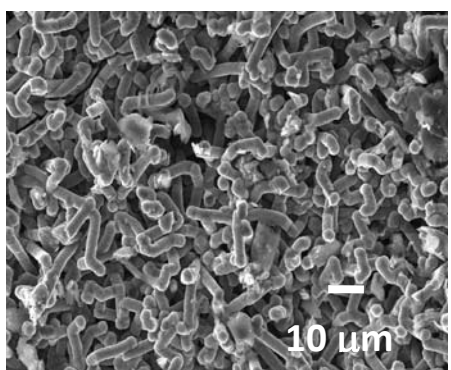
(a) $H_2/MTS = 4.66$



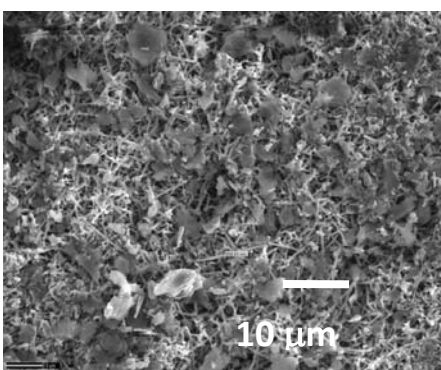
(b) $H_2/MTS = 2.33$



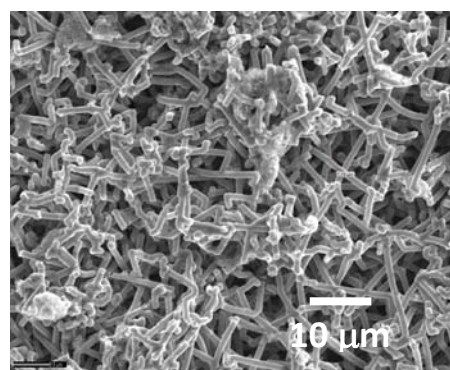
(c) $H_2/MTS = 1.16$



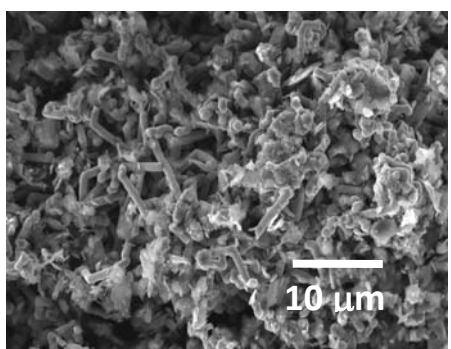
(d) $H_2/MTS = 9.3$



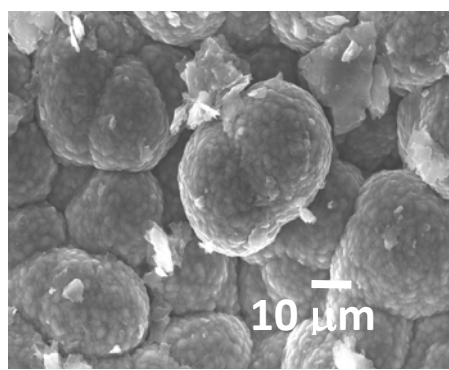
(e) $H_2/MTS = 4.65$



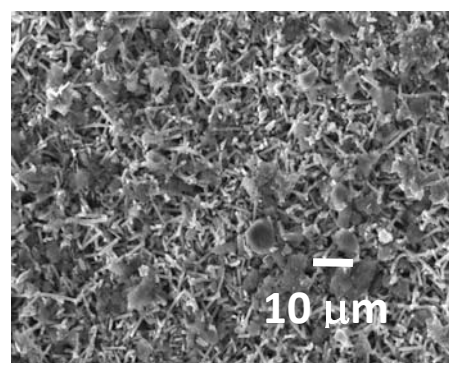
(f) $H_2/MTS = 2.32$



(g) $H_2/MTS = 14.0$

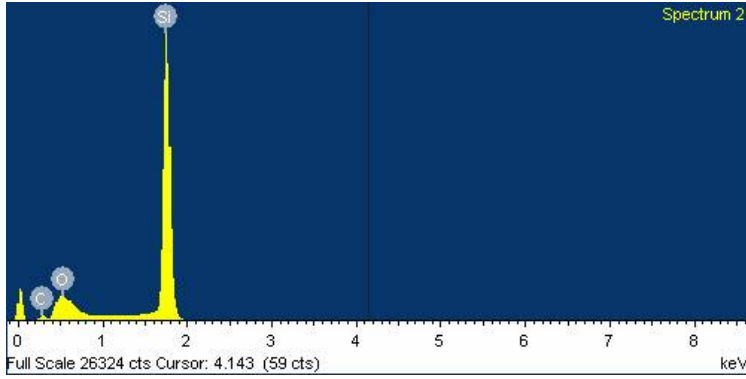


(h) $H_2/MTS = 7.0$

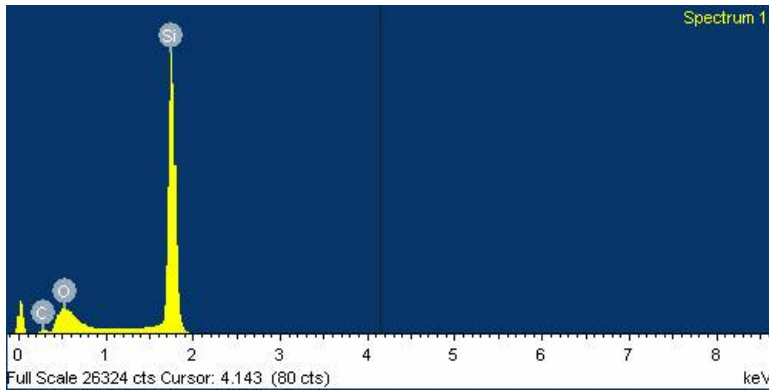


(i) $H_2/MTS = 3.5$

Fig. 6.3 (a-i): SEM micrographs of the coatings obtained with various processing parameters (a) deposition at $H_2/MTS= 4.66$ (b) deposition at $H_2/MTS=2.33$ (c) deposition at $H_2/MTS=1.16$ (d) deposition at $H_2/MTS= 9.3$ (e) deposition at $H_2/MTS= 4.65$ (f) deposition at $H_2/MTS=2.32$ (g) deposition at $H_2/MTS=14.0$ (h) deposition at $H_2/MTS=7.0$ (i) deposition at $H_2/MTS=3.5$



(a)



(b)

Fig. 6.4: EDS spectrum of the coating for conditions of deposition at (a) $H_2/MTS= 7$ and (b) deposition at $H_2/MTS= 4.66$

S.No.	Weight %C	Weight %O	Weight %Si
Spectrum (a)	35.85	4.15	60.0
Spectrum (b)	34.2	5.75	60.05

6.3.1. Effect of MTS feed rate

The effect of MTS feed rate in the mixed gas was investigated at different hydrogen concentrations (by volume %) keeping other operating parameters constant and the results are presented in Fig. 6.5(a). The figure shows that with increase in MTS feed rate at various hydrogen concentrations in mixed gas, the deposition rate increased. At 20% hydrogen with increasing MTS flow rate the deposition rate increases initially and gets saturated at 2 ml/min while in the case of 40% hydrogen (Exp. 4, 5 & 6) and 60% hydrogen (Exp. 7, 8 & 9) there is a linear increase in deposition rate with increase in MTS feed rate and reaches saturation at 3.0 ml/min. It is observed that at 20% hydrogen with increasing MTS feed rate the preferred orientation of SiC growth is in {111} i.e. whisker formation is observed (Fig. 6.3 (a–c)) at higher flow rate of MTS. This indicates that when 20% hydrogen is used with MTS the concentration of intermediate gaseous reactant does not increase with increase in MTS concentration in the depositing gaseous mixture leading to growth of whiskers and the concentration of gaseous reactant gets saturated early. It is verified from calculation of the order of the reaction also.

The MTS dissociation does not affect the deposition rate as there is no change in order of reaction which means there is enough number of intermediate reactants that is present, which govern the kinetics and morphology of the deposit. It is seen that at 40% hydrogen at higher MTS feed rate (3ml/min) there is dense deposition. Lower MTS feed rate shows formation of whiskers i.e. preferred orientation is [111] while at higher MTS feed rate the preferred orientation is [220]. While increase of 40% hydrogen, the concentration of intermediate gaseous reactants increases with increasing MTS concentration leading to the grain growth.

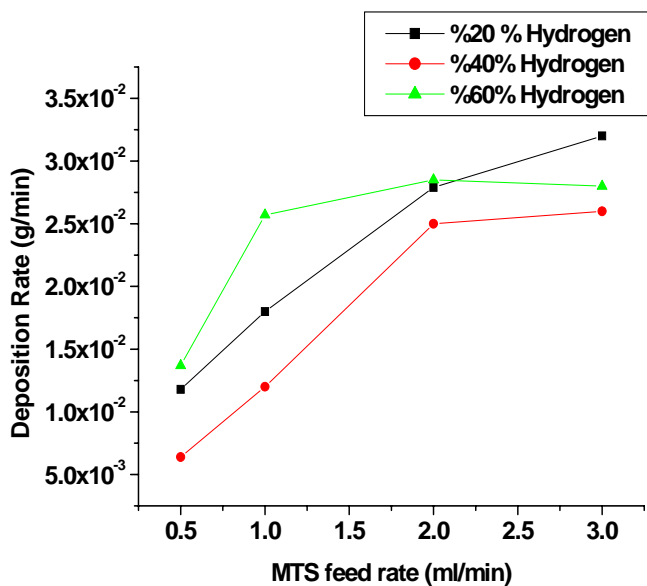


Fig. 6.5(a): Effect of variation of MTS feed rate at different hydrogen concentrations on the deposition rate

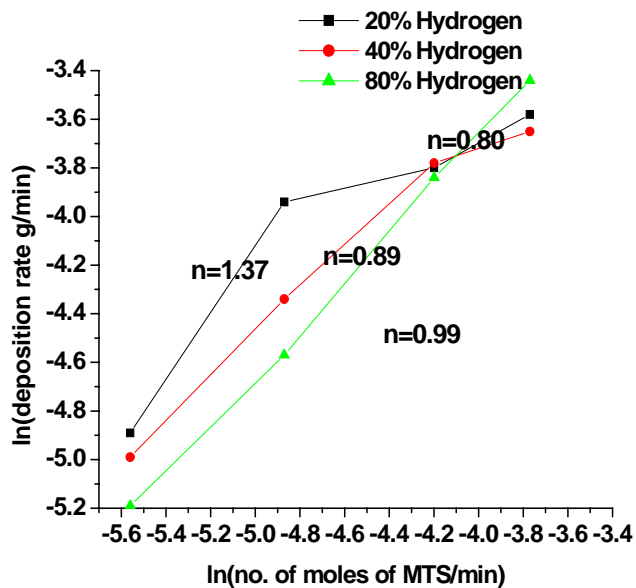


Fig. 6.5(b): Plot of ln (no. of moles of MTS) vs. ln (deposition rate) at different hydrogen concentration

It can be observed by the order of reaction at different stages. It is seen from Fig. 6.5(b) that the reaction order with respect to number of MTS moles is greater than 1.0 at 20% hydrogen with increasing number of moles of MTS but decreases to 0.8 as the saturation is achieved. Initially the MTS concentration effect the deposition rate after certain feed rate it does not show any effect. These results indicate that the reaction is very fast at higher concentrations of MTS and hence the deposition rate does not depend upon the dissociation rate of MTS. While the order of reaction for 40% hydrogen and 60% hydrogen was found to be 0.89 and 0.99, respectively indicating that the order of reaction with respect to number of moles of MTS is nearly 1.0. It means enough reactants are generated at high feed rate of MTS which is good enough for grain growth, even at saturation point.

6.3.2. Effect of hydrogen gas flow rate on deposition rate

It is expected that the dissociation of MTS molecule should occur faster with increase in hydrogen flow but the reverse trend in deposition rate is observed for MTS feed rate at ≤ 1.0 ml/min. This may be due to the HCl, by-product of both homogeneous and heterogeneous reactions which inhibit SiC growth [37, 38, 168-171] by chemical adsorption on the surface. Another possible reason may be due to the excess production of by-products gas, HCl along with argon which sweeps out the converted SiC particles from the reactor before deposition can take place at such high deposition temperature.

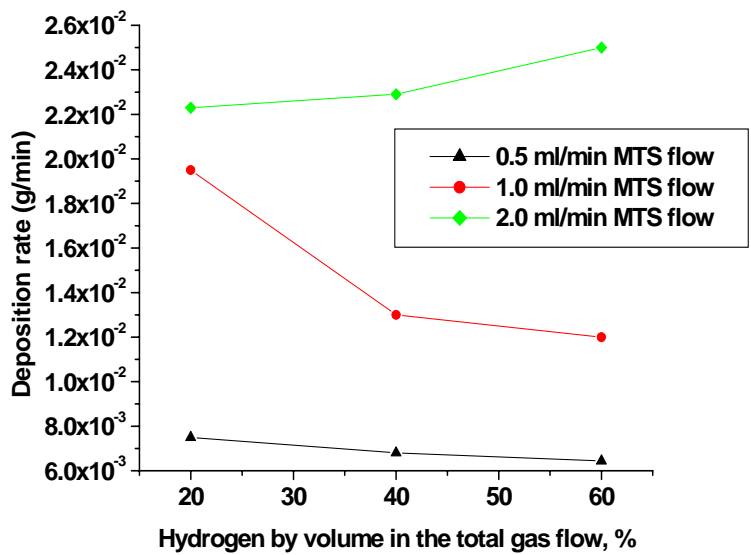


Fig. 6.6(a): Effect of H₂ content in the diluent gases on deposition rate

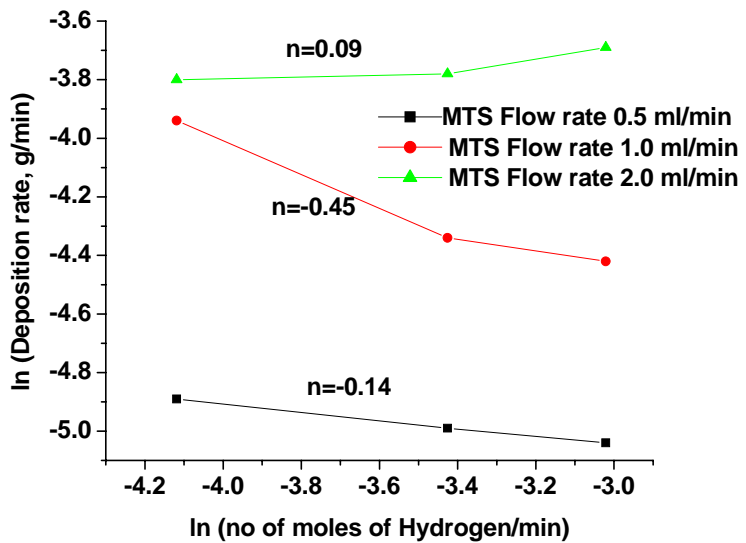


Fig. 6.6(b): Plot of ln of (no. of moles of hydrogen) vs. ln of (deposition rate) at different MTS flow rate

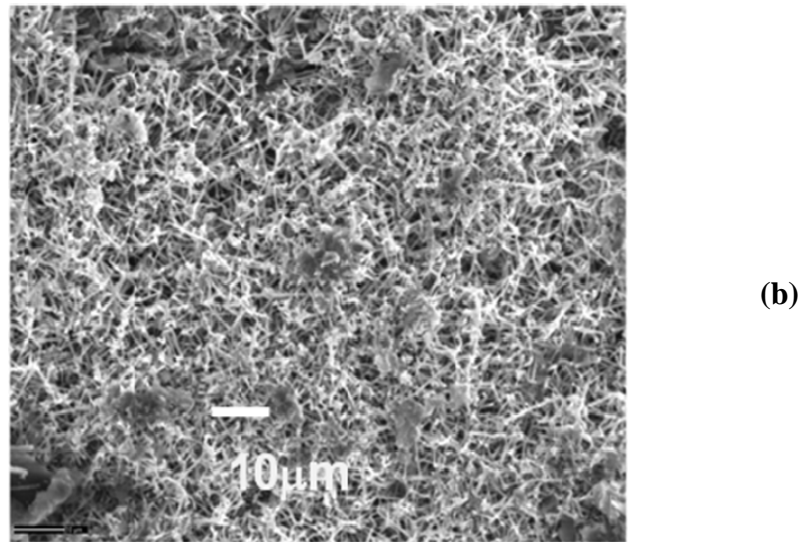
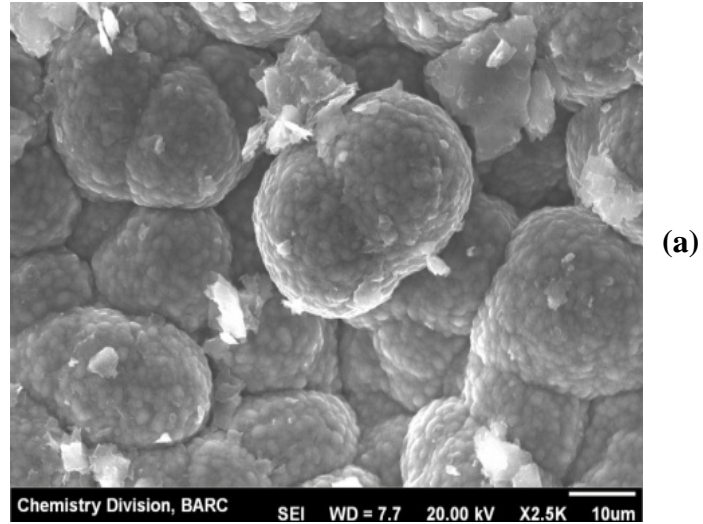


Fig. 6.6 (c): Effect of H₂ content in the diluent gases on the microstructure of deposit at MTS=1.0ml/min for (a) 60% hydrogen & (b) 20% hydrogen

However for 100% hydrogen concentration (zero concentration of argon) in the feed gas, it was found to give maximum conversion resulting in higher deposition rate. This result may be due to minimum effect of total gas flow when inert gas flow is zero. At 0.5ml/min MTS feed rate there is grain growth at lower hydrogen concentration i.e. it has growth along direction [220], with increasing hydrogen concentration there is whisker formation i.e. preferred orientation (Fig 6.3 (a, d & g)). Competitive adsorption of HCl and sweeping of SiC particles is the reason for low concentration of reactants at high hydrogen percentage in the total gas for the case of 0.5ml/min feed rate of MTS which leads to whisker growth at higher hydrogen concentration. For MTS flow rate 1.0 ml/min with increasing hydrogen concentration the preferred orientation of growth is in [220] i.e. the grain growth is observed in Fig. 6.3 (b, e & h) respectively.

In case of MTS feed rate of 1.0 ml/min the deposition rate is decreasing with increasing hydrogen flow and grain growth is occurring as seen from Fig. 6.6 (c) that may be due to enough concentration of intermediate reactants in the feed gas. It can be seen from the order of the reaction (0.5 in this case) that enough MTS was getting decomposed. While for MTS feed rate 0.5 ml/min and 2.0 ml/min, there is no appreciable effect of concentration of number of moles of MTS on the deposition rate, but there is an appreciable effect at MTS feed rate of 1.0 ml/min. In case of MTS feed rate greater than 1.0 ml/min (e.g. for MTS feed rate 2.0 ml/min) the deposition rate increases with increase in hydrogen flow rate resulting in as expected grain growth as seen in Fig. 6.3 (c, f & i).

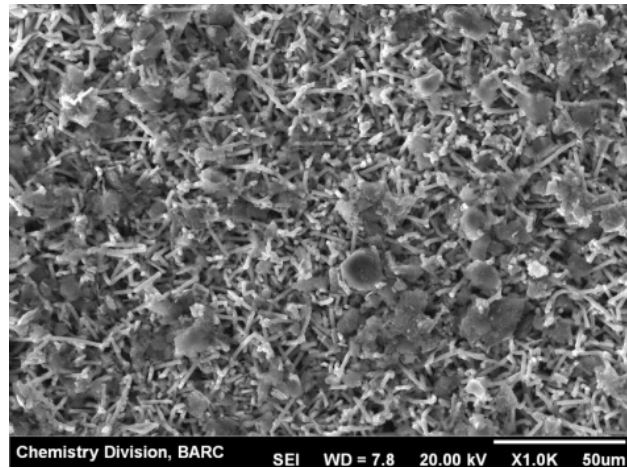
6.3.3. Effect of inert gas flow rate on coating rate

The studies by Motojma et al. [172] have reported that argon addition to source gas under atmospheric pressure lessens the co-deposition of free silicon with SiC and accelerates the deposition of single phase SiC. Experiments were conducted at various argon percentages in the mixed gas feed and its effect on the SiC deposits is presented. Although carrier gas does not take part in the reaction but it can influence the deposition rate. It has been observed that with change in the percentage of argon in the total gas mixture the deposition rate changes.

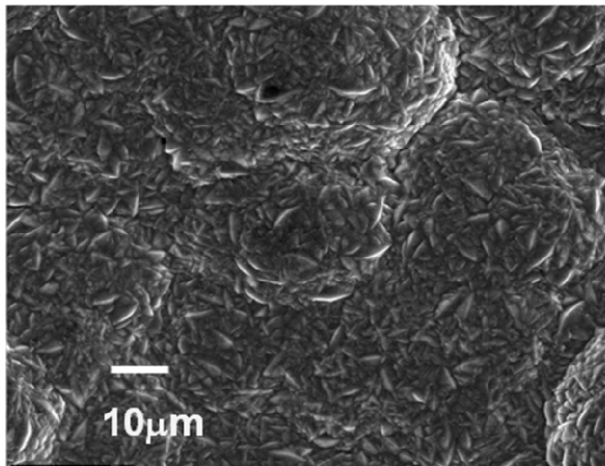
Though there is an increasing trend in the deposition rate at MTS flow rate of 0.5 ml/min and at 1.0 ml/min but at 2.0 ml/min, there is decrease in deposition rate. The reverse trend has been observed in this case with respect to hydrogen percentage in the total gas mixture. At much higher deposition temperature mass transfer mechanism has been observed. At MTS feed rate 0.5 ml/min at lower concentration whisker growth is observed and at higher concentration of argon grain growth in [220] direction is observed. The changes in microstructure with increasing total gas flow rate are shown in Fig. 6.7.

It is possible that for MTS feed rate of 0.5 ml/min the concentration of intermediate at the deposition surface was low at low argon percentage and when the argon percentage is higher it carries more intermediate reactant species at the deposition surface resulting in increase of deposition rate (grain growth). For the MTS flow rate of 1.0 and 2.0 ml/min the reverse trend is obtained, at higher argon concentration the preferred orientation is [111] even though the deposition rate increase with increase in argon concentration in case of MTS feed rate of 1.0 ml/min.

It can be explained by the fact that enough concentration of reactants was present at the deposition surface for low argon percentage and as the argon percentage increases in the mixed gas the sweeping of intermediate reactant species dominate the deposition, resulting in whisker growth as seen in Fig. 6.7 (c). It is seen from Fig. 6.7 (a & b) that the effect of argon gas is more pronounced than the hydrogen gas in the system.



(a)



(b)

Fig. 6.7: Effect of total gas in the diluent gases on microstructure for (a) total flow at 2 lpm & (b) 4 lpm

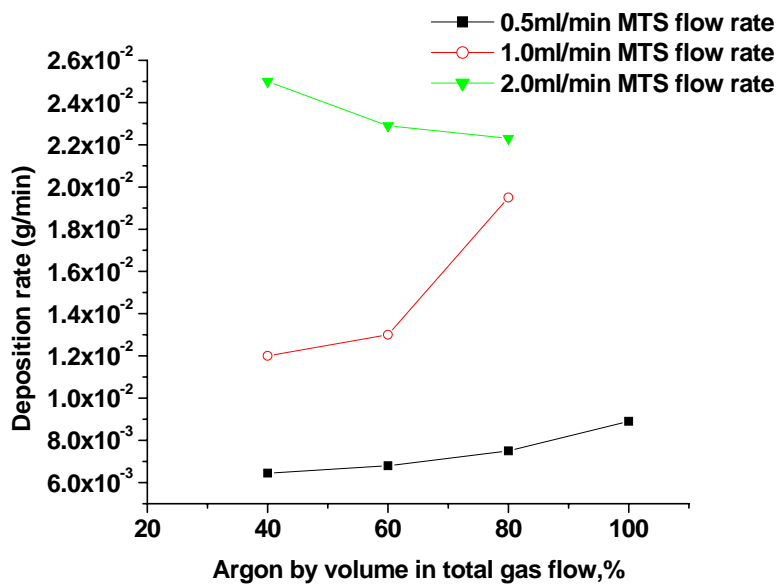


Fig. 6.7(a): Effect of argon gas on the deposition rate

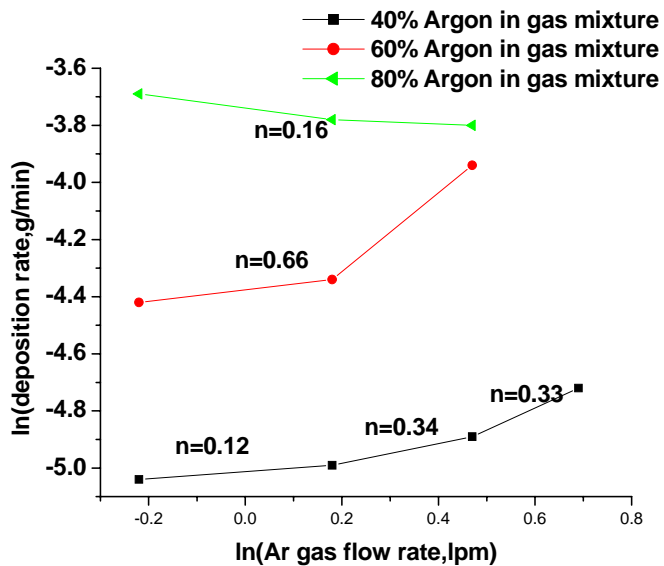
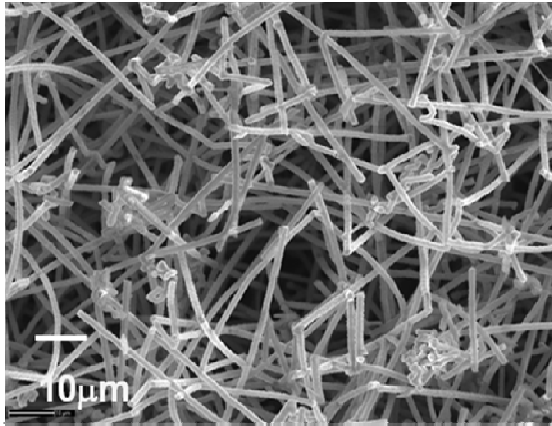
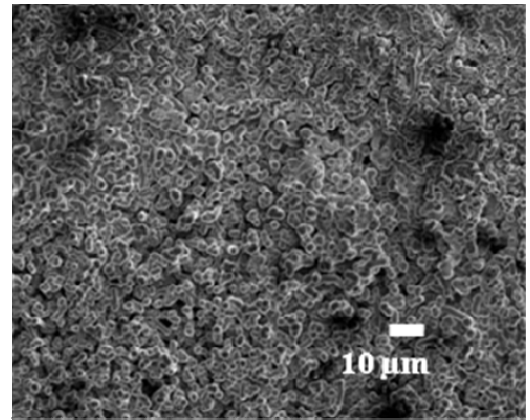


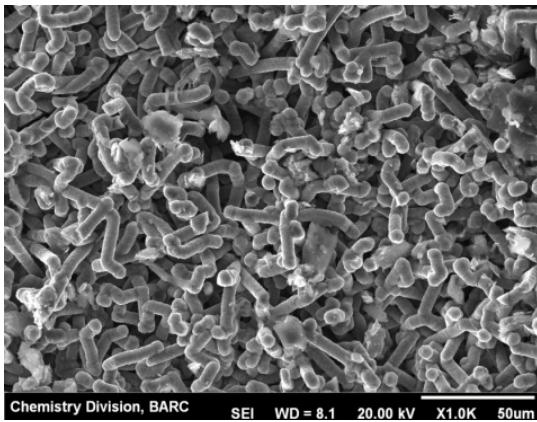
Fig. 6.7(b): Plot of ln (no of moles of argon) with ln (deposition rate)



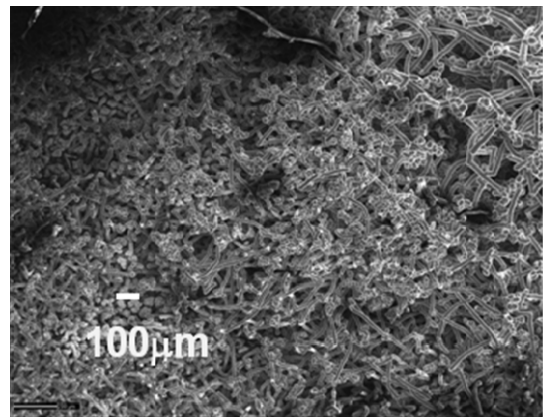
(a)



(b)



(c)



(d)

Fig. 6.7 (c): Effect of argon gas on the microstructure at (a) 0%Ar, (b) 40%Ar, (c) 60%Ar, (d) 100%Ar

6.4. Conclusions

SiC coating was developed using chemical vapor deposition technique on the 3D surface of the C/C composite block in a hot wall vertical reactor at temperature of 1400°C. The effects of the process coating parameters on deposition rate and morphology of CVD coated SiC were studied. The coating was identified as β -SiC from XRD analysis. The preferred orientation was found to be (111) plane. It has been observed that for obtaining dense SiC coating the MTS feed rate should be on the higher side (≥ 1.0 ml/min) along with higher hydrogen percentages in the mixed gas with respect to argon percentage. It was observed in the present studies that not only the percentage of hydrogen but the percentage of argon in the total gas mixture also affects the deposition rate and the morphology of the SiC deposit. The effect of argon was found to be more pronounced than the hydrogen gas in the present system.

CHAPTER 7

CHAPTER 7

SUMMARY AND FUTURE SCOPE OF THE WORK

Compact High Temperature Reactor (CHTR) and Advanced Heavy Water Reactor (AHWR) need high density isotropic type graphite and also carbon-carbon composite for various critical structural components. The present work dealt with preparation and characterization of the carbon/carbon composites. The objective of this work was to develop carbon composite materials with reasonably high density as well as amorphous isotropic carbon for use in thermal reactors. An amorphous structure is needed in order to avoid accumulation of Wigner energy. This was achieved by carrying out development of carbon-carbon composites by using different precursors. Subsequently efforts will be taken up for the fabrication of some test components for evaluating the performance of the same in our novel reactors.

The composites were prepared using petroleum coke, carbon black PAN carbon fiber both chopped and matted. These materials were characterized for their properties. The petroleum coke based samples were found to be amorphous at lower temperatures (below 800°C), but they tend to graphitize at higher temperatures. They also showed the accumulation of Wigner energy, which limits their use as neutron scatterer in the Advanced Heavy Water Reactor (AHWR). As these samples were found to be graphitizable in nature, the next sets of samples were made from chopped PAN fiber and phenol formaldehyde resin as binder, which was non-graphitizable in nature. The composite made with 20 vol% fiber heat treated at 1000°C showed the desired property in

terms of amorphousness and isotropicity. The samples with lower volume percentage of fiber (10 vol%) developed crack during processing. The increase in the percentage of fiber volume enhances stress-graphitization as observed in the case of 50 vol% fiber based sample. The samples with 20 vol% fiber tended to develop anisotropy when heated to 2000°C. Basically the shape of the fibers causes the development of stress at fiber matrix interface. This problem was eliminated by choosing the spherical shape of the second phase (carbon black). Carbon black-phenolic resin composites have been prepared through a novel technique. It was found that the carbonization of the phenolic resin pieces prior to composite preparation helps in many ways. The shrinkage of the product was found to be lesser as the volatile matter evolved during carbonization was lesser. Thus the possibility of crack formation also reduces. Therefore higher rate of heating could be employed there by helping in the decrease in production cost. Composite with a density up to 1320 kg/m³ was obtained without any impregnation by this method as compared to 1270 kg/m³ with the PAN fiber based sample after four cycles of impregnation. The structural characterization suggests that the carbon black-phenolic resin carbon composite fulfills the criterion of the scattering material. Its C_p value was found to be more than that of the graphite, which suggests a reduced probability of release of Wigner energy. This material has to be densified to impart additional irradiation stability. Further composite fabrication using 2-D matted PAN carbon fiber for the development of carbon-carbon composites was carried out. The carbonization of the preforms to remove the volatiles was subsequently followed by densification of these samples using liquid impregnation technique. To achieve the required density the impregnation was carried out with varying process controls and characterized after

suitable heat treatments. Optical microscopy with polarized light, electron microscope, XRD analysis, X-ray Tomography and Micro Laser Raman spectroscopy was used to characterize the microstructure and get a clear understanding of the microstructural details and to estimate the degree of graphitization that is achieved finally. C/C composites with density of 1470 kg/m^3 were developed with two cycles of impregnation and carbonization. These composites were found to be amorphous in nature from the XRD even after heat treatment up to 1800°C . Further work on irradiation stability was carried out to see the stability of these materials under irradiation.

As the main aim of this was to develop a composite for advanced reactor applications, hence due concern would be given to the radiation damage studies of these materials by conducting relevant irradiation experiments. The carbon-carbon (C/C) composite samples have been irradiated at varying fluencies with thermal neutrons at APSARA Reactor in Bhabha Atomic Research Center, Trombay. The energy spectrum for irradiation was 98% thermal neutron component for which neutron energy was up to 0.55 eV and 2% is epithermal component (above 0.55 eV). It was observed from the XRD analysis of the irradiated and unirradiated samples that the value of d_{002} peak for the unirradiated samples is higher than that of the irradiated samples indicating the tendency to get ordered structure. This was also inferred from the Raman spectroscopy. The I_G/I_D ratio of irradiated samples was found increase with increasing fluence when compared to unirradiated samples initially but decreased further with increasing fluence. The stored energy with respect to the fluence level was obtained from the DSC, which indicated that simple defects created due to low fluence of irradiation are annealed by heating accompanied by release of the stored energy at lower temperature. On the other hand the

complex defects are formed require high temperatures are required for annealing these defects. The flux/fluence used is lower than the actual scenario in the upcoming compact high temperature reactor; however the present study could definitely be an initial step in the direction of investigation of damage caused by neutrons on carbon/carbon composite materials for its use in the upcoming reactor. Currently the available flux was low in the range of 10^{12} n/cm²/s. However, these samples have to be evaluated by irradiating at a higher dose for potential nuclear application. There were severe limitations of not being able to use the fluence of 10^{20} n/cm². However, an extension of work on carbon-carbon composites irradiation with higher flux in some international neutron irradiation facility would be taken up in near future. Currently some irradiation studies with high energy neutrons are being carried out. However these investigations are out of scope of the present work and hence will be taken up in future.

In order to ensure the long life of the components in the reactors these are need to be coated with pyrolytic carbon (PyC) and silicon carbide (SiC) for improved mechanical, chemical and irradiation stability. PyC and SiC are to be deposited by chemical vapour deposition (CVD) technique. Although carbon-carbon composite materials possess excellent properties, they are prone to oxidation at high temperatures as conventional carbon materials when exposed to oxidizing atmospheres. Hence they can be used in environment consisting of vacuum or inert gases. As these carbon-carbon composites will experience high temperature and severe environment it is necessary to coat these composites with suitable protective layer coating. Hence protocol for SiC coating was developed using chemical vapor deposition technique on the 3D surface of the C/C composite block in a hot wall vertical reactor at temperature of 1400°C. The effects of the

process coating parameters on deposition rate and morphology of CVD coated SiC were studied. The coating was identified as β - SiC from XRD analysis. In the present studies it was found that not only the content of hydrogen but also the content of argon in the total gas mixture affects the deposition rate and the morphology of the SiC deposit. The effect of argon was found to be more pronounced than the hydrogen gas in the present system. It was possible to achieve the SiC coating using the commercially available MTS. Further work on studies of oxidation behavior of these coating will be taken up in near future course of work. Alternative chlorine free precursors are being developed which also will be used for the SiC coating as MTS is highly corrosive in nature. Consequently, intense research over the past years have been focused on the elaboration of SiC based materials from precursors such as silane plus hydrocarbon, organosilicon single compound precursors and organosilicon polymer. Among the SiC precursors most focus is on the compounds, which are non corrosive, non toxic and environment friendly.

An extension of the present work not included in thesis

Apart from the coating of the carbon-carbon composites, development of protective coatings for the containment of fission products within the fuel particle is also being studied. The CHTR fuel is designed to operate at high temperatures, withstand high burn-up and has long core resident time. A typical CHTR fuel bed consists of prismatic BeO moderator block with centrally located graphite fuel tube carrying fuel compacts. Schematic of fuel particle is shown in Fig. 7. 1. A typical TRISO coated fuel particle has a kernel (500 μm diameter) comprising of fissile, fertile and burnable poison materials followed by four coating layers.

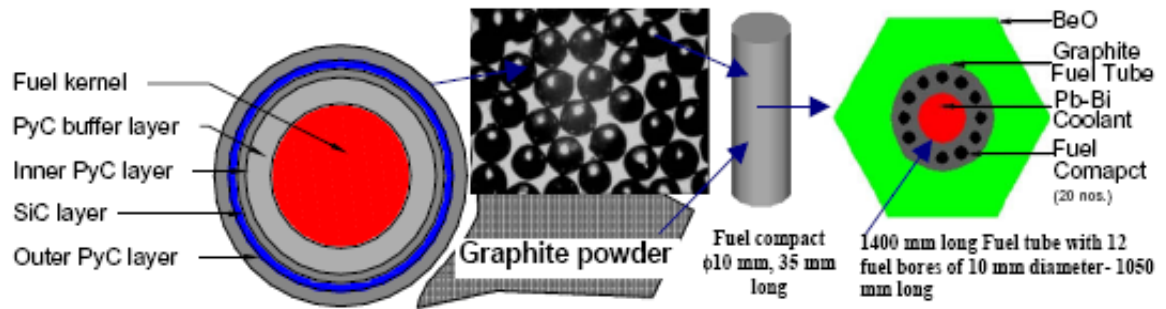


Fig.7.1 Schematic of TRISO coated fuel particle, compact and single fuel bed

The functional requirements and proposed dimensions of these layers are as follows: (a) Low-density pyrolytic carbon (PyC) buffer layer: This porous layer (90 μm thick) acts as an absorber for fission recoils and provides volume to accommodate fission products and kernel swelling. (b) Inner high-density PyC layer: This layer (30 μm thick) serves as a barrier to gross diffusion of fission products and fission gases. This is to protect integrity of subsequent SiC layer. (c) Silicon carbide (SiC) interlayer: This layer (30 μm thick) contains gaseous fission products released by the kernel and thus acts like a pressure vessel. This also acts as a pressure vessel. It contains gaseous fission products released by the kernel and thus acts like a pressure vessel. This also acts as an additional diffusion barrier to metallic fission products. The thickness needs to be adequate to withstand the developed pressure and corrosion attacks by fission products. (d) Outer high-density PyC layer: This layer (50 μm thick) as well as inner PyC layer, on irradiation, puts SiC layer into compression to limit stresses. Additionally it provides chemical protection to SiC layer. It also provides bonding surface for making compacts. There is much importance of SiC in nuclear energy applications. In TRISO-coated fuel

particles for high temperatures reactors (CHTR, HTGR), one of the layers is SiC coating. In particular, the SiC layer acts as a diffusion barrier to metallic fission products and a miniature pressure vessel of the particle. The Fig. 7.2 shows the SEM images of the TRISO coated particle containing the SiC layer sandwiched between the PyC prepared as an extension of the present work.

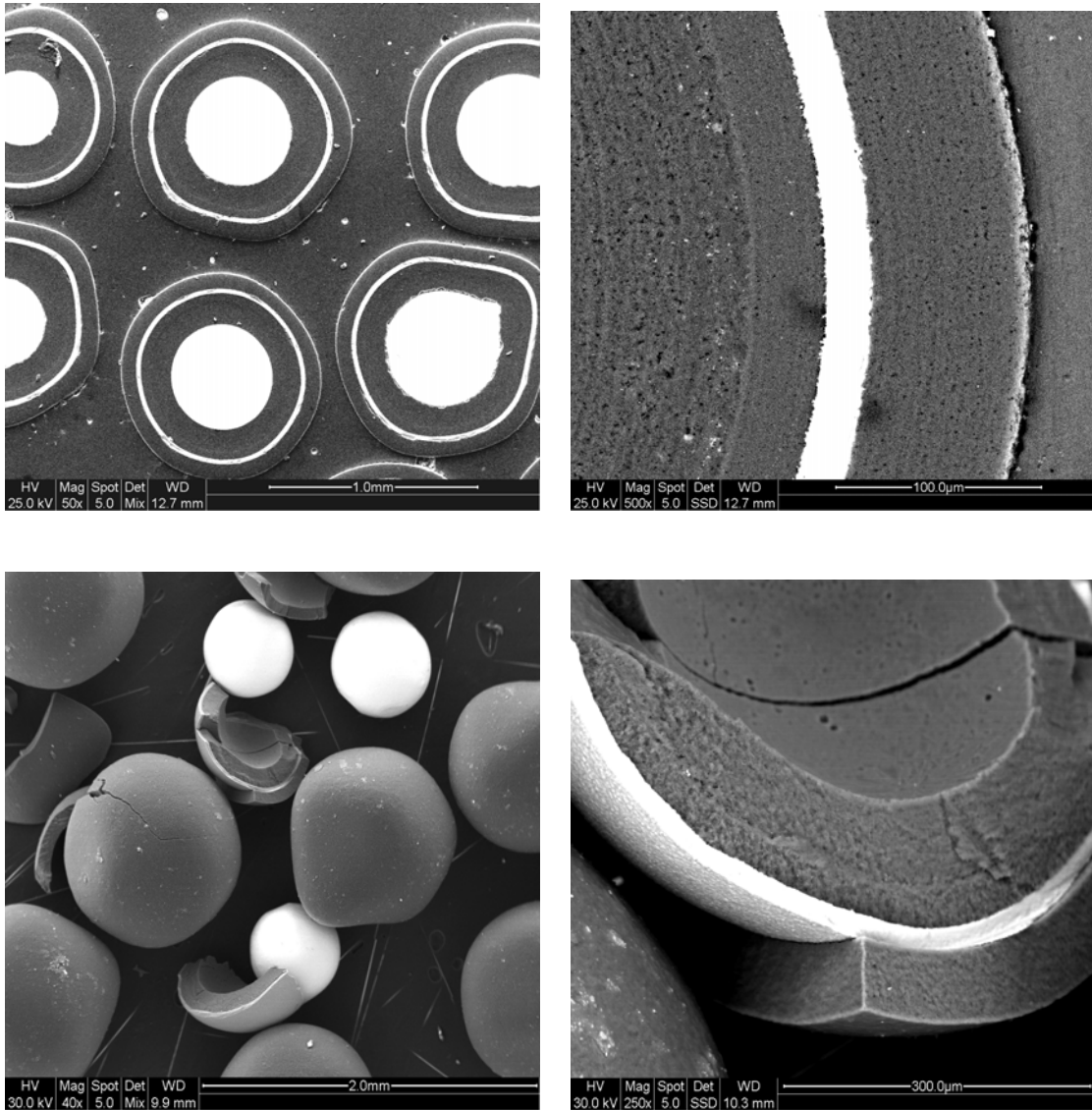


Fig. 7.2: SEM images of the TRISO coated zirconia particle

Coating has been developed using surrogate 500 μm zirconia microspheres. Three isotropic layers of graded density of pyrolytic carbon and silicon carbide over a buffer (porous) carbon layer was coated over the spherical particle. The coatings were developed using a high temperature spouted bed reactor. Uniform coating of pyrolytic carbon was obtained using acetylene gas. The SiC coating was developed using methyl trichlorosilane (MTS). The SEM images of the coated particles showing the different layers of uniform thickness are shown in Fig. 7.2. Raman Spectroscopy verified the β -SiC phase of isotropic layer of silicon carbide.

REFERENCES

1. Graphite Moderator Lifecycle Behavior, IAEA – Tecdoc., 90 (1998) 32.
2. G. B. Engle, and W. P. Eatherly, High Temp.–High Press, 4 (1972) 119.
3. B. T. Kelly, editor. Physics of Graphite. London: Applied Science Publishers, 1981.
4. B. T. Kelly and T. D. Burchell, Carbon, 32 (1994) 499.
5. T. D. Burchell. Carbon Materials for Energy production and Storage. In Design and Control of structure of Advanced Carbon materials for Enhanced Performance. B. Rand et al, editor. Kluwer Academic Publishers, (2001), 277.
6. E. Fitzer, L. M. Manocha, Carbon Reinforcements and Carbon/Carbon Composites, pp 17-25, 100-105, 288-300, Springer-Verlag Berlin Heidelberg New York, (1998).
7. Timothy. D. Burchell, Carbon Materials for Advanced Technologies, 1st Ed., pp 1, 458-473, Elsevier Science Ltd, Oxford OX5 1GB, UK, 1999.
8. G. Savage In: Carbon/carbon composites New York: Oxford University Press, (1993) 117.
9. B. Rand Matrix Precursors for Carbon- carbon composites London: Royal Society of Chemistry, (1993) 67.
10. Houdayer, M., Spitz, j and Tran Van, D, French Patent No.81,22163, 1981, US patent No.4, 472454, 1984.
11. E. Fitzer, Carbon, 25 (1987)163.
12. P. Delhaes, Carbon, 40 (2002) 641.
13. He-Jun Li, Xiang-Hui Hou, Yi-Xi Chen, Carbon, 38 (2000) 423.
14. Zhong-hua Tang, Dian-ning Qu, Jie Xiong, Zhi-qiang Zou, Carbon, 41 (2003) 2703.

15. S. Vaidyaraman, W. J. Lackey, P. K. Agrawal, Michael, A. Miller,
Carbon, 34 (1996) 347.
16. D. Rovillain, M. Trinqucoste, E. Bruneton, A. Derre, P. Davida, P. Delhaes,
Carbon, 39 (2001) 1355.
17. Y. G. Roman, J. F. A. K. Kotte & M. H. J. M. de Croon,
J. Eur. Ceram. Soc., 15 (1995) 875.
18. E. Fitzer and W. Huttner, J. Phys. D, Appl. Phys., 14 (1981) 347.
19. W. Kowbel and C. H. Shan, Carbon, 28 (1990) 287.
20. K. Y. Sohn, Seh-Min Oh and Jai-Young Lee, Carbon, 26 (1988) 157.
21. J. D. Buckley, Ceram Bull., 67 (1988) 364.
22. J. E. Sheehan, Ann Rev Mater Sci., 24 (1994)19.
23. M. E. Westwood, J. D. Webster, R. J. Day, F. H. Hayes, R. Taylor,
J. Mat. Sci.,31 (1996) 1389.
24. H. Fritze, J. Jojie, T. Witke, C. Ruscher, S. Weber, S. Scherrer,
J. Eur. Ceram Soc., 18 (1988) 2351.
25. F. Smeacetto, M. Ferraris, Carbon, 40 (2002) 583.
26. R. Luo, J.Cheng, T. Wang, Carbon, 40 (2002)1965.
27. Q. Fu, He-Jun Li, X. Shi, Li, Sun, Scripta Materialia, 52 (2005) 923.
28. R. Bruetsch, Thin Solid Films, 126 (1983) 313.
29. A. Ravesh, A. Inspektor, U. Carmi, and R. Auni,
J. Vac. Sci. Technol. A, 5 (1987) 2836.
30. C. A. A. Cairo, M. L. A. Gracca, C. R. M. Silva, J. C Bressiani,
J. Eur Ceram.Soc., 21 (2001) 325.
31. L. F. Cheng, Y.D Xu, L. T. Zhang, Carbon, 38 (2000) 1493.
32. S. Lloyd, N. Avery, M. Pal, Carbon, 39 (2001) 991.

33. A. Ordine, C. A. Achete, O. R. Mattosa, I. C. P Margaret, S. S Camargo Jr.,
T. Hirsch, Surf Coat. Technol., 133-134(2000) 583.
34. S. K. Gong, H. B. Xu, Q. H. Yu, C. G. Zhou,
Surf. Coat. Technol., 130 (2000) 128.
35. K. L. Choy, Prog. Mater. Sci., 48 (2003) 57.
36. W. G. Zhang, K. J. Huttinger, Chem. Vap. Deposition., 13 (2001) 167.
37. Y. J. Lee, D. J. Choi, S. S. Kim, H. L. Lee, H. D. Kim,
Surf. Coat. Technol., 177-178 (2004) 415.
38. A. K. Costa, S. S. Camargo Jr., C. A. Achete, R. Carius,
Thin Solid Film., 243 (2000) 377.
39. J. D Buckley, Ceram Bull., 67 (1988) 364.
40. J. E Sheehan, Ann. Rev. Mater. Sci., 24 (1994)19.
41. M. E Westwood, J. D Webster, R. J. Day, F. H. Hayes, R. Taylor,
J. Mater. Sci., 31 (1996)1389.
42. D. L. Schmidt, K. E Davidson, L. S. Theibert. SAMPE J, 35 (3) (1999) 27.
43. D. L. Schmidt, K. E Davidson, L. S. Theibert. SAMPE J, 35 (4) (1999) 5.
44. D. L. Schmidt, K. E Davidson, L. S. Theibert. SAMPE J, 35 (5) (1999).47.
45. G. Savage In: Carbon/carbon composites, New York, Oxford University Press,
(1993) 117.
46. L. V. Azaraffi, Elements of X-ray crystallography, M. C. Grow Hill Book
Company, New York, (1968).
47. B. D. Cullity, Elements of X-ray Diffraction, Addison Wesley Publishing
Company, Inc. Massachusetts, U. S. (1965).
48. L. Babout, P. M. Mummery, T. J. Marrow, A. Tzelepi, P. J. Withers.
Carbon, 43 (2005) 765.

49. L. Babout, P. M. Mummery, T. J. Marrow, P. J. Withers,
Scripta Mater.,54 (2006) 829.
50. N. Douarache, D. Rouby, G. Peix, J. M. Jouin, Carbon 39 (2001) 1455.
51. C. Berre, S.L. Fok, B. J. Marsden, L. Babout, A. Hodgkins, T. J. Marrow et al.,
J. Nucl. Mater.,352 (2006) (1-3) 1.
52. Robertson, Ad. Physics, 35 (1986) 317.
53. D. S. Knight and W. B. White, J. Mater. Res., 4 (1989) 385.
54. P. K. Bachmann and D. U. Wiechert, Diamond Rel. Mater., 1 (1992) 422.
55. L. Nikiel and P. W. Jagodzinski, Carbon, 31 (1993) 1313.
56. R. J. Nemanich, J. T. Glass, G. Lucovsky and R. E. Shroder,
J. Vac. Sci. Technol. A., 6 (1988) 1783.
57. L. Fayette, B. Marcus, M. Mermoux, L. Abello and G. Lucazeau,
Diamond Rel. Mater., 3 (1994) 438.
58. F. Tuinstra and J. L. Koenig, J. Chem. Phys., 53 (1970) 1126.
59. M. Yoshikawa, G. Katagiri, H. Ishida and A. Ishitani,
Sol. State. Comm.,66 (1988) 1177.
60. W. D. Kunrary, Property Measurement at high Temperature, John Wiley and
Sons, Inc., New York, (1959)
61. J. Valentich, Instrument and control System, 42 (1969) 91.
62. A. Guinier and G. Fournet, in: John Wiley and Sons, Inc, New York (Eds), Small-
Angle Scattering of X-rays, 19 (1955).
63. S. Mazumder, D. Sen, T. Saravanan, P. R. Vijayaraghavan,
J. Neutron Research, (2001) 39.
64. J. A. Lake, J. Appl. Cryst., 23 (1967) 191.
65. Th. Gerber, G. Walter, P. W. Schmidt, J. Appl. Cryst., 24 (1991) 278.

66. A. J. Allen, *J. Am. Ceram. Soc.*, 88 (2005) 1367.
67. S. Knight Diane, B. J. White William. *Mater. Res.*, 4 (1989) 385.
68. K. Dasgupta, M. Roy, A. K. Tyagi, S. K. Kulshreshtha, Ramani Venugopalan, D. Sathiyamoorthy, *Compos. Sci. Technol.*, 67 (2007) 1794.
69. A. K. Patra, S. Ramanathan, D. Sen, S. Mazumder, *J. of Alloys and Compounds*, 397 (2005) 300-305.
70. S. Mazumder, et al, *J. Phys.: Condens. Matter* 13 (2001) 5089.
71. D. Sen, J. Bahadur, S. Mazumder; *Eur. Phys. J. B* (2009) Web Published (DOI : 10.1140/epib/e2009-00270-8) and references there in.
72. H. Peterlik, P. Fratzl and K. Kromp *Carbon*, 32 (1994) 939.
73. R. Venugopalan, D. Sathiyamoorthy, R. Acharya and A.K. Tyagi, *J. Nucl. Mat.*, 404 (2010) 19.
74. R. E. Nightingale, *Nuclear Graphite* (Academic Press, New York, London), 1962.
75. B. T. Kelly, *Prog. Nucl. Energ.*, 2 (1978) 21.
76. V. I. Klimenkov, Y. N. Aleksenko, *USSR Acad. Sci. Phys.*, 2 (1956) 226.
77. T. D. Burchell. *Phys. Scripta T.*, 64 (1996) 17.
78. T. Iwata, *J. Nucl. Mater.*, 134 (1985) 361.
79. G. H. Kinchin and R. S. Pease, *Rep. Phys. Prog. Phys.*, 18 (1) (1955).
80. F. Banhart, *Rep. Prog. Phys.*, 62 (1999) 1181.
81. A. Seeger, *Rad. Eff. Deffects Solids.*, 355 (1989) 111.
82. A. Seeger, W. Frank, *Solid State Phenomena.*, 125 (1988) 3.
83. Linhua Zou, Baiyun Huang, Yong Huang, Qizhong Huang, Chang'an Wang., *Materials chemistry and physics*, 82 (2003) 654.
84. J. Marie, J. Mering, *Chemistry and Physics of Carbon*, 6 (1970) 125.
85. R. E. Franklin, *Acta. Crystallogr.*, 4 (1951) 253.

86. B. E. Warren, *Phys. Rev.*, 59 (1941) 693.
87. J. Biscoe, B. E. Warren, *J. Appl. Phys.*, 13 (1942) 364.
88. R. E. Franklin, *Acta. Cryst.*, 3 (1950) 107.
89. S. Ergun, *Chemistry and Physics of Carbon*. Ed, P. L. Walker (Marcel Dekker, New York), 1967.
90. S. Ergun, *Carbon*, 14 (1976) 39.
91. W. Ruland, *Chemistry and Physics of Carbon*. Ed, P. L. Walker (Marcel Dekker, New York), 1968.
92. P. Scherrer. *Nachr. Ges. Wiss. Gottingen*, 2 (1918) 98.
93. K. Dasgupta, P. Barat, A. Sarkar, P. Mukherjee, D. Sathiyamoorthy, *Applied Physics A-Materials Science and Processing*. 87 (2007) 721.
94. G. V. Dienene, *J. Appl. Phys.*, 24 (1953) 666.
95. S. D. Preston, G. T. Melvin, *Results from the 1997/98 Stored energy Survey of Windscale Pile I, IAEA Technology plc Report AEAT-3400 WPTC 73, 1998.*
96. H. Bridge, D. Mottershead, *J. Nucl. Mater.*, 20 (1966) 281.
97. J. H. W. Simmons, *Radiation Damage in Graphite*, 1965.
98. J. C. Bell, H. Bridge, A. H. Cottrell, G. B. Greenough, W. N. Reynolds, J. W. H. Simmons, *Stored energy in the graphite of power producing reactors*, *Phil. Trans. Roy.Soc. A.*, 254 (1962) 361.
99. R. Bruetsch, *Thin Solid Films*, 126 (1983) 313.
100. R. Koc, S. V. Cattamanchi, *J. Mater. Sci.*, 33 (1998) 2537.
101. J. Wang, I. Risa, T. Takayuki, *Energy and Fuel*, 14 (2000) 1108.
102. C. Y. Che, C. I. Li, S. H. Chen, *Br. Ceram. Tras.*, 99 (2000) 57.

103. A. W. Weimer, K. J. Nilsen, G. A. Cochran, R. P. Roach,
AIChE. J., 39 (1993) 493.
104. P. Martin, R. Ecke, E. Muller, J. Eur. Ceram.Soc., 18 (1998) 1737.
105. H. Tanaka, Y. Karachi, Ceram.Int., 14 (1988) 109.
106. I. Hasegawa, T. Nakamura, S. Motojima, and M. Kajiwara,
J. Mater. Chem., 59 (1995) 193.
107. W. P. Cannon, S. C. Donforth, J. H. Flint, J. S. Haggoty and R. A. Marra,
J. Am. Ceram. Soc., 65 (1982) 324.
108. W. P. Cannon, S. C. Donforth, J. H. Flint, J. S. Haggoty, and H. K. Bowen,
J. Am. Ceram., Soc., 65 (1982) 330.
109. Y. Suyama, R. A. Marra, J. S Haggaty and H. K Bowen,
Am. Ceram. Soc. Bull., 64 (1985) 1356.
110. M. Cauchetier, O. Croix, and M. Luce, Adv. Ceram. Mater., 3 (1988) 548.
111. H. L. Marcus, D. L. Bourell, Adv. Mater. Processes, 144 (1993) 28.
112. A. J. Steckl, IEEE Trans. Electron. Devices, 39 (1992) 64.
113. H. Nagasawa, K. Yagi, Phys. Stat. Sol. B, 202 (1997) 335.
114. R. Scholz, U. Go Sele, F. Wishmeyer, E. Niemann,
Appl. Phys. A, 66 (1998) 59.
115. F. Biasioli, F. Boschetti, E Barborini, P. Piseri, P. Milani, S. Iannotta, Chem.
Phys. Lett., 270 (1997) 115.
116. F. Biasioli, F. Boschetti, P. Piseri, P. Milani, S. Iannotta,
Chem. Phys. Lett., 301 (1999) 109.
117. M. Baaloch, A. V. Hamza, Appl. Phys. Lett., 63 (1993) 150.
118. G. Ciullo, M. Moratti, T. Toccoli, S. Iannotta, Phil. Mag. B, 80 (2000) 635.

119. P. Milani, S. Iannotta, Cluster Beam Synthesis on Nano-structured Materials, Springer, Berlin, (1999) ISSN 4437.
120. A. Sherman, Chemical vapor deposition for microelectronics. Park Ridge (NJ): Noyes, (1987).
121. D. W. Hess, D. B. Graves. In: M.L. Hitchman, K F. Jensen, editors. CVD principles and applications. San Diego: Academic Press, (1993) 387 [Chapter 7].
122. A. Dehbi-Alaoui, Vacuum, 46 (1995) 1305.
123. Y. Catherine In, G. S. Mathad, G. C. Schwartz, G. Smolinsky, editors. Plasma processing. Pennington: Electrical Society, (1985) 317.
124. S. J. C. Irvine, In D. A. Glocker, S. I. Shah, editors. Handbook of thin film process technology, B1.3 Bristol (UK), Institute of Physics, 1995.
125. T. F. Deutsch, D.J. Ehrlich, R. M. Osgood, Appl. Phys. Lett., 35 (1979) 175.
126. R. M. Osgood and T. F. Deutsch, Science, 227 (1985) 709.
127. I. P. Herman, Chem Rev., 89 (1989) 323.
128. V. R. McCrary, V. M. Donnelly In, M.L. Hitchman, K. R. Jensen, editors. Chemical vapour deposition. London: Academic Press, 1993.
129. L. Niinisto, M. Ritala, M. Leskela, Mat. Sci. Engg. B. Solid-State Mat Adv Technol., 41 (1996) 23.
130. J. E. Lau, K. W. Barth, G. G. Peterson, D. Endisch, A. Topol, A. E. Kaloyeros, J. Electrochem. Soc., 145 (1998) 4271.
131. K. J. Bachmann, C. Hoepfner, N. Sukidi, A. E. Miller, C. Harris, D. E. Aspnes, Appl. Surf. Sci., 112 (1997) 38.

132. A. Koukitu, T. Taki, *Appl. Surf. Sci.*, 112 (1997) 63.
133. M. A. Herman, J. T. Sadowski, *Crystal Res Technol.*, 34 (1999) 153.
134. T. Suntola In, D. A. Glocker, S. I. Shah, editors. *Handbook of thin film process technology*, B1:5.1. Bristol (UK), Institute of Physics, (1995).
135. H. S. Park, J. S. Min, J. W. Lim, S. W. Kang, *Appl. Surf. Sci.*, 158 (2000)
136. *CVD metalorganics for vapour phase epitaxy product guide and literature review*, Danvers (MA): Morton International, Advanced Materials, (1993).
137. S. K. Ghandhi, I. B. Bhat, *MRS Bulletin*, 11 (1988) 37.
138. R. D. Dupuis, In: Glocker, D.A., Shah, S.I. editors. *Handbook of thin film process technology*, B1.1:1. Bristol (UK): Institute of Physics, (1995).
139. A. C. Jones, *J. Cryst. Growth*, 129 (1993) 728.
140. J. P. Duchemin, *J. Vac. Sci. Technol.*, 18 (1981) 753.
141. M. J. Ludowise, *J. Appl. Phys.*, 58 (1985) R31.
142. G. B. Stringfellow, *Organometallic vapour phase epitaxy, theory and practice*. San Diego (CA): Academic Press, (1989).
143. N. Putz, H. Heinecke, M. Heyen, P. Balk, M. Wayers, H. Luth, *J. Cryst. Growth*, 74 (1986) 292.
144. J. P. Senateur, C. Dubourdiou, V. Galindo, F. Weiss, *Application of pulsed injection MOCVD to the deposition of oxide single layers and superlattices*. In: Choy KL, editor. *Innovative/cost-effective processing of films and powders*. London: Imperial College Press, (2002).
145. A. A. Molodyk, O. Y. Gorbenko, A. R. Kaul, *J. Alloys Comp.*, 951 (1997) 303.
146. O. Y. Gorbenko, A. A. Bosak, *J. Cryst. Growth*, 186 (1998) 181.
147. M. Leskela, H. Mosla, L. Ninistro, *Supercond. Sci. Tech.*, 6 (1993) 627.

148. O. Y. Gorbenko, A. R. Kaul, G. Wahl, *Chem Vapour Deposit*, 3 (1997) 4.
149. K. L. Choy, Vapour processing of nanostructured materials. In: Nalwa, H.S., editor. *Handbook of nanostructured materials and nanotechnology*. San Diego (CA), Academic Press, (2000) 533.
150. W. S. Rayleigh, *The theory of sound*, Vol. 2. New York, Dover, (1945).
151. G. I. Taylor, *Proc R Soc London Ser, A*, 280 (1964) 383.
152. G. Blandenet, Y. Lagrade, *Thin Solid Films*, 77 (1981) 81.
153. K. Omura, P. Veluchamy, M. Tsuji, T. Nishio, M. Murozono, *J. Electrochem. Soc.*, 1462 (1999) 13.
154. K. L. Choy, W. Bai, S. Charojrochkul, B. C. H. Steele, *J. Power Source*, 71 (1998) 361.
155. K. L. Choy, H. K. She. *Mater. Sci. Eng. A*, 281 (2000) 253.
156. A. O. Isenberg In, J. D. E McIntyre, S. Srinivasan, F. G. Will, editors. *Proceedings of the symposium on electrode materials and processes for energy conversion and storage*. Pennington (NJ): Electrochemical Society, (1977) 572.
157. N. Q. Minh, T. Takahashi, *Science and technology of ceramic fuel cells*. The Netherlands, Elsevier Science, (1995).
158. Van, Dieten V. *Electrochemical vapour deposition of SOFC interconnection materials*. PhD thesis. The Netherlands: Delft University of Technology, (1994).
159. A. O. Isenberg, *Solid State Ionics*, 3–4 (1984) 431.
160. M. Inaba, A. Mineshige, S. Nakanishi, I. Nishimura, A. Tasaka, K. Kikuchi, *Thin Solid Films*, 323 (1998) 18.
161. M. F. Carolan, J. N. Michaels, *Solid State Ionics*, 37 (1990) 189.
162. T. L. Starr, *Ceram Eng Sci Proc.*, 9 (1988) 803.

163. R. L. Bickerdike, A. R. G. Brown, G. Hughes, H. Ranson, Proc. 5th Conf. on Carbon. New York, Pergamon Press, (1962) 575.
164. T. Haug, H. Knabe, U. Ehrmann, In: Auner N, Weiss J, editors. Organosilicon Chemistry, Weinheim (Germany): VCH, (1994) 303.
165. W. J. Lackey, Ceram. Eng. Sci. Proc., 10 (1989) 577.
166. D. P. Stinton, T. M. Besmann, R. A. Lowden,
Am. Ceram. Soc. Bull., 67 (1988) 350.
167. T. M. Besmann, D. P. Stinton, R. A. Lowden, MRS Bulletin, 13 (1988) 45.
168. D. N. Lee, J. Mater. Sci., 24 (1989) 4375.
169. D. J. Ching, W. J. Shyy, D. H. Kuo and M. H. Hon,
J. Electrochem. Soc., 134 (1987) 3145.
170. T. M. Bessman, B. W. Sheldon, T. S. Moss III, M. D. Kaster,
J. Am. Ceram. Soc., 75 (1992) 2899.
171. D. Lespiaux, F. Langlias, R. Naslain, S. S. Schamm,
J. Eur. Ceram. Soc., 15 (1995) 81.
172. S. Motojima and Mistutaka Hasegawa, Thin solid Films, 186 (1990) L39.

Publications out of the present work

JOURNAL PUBLICATIONS

1. Novel isotropic high density amorphous carbon composite for moderator application in low temperature thermal reactors.
K. Dasgupta, M. Roy, A. K. Tyagi, S. K. Kulshrestha, **Ramani Venugopalan** and D. Sathiyamoorthy
Composite Science and Technology 67 (2007) 1794-1801
2. Neutron irradiation studies on low density pan fiber based carbon /carbon composites.
Ramani Venugopalan, D. Sathiyamoorthy, R. Acharya and A. K. Tyagi,
J. Nucl. Mater. 404 (2010)19-24.
3. Preparation and microstructural characterization of carbon/carbon composite,
Ramani Venugopalan, D. Sathiyamoorthy and A. K. Tyagi ,
World Journal of Engineering (Accepted)
4. Morphological study of SiC coating developed on 2D Carbon Composites using MTS precursor in a hot wall vertical reactor.
Ramani Venugopalan, Jyoti Prakash, J. Nuwad, C. G. S Pillai, A. K. Tyagi, and D. Sathiyamoorthy.
Int J. Mater. Res. (Communicated)
5. Effect of impregnation mediated densification on the structure and properties of PAN-fiber based carbon composite.
Ramani Venugopalan, Mainak Roy, Rekha Rao, Sussie Thomas, D. Sathiyamoorthy and A. K. Tyagi
(Communicated)

IN PROCEEDINGS

6. Development of Carbon Composite With SiC Coating For High Temperature Nuclear Applications
Ramani Venugopalan, Jyoti Prakash, J. Nuwad, C. G. S Pillai, A. K. Tyagi, and D. Sathiyamoorthy
Published in the Proceedings of International Conference on Carbon Nanotechnology: Potential Challenges held at IIT Kanpur on 15-17 Dec.2010, pp 84-85.
7. Development of carbon-carbon composite: its characterisation and irradiation studies. **Ramani Venugopalan**, D. Sathiyamoorthy and A. K. Tyagi
Published in the Proceedings of FACC-2009 held on Nov 25-27, 2009 at Habitat Centre New Delhi.

8. SANS Study of Porosity in PAN Carbon Fiber Based C/C Composites.
R. Venugopalan, D. Sathiyamoorthy, A. K. Patra, J. Bahadur, P. U. Sastry and A. K. Tyagi
Published in the Proceedings of DAE Solid State Physics Symposium, Vol. 54 (2009), pp-1129-30 held at The Maharaja Sayajirao University of Baroda, Vadodara on Dec 14-18, 2009.

9. Pore Structure of Neutron Irradiated PAN Fiber Based Carbon-Carbon Composites: A Small Angle X-ray Scattering Study,
A. K. Patra, **Ramani Venugopalan**, P. U. Sastry and D. Sathiyamoorthy
Published in the Proceedings of ISMC-2010 held at BARC, Mumbai on Dec 7-11, 2010, pp 308.

Novel isotropic high-density amorphous carbon composites for moderator applications in low-temperature thermal reactors

K. Dasgupta^a, M. Roy^{b,*}, A.K. Tyagi^b, S.K. Kulshreshtha^b,
Ramani Venugopalan^a, D. Sathiyamoorthy^a

^a Powder Metallurgy Division, Bhabha Atomic Research Centre, Mumbai-400085, India

^b Chemistry Division, Bhabha Atomic Research Centre, Mumbai-400085, India

Received 28 March 2006; received in revised form 20 October 2006; accepted 29 October 2006

Available online 19 December 2006

Abstract

Making of high-density amorphous carbon composites with substantial thermal and radiation stability is a challenge in itself. Two series of carbon composites were synthesized by making use of novel precursor materials like polyacrylonitrile (PAN) based carbon fibers and carbon black (CB) powder along with phenol formaldehyde resin as binder. The samples were extensively characterized using a large number of characterization techniques. Carbon composites made by this technique are found to retain very high-degree of isotropicity and amorphous nature even when heat-treated at ~1500 °C and above. Besides, they are found to exhibit excellent thermo-mechanical properties like specific heat, compressive strength and coefficient of thermal expansion. Stock composition was varied to find its effect on the thermo-mechanical properties and isotropicity of the samples.

© 2006 Elsevier Ltd. All rights reserved.

Keywords: A. Amorphous; A. Carbon composite; B. Mechanical properties; B. Microstructure

1. Introduction

Use of graphitic carbon as moderator material is strictly not recommended for nuclear reactors operating below 250 °C, as this might lead to the sudden release of Wigner energy that is locked up in graphite as a result of atoms dislodged from their normal lattice points by impinging radiation, often causing serious accidents [1,2]. Graphite is also likely to undergo post-irradiation densification, thereby inflicting severe changes in the fabricated structures and hence causing failure in them. However despite all these drawbacks, graphitic carbon due to its excellent neutron scattering properties, still continues to be the unanimous choice for the moderator material in high-temperature nuclear reactors [3–5] where the aforesaid drawbacks are essentially overcome due to high-temperature annealing.

Therefore the question arises whether a carbon-based material could be developed that suits the moderator requirements in low-temperature thermal reactors? Obviously the basic requirements are that the material should be amorphous, dense and with very high degree of isotropicity in them. Conventionally amorphous carbon is prepared from petroleum coke. But it tends to graphitize during high temperature processing at and above 900 °C, hence making it useless for the proposed application. So, the key issue remains that the material should retain its isotropic nature even after heat-processing at ~1500 °C and above typically required for structural fabrication. Besides, there should not be much radiation-induced modification of its thermo-mechanical properties. Unfortunately, such a novel carbon with high degree of thermal and radiation stability does not exist. So attempts were made to develop carbon composites that encompass most of the properties and yet remain isotropic over a wide range of temperatures by judiciously choosing the right starting materials that yielded hard and non-graphitizing forms of carbon [6]. In

* Corresponding author. Tel.: +91 22 25590292; fax: +91 22 25505151.
E-mail addresses: kdg@magnum.barc.ernet.in (K. Dasgupta), mainak73@yahoo.com (M. Roy).

this article, we report on synthetic routes for making of novel carbon composites that not only retain isotropicity over a wide range of stock composition but also remain amorphous when heat-treated at high temperatures. Besides these materials offer excellent thermo-mechanical properties such as low coefficient of thermal expansion, high specific heat, high compressive strength etc. and can be processed at very high heating rates typically ~ 50 – 100 °C/h as against 5 °C/h recommended for standard petroleum coke samples. An exhaustive study has been carried out on different thermo-mechanical and other material properties of the samples using a wide range of characterization techniques. Herein, we discuss the results of our investigation on carbon composites made from carbonized PAN fiber i.e., carbon fibers and carbon black powder in comparison with a standard carbon sample made from petroleum coke.

2. Experimental

2.1. Sample preparation

2.1.1. Petroleum coke based samples

As reference a sample was prepared from nuclear grade petroleum coke mixed with 25% phenol formaldehyde binder following standard recipe available in the literature [1]. Pellets (10 mm diameter and 10 mm height) were made in a uniaxial press under a pressure of 350 MPa. They were then heat-treated at ~ 1000 °C in an inert atmosphere to get the desired product.

2.1.2. Carbon fiber based samples

Carbonized PAN (polyacrylonitrile) fibers were chopped into pieces typically ~ 2 mm in length and dispersed in phenol formaldehyde resin matrix in different weight fractions. The resin along with the fiber was then cast in a dye having 10 mm diameter and 10 mm height and was heat-treated to ~ 1000 °C in an inert (argon) atmosphere at the rate of 50 °C/h to obtain the desired product. Carbon composites made with 10, 20, 30 and 50 wt% of carbon fibers were characterised ex-situ using a number of techniques.

2.1.3. Carbon black based samples

Phenol formaldehyde resin (liquid Resol type) was cured at 200 °C and crushed into small pieces. They were subsequently carbonized at a temperature of 1000 °C in inert atmosphere. The heating rate was maintained at 100 °C/h in the temperature range of 200 °C– 750 °C. The carbonized product was milled and sieved into different size fractions. The powder was leached by hydrochloric acid to remove metallic impurities like iron that came in from milling. Powder having size below 75 μm was used in the present study. This carbon powder was mixed with 0–15 wt% of carbon black (N330 grade of surface area 83 m^2/g) and phenol formaldehyde binder varying from 10% to 20% by weight. Pellets (~ 10 mm diameter and 10 mm height) were

made in a uniaxial press under a pressure of 350 MPa. The green pellets were heat treated upto 1000 °C at a heating rate of 100 °C/h in inert atmosphere to remove volatile organic impurities from the binder.

2.1.4. Densification of the samples

Densification of carbon samples was carried out by impregnation technique. Residual open pores in the samples were impregnated with liquid phenol formaldehyde resin under pressure of 24 kg/cm^2 and then it was carbonized at ~ 1000 °C under inert atmosphere. Heating rate was maintained at ~ 100 °C/h. Impregnation for different span of time and subsequent carbonization was carried out in cycles until there was no appreciable change in the density of the samples.

All samples were subsequently heat-treated at 1500 °C to explore the effect of high-temperature processing on the micro-structural modification of the materials.

2.2. Sample characterization

Chemical analysis of the samples was done by atomic emission spectroscopy (AES). Bulk density of the samples was measured by conventional Archimedes principle using distilled water. Specific heat (C_p) data were obtained using a differential scanning calorimeter (DSC) (Mettler make). Coefficient of thermal expansion (CTE) and compressive strength (CST) measurements were carried out, respectively, using a dilatometer and a universal testing machine. Reflection microscopy was done on polished samples using a polarized light source. A retarder plate (λ plate) that introduces a phase shift of 551 nm was used in combination with a set of cross-polarisers to study the samples and a Newton chart for phase shift was used to decode the extent of anisotropy in the samples from different colourations in the micrographs. X-ray diffraction patterns were recorded in a Philips X-ray diffractometer PW 1710 using Cu K_α line (1.54060 Å) from an X-ray generator operated at ~ 30 kV and 20 mA. Micro-Raman measurements were done using a LABRAM-I spectrometer (ISA make) in a backscattering geometry and with spectral resolution of 2 cm^{-1} . The 488 nm line of a 10 mW Ar^+ laser was focused onto the sample using a $10\times$ microscope (Olympus make) objective that corresponds to a spot of less than 1 mm for excitation and a Peltier cooled charge coupled device (CCD) was used for multi-channel detection.

3. Results and discussion

Nuclear grade (N-grade) material was obtained by both the proposed synthetic routes and also from N-grade petroleum coke. Elemental analysis of the samples (Table 1) shows impurities like boron, cadmium and cobalt, with very high neutron cross-section below ppm level. Other impurities also comply with nuclear standards. These metallic impurities especially iron are believed to have been incorporated during milling of the samples. It was observed

Table 1
Impurity analysis data of carbon samples prepared from different sources (ppm)

Source	Boron	Cadmium	Cobalt	Iron
N-grade petroleum coke	<1	0.5	0.3	380
Carbon fiber	<1	0.7	0.6	400
Carbon black	<1	ND ^a	ND	620

^a ND implies not detected, i.e., below detection limit of AES.

that density of the petroleum coke-based samples at a given temperature increased initially and then decreased steadily with weight fraction of the binder. Initially the binder bridges the inter-particle gap thus increasing the sample density, while excess of it contributes to porosity in the sample as it volatilizes during carbonization. Maximum density (~1710 kg/m³ @ 1000 °C) was obtained with 25 wt% of binder composition. A standard carbon sample synthesized by cracking this stock composition i.e., 75% petroleum coke and 25% binder at ~1000 °C has been used during the present study as a reference material for comparing its thermo-mechanical and other material properties with those obtained from carbon fiber and carbon-black. Fig. 1 shows the variation in density of the two sets of samples as a function of their constituents. The dotted line represents the standard sample made from petroleum coke. Density of carbon fiber based samples increases monotonically with fiber content i.e., with decreasing matrix element. Incomplete binding of the matrix resin with fiber leads to open porosity and hence decrease in the sample density with decreasing percentage of fiber. Carbon-black based samples have higher density than carbon fiber based samples because of lower % porosity but no systematic variation of the sample density with wt% of carbon-black is observed for these samples. For a given wt% of CB, highest sample density is attained with 15% binder that falls off on both sides of it due to binder-effect as has already been

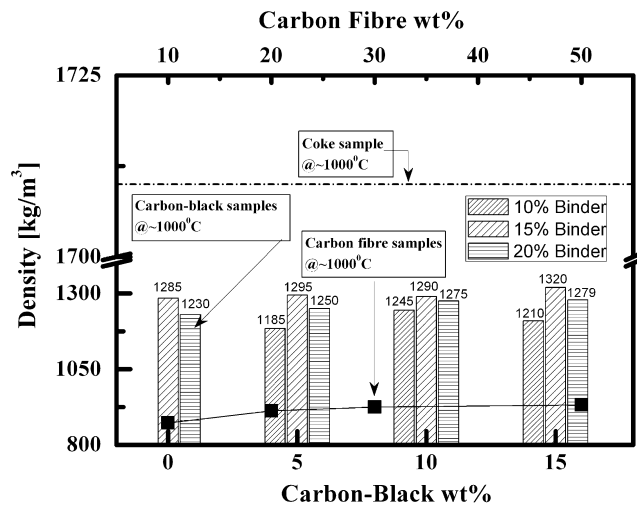


Fig. 1. Variation of density in both PAN based carbon fiber and CB samples as a function of their constituents.

explained in case of petroleum coke based samples. The hypothesis is supported by open pore analysis of CB samples (Fig. 2) that shows samples made with 15% binder having lowest percentage of open porosity for a given wt% of CB. Density of the standard coke sample is however very much higher as compared to both carbon fiber and CB based samples. In order to increase their density further, the samples were subjected to impregnation and subsequent carbonization as described in detail in the experimental part. After several cycles of impregnation (Fig. 3) it was found that density increased only by 15% (density 1512 kg/m³) in case of 15 wt% CB sample while it increased by more than 40% (density 1510 kg/m³) in case of 20 wt% PAN based carbon fiber sample, indicating greater percentage of open pores in as-grown carbon fiber samples. However one major disadvantage of this

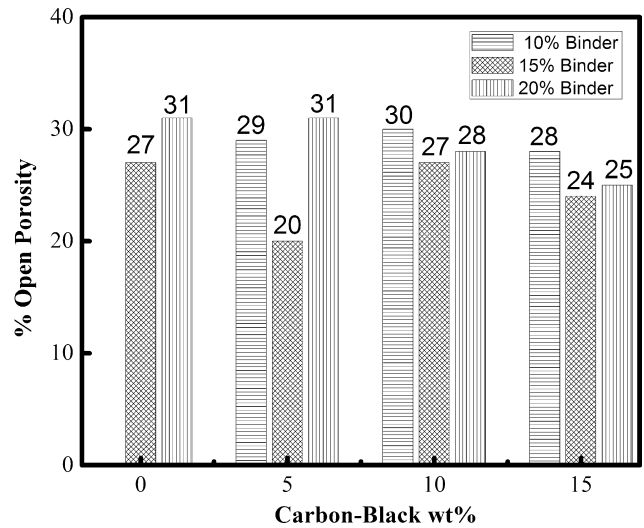


Fig. 2. Open porosity analysis of CB samples as a function of their constituents.

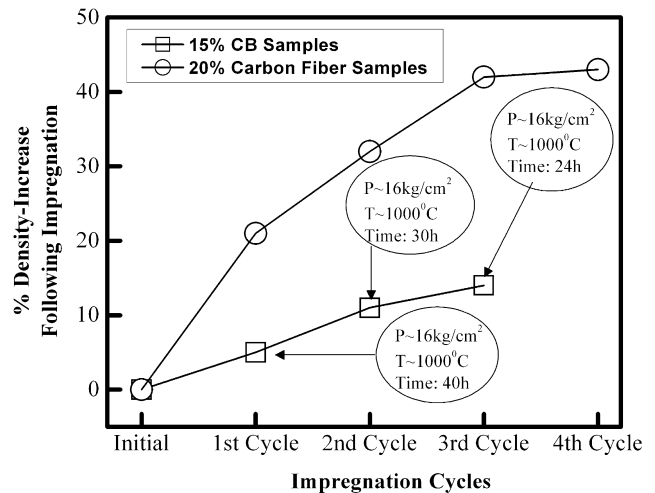


Fig. 3. Increase in density of PAN fiber and CB samples as a function of impregnation cycle.

impregnation technique is that during high-temperature processing, stress is developed in the samples due to unequal expansion of the matrix and core material, often resulting in the formation of cracks in them. Fig. 4 shows the variation in compressive strength of the same set of samples as a function of their constituents. The dotted line as in the previous graph represents the standard coke sample. By and large the trend is the same as that observed for density. In case of CB samples, 15% binder yields the highest compressive strength irrespective of wt% of CB, while it is highest for 50% carbon fiber sample. The most significant observation is that CST of the 50% PAN based carbon fiber sample and a few other CB samples far exceeds that of the standard coke sample. Coefficient of thermal expansion (CTE) along two mutually perpendicular directions has been recorded for the samples and is presented along with that of the standard coke sample in Fig. 5(a) and (b). It is observed that CTE_{\parallel} increases while CTE_{\perp} first increases and then steadily decreases with wt% of fiber in carbon fiber samples. In case of CB samples, CTE_{\parallel} varies rather unevenly while CTE_{\perp} exhibits an increasing trend with wt% CB for a given percentage of binder. However, it may be noted that for the entire range of composition studied CTE values for both carbon fiber and CB samples are very much lower than the standard coke sample as required for the proposed application. Moreover, CTE_{\parallel} and CTE_{\perp} values differ significantly in the standard coke sample implying development of anisotropic graphite phase in it, whereas there is not much of difference in the values for the CB and carbon fiber samples except for the 50% fiber composition. Fig. 6 shows the mean specific heat of the carbon fiber samples and CB samples with 15% binder composition over the temperature range of 50–550 °C. Samples with 15% binder have been typically chosen as they exhibit higher specific heat and excellent material properties over other binder compositions. Mean specific heat decreases drastically from 1710 to 1120 J/(kg K) as

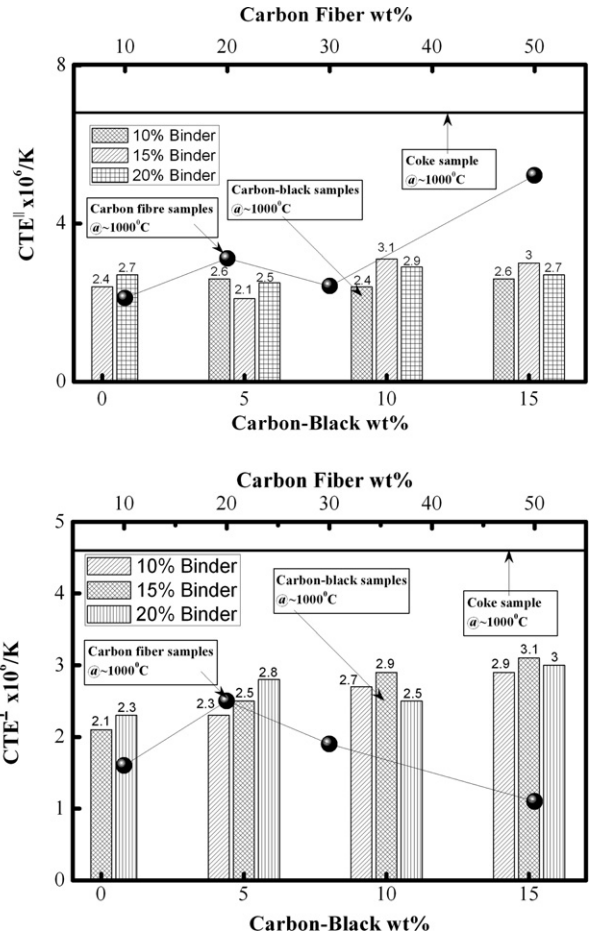


Fig. 5. Variation of coefficient of thermal expansion along two mutually perpendicular directions in both PAN based carbon fiber and CB as a function of their constituents.

fiber increases from 10% to 20% and then tends to saturate at higher wt% of fiber. In contrast, specific heat first increases significantly from 1210 to 1700 J/(kg K) upon addition of 10% carbon black and then decreases at higher

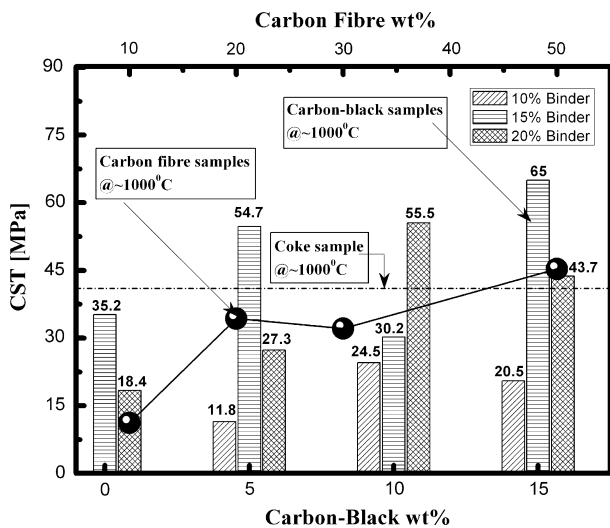


Fig. 4. Variation of compressive strength in both PAN based carbon fiber and CB samples as a function of their constituents.

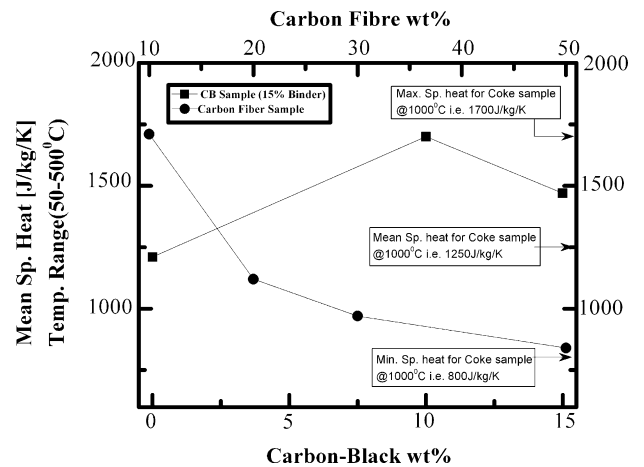


Fig. 6. Variation of mean specific heat measured in the temperature range of 50–550 °C in both PAN based carbon fiber and CB as a function of their constituents. Inset: Plot of specific heat of 15% binder CB samples as a function of temperature.

wt% of CB. It is well known that higher specific heat minimizes the risk of releasing Wigner energy suddenly [1]. The arrows in the graph describe the mean (1250 J/(kg K)), upper (1700 J/(kg K)) and lower (800 J/(kg K)) limiting values of specific heat for the standard coke sample in the specified range. Although the mean values are slightly lower for carbon fiber samples, they are very much on the higher side for CB samples as compared to the standard. Besides all data points for both the samples measured in the specified temperature range lie within the limiting band for the standard sample. Apart from these very important thermo-mechanical parameters discussed above, the material property that matters most for the proposed application is the isotropic and amorphous nature of the samples. The extent of anisotropy in amorphous carbon sample due to formation of graphitic phase can be qualitatively studied using an optical polarized microscope equipped with a set of cross-polarizers and a retarder plate (λ -plate) [7,8]. According to Newton's chart for evaluation of phase shifts, a λ -plate that introduces a shift of 551 nm would show up an isotropic phase as blurred magenta colored background [black in gray scale], while the anisotropic graphite crystals would appear either as greenish blue or deep yellow [bright patches with contrast in gray scale] depending on whether its aromatic plane is perpendicular or parallel to the λ -plate. Development of such coloration (greenish/yellowish) due to anisotropic graphite phase is referred to as optical activity. The technique has been described in detail in one of our previous articles [7]. Fig. 7(a) shows the micrograph of the standard coke sample that clearly shows development of optical activity due to the formation of graphite micro-crystallites. Fig. 7(b) shows the micrograph of the same sample heat treated at $\sim 1500^\circ\text{C}$. It is evident from the figure that the graphite micro-crystallites have grown bigger upon heat treatment resulting in enhanced optical activity of the sample. The observation is also supported from XRD measurements that will be discussed subsequently. Fig. 8(a) and (b) shows the micrographs of two typical samples grown with 20% and 50% carbon fiber. The optical activity of the 50% fiber sample is quite high (Fig. 8(b)), whereas the 20% fiber sample barely shows any activity (Fig. 8(a)). This has been explained on the basis of graphitization due to stress induced by the fiber ends. The stress distribution along the fiber length due to fiber matrix interaction during heat treatment of composite is uneven. The stress is maximum at the fiber end and minimum at the fiber centre [8]. The greater is the fiber content the more is the stress generated at the fiber matrix interface, which lead to anisotropy by means of graphitization. However, even after heating to 1500°C , no optical activity is developed in the 20% fiber sample [Fig. 8(c)]. The carbon-black samples on the contrary do not show up any activity for the entire range of composition discussed above. Fig. 9 (a) shows the micrograph of a typical CB sample with 15% CB and 15% binder composition. Extensive magenta background [black in gray scale] confirms the isotropic nature of the composite. The

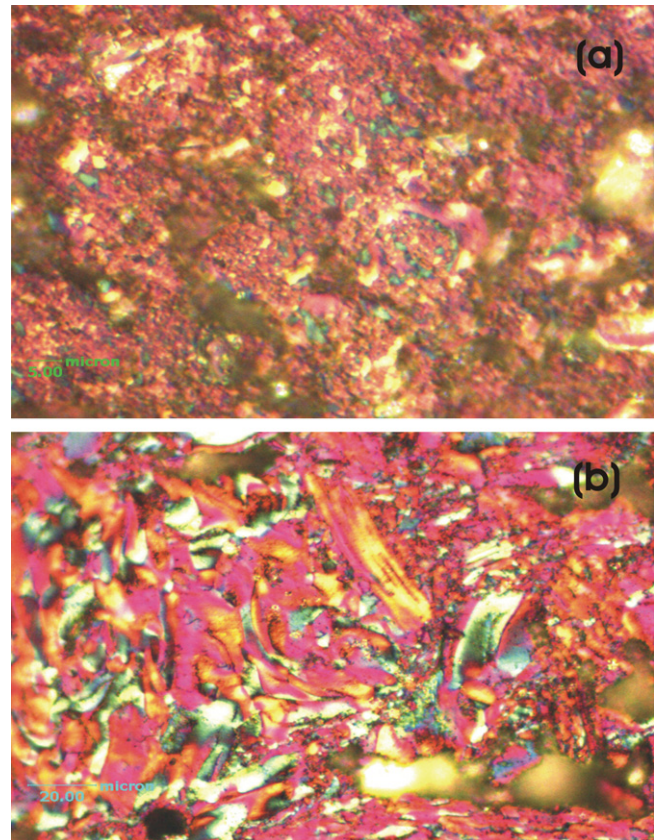


Fig. 7. Polarized optical micrographs of carbon composites made from petroleum coke heat-treated at (a) $\sim 1000^\circ\text{C}$ and (b) $\sim 1500^\circ\text{C}$.

sample remains isotropic and amorphous even when heated to 1900°C [Fig. 9(b)] implying that no stress is developed at the interface of as-grown CB samples. Here, the CB particles because of their near spherical geometry actually act as stress reliever as against the pointed fiber ends in carbon fiber based samples. Turbostratic modeling of XRD data provides a simple and straightforward technique for quantitative estimation of the degree of graphitization in amorphous carbon [9]. According to this model, the limiting value for the distance between two adjacent layers in turbostratic graphite is taken to be 0.344 nm, while that for pure 100% graphitic structure is taken to be 0.3354 nm. The percentage degree of graphitization in turbostratic graphite is therefore defined in terms of deviation of the interlayer spacing from that of the pure structure according to the equation

$$\begin{aligned} \text{\%Degree of graphitization} \\ = \{(3.44 - d_{002}) / (3.44 - 3.354)\} \times 100 \end{aligned} \quad (1)$$

where d_{002} denotes the interlayer spacing as obtained from the analysis of the XRD peak at $\sim 27^\circ$. According to this model any sample having an interlayer spacing higher than that of the limiting value i.e., 0.344 nm is considered to be 100% amorphous or isotropic in nature. The turbostratic model has also been used to analyze amorphous carbon [10] and is found to work well for all the

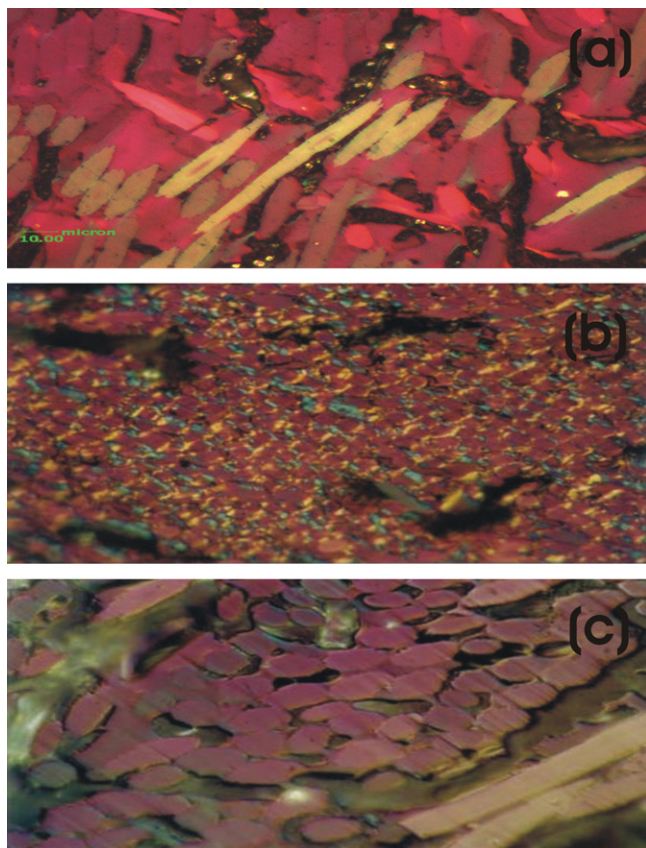


Fig. 8. Polarized optical micrographs of carbon composites made from (a) 20%, (b) 50% PAN based carbon fiber heat-treated at ~ 1000 °C and (c) 20% PAN fiber heat-treated at ~ 1500 °C.

carbon samples under discussion irrespective of their source and composition. Results on structural analysis and % degree of graphitization along with detailed sample composition are given in Table 2. As evident from the table, the standard coke sample is 25% graphitic. Except for the 50% fiber sample which exhibits graphitization of 73%, all carbon fiber and CB samples are found to be isotropic or 100% amorphous in nature for the entire range of composition discussed above. Although it is ascertained that as-grown CB samples are by and large isotropic in nature on a macroscopic scale and remains so even after heat treatment of 1500 °C, it remains to be verified at microscopic level especially in the context of the novel densification process discussed above that involves impregnation of the open pores by liquid resin under high-pressure followed by carbonization. Micro-Raman spectroscopy in combination with polarized microscopy provides a direct probe to the issue. Fig. 10 shows the μ -Raman spectra of three representative CB samples made from a fixed (15%) binder composition but with different wt% of CB. For comparison, Raman spectrum of a standard graphitic sample is also attached to the figure. The graphitic sample exhibits a strong and sharp peak at ~ 1580 cm^{-1} corresponding to zone centre vibrational mode of E_{2g} symmetry labeled 'G' peak and a hump at ~ 1355 cm^{-1} called 'D' peak, assigned to have originated from disorder, induced in the

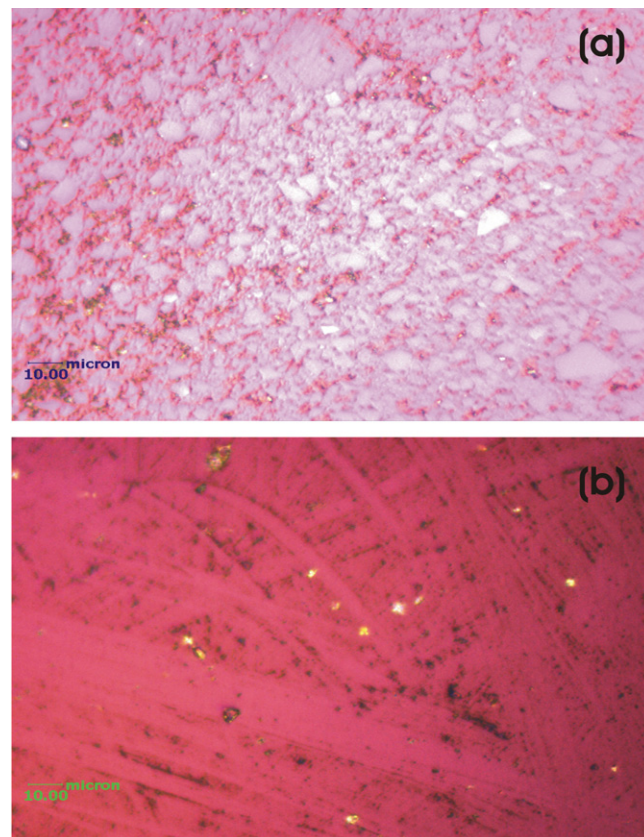


Fig. 9. Polarized optical micrographs of carbon composites made from CB heat-treated at (a) ~ 1000 °C and (b) ~ 1500 °C.

sample along its graphitic planes [11]. It is known from the literature that with decreasing long-range order the peaks become broader [12] and 'D' peak intensity relative to that of 'G' peak (i.e., D/G ratio) increases, often exceeding that of the later. The spectra are fitted with multi-

Table 2
% Graphitization in samples processed @ 1000 °C

Source	CB (wt%)	Binder (wt%)	PAN fiber (wt%)	Matrix (wt%)	d_{002} Graphitization %
Petroleum coke		25	75	3.42	25
Carbon black	0	15	85	3.48	NIL
	0	20	80	3.47	NIL
	5	10	85	3.49	NIL
	5	15	80	3.50	NIL
	5	20	75	3.52	NIL
	10	10	80	3.49	NIL
	10	15	75	3.50	NIL
	10	20	70	3.51	NIL
	15	10	75	3.50	NIL
Carbon fiber	15	15	70	3.52	NIL
	15	20	75	3.51	NIL
		10	90	3.50	NIL
		20	80	3.49	NIL
		30	70	3.48	NIL
		50	50	3.38	73

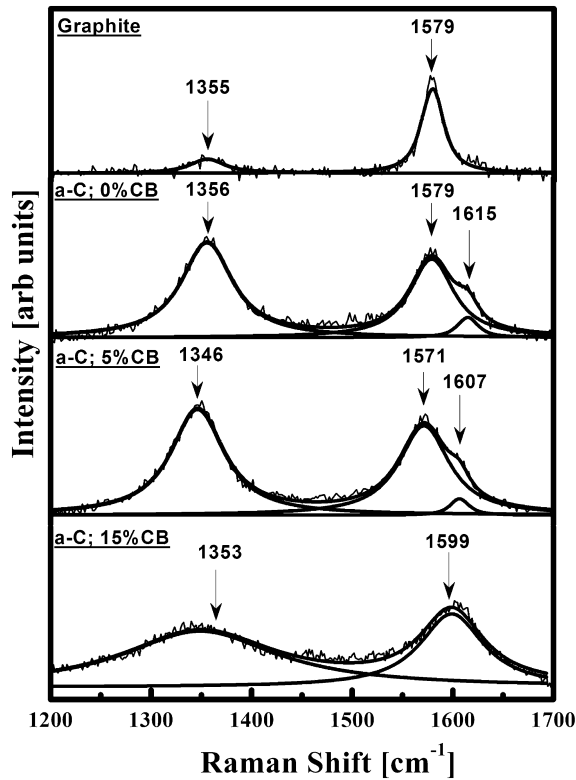


Fig. 10. Raman spectra of carbon composites made with 0, 5 and 15 wt% of CB along with a standard graphite sample.

Lorentzian line shape in order to extract quantitative information regarding peak position, FWHM and D/G ratio from the fitted parameters. It may be seen from the graph that both the 'D' and 'G' bands get broadened and D/G ratio increases in case of samples made from 0% and 5% of CB as compared to that of graphite, implying significant disorder in the samples. Apart from the 'D' and 'G' bands, another band at $\sim 1610 \text{ cm}^{-1}$ that corresponds to first order zone boundary phonon mode also appears in these samples. The bands are further broadened in case of samples made from 15% CB indicating an increase in their amorphous nature with increasing weight percentage of CB. Fig. 11 shows the Raman spectra of 15% CB sample before and after impregnation cycle. No appreciable change in the Raman profile could be observed following impregnation of the samples. This is further supported from the respective polarized optical micrographs (inset of Fig. 11) that do not show up any sign of optical activity in the samples even after third cycle of impregnation. In order to get a quantitative estimation of the trapped Wigner energy composites made from both carbon fiber and CB, they are subjected to irradiation by different projectiles. Results of irradiation tests on composites made from varying stock composition will be communicated separately in future. Finally a channel tube having diameter of 75 mm and length of $\sim 1.4 \text{ m}$ (Fig. 12 shows photograph of the channel tube actually used) has been fabricated with amorphous carbon composite made by the proposed tech-

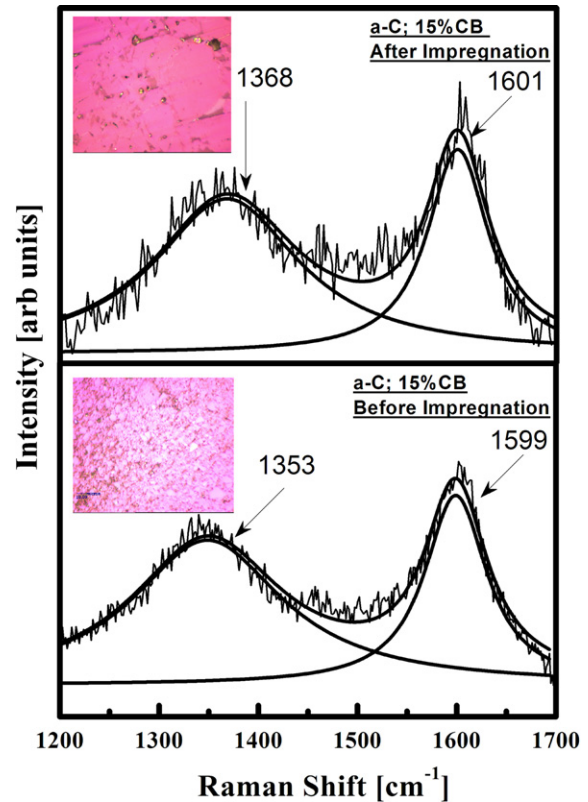


Fig. 11. Raman spectra of 15% CB composite samples before and after impregnation cycles. Inset: Corresponding polarized optical micrographs.

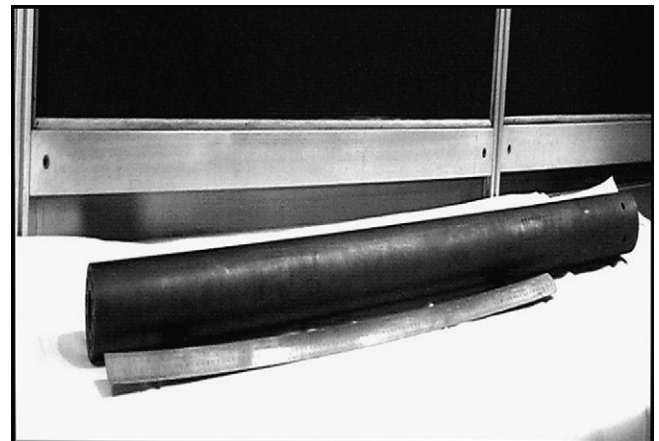


Fig. 12. Photograph of the channel tube made with 15% CB carbon composite.

nique from a stock composition of 15% CB and 15% binder and is ready to be tested under actual reactor conditions.

4. Conclusions

Two novel processing routes that involve use of carbonized polyacrylonitrile fibers and carbon black powder for making nuclear grade amorphous carbon composites have been proposed. It has been demonstrated that composites made from both these routes show very high density and

exceptional thermo-mechanical properties like coefficient of thermal expansion, compressive strength, specific heat etc. and are isotropic and amorphous over a wide range of stock composition that reduces the risk of releasing Wigner-energy when used as moderator material in thermal reactors. This has been verified from experiments carried out under actual reactor conditions.

Acknowledgements

The authors would like to express their sincere gratitude to Dr. S. Banerjee, Director, Bhabha Atomic Research Centre, Shri B.P. Sharma, Associate Director (S), Materials Group, Bhabha Atomic Research Centre, Dr. Tulsi Mukherjee, Director, Chemistry Group, Bhabha Atomic Research Centre and Shri R.K. Sinha, Director, Reactor Development and Design Group, Bhabha Atomic Research Centre for their constant support and encouragement. The authors also thank the Carbon Research Group of National Physical Laboratories, New Delhi, for their technical and scientific support.

References

- [1] Nightingale RE, editor. Nuc Graphite. New York and London: Academic Press; 1962.
- [2] Graphite Moderator Lifecycle Behavior, IAEA – Tecdoc 1998;90: 32–6.
- [3] Engle GB, Eatherly WP. High Temp.–High Press. 1972;4:119.
- [4] Kelly BT, editor. Phys. Graphite. London: Applied Science Publishers; 1981.
- [5] Kelly BT, Burchell TD. Carbon 1994;32:499.
- [6] Franklin RE. Proc. R. Soc. Lond A 1957;209:196–218.
- [7] Dasgupta K, Sathiyamoorthy D. Mater. Sci. Tech. Ser 2003;19: 995.
- [8] Oberlin A, Bonnamy S, Lafdi K. Structure and texture of carbon fibers. In: Donnet JB, Wang TK, Rebonillat S, Peng JCM, editors. Carbon Fibers. New York: Dekker; 1998. p. 85–159.
- [9] Pacault A. In: Walker Jr PL, editor. Chem. Phys. Carbon, Vol. 7. New York: Marcel Dekker; 1971. p. 107–54.
- [10] Dasgupta K, Krishna PSR, Chitra R, Sathiyamoorthy D. Carbon Sci. 2003;4:10–3.
- [11] Knight Diane S, White William B. J. Mater. Res. 1989;4:385.
- [12] Bachmann Peter K, Wiechert Detlef U. In: Clausing RE et al., editors. Diamond and Diamond-Like Films and Coatings. New York: Plenum Press; 1991.

Provided for non-commercial research and education use.
Not for reproduction, distribution or commercial use.



This article appeared in a journal published by Elsevier. The attached copy is furnished to the author for internal non-commercial research and education use, including for instruction at the authors institution and sharing with colleagues.

Other uses, including reproduction and distribution, or selling or licensing copies, or posting to personal, institutional or third party websites are prohibited.

In most cases authors are permitted to post their version of the article (e.g. in Word or Tex form) to their personal website or institutional repository. Authors requiring further information regarding Elsevier's archiving and manuscript policies are encouraged to visit:

<http://www.elsevier.com/copyright>



Contents lists available at ScienceDirect

Journal of Nuclear Materials

journal homepage: www.elsevier.com/locate/jnucmat

Neutron irradiation studies on low density pan fiber based carbon/carbon composites

Ramani Venugopalan^{a,*}, D. Sathiyamoorthy^a, R. Acharya^b, A.K. Tyagi^c

^a Powder Metallurgy Division, Bhabha Atomic Research Centre, Mumbai 400 085, India

^b Radiochemistry Division, Bhabha Atomic Research Centre, Mumbai 400 085, India

^c Chemistry Division, Bhabha Atomic Research Centre, Mumbai 400 085, India

ARTICLE INFO

Article history:

Received 26 February 2009

Accepted 14 June 2010

ABSTRACT

Carbon has been extensively used in nuclear reactors and there has been growing interest to develop carbon-based materials for high-temperature nuclear and fusion reactors. Carbon–carbon composite materials as against conventional graphite material are now being looked into as the promising materials for the high temperature reactor due their ability to have high thermal conductivity and high thermal resistance. Research on the development of such materials and their irradiation stability studies are scant. In the present investigations carbon–carbon composite has been developed using polyacrylonitrile (PAN) fiber. Two samples denoted as Sample-1 and Sample-2 have been prepared by impregnation using phenolic resin at pressure of 30 bar for time duration 10 h and 20 h respectively, and they have been irradiated by neutrons. The samples were irradiated in a flux of 10^{12} n/cm²/s at temperature of 40 °C. The fluence was 2.52×10^{16} n/cm². These samples have been characterized by XRD and Raman spectroscopy before and after neutron irradiation. DSC studies have also been carried out to quantify the stored energy release behavior due to irradiation. The XRD analysis of the irradiated and unirradiated samples indicates that the irradiated samples show the tendency to get ordered structure, which was inferred from the Raman spectroscopy. The stored energy with respect to the fluence level was obtained from the DSC. The stored energy from these carbon composites is very less compared to irradiated graphite under ambient conditions.

Crown Copyright © 2010 Published by Elsevier B.V. All rights reserved.

1. Introduction

Carbon is a wonderful material having wide range of structures and possess several excellent properties such as their capability to withstand high temperature (up to 3000 °C in protective environment), increased strength up to 2500 °C, chemical inertness, low coefficient of thermal expansion, low friction, good thermal and electrical conductivities, low density and good thermal shock resistance. Carbon and carbon-based materials are used in nuclear reactors and in the recent past there has been growing interest to develop graphite and carbon-based materials for high-temperature nuclear and fusion reactors. Efforts are underway to develop carbon materials with high density as well as amorphous isotropic carbon for use in low temperature thermal reactors. An amorphous structure is needed in order to avoid accumulation of Wigner energy [1], which is the stored energy in carbon lattice due to dislocation of atoms induced by irradiation. This amorphous carbon should be isotropic and dense in order to achieve dimensional stability under irradiation.

Graphitic carbon due to its excellent neutron scattering properties, continues to be the unanimous choice for the moderator material in high-temperature nuclear reactors [2–4] where the aforesaid drawbacks are essentially overcome due to high-temperature annealing. The effect of particle irradiation on graphite has gained lot of importance due to its use as nuclear material. Some literature on irradiation behavior of graphite [5–8] and stored energy in graphite [9,10] is available. However the studies on radiation damage in the disordered forms of carbon are scant. Few investigations on heavy ion irradiation of disordered carbon in carbon/carbon (C–C) composite made of particulates and chopped carbon fibers have been reported, but there is not much literature on architecture carbon/carbon composites. Burchell et al. [11] irradiated 1D, 2D, and 3D C–C composites at 600 °C up to damage doses 1.5dpa. 3D C–C composites were shown to have more isotropic dimensional changes than that of 1D or 2D composites.

The present study aims at determining if the particle irradiation causes formation of crystalline phase in the amorphous carbon leading to any storage of Wigner energy. There is a possibility of self-organization phenomena under irradiation leading to localized ordered arrangement in disordered structure of atoms in amorphous samples leading to crystallinity [12–14]. In the present work, we have carried out neutron irradiation on the carbon–carbon

* Corresponding author. Tel.: +91 022 25590499; fax: +91 022 5505151.

E-mail address: rvg@barc.gov.in (R. Venugopalan).

composites. We have characterized the structural parameters like extent of local ordering along *c*-axis, the average spacing of the $d_{(002)}$ i.e. the (0 0 2) crystallographic planes using X-ray diffraction (XRD) technique. This is further validated using Raman spectroscopy.

2. Experimental

2.1. Preparation of carbon/carbon composite samples

The fabrication of a suitable preform is the first step for manufacturing the carbon–carbon composite. This may also be referred to as fiber architecture. It not only imparts rigidity to the composite, but also in combination with fiber properties it determines the properties of the composite. In the present studies preform has been made using PAN carbon fibers. PANEX 35 carbon fiber of yield 48 K has been used. The carbon fiber diameter was 7.2 μm . In the present work green preform in the shape of rectangular blocks have been fabricated using 2D matted PAN carbon fiber which was stacked to a 2-D preform using phenol formaldehyde resin. This preform was cut into 1" \times 1" \times 0.4" size and carbonized at a slow heating rate of 0.1 $^{\circ}\text{C}/\text{min}$ in inert atmosphere. This carbonized samples had density of 1100 kg/m^3 . The carbonized sample is highly porous and has to be densified for any application. Hence

these samples were densified by resin impregnation technique up to two cycles. The samples were impregnated with liquid phenol formaldehyde resin under a pressure of 30 bar and with varying time duration of 10 and 20 h. The impregnated samples were cured and then carbonized at 1000 $^{\circ}\text{C}$ under inert atmosphere with a heating rate of 6 $^{\circ}\text{C}/\text{h}$. The samples were then further subjected to a second cycle of impregnation at the same pressure and varying time duration as carried out during the first cycle. These samples were then cured and carbonized as done in the first cycle. Two cycles of impregnation and carbonization were carried out and then used for further studies.

2.2. Irradiation of the samples

The carbon–carbon (C–C) composite samples have been irradiated with thermal neutrons at Apsara Reactor in Bhabha Atomic Research Center, Trombay. The energy spectrum for irradiation was 98% thermal neutron component for which neutron energy was up to 0.55 eV and 2% is epithermal component (above 0.55 eV).

Two samples, Sample-1 and Sample-2 having density of 1314 kg/m^3 and 1310 kg/m^3 respectively were taken for these studies. Sample-1 was prepared by impregnation of resin at 30 bars for 10 h while Sample-2 was prepared by impregnation at

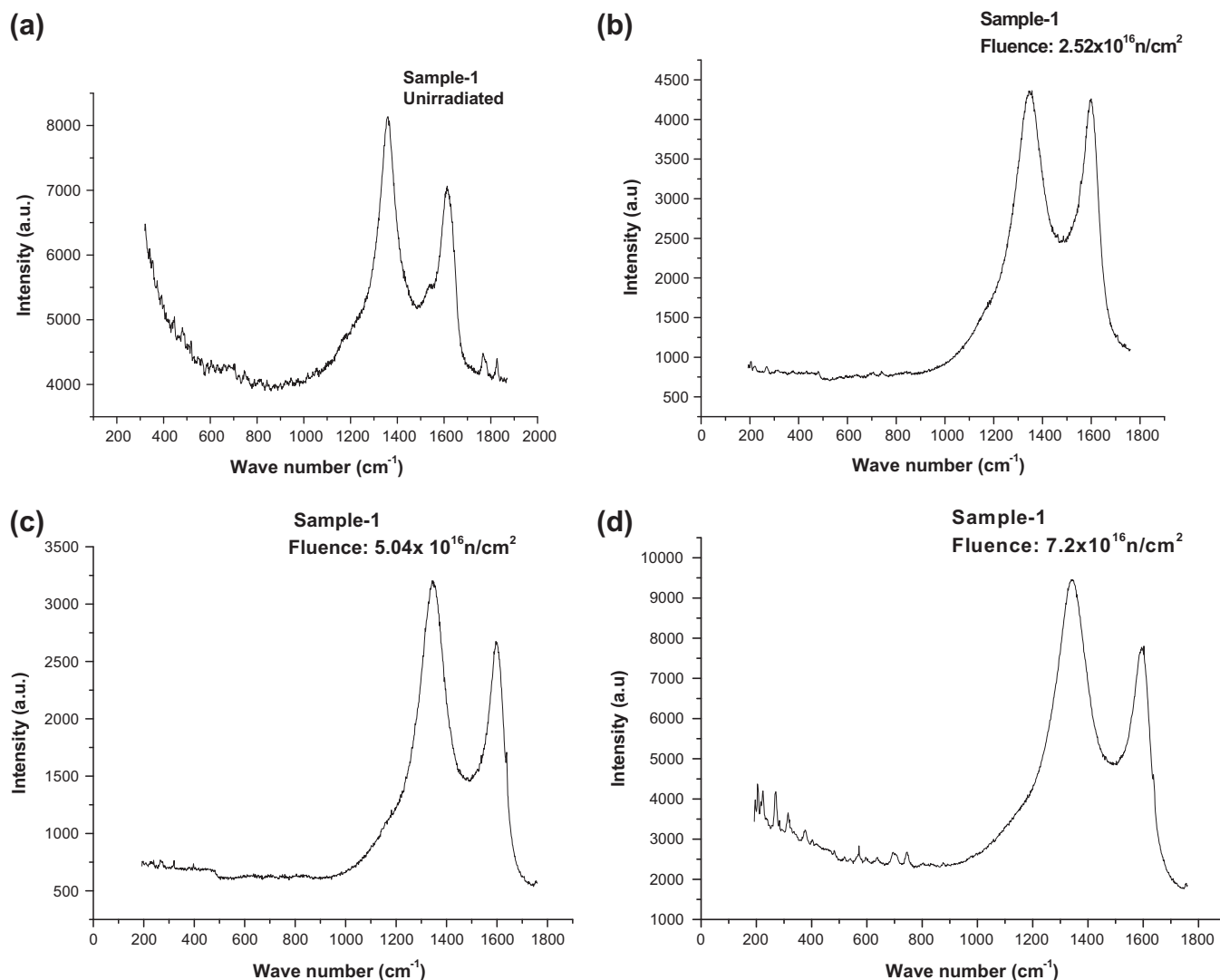


Fig. 1. Change in I_G/I_D for unirradiated and irradiated carbon/carbon composites Sample-1 at fluence levels: (a) unirradiated, (b) 2.52×10^{16} n/cm^2 , (c) 5.04×10^{16} n/cm^2 and (d) 7.2×10^{16} n/cm^2 .

30 bars for 20 h. The irradiation flux was 1×10^{12} n/cm²/s for seven hours, fourteen hours and twenty hours for both Sample-1 and Sample-2. The respective fluence was 2.52×10^{16} n/cm², 5.04×10^{16} n/cm² and 7.2×10^{16} n/cm² at temperature of 313 K during irradiation. The stored energy in the composite due to irradiation was measured using DSC and the changes in the structure were observed by X-ray diffraction and Raman spectroscopy.

2.3. Characterisation of the irradiated sample

XRD technique is employed to characterize the degree of graphitization of carbon-carbon composites with low crystallinity. X-ray diffraction patterns were recorded using a Philips X-ray diffractometer PW 1710 using monochromatised Cu K α line (1.5418 Å) from an X-ray generator operated at ~30 kV and 20 mA. Samples

were scanned in a step of 0.02°/step over the angular range of (2 θ) from 10° to 70°. Micro Raman measurements were done using a LABRAM-I spectrometer (ISA) make in a back scattering geometry. The stored energy release spectra were measured by a differential scanning calorimeter at a constant heating rate in argon atmosphere. Both the samples were heated at the rate of 5 °C/min from RT to 1000 °C.

3. Results and discussion

3.1. Raman spectroscopy studies

Raman spectroscopy was used for the structural analysis and to find if graphitization was occurring during the processing of the samples. Usually Raman spectra of most of the carbon-graphite

Table 1
Variation of I_G/I_D with irradiation fluence levels.

S. No	Sample code	I_G/I_D			
		Unirradiated	2.52×10^{16} n/cm ²	5.04×10^{16} n/cm ²	7.2×10^{16} n/cm ²
1	Sample-1	0.73	0.87	0.85	0.80
2	Sample-2	0.82	0.92	0.93	0.91

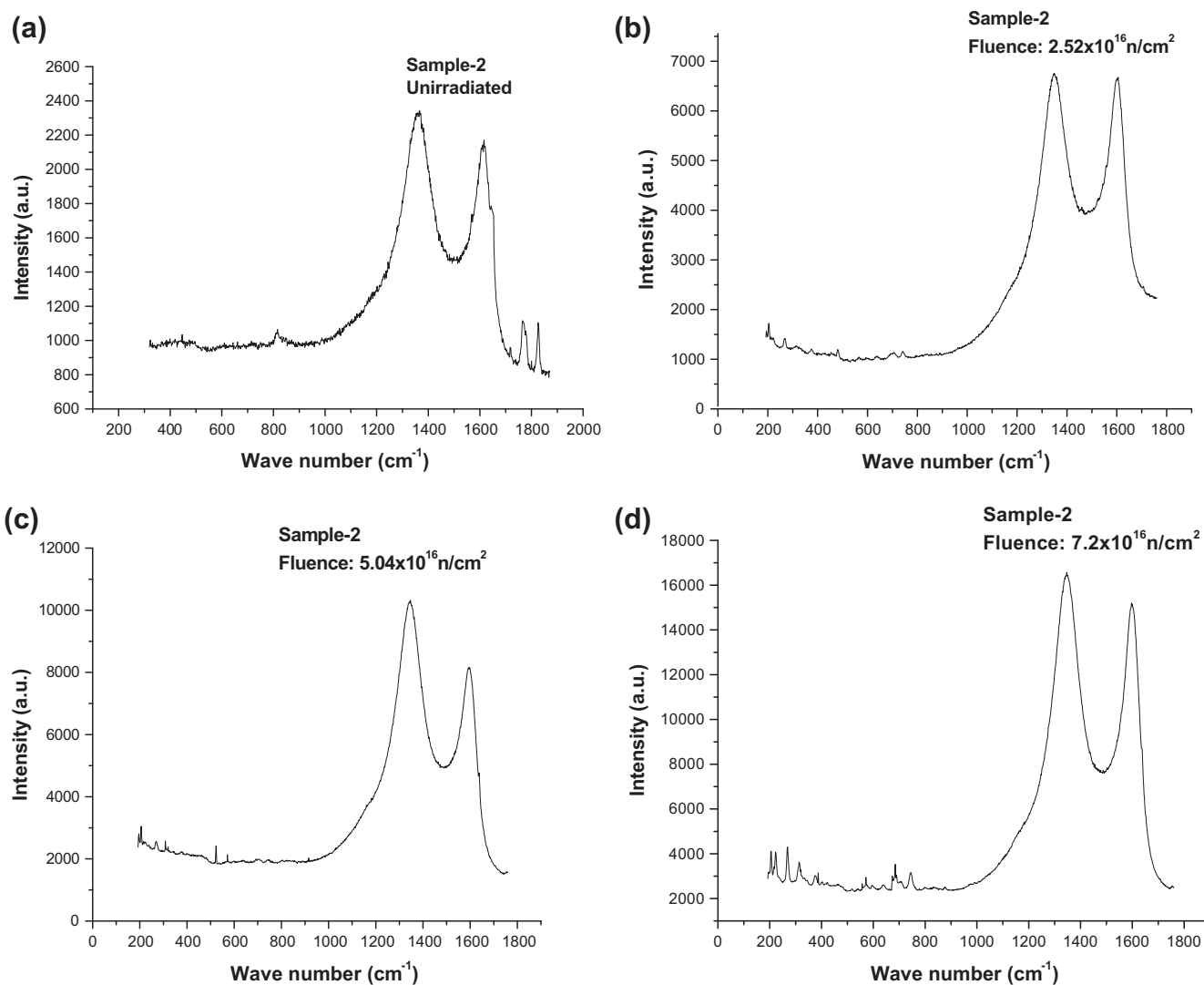


Fig. 2. Change in I_G/I_D for unirradiated and irradiated carbon/carbon composites. Sample-2 at fluence levels: (a) unirradiated, (b) 2.52×10^{16} n/cm², (c) 5.04×10^{16} n/cm² and (d) 7.2×10^{16} n/cm².

materials contain two peaks at $\sim 1580\text{ cm}^{-1}$ and at $\sim 1360\text{ cm}^{-1}$ except for natural graphite, which has a single sharp Raman band at 1580 cm^{-1} [15]. The 1580 cm^{-1} peak i.e. 'G' peak is known to correspond to graphite structure and the 1360 cm^{-1} peak is correlated to graphitized carbon structure called 'D' peak, assigned to have originated due to the disorder. The ratio of the integrated intensities of the two peaks, I_D/I_G has been considered to be a good parameter to estimate the degree of graphitization. The higher the ratio of I_D/I_G , lower is the degree of graphitization of the carbon materials. The 1580 cm^{-1} peak comes from the flex vibration of chemical bonds in atomic hexagonal net plane while the 1360 cm^{-1} peak is associated with local unsymmetrical structure, which exists, in graphitized carbon or non-integrity graphite crystals containing defects.

The change in structural parameters and the energy stored due to displacement of atoms from lattice position during irradiation have been studied using Raman Spectroscopy. From Fig. 1a–d shows the variation of I_G/I_D ratio of irradiated Sample-1. From Table 1 it is seen that the I_G/I_D ratio increased from 0.73 to 0.87 with increase in fluence and then further decreased with further increase in fluence. Fig. 2a–d shows the variation of I_G/I_D ratio of irradiated Sample-2. While in Sample-2 there was an increase in the ratio of I_G/I_D with increase in fluence from 0.82 to 0.93 and remains almost same on further increase in fluence. Study was carried out to see if the different processing parameters caused marked change in the I_G/I_D ratio of irradiated Sample-1 and Sample-2. There was no appreciable change observed which may be due to the fact that both had nearly the same density. It can be inferred that density is the factor which governs the irradiation defects rather than the processing parameter.

3.2. XRD studies

Carbon–carbon composites are composed of carbon fibers and carbon matrix, which are fabricated by different processing techniques. The carbon matrix is usually obtained by either impregnation with an organic precursor or chemical vapor infiltration (CVI) or by combination of these two ways that lead to hybrid matrix. The degree of graphitization in carbon–carbon composites is inhomogeneous and this is the reason why the material is difficult to graphitize. According to Bragg equation, the interlayer spacing d_{002} can be obtained and on the basis of the model given by Maire and Mering [16], the degree of graphitization can be calculated from the equation given below:

$$g(\%) = (0.3440 - d_{(002)}/0.3440 - 0.3354) \times 100 \quad (1)$$

where g is the degree of graphitization, 0.3440 is the interlayer spacing of fully non graphitized carbon (in nm), 0.3354 is the interlayer spacing of the ideal graphite crystallite and the $d_{(002)}$ is interlayer spacing obtained from XRD. 0.3440 nm represents a specific structure proposed by Franklin [17] who considered it as interlayer spacing of non graphitic carbon, i.e. the turbostratic structure put forward by Warren and co-workers [18,19]. Sometimes the apparent interlayer spacing of turbostratic structure is greater than 0.344 nm, as $d_{(002)} > 0.3440\text{ nm}$, $g < 0$ in Eq. (1) represents a structure which is far from ideal graphite structure.

From the XRD patterns Fig. 3a and b of the irradiated and unirradiated samples it is found that the d_{002} peaks for the irradiated samples are becoming broader and appearance of a new peak indicate the tendency to get ordered structure. Table 2 gives the change in d_{002} values of unirradiated and irradiated Sample-1 and Sample-2.

XRD is the most common analytical tool for determining structure of the ordered and disordered carbons [20–23]. In graphite the carbon layers have the ABAB-stacking along the c -axis. The disorder

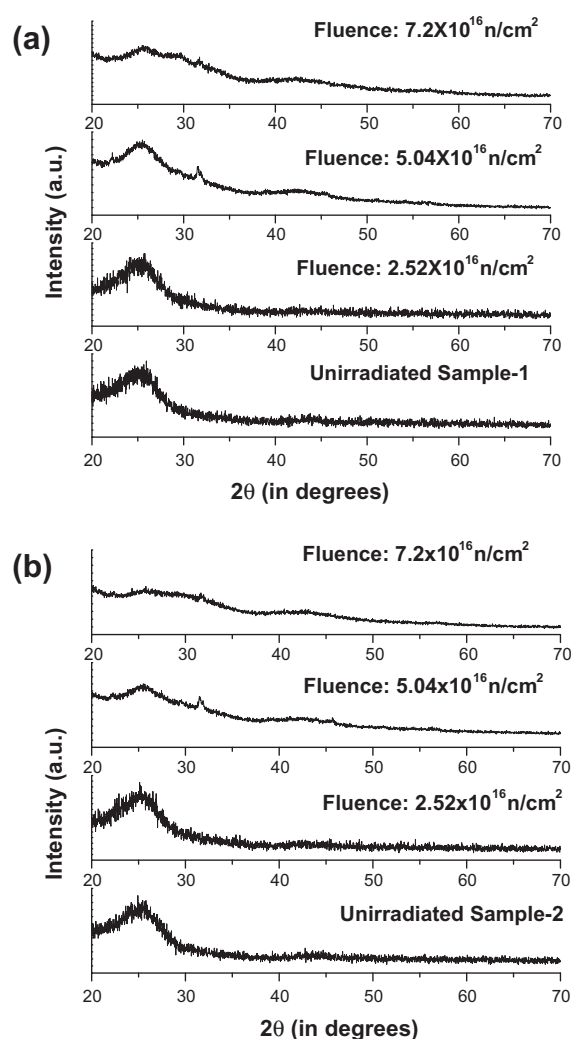


Fig. 3. XRD patterns of irradiated carbon/carbon composite: (a) Sample-1 and (b) Sample-2 at different fluences.

Table 2
Variation of d_{002} with different fluence levels.

Dose (neutron) (n/cm^2)	Sample-1 d_{002} (Å)	Sample-2 d_{002} (Å)
Unirradiated	3.66	3.719
2.52×10^{16}	3.60	3.64
5.04×10^{16}	3.51	3.49
7.2×10^{16}	3.49	3.50

can occur due to random shifts between the adjacent layers, unorganized carbon atoms which are not part of the layer, presence of local 3R stacking and strain in the layers. These defects affect the extent of local ordering L_c along c -axis designated as crystalline height.

3.3. DSC studies

The neutrons transfer their kinetic energy by knock off of atoms from the lattice when the carbon–carbon composites are irradiated. These in turn cause displacement cascades by successive collisions. Stored energy arises due to the fact that after irradiation by neutrons the crystal lattice of graphite possesses increased potential energy due to the presence of defects stable under the

conditions at which the irradiation was carried out. The defects are of two general types, vacancy and interstitial, but with varying complexity depending on the irradiation conditions. Defects may be annealed to more stable configuration by increasing the vibrational energy of the lattice by heating. Most of the energy release may be caused by the annihilation of interstitials and vacancies. The stored energy was measured by release of the energy at constant rate. Fig. 4a and b shows the DSC plot, of the energy release rate with respect to temperature for the irradiated samples. The samples were heated at constant rate of heating of 5 °C per minute in the range from RT to 1000 °C. The stored energy is obtained from the area under the curve. The stored energy release data for Sample-1 and Sample-2 at varying fluence levels is given in Table 3.

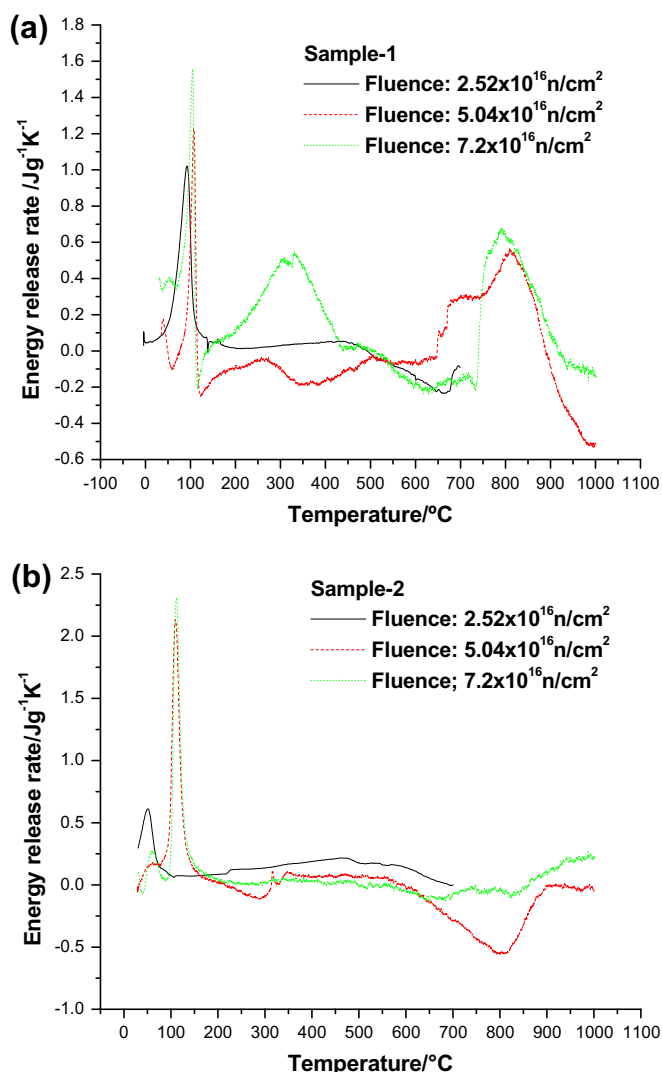


Fig. 4. Stored energy release spectra of carbon/carbon composite at different fluence levels: (a) Sample-1 and (b) Sample-2.

Table 3
Stored energy at different irradiation fluence levels.

Dose (n/cm ²)	Sample-1 stored energy (J/g) (RT–1000 °C)	Sample-2 stored energy (J/g) (RT–1000 °C)
2.52×10^{16}	82.20	100.02
5.04×10^{16}	119	66
7.2×10^{16}	185	51.65

The stored energy is found to increase with increasing fluence in Sample-1. At lower fluence the defects are simple and are getting annealed at around 100 °C. While at higher fluence levels complex defects are formed which are getting annealed by heating at higher temperatures. In Sample-2 the stored energy was found to decrease with increasing fluence indicating that the defects created are less and simple in nature and are getting annealed at lower temperatures. It has been earlier reported in literature [24] that the stored energy decreases with increase in fluence level for ion irradiation of both carbon black based composite and PAN based composite. Irradiation at high doses causes formation of complex defects and the stored energy may be released at higher temperatures. The samples in our experiments are carbon/carbon composites made of reinforced PAN fiber and matrix of carbon char obtained from phenol formaldehyde resin. Both the carbon present in the samples is in disordered form. The amount of energy stored in graphite varies with the crystallite size, more energy being stored in the more highly crystalline material [25]. In case of irradiated graphitic samples they require high activation energy to overcome the activation barrier to reach at a lower energy state (stable form) and so higher temperature is required. So the energy release peak is seen around 150–200 °C for graphite samples irradiated at 30 °C associated with the recombination of single interstitials and vacancies. With increasing neutron dose this peak becomes broader and maximum release rate is reduced. The disordered carbon is already at higher energy level and the activation energy barrier is less, as compared to graphite therefore lower temperature is sufficient to overcome the activation energy barrier. The accumulation of stored energy in graphite is both dose and irradiation temperature dependent. With increasing irradiation temperature the total amount of stored energy and its peak rate of release diminish and above temperature of ~300 °C stored energy ceases to be a problem. The amount of stored energy in graphite irradiated at ambient temperature is very large, which is 2700 J/g, can be stored as lattice defects. This heat, when released under adiabatic conditions would cause an increase in temperature of ~1300 °C. Annealing is required as observed in highly irradiated graphite [26–29] where the sample has to be heated to 2000 °C to release all the stored energy.

4. Conclusions

The neutron irradiated carbon composite samples have been characterized by XRD and Raman spectroscopy before and after neutron irradiation. DSC studies have also been carried out to see the stored energy release behavior due to irradiation. From the XRD analysis of the irradiated and unirradiated samples it is found that the values of d_{002} peaks for the unirradiated samples are higher than that of the irradiated samples indicating the tendency to get ordered structure. This is also inferred from the Raman spectroscopy. The I_G/I_D ratio of irradiated samples was found to increase with increasing fluence when compared to unirradiated samples initially but decreased further with increasing fluence in Sample-1. While in Sample-2 there was an increase in the ratio of I_G/I_D with increase in fluence and is almost same on further increase in fluence. The stored energy with respect to the fluence level was obtained from the DSC. These results indicate that simple defects created due to low fluence of irradiation are annealed by heating and releasing the stored energy at lower temperature while if complex defects are formed high temperatures are required for annealing these defects. The flux/fluence used is lower than the actual scenario in the upcoming compact higher temperature reactor; however the present study could definitely be an initial step in the direction of investigation of damage caused by neutrons on carbon/carbon composite materials for its use in the

upcoming reactor. Currently the available flux was low in the range of 10^{12} n/cm²/s. However these samples have to be evaluated by irradiating at a higher dose for any nuclear application. We have severe limitation of not being able to use the fluence of 10^{20} n/cm². However an extension of work on carbon/carbon (C/C) composites irradiation with higher flux in some international neutron irradiation facility would be taken up in near future. Currently some irradiation studies with high energy neutrons are being carried out. The results of which will be discussed in forthcoming publication.

References

- [1] Graphite Moderator Lifecycle Behavior. IAEA – Tecdoc. 90 (1998) 32.
- [2] G.B. Engle, W.P. Eatherly, High Temp. – High Press. 4 (1972) 119.
- [3] B.T. Kelly, Physics of Graphite, Applied Science Publishers, London, 1981.
- [4] B.T. Kelly, T.D. Burchell, Carbon 32 (1994) 499.
- [5] R.E. Nightingale, Nuclear Graphite, Academic Press, New York, London, 1962.
- [6] B.T. Kelly, Prog. Nucl. Energy 2 (1978) 21.
- [7] V.I. Klimenkov, Y.N. Aleksenko, USSR Acad. Sci. Phys. 2 (1956) 226.
- [8] T.D. Burchell, Phys. Scripta T 64 (1996) 17.
- [9] T. Iwata, J. Nucl. Mater. 134 (1985) 361.
- [10] K. Dasgupta, M. Roy, A.K. Tyagi, S.K. Kulshreshtha, D. Sathiyamoorthy, Compos. Sci. Technol. 67 (2007) 1794.
- [11] T.D. Burchell, Carbon materials for energy production and storage, in: B. Rand et al. (Eds.), Design and Control of Structure of Advanced Carbon Materials for Enhanced Performance, Kluwer Academic Publishers, 2001.
- [12] F. Banhart, Rep. Prog. Phys. 62 (1999) 1181.
- [13] A. Seeger, Rad. Eff. Deffects Solids 355 (1989) 111.
- [14] A. Seeger, W. Frank, Solid State Phenomena 125 (1988) 3.
- [15] Linhua Zou, Baiyun Huang, Yong Huang, Qizhong Huang, Chang'an Wang, Mater. Chem. Phys. 82 (2003) 654.
- [16] J. Marie, J. Mering, Chem. Phys. Carbon 6 (1970) 125.
- [17] R.E. Franklin, Acta Crystallogr. 4 (1951) 253.
- [18] B.E. Warren, Phys. Rev. 59 (1941) 693.
- [19] J. Biscoe, B.E. Warren, J. Appl. Phys. 13 (1942) 364.
- [20] R.E. Franklin, Acta Cryst. 3 (1950) 107.
- [21] S. Ergun, P.L. Walker (Eds.), Chemistry and Physics of Carbon, Marcel Dekker, New York, 1967.
- [22] S. Ergun, Carbon 14 (1976) 139.
- [23] W. Ruland, P.L. Walker (Eds.), Chemistry and Physics of Carbon, Marcel Dekker, New York, 1968.
- [24] K. Dasgupta, P. Barat, A. Sarkar, P. Mukherjee, D. Sathiyamoorthy, Appl. Phys. A: Mater. Sci. Process. 87 (2007) 721.
- [25] G.V. Dienene, Physics 24 (1953) 666.
- [26] S.D. Preston, G.T. Melvin, Results from the 1997/98 Stored energy Survey of Windscale Pile I, IAEA Technology plc Report AEAT-3400 WPTC 73, 1998.
- [27] H. Bridge, D. Mottershead, J. Nucl. Mater. 20 (1966) 281.
- [28] J.H.W. Simmons, Radiation Damage in Graphite, Pergamon Press, Oxford, 1965.
- [29] J.C. Bell, H. Bridge, A.H. Cottrell, G.B. Greenough, W.N. Reynolds, J.W.H. Simmons, Philos. Trans. Roy. Soc. A 254 (1962) 361.